

C71-52/301

NASA CR-111861  
C71-52/301  
COPY

# PLANETARY TERMINAL DESCENT AND LANDING RADAR

## FINAL REPORT

Contract NAS 1-7696

JANUARY 1971

Prepared for  
NATIONAL AERONAUTICS AND SPACE ADMINISTRATION  
Langley Research Center  
Hampton, Virginia



**Autonetics**  
North American Rockwell

3370 Miraloma Avenue  
Anaheim, California 92803

## ABSTRACT

This program was initiated to procure a model R146-A bi-mode radar configured to provide three-dimensional velocity readout and to indicate slant range to the ground over a wide range of velocities and altitudes. The equipment construction was completed in January 1969 and was flight tested in a company-owned B-26 aircraft during the next several months. The test results indicated a lower operating limit of approximately 100-ft altitude in the  $J_3$  Bessel sideband mode. The system was modified to provide switch selectable operation in  $J_1$ ,  $J_2$ , or  $J_3$  Bessel sideband modes and was then flight tested in a Jet Ranger helicopter. The results of this flight test indicated performance degradation due to the poor sidelobe structure of the Luneberg lens. Dual constant K antennas were fabricated and the system was configured to permit operation in either a single or dual antenna configuration. The system was again flight tested in the Jet Ranger helicopter and good performance was obtained. Three-dimensional tracking of both positive and negative velocities down to zero ft/sec were obtained with an average error of less than 1.5 ft/sec corresponding to approximately 0.218 percent of full scale (680 ft/sec). Altitude performance was measured from 10,000 ft to touchdown using on-board instrumentation and ground truth data supplied by the Pacific Missile Range at Pt. Mugu, California. It has been difficult to correlate the altitude data, but it appears that accuracies of better than  $\pm 5$  ft or 5 percent of value were obtained over the full altitude range to touchdown.

The resultant system for performance was satisfactory but the equipment was bulky. A modification program has been recommended that would result in a much smaller unit with improved performance.

## FOREWORD

This report was prepared by North American Rockwell Corporation, Autonetics Division, Anaheim, California, on NASA Contract NASI-7696, "Planetary Terminal Descent and Landing Radar". The work was sponsored by the Flight Instrument Division of the Langley Research Center. Richard Harrington was Project Engineer at the beginning of the program and continued in that capacity through February 28, 1969. W. A. Southall then assumed project responsibility.

The program results presented began in May 1968, and were completed in December 1970 and represent a joint effort of the Sensor Systems Group and the Flight Test Facility. Program Manager, G. M. Sallus, was responsible for the overall program management, and R. N. Parker, Chief Engineer, was responsible for the design and development activity.

The chief contributors and their fields of interest were: L. R. Frasure, W. R. Fried, R. Boehringer, and T. G. Sprague in electrical design; A. McLeod in antenna feedhorn design; H. F. Twilley and E. Jeseck in flight test planning, coordination and instrumentation.

This report is the final Technical Report and includes all the work done on Contract NASI-7696.



## NOMENCLATURE

$e_1$	Transmitted FM signal
$E_1$	Max amplitude of transmitted signal
$f_c$	Transmitted carrier frequency
$m$	Transmitted modulation index
$f_m$	Modulation frequency
$t$	Time
$e_2$	Local oscillator FM signal
$E_2$	Max amplitude of LO signal
$f_{1F}$	Intermediate frequency
$e_3$	Echo FM signal
$E_3$	Max amplitude of echo signal
$f_d$	Doppler frequency due to vehicle motion
$t$	Round-trip delay time
$e$	Mixer output signal
$J_n$	Bessel Sideband of $n^{\text{th}}$ order
$M$	Received modulation index
$n$	Sideband Order
$f_{1F_2}$	Second intermediate frequency
$V$	Velocity of vehicle
$\lambda$	Transmitted wavelength
$a$	Magnitude of $f_a$
$a'$	Magnitude of $f_a'$
$b$	Magnitude of $f_b$
$b'$	Magnitude of $f_b'$

## NOMENCLATURE (Cont)

<b>S</b>	<b>Signal</b>
<b>N</b>	<b>Noise</b>
$p_t$	<b>Average transmitted power</b>
$G_o$	<b>Antenna gain (max)</b>
$\omega$	<b>Antenna pattern factor</b>
$\sigma_o$	<b>Back-scattering cross section per unit area of the scattering surface</b>
<b>K</b>	<b>Boltzmann's constant</b>
<b>T</b>	<b>Absolute temperature</b>
<b>B</b>	<b>Bandwidth</b>
<b>L</b>	<b>System RF losses</b>
<b>E</b>	<b>Modulation efficiency factor</b>
$\lambda_m$	<b>Modulation wavelength</b>
<b>K</b>	<b>Received modulation constant</b>
$K_1 = \frac{K}{2}$	
$K_2 = K_1^2$	
$\Phi$	<b>Maximum received modulation phase angle</b>
$M_o$	<b>Modulation index of the 1<sup>st</sup> zero crossing of an individual Bessel sideband</b>
$M_p$	<b>Modulation index of the 1<sup>st</sup> peak of an individual Bessel sideband</b>
$V_{ref}$	<b>Reference voltage</b>
$t_d$	<b>Time delay</b>
<b>l</b>	<b>Filter length</b>
$V_g$	<b>Group Velocity</b>
$\omega$	<b>Frequency (general)</b>
$\omega_o$	<b>Frequency of interest</b>
$\beta$	<b>Phase shift per filter section</b>

## NOMENCLATURE (Cont)

NB	Noise bandwidth
$T_I$	Integration time
$t_r$	Rise time
N	Number of filter sections
F	Image focus point
F'	Object focus point
R	Spherical radius
$R^1$	Hypothetical spherical radius
$\eta$	Refraction index
$\phi$	Angle between the velocity vector and the projected beam center of radiation.
$V_x$	Heading velocity
$V_y$	Drift velocity
$V_z$	Vertical velocity
$D_1$	Doppler frequency from beam No. 1
$D_2$	Doppler frequency from beam No. 2
$D_3$	Doppler frequency from beam No. 3
$K_x$	Heading velocity constant
$K_y$	Drift velocity constant
$K_z$	Vertical velocity constant
$\gamma_i = \psi$	Depression angle complement of individual antenna beams
$\theta_i$	Projected azimuth angle of individual antenna beams ( <b>splay angle</b> )
r	Range to scattering surface
c	Velocity of light
h	Altitude
$\psi$	Beam incidence angle

## NOMENCLATURE (Cont)

$f_a$	Doppler frequency return from beam intercept closer to vertical than boresight.
$f_a'$	Image of $f_a$
$f_b'$	Image of $f_b$
R	Lens radius
$L_0$	Ref path from lens to horn
f	Focal length of lens
$\eta$	Lens index of refraction
u, V, $\omega(u, V)$	Truncation surface coordinates
A, B, f(A, B)	Lens spherical surface coordinates
$\theta$	Feed horn exit ray angle from broadside
$L_1$	Arbitrary path length for ray having at $\theta$ angle
$\delta L$	Normalized path length error
$\Sigma$	Lens dielectric constant
F	Lens focal distance
$\psi$	Feed scan position

## BEAM GEOMETRY NOMENCLATURE

$p_i$	Unit vector from the axis to an individual beam
$l_i$	Direction cosine in X direction of an individual beam
$m_i$	Direction cosine in Y direction of an individual beam
$u_i$	Direction cosine in Z direction of an individual beam
$\theta_i$	Projected azimuth angle of an individual beam position
$\gamma_i$	Direction angle of an individual beam with respect to the Z axis
$\alpha_i$	Direction angle of an individual beam with respect to the X axis



## BEAM GEOMETRY NOMENCLATURE (Cont)

$\beta_i$	Direction angle of an individual beam with respect to the <b>Y axis</b> .
$f_{d_i}$	Doppler frequency shift from an individual beam.
$d_i$	Doppler frequency return from an individual beam position.
$\lambda_i$	Wavelength of the transmitted frequency for an individual beam.
$V_x$	Velocity component in the x direction
$V_y$	Velocity component in the y direction
$V_z$	Velocity component in the z direction



## INTERIM REPORTS

The following documents were generated during the course of the program:

C8-2980/401 "Planetary Terminal Descent and Landing Radar, Model R146A, Flight Test Plan".

T9-609/401 "Doppler Navigation Error Analysis for R146A Planetary Terminal Descent and Landing Radar". March 20, 1969.

T9-816/401 "Planetary Terminal Descent and Landing Radar Mechanization Modification to  $J_2$  Bessel Sideband for Improved Low Altitude Performance". April 17, 1969.



## TABLE OF CONTENTS

	Page
Abstract .....	ii
Foreword .....	iii
Nomenclature .....	v
Interim Reports .....	xi
1.0 INTRODUCTION AND SUMMARY .....	1-1
1.1 Mission Requirements .....	1-4
1.2 Modulation Techniques Trade-off .....	1-6
1.3 FM/CW Mode Analysis and Design Considerations .....	1-11
1.3.1 FM/CW Doppler and Altimeter Radar Theory - General Signal Analysis .....	1-13
1.3.2 Velocity Measurement .....	1-16
1.3.3 Altitude Measurement .....	1-19
1.3.4 Signal-to-Noise Ratio Characteristics .....	1-23
1.3.5 Choice of Critical Parameters .....	1-25
2.0 EQUIPMENT DESCRIPTION .....	2-1
2.1 Functional Description .....	2-1
2.2 Physical Characteristics .....	2-9
2.3 Performance Characteristics .....	2-10
2.4 Description of Equipment Components .....	2-10
2.4.1 Master Frequency Generator .....	2-10
2.4.2 Mode Switching .....	2-26
2.4.3 Transmitter .....	2-33
2.4.4 Microwave Components .....	2-38
2.4.5 Antenna .....	2-46
2.4.6 Receiver Design Considerations .....	2-61

## TABLE OF CONTENTS (Cont)

	Page
2.4.7 Leakage Elimination Filter (LEF) . . . . .	2-81
2.4.8 Velocity Tracker . . . . .	2-84
2.4.9 FM/CW Altitude Channel . . . . .	2-92
2.4.10 Phase Lock Loop. . . . .	2-100
2.4.11 ICW Range Tracking Loop . . . . .	2-109
2.4.12 Velocity Readout Circuitry . . . . .	2-116
2.4.13 Panel Controls and Electronic Chassis . . . . .	2-132
2.4.14 Power Supplies . . . . .	2-136
3.0 FLIGHT TEST . . . . .	3-1
3.1 General Description . . . . .	3-1
3.2 B-26 Flight Test Program . . . . .	3-2
3.3 Helicopter Flight Test Program . . . . .	3-5
3.4 Instrumentation and Signals Recorded . . . . .	3-10
3.5 Modes Tested . . . . .	3-11
3.6 Flight Profiles . . . . .	3-12
3.7 Terrain Types . . . . .	3-13
3.8 Air Force Flight Test Center and Pacific Missile Range Tests . . . . .	3-14
4.0 DATA REDUCTION . . . . .	4-1
4.1 General Discussion . . . . .	4-1
4.1.1 Information Content on Signals . . . . .	4-1
4.1.2 Data Reduction Techniques and Interpretation of Results . . . . .	4-4
4.1.3 Accuracy Determination . . . . .	4-19
5.0 Conclusions and Recommendations . . . . .	5-1
5.1 Conclusions . . . . .	5-1
5.2 Recommendations . . . . .	5-9

## LIST OF ILLUSTRATIONS

Figure		Page
1.	Transmitted Spectrum . . . . .	1-17
2.	Local Oscillator . . . . .	1-17
3.	Received Spectrum . . . . .	1-17
4.	Received Spectrum at Intermediate Frequency . . . . .	1-17
5.	Received Spectrum at Second Intermediate Frequency . . . . .	1-17
6.	System Beam Configuration . . . . .	1-20
7.	Altimeter Signal After Frequency Fold-Over . . . . .	1-22
8.	Altimeter Signal After Filtering . . . . .	1-22
9.	Altimeter Signal After Squaring . . . . .	1-22
10.	Bessel Functions for Small Arguments . . . . .	1-26
11.	$J_1^2$ (M) Function for Small Arguments . . . . .	1-28
12.	$1/r^2$ Function for Small r . . . . .	1-28
13.	Signal-to-Noise Ratio vs Range for $J_1$ FM/CW System . . . . .	1-28
14.	PTDLR Block Diagram . . . . .	2-2
15.	Transceiver . . . . .	2-11
16.	Processor . . . . .	2-12
17.	High Frequency Generator . . . . .	2-15
18.	60.000 MHz Generator . . . . .	2-17
19.	60.378 MHz, 60.4158 MHz, and 415.8 KHz Reference Generators . . . . .	2-18
20.	L. O. Reference Switching . . . . .	2-19
21.	60.4158 MHz Drivers . . . . .	2-20
22.	Low Frequency Generator . . . . .	2-22
23.	126 KHz, 189 KHz, and 378 KHz XTAL Oscillators . . . . .	2-23

LIST OF ILLUSTRATIONS (Cont)

Figure	Page
24. Modulation Frequency Driver . . . . .	2-24
25. 378 KHz Harmonic Generator . . . . .	2-25
26. 756 KHz Harmonic Generator . . . . .	2-27
27. Mode Switching and Range Readout - Block Diagram . . . . .	2-28
28. Mode Switching . . . . .	2-29
29. Ke Band Source . . . . .	2-36
30. RF Hardware . . . . .	2-41
31. Luneberg Lens Geometry . . . . .	2-48
32. Graph of Loss Tangent as a Function of Refraction Index for Two Low Density Artificial Dielectrics . . . . .	2-49
33. Luneberg 10.5 in. Lens . . . . .	2-51
34. H-Plane Radiation Patterns for 10.5 in. Luneberg Lens . . . . .	2-52
35. Luneberg Lens Beam Pattern . . . . .	2-53
36a. PTDLR Single Antenna Concept . . . . .	2-55
36b. PTDLR Dual Antenna Concept . . . . .	2-55
37. Physical Comparison of Geometrical Properties of Conventional Hemispherical Scanning Lens with the Thin Cap Multiple Beam Constant "K" Lens . . . . .	2-57
38. Constant "K" Cap Lens Geometry . . . . .	2-58
39. Aperture Phase Correction as a Function of Lens Radius. . . . .	2-59
40. Antenna Beam Patterns . . . . .	2-63
41. Received Power vs Range . . . . .	2-65
42. FM/CW Alternate Channel Gain Distribution . . . . .	2-66
43. FM/CW Velocity Channel Gain Distribution . . . . .	2-67
44. Preamplifier Schematic . . . . .	2-72
45. I. F. Amplifier . . . . .	2-79



LIST OF ILLUSTRATIONS (Cont)

Figure		Page
46.	AGC Amplifiers . . . . .	2-80
47.	Leakage Elimination Filter (Alt. Channel) . . . . .	2-82
48.	Leakage Elimination Filter (Velocity Channels) . . . . .	2-83
49.	L. E. F. Ref. Gen. (Velocity Channel) . . . . .	2-85
50.	Velocity Tracker Schematic . . . . .	2-87
51.	Amplitude and Phase Response . . . . .	2-90
52.	Velocity Tracker . . . . .	2-93
53.	FM/CW Altitude Tracker . . . . .	2-95
54.	FM/CW Altitude Channel Schematic . . . . .	2-96
55.	Alt. Smoothing Loop ( $\emptyset$ Lock) #1 . . . . .	2-101
56.	Phase Lock Loop #2 . . . . .	2-104
57.	Phase Lock Loop #2 Schematic . . . . .	2-108
58.	Received Spectra (ICW) . . . . .	2-112
59.	ICW Tracker . . . . .	2-117
60.	ICW PRF Tracking Loop Schematic . . . . .	2-118
61.	Meter Board . . . . .	2-120
62.	PTDLR Beam Geometry . . . . .	2-122
63.	Control Chassis . . . . .	2-137
64.	Wiring Diagram . . . . .	2-139
65.	B-26 A/C . . . . .	3-3
66.	Helicopter Installation . . . . .	3-7
67.	Helicopter Installation . . . . .	3-8
68.	Dual Antenna Installation . . . . .	3-9
69.	Flight Card . . . . .	3-16

**LIST OF ILLUSTRATIONS (Cont)**

<b>Figure</b>		<b>Page</b>
70.	Processing Improvement . . . . .	4-8
71.	Data Reduction Set-Up . . . . .	4-9
72.	Doppler Spectra . . . . .	4-12
73.	LEF Improvement . . . . .	4-15
74.	Doppler Return vs Terrain Type . . . . .	4-17
75.	Preliminary Data Reduction . . . . .	4-21
76.	Altitude Comparison, Run 15 . . . . .	4-27
77.	Altitude Comparison, Run 16 . . . . .	4-28
78.	Velocity Comparison, Run 15 . . . . .	4-29
79.	Velocity Comparison, Run 16 . . . . .	4-30
80.	FM/CW Velocity Comparison . . . . .	4-31
81.	ICW Velocity Comparison . . . . .	4-32
82.	Proposed PTDLR Transmitter Mechanization . . . . .	5-6
83.	Flat Plate Antenna . . . . .	5-8

## LIST OF TABLES

Table	Page
1. Terminal Descent and Landing Radar Modulation Technique Trade-Offs . . . . .	1-8
2. Performance Characteristics . . . . .	2-13
3. K Band Power Source (Multiplier Amplifier Chain) T-3070 . . . . .	2-37
4. Luneberg Antenna Characteristics . . . . .	2-46
5. Typical Properties of the Composite Luneberg Lens Medium Used by Armstrong Cork Co. . . . .	2-49
6. Sidelobe Improvement . . . . .	2-60
7. FM/CW Altitude Channel Signal Levels . . . . .	2-68
8. FM/CW Velocity Channel Signal Levels ( $J_3$ Worst Case) . . . . .	2-70
9. FM/CW Velocity Channel Signal Levels ( $J_3$ Nominal Case) . . . . .	2-71
10. Pt Mugu Flight Summary . . . . .	3-17
11. PTDLR Tape Data Points - Helicopter . . . . .	4-11



## 1.0 INTRODUCTION AND SUMMARY

Under the authorization of contract NAS1-7696, the Autonetics Division of North American Rockwell has successfully completed a 30-month program to develop, evaluate, and deliver a multiple beam doppler radar system. The objective of the program was to develop and implement a prototype of Autonetics R146 Bi-mode Radar for performance evaluation purposes.

The evaluation model has been designed to provide three-dimensional velocity information over the velocity range of from minus 680 ft/sec through zero to plus 680 ft/sec and simultaneously provide slant range to the ground over an altitude range of from zero feet to 30,000 feet. Considerable flexibility has been incorporated in the design to permit evaluation of system performance in a number of rapidly implemented configurations. These include  $J_1$ ,  $J_2$ , or  $J_3$  Bessel sideband operation with high or low modulation index in a single or dual antenna configuration. Three separate flight test programs have been conducted during the course of this program with the system in a number of different configurations. The flight test vehicle was fully instrumented to permit the recording of a number of pertinent radar signals and flight path geometries. After each flight test program was completed, sufficient data reduction was performed on the flight data tapes to enable evaluation of system performance in the particular modes being tested. Subsequent analysis of the data identified design concept, hardware, and mode changes that should be made to improve overall system performance. The identified changes were then implemented prior to the next flight test program.

The most optimum system configuration from a performance point of view was selected on the last flight test program which was conducted at the Pacific Missile Range (PMR) facility at Pt Mugu, Calif. Ground truth determination of vehicle velocity components and space positioning was provided by two tracking Askania Cameras. The ground truth records are in the form of digital tapes. NASA has implemented a data reduction program using the computer facilities at Langley Research Center (LRC) to establish the ultimate Planetary Terminal Descent and Landing Radar (PTDLR) system accuracy achieved by comparing the PMR tapes with the PTDLR flight test data tapes recorded simultaneously. This effort is required in order to establish quantitative accuracy numbers. A modified B-26 aircraft was used during the first flight test and provided the relatively high altitude (to 12K ft) and high velocity (400 ft/sec) evaluation capability and a Bell Jet Ranger helicopter was used to provide low altitude (zero ft) and low velocity (hover) evaluation capability during the last two flight test programs.

Data reduction activities conducted at Autonetics and at the LRC facilities indicate that high quality altitude and three-dimensional velocity information is produced over all obtainable combinations of altitude and velocity within the performance envelope of the particular flight test vehicles.

The performance of the R146A has generally exceeded the original specifications for velocity and altitude with respect to both scale and accuracy.

Recommended items for future efforts include the following:

- a. Incorporation of a  $K_e$  band circulator to allow for improved single antenna capability. The installation of the filter should allow the

leakage to approach the receiver noise level. A further improvement can be accomplished by utilizing the leakage elimination filters.

- b. A new transmitter utilizing a phase-locked gunn oscillator is recommended. Advantages of this implementation include lower transmitter and L.O. power levels required, greater suppression of unwanted carrier and sideband frequencies, reduced filter requirements, and removal of the transmitter/receiver path length matching problem.
- c. Incorporation of a new, low-cost, lightweight, flat-plate antenna will provide an appropriate size and volume for aircraft, STOL and VTOL applications. The volume contained under the antenna segments may be utilized to house microelectronic circuitry associated with each antenna beam.
- d. The data processing circuitry is a candidate for hybrid thin-film circuitry. Other portions of the circuitry are candidates for hybrid thin film, or microwave integrated-circuit improvements for weight, size and reliability improvements.
- e. Application of MOS technology will allow for an improved tracker. A digital velocity tracker has been developed which provides a high degree of accuracy and has no offset bias error.

It is believed that the flight test results utilizing the evaluation model have demonstrated feasibility of the system. A system utilizing the above recommended improvement should lead to a low-cost combined velocity and altitude flight instrument which would be highly compact, accurate and reliable.

## 1.1 **Mission Requirements**

In order to determine a system configuration and operating parameters, it is necessary to establish the mission requirements that the system is intended to fulfill. The Autonetics R146 radar system was originally formulated to provide three-dimensional velocity and altitude information during the terminal guidance phase of a soft landing instrument capsule on the Martian surface. An extensive tradeoff study was conducted to establish the unique mission requirements for this space probe in order to determine the optimum system configuration. Mechanical restraints, prime power and maximum weight limitations, reliability requirements, terminal landing flight profiles, and a number of other related parameters were considered during the tradeoff phase to arrive at the R146 Bi-mode radar concept as the most suitable configuration.

Although the original design considerations were based on the requirements necessary to provide terminal guidance for an unmanned instrument capsule, there are a number of other applications for a similar device.

For some time a radar has been required to furnish, from the same equipment, a measurement of velocity for navigational purposes and a measurement of absolute altitude above terrain. This requirement has become particularly acute recently because of the increased use of helicopters and light aircraft which require both of these pieces of information. Such a radar may also be required for low-altitude terrain following, for all-weather landing and for certain space applications such as manned lunar landing and satellite rendezvous. All of these vehicles are limited in allowable weight and volume for electronic equipment and antennas.

Airborne Doppler navigation radars of different types have been developed and have found extensive use in both military and civil operations. Also, various types of radar altimeters have been in existence for quite a long time and are in widespread use today. Ever since the advent of Doppler radar systems, the extraction of altitude information from the same equipment looked like an obvious next step, and several attempts



have been made to achieve it. Most of these attempts have been faced with considerable difficulty and have resulted either in the abandonment of the attempt or in the design of an approach which actually represented the inclusion of two separate functions in one equipment, operating on a sequential, time-shared basis. The major reasons for these difficulties are the incompatibilities of certain critical radar parameters to velocity and altitude measurements. Notable among these are the PRF, in pulse systems, and the modulation frequency and/or modulation waveform in FM/CW systems. Specifically, altitude and velocity ambiguities and loss in accuracy have been typical problems in these previous approaches. Also, problems of aircraft attitude excursions (pitch and roll) and associated antenna pattern considerations have represented difficult design problems.

The resultant PTDLR system represents a genuine integration of the velocity measuring and altitude measuring functions in the same equipment, i. e., they stem from the same antenna-receiver-transmitter, in such a manner that both pieces of information are available at the same time, using the same received signal, and almost completely common circuitry. Hence, the approach results in a considerable saving in weight, size and cost. In addition, the particular configuration described is capable of measuring three-dimensional velocity information through zero velocity to negative velocities without loss of sense, (as is required in a helicopter, VTOL aircraft or lunar landing vehicle) and absolute altitude above terrain, both with very high accuracy and down to zero feet altitude.

A velocity and altitude measuring radar for helicopters, light aircraft and VTOL aircraft must be capable of actual operation down to zero

foot altitude, particularly if application of the equipment for all-weather landing is envisioned. The equipment must be capable of three dimensional velocity measurement through zero to negative and of operating under considerable attitude excursions over both land and water. It must have high accuracy of velocity for integration into navigational position information and the altitude accuracy must be high particularly at low altitudes. It must be relatively light and small, have a small antenna and/or small radome cut-out and low primary power consumption, preferably at low DC voltage levels. Finally, it must be very high in reliability and maintainability and low in cost.

## 1.2 Modulation Techniques Trade-off

For coherent radar operation which is required for the three-dimensional velocity and altitude measurement, three possible techniques or combinations thereof are available:

Pure CW for velocity and Linear FM/CW for range

Bessel Sideband FM/CW for both velocity and range

ICW (interrupted CW or Coherent Pulse) for both velocity and range

A summary of the characteristics of each of these techniques is presented in Table 1.

The pure CW (Doppler velocity) and linear FM/CW (altimeter) are the simplest and also the oldest of these techniques. Both techniques have the same electrical performance properties from several viewpoints; namely, transmitter-receiver isolation (leakage characteristics), susceptibility to interference due to reflections from nearby objects and due to vibration, and antenna aperture utilization. Both techniques can be considered equally poor in all these properties. While both techniques appear

on the surface to be attractively simple in design, extreme care must be exercised in practical equipment configurations, to reduce transmitter-receiver leakage levels, problems due to reflections from nearby objects, and vibration problems, including acoustic coupling through any surrounding atmosphere. (Acoustic coupling has been a serious problem in the design of CW radars to be used in the Earth's atmosphere.) It also caused problems in the testing of the lunar landing radars which had to be tested on Earth.

In both the pure CW and linear **FM/CW** techniques, a space-duplexed or dual antenna arrangement is required to reduce transmitter-receiver leakage signals to manageable levels. This represents a waste of the available antenna space, since, effectively, only a portion of the available antenna aperture is used.

From a theoretical point of view, the similarity of pure CW and linear **FM/CW** is evident when one considers that the linear **FM/CW** configuration makes use of the zero-order ( $J_0$ ) Bessel sideband which is exactly the same as the carrier of the pure CW system. Similarly, the basic high altitude performance capabilities of the two systems are usually limited by signal-to-leakage ratios rather than by signal-to-noise ratios. The pure CW technique is capable of Doppler-velocity measurement only and is not capable of ranging. (The linear **FM/CW** technique does, of course, have a ranging capability.)

The Bessel sideband **FM/CW** technique has been used extensively in recent years and combines some of the advantages of CW and pulse techniques. The simplicity of radars using this technique does not depart greatly from that of the CW technique, while the transmitter-receiver

Table 1. Terminal Descent and Landing Radar Modulation Technique Trade-Offs

	Pure CW and Linear FM/CW	Bessel Sideband FM/CW	ICW	Bessel FM/CW/ICW
Efficiency	High (50-100 percent)	Moderate (10-20 percent)	High (50 percent)	Medium-to-High (10-50 percent)
Ranging Capability	Pure CW: Not Capable Linear FM/CW: Capable	Inherently Capable	Inherently Capable	Inherently Capable
Transmitter-Receiver Isolation	Severe Leakage Problem (marginal at 90 db)	Good Isolation (30 db adequate)	Excellent Isolation (transmitter off)	Excellent Isolation (30 db adequate)
Antenna Aperture Utilization	Space Duplexing Requires Twice Antenna Size	Single Antenna Feasible	Single Antenna Feasible	Single Antenna Feasible
Near-In Reflections	Severe Problem	No Problem	No Problem	No Problem
Range Ambiguities at High Altitude and Velocities	Linear FM/CW is Ambiguous Unless Velocity Correction Supplied	Ambiguous Range Information	Unambiguous Range Information	Unambiguous Range Information
High Altitude Performance	Poor	Moderate	Excellent	Excellent
Low Altitude Performance	Excellent	Very Good	Poor	Excellent
Complexity	Low	Moderate	Moderate	Moderate
Weight	Low for Equipment High for Antennas	Low	Moderate	Moderate
Vibration, Microphonics	Severe Problem	No Problem, Sideband is out of Microphonic Spectrum	No Problem	No Problem

isolation properties of this technique are inherently good. The inherent isolation is based on the use of one of the Bessel sidebands other than the zero-order sideband, since all of the other sidebands have the property of resulting in zero signal at zero range, and very small signals at short distances from the antenna. Zero range is equivalent to the basic transmitter-receiver leakage path while typical reflections from nearby objects, such as radome and vehicle structures, represent signals returning from short distances.

The Bessel sideband **FM/CW** technique can also be used for ranging by means of a phase measurement of the selected Bessel sideband with respect to the transmitted modulation phase.

There is, however, a basic limitation in the Bessel sideband **FM/CW** technique for the measurement of velocity and altitude at high altitudes and at high velocities. This limitation has three basic reasons: high altitude range measurement requires low modulation frequencies which leads to incompatible ambiguities in the presence of large Doppler shifts due to high velocity; a single antenna Bessel sideband **FM/CW** system exhibits an ultimate leakage limitation; and, since only a single harmonic sideband is used, the efficiency factor of the Bessel sideband **FM/CW** technique is only moderate, e. g., in the order of -5db for the third order sideband. For these reasons, the **FM/CW** technique does not appear to be attractive for operation at high altitudes and large velocities.

The ICW (Interrupted Continuous Wave, also called high-duty-cycle-coherent-pulse) modulation technique exhibits excellent high altitude performance properties as well as excellent transmitter-receiver isolation characteristics. The excellent high altitude and high velocity performance properties of the ICW technique are based on the following factors:

- a. The efficiency factor of the ICW system is **extremely high**, approaching that of the pure CW technique.
- b. Since the receiver is gated-off while the transmitter is on (and vice versa), **excellent isolation performance results**.
- c. No velocity-range ambiguities exist since the Doppler shift of the carrier is used for velocity measurement and the PRF is used for range measurement.

The ICW modulation, in order to be used at its maximum efficiency, must be operated at 50 percent duty cycle for both transmission and reception. Since the pulse repetition frequency must therefore be changed with changing range, the pulse repetition frequency can be servoed to keep the receiving duty factor at 50% at all times. The value of the PRF then becomes a measure of range. Both the ICW doppler and servoed PRF ranging technique have been successfully demonstrated during the past few years. The greatest limitation of the ICW technique lies in its performance properties at low altitudes above the terrain. Operation at short ranges requires extremely short pulse rise times and presents very difficult gating problems. So-called overlap transmitter-receiver gating has been attempted in order to achieve low altitude operation but has not been very successful since it results, effectively, in quasi-CW operation. The servoed PRF method of range measurement also leads to extremely high pulse repetition rates at short ranges, making the technique impractical or very difficult to implement. For these reasons, the ICW technique does not appear attractive for low altitude operation.

The choice of modulation techniques is dependent upon the maximum range at which the PTDLR is required to perform.

For operation up to 30,000 ft the most suitable configuration is a combination of ICW and Bessel sideband FM/CW, in order to make use of the good high altitude and high velocity performance of the ICW technique and the good low altitude performance of the FM/CW technique. Although it may be theoretically possible to extend either technique to its limit, this is not a desirable or sound engineering approach from the viewpoint of operational reliability and installation tolerances.

Solid-state transmitters such as varactor and step-recovery diode multiplier chains can accommodate both ICW and Bessel sideband FM-CW modulation by simply changing the modulation on the driving oscillator appropriately. This can be accomplished because the Bessel sideband FM/CW technique, in contradistinction to the linear FM/CW technique, uses very narrow-band sinusoidal modulation at low modulation indices and a crystal oscillator can easily be "pulled" for frequency modulation or gated for ICW modulation. Hence, the ICW and Bessel sideband FM/CW modulations can be generated in a completely common transmitter-receiver.

### 1.3 FM/CW Mode Analysis and Design Considerations

Various types of FM/CW altimeters have been developed in the past. The two types in use today can be categorized as (1) frequency measurement and (2) variable frequency deviation.

The frequency measurement type generally uses low frequency, wide deviation and triangular modulation, in such a manner that the difference frequency generated by heterodyning the transmitted and received signals is a function of altitude. The variable frequency deviation type, which is a more recent development, is based on the use of sinusoidal modulation, the

measurement of the amplitude of one or more of the **modulation sidebands** and the variation of the frequency deviation as a function of altitude so as to maintain the modulation index constant.

The frequency measurement method, whose development goes back to before World War II, is plagued by a number of well-known disadvantages, particularly as regards accuracy under certain operational conditions. These disadvantages include errors due to Doppler shifts caused by vertical and horizontal motion of the vehicle, errors due to changes in the modulation waveform and modulation characteristics of the transmitter, and errors caused by incidental modulation noise due to vehicle vibration. They also exhibit a quantization (step) error due to the low deviation frequency used and so-called "false target acquisition" phenomena due to the wide antenna beamwidths used in typical systems. The modulation frequency and deviation required for this type of system are not compatible with the FM/CW Doppler velocity measurement function. The variable frequency deviation system does not have the quantization error problem of the frequency measurement system, but it is sensitive to amplitude and modulation effects, since the modulation index control is generally obtained by measuring amplitude.

If the Fourier spectrum of the signal which is the beat between the transmitted and received signal of the FM/CW radar is carefully analyzed, it is seen, as will be shown in the following section, that the relative phase of each of the sidebands of this signal is a function of the relative delay and, hence, of the altitude of the vehicle. Thus, it is possible to select one of these sidebands and to compare its phase with that of the reference modulation oscillator and thereby obtain a measurement of altitude. This



is based strictly on a measurement of phase and hence is not disturbed by amplitude effects, by changes in modulation waveform or by a change in modulation index. Also, by means of a squaring technique, the theory of which will be described later, the effects of Doppler noise due to vehicle motion can be eliminated.

In summary, an FM/CW phase measuring altimeter technique is selected, which is based on the relative phase measurement of one of the sidebands of the spectrum which is the beat between the transmitted and received signals. The accuracy of the technique is therefore not deteriorated by amplitude or frequency (Doppler) effects. The accuracy of altitude determination is primarily a function of the precision with which the phase measurement can be made; due to the current state-of-the-art, precision of the measurement can be extremely high.

As a result, the FM/CW phase altimeter technique and the FM/CW Doppler technique are found to be completely compatible and, hence, ideally suited for integration into one equipment which provides simultaneous velocity and altitude measurement.

A mathematical treatment of the FM/CW radar under discussion, which will help to give a spectral picture of the signals present in the system, is given in the next section.

### 1.3.1 FM/CW Doppler and Altimeter Radar Theory - General Signal Analysis

If the transmitted signal is a sinusoidally frequency-modulated microwave signal of the form

$$e_1 = E_1 \sin (2\pi f_c t + m \sin 2\pi f_m t),$$

where

$$f_c = \text{transmitted carrier frequency}$$

$m$  = transmitted modulation index

$f_m$  = modulation frequency;

and if the local oscillator signal is of the form

$$e_2 = E_2 \sin [2\pi(f_c + f_{IF}) t + m \sin 2\pi f_m t], \quad (2)$$

where

$f_{IF}$  is the intermediate frequency;

and if the echo signal is of the form

$$e_3 = E_3 \sin [2\pi(f_c + f_d) (t - \tau) + m \sin 2\pi f_m (t - \tau)], \quad (3)$$

where

$f_d$  = Doppler shift frequency due to vehicle motion

$\tau$  = round-trip delay time;

then these three signals will appear at the radar mixer crystal. While the exact crystal law will not affect the results materially, a square law crystal is assumed and an output signal  $e$  of the following form results:

$$\begin{aligned} e &= (e_1 + e_2 + e_3)^2 \\ &= (e_1^2 + e_2^2 + e_3^2 + 2e_1e_2 + 2e_2e_3 + 2e_3e_1). \end{aligned} \quad (4)$$

The first three terms of (4) will generate dc components and signals at twice the carrier frequency, and are therefore not of interest here. The  $2e_1e_2$  term represents the mixture of transmitter leakage and local oscillator signal, and while it is of interest in detailed system design, it is not significant in an explanation of the basic principles of the radar under discussion. The  $2e_1e_3$  term is of importance in non-IF FM/CW radar systems, where sense of velocity motion is lost; but it is not of importance here, since the resultant signal is in too low a frequency range to be passed by the IF amplifier.

This leaves the  $2e_2e_3$  term as the only one to be considered here. Thus, we have (dropping the factor 2)

$$e_2e_3 = E_2E_3 \sin [2\pi(f_c + f_{IF}) t + m \sin 2\pi f_m t] \sin [2\pi(f_c + f_d) (t + \tau) + m \sin 2\pi f_m (t - \tau)]. \quad (5)$$

This trigonometric expression will give two terms, the second one of which is at twice the carrier frequency and is therefore rejected. The only remaining term of interest has the form

$$\left\{ \frac{E_2E_3}{2} \cos [2\pi(f_{IF} - f_d) t + 2\pi(f_c + f_d) \tau + \left( 2m \sin 2\pi f_m \frac{\tau}{2} \right) \cos 2\pi f_m \left( t - \frac{\tau}{2} \right)] \right\} \quad (6)$$

This signal is at the intermediate frequency  $f_{IF}$  and is a frequency-modulated signal, which is modulated at frequency  $f_m$  and with a modulation index  $M = 2m \sin [2 f_m (\tau/2)]$ .

In (6), the term  $2\pi(f_c + f_d)\tau$  is an RF phase term which is of no particular interest here and which will continue to be neglected. If (6) is now expanded, using the well-known Bessel identities (6)

$$\begin{aligned} \cos (x \cos y) &= J_0(x) - 2J_2(x) \cos 2y \\ &\quad + 2J_4(x) \cos 4y - \dots \end{aligned}$$

$$\sin (x \cos y) = 2J_1(x) \cos y - 2J_3(x) \cos 3y + \dots$$

the following expression results:

$$\begin{aligned} \cos [2\pi(f_{IF} - f_d) t] &[J_0(2m \sin 2\pi f_m \frac{\tau}{2}) \\ &- 2J_2(2m \sin 2\pi f_m \frac{\tau}{2}) \cos 4\pi f_m (t - \frac{\tau}{2}) + \dots ] \\ &+ \sin [2\pi(f_{IF} - f_d) t] [2J_1(2m \sin 2\pi f_m \frac{\tau}{2}) \\ &\quad \cos 2\pi f_m (t - \frac{\tau}{2}) - \dots ] \end{aligned} \quad (7)$$

Further mathematical manipulation and substitution of  $M = 2m \sin [2\pi f_m T/2]$  results in a series of sidebands centered at frequency  $f_{IF} - f_d$ , as follows:

$$\begin{aligned}
 & J_0(M) \cos 2\pi(f_{IF} - f_d)t \\
 & - J_1(M) \sin 2\pi[(f_{IF} - f_d)t + f_m(t - \frac{T}{2})] \\
 & - J_1(M) \sin 2\pi[(f_{IF} - f_d)t - f_m(t - \frac{T}{2})] \\
 & - J_2(M) \cos 2\pi[(f_{IF} - f_d)t - 2f_m(t - \frac{T}{2})] \\
 & - J_2(M) \cos 2\pi[(f_{IF} - f_d)t + 2f_m(t - \frac{T}{2})] + \dots \quad (8)
 \end{aligned}$$

Spectral representations of the transmitted signal, received signal, local oscillator signal and the signal at the intermediate frequencies are shown in Figures 1 - 5. Figure 4, for example, is a graphical representation of (8).

### 1.3.2 Velocity Measurement

It will be noted that the two received spectra in Figures 2 and 4 are shown with the harmonic sidebands Doppler-shifted by a frequency  $f_d$  due to aircraft motion. Also they are not pure line frequencies, but, rather, have a finite width and a roughly Gaussian, noise-like shape associated with them. This is due to the finite beamwidth of the antenna and the random, noise-like nature of the back-scattering phenomenon.

Also, it is important to note that for a helicopter system, in which negative speeds are to be measured with proper sense, an intermediate frequency  $f_{IF}$  must be used in order to prevent fold-over about  $f_c$  and the resulting loss of sense. Furthermore, additional heterodyning is permitted, but an offset frequency, such as  $f_{IF2}$  in Figure 5, must be maintained all the way down to the frequency measuring (tracking) circuits in order not to lose the sense of direction of motion. Previously developed

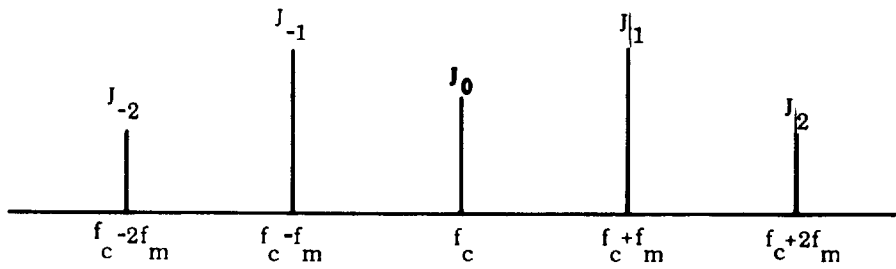


Figure 1. Transmitted Spectrum

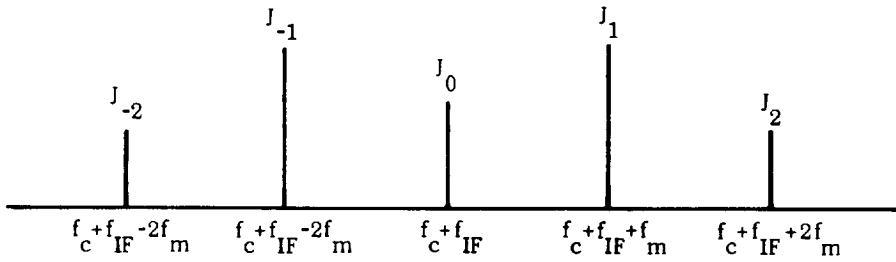


Figure 2. Local Oscillator

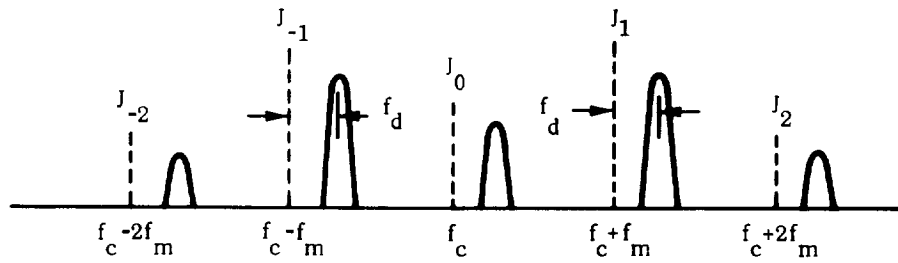


Figure 3. Received Spectrum

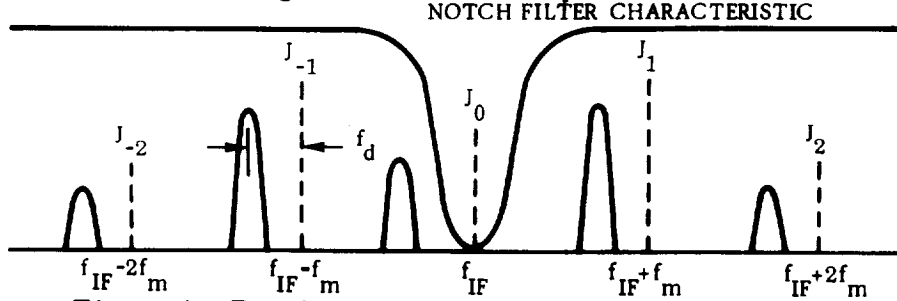


Figure 4. Received Spectrum at Intermediate Frequency

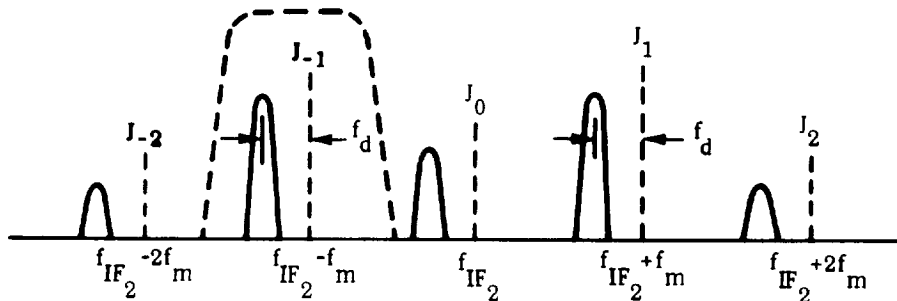


Figure 5. Received Spectrum at Second Intermediate Frequency

FM/CW Doppler systems have permitted such "folding" about zero frequency somewhere in the system, thereby losing this sense information.

As regards velocity measurement, it is seen from (7) and (8) and Figures 4 and 5 that it is merely necessary to filter out the desired sideband at frequency  $f_{IF} + nf_m$ , where  $n$  is the sideband order, or at the second intermediate frequency  $f_{IF_2} + nf_m$ ; and to feed the resulting signal to a frequency tracking circuit [1], [3], [5] which will measure the average displacement or center of area of the  $f_d$  spectrum with respect to a reference frequency.

This average Doppler frequency displacement  $f_d$  will then be a measure of the vehicle's velocity component along the antenna beams by virtue of the well-known Doppler equation

$$f_d = \frac{2V}{\lambda} \cos \phi \quad (9)$$

where

$V$  is the velocity of the vehicle

$\lambda$  is the transmitted wavelength

$\phi$  is the angle between the velocity vector and the beam center of radiation.

If three noncoplanar symmetrical antenna beams are used, then for a pitch and roll stabilized antenna, the three orthogonal velocity components  $V_x$  (heading velocity),  $V_y$  (drift velocity) and  $V_z$  (vertical velocity) can be obtained as a function of the three doppler frequencies  $D_1$ ,  $D_2$  and  $D_3$ : (A detailed derivation can be found in section 2.4.12).

$$V_x = K_x (D_1 - D_2) \quad (10)$$

$$V_y = K_y (D_4 - D_1) \quad (11)$$

$$V_z = K_z (D_2 + D_4) \quad (12)$$

where  $K_x$ ,  $K_y$  and  $K_z$  are constants containing the transmitted wavelength and beam look angles for the beam configuration shown in Figure 6.

Specifically

$$K_x = \frac{\lambda}{4 \cos \theta \sin \gamma} \quad (13)$$

$$K_y = \frac{\lambda}{4 \sin \theta \sin \gamma} \quad (14)$$

$$K_z = \frac{\lambda}{4 \cos \gamma} \quad (15)$$

where

$\alpha$  = depression angle complement of antenna beams

$\theta$  = projected azimuth angle of antenna beams

### 1.3.3 Altitude Measurement

As regards the altitude measuring technique, reference is again made to (7) and (8) and Figures 4 and 5. It will be noted from (7) and (8) that the phase of each of the sidebands of the received spectrum is a function of the round trip delay time  $\tau$  and, hence, of the range to the ground. Specifically, it is seen that the phase of each of the received sidebands is  $n2\pi f_m \tau/2$ , where  $n$  is the order of the sideband. Hence one might select one of the sidebands and compare its phase with that of the transmitter modulation oscillator. Such a comparison would then eventually appear to yield an angle equivalent to  $\tau/2$  so that the range to the ground  $r$  is given by

$$r = \frac{\tau c}{2} \quad (16)$$

where  $c$  is the velocity of light.

Absolute altitude would then appear to be obtainable by relating range to altitude by the cosine of the beam incidence angle,  $\psi$ ; namely,

$$h = r \cos \psi. \quad (17)$$

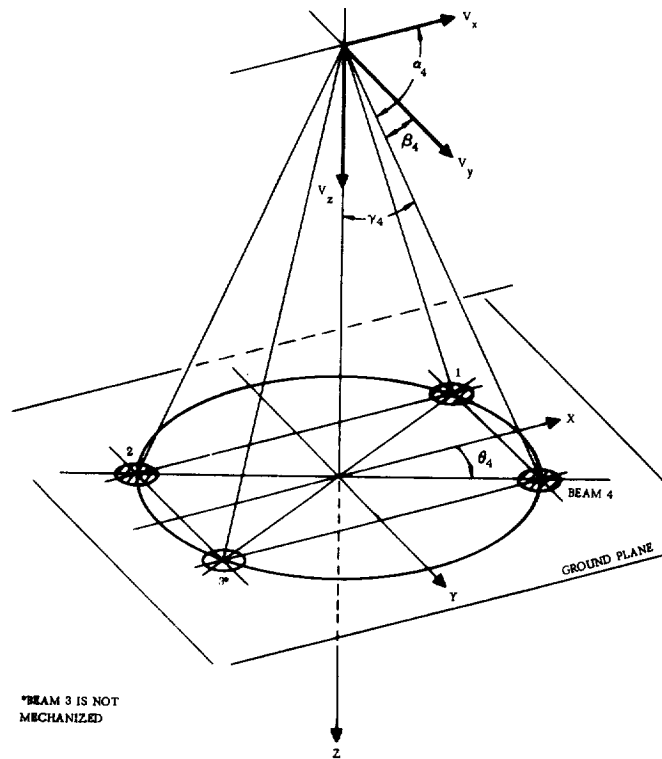


Figure 6. System Beam Configuration

There is one difficulty with this, however: the received signal sidebands are not located at  $f_m$ ,  $2f_m$ , etc., but rather are Doppler-shifted by  $f_d$  due to the motion of the vehicle. This is shown mathematically in (8) by the terms  $\sin 2\pi ([f_{IF} - f_d] t + f_m (t - (\tau/2)))$ , etc., and graphically by the spectral representations in Figures 4 and 5.

A technique has been developed, however, which not only circumvents this problem but also eliminates the fluctuation noise on the altitude information, which is associated with the received signal due to the noise-like nature of the Doppler-shifted signal. The process can best be explained by reference to Figures 4, 7, 8 and 9. In order to place the signals into the frequency regions of  $nf_m$ , it is necessary to use both the sidebands of whatever order is selected. For this purpose the received spectrum needs to be folded about its center. This is contrary to the Doppler velocity



measurement where no folding was permitted. Of course, in the case of altitude measurement, the problem of loss of sense does not exist. The folding process is accomplished by heterodyning the spectrum of Figure 4, which is centered at  $f_{IF}$ , with a signal of frequency  $f_{IF}$ . The resulting signal is a spectrum at dc, as shown in Figure 7. This  $J_1$  pair is shown after filtering in Figure 8. It should now be noted from Figure 8 that although the two spectra of the pair are noise-like in character, they are coherent with respect to one another, since they originated from the same signal at the same time. Furthermore, due to the folding process, the two spectra are a mirror-image pair, located symmetrically on either side of  $f_m$ , each at an average distance of  $f_d$ . This signal can also be regarded as a double-sideband suppressed carrier signal, with frequency  $f_m$  being the carrier and the  $\pm f_d$  spectra the sidebands. If this signal is fed to a square law, frequency doubling device, it can be shown mathematically (and graphically from Figure 8) that the squaring process will essentially reconstruct a narrow "carrier" spike, located at  $2f_m$ . Let us illustrate this with the two unsymmetrical but coherent mirror-image spectra of Figure 8. At the output of the square law doubler, the sum of the signals at  $f_b$  and  $f_b'$  will lie at  $2f_m$ , the sum of the signals at  $f_a$  and  $f_a'$  will also lie at  $2f_m$ , and so on. Hence, squaring of the signal will reconstruct a carrier spike at  $2f_m$ . This is shown graphically in Figure 9.

Since this signal is essentially a narrow frequency spike, the noise-like character of the signal before squaring, as shown in Figure 8, has essentially been removed; i. e., the Doppler fluctuation noise of the signal has been eliminated. The phase of this signal (located at  $2f_m$ ) need now only be compared with the reference phase of the frequency-doubled

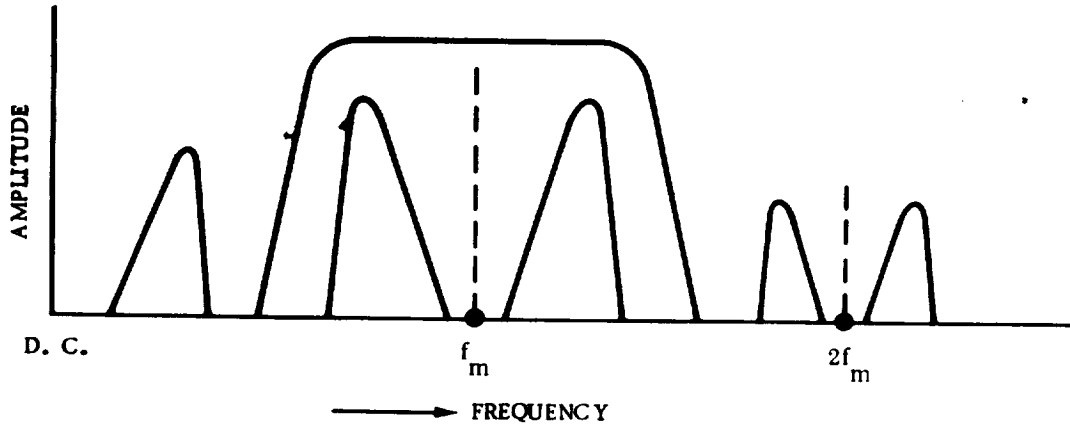


Figure 7. Altimeter Signal After Frequency Fold-Over

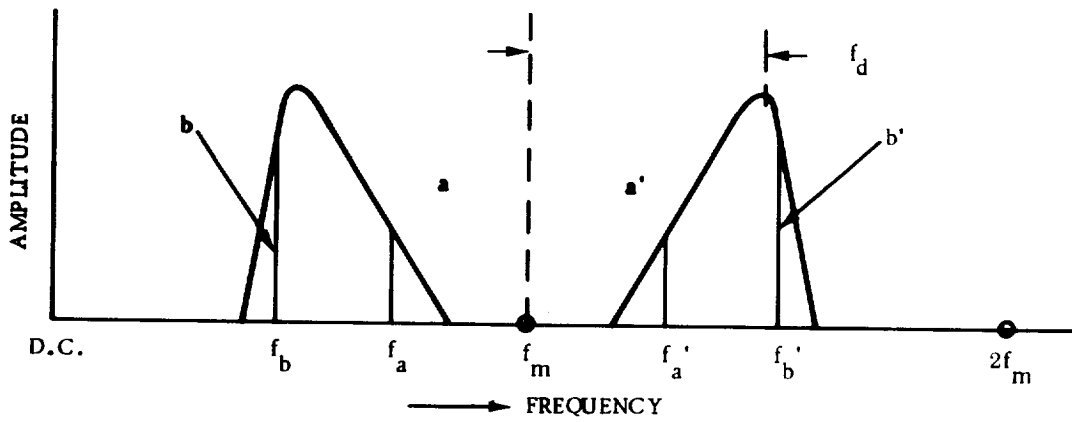


Figure 8. Altimeter Signal After Filtering

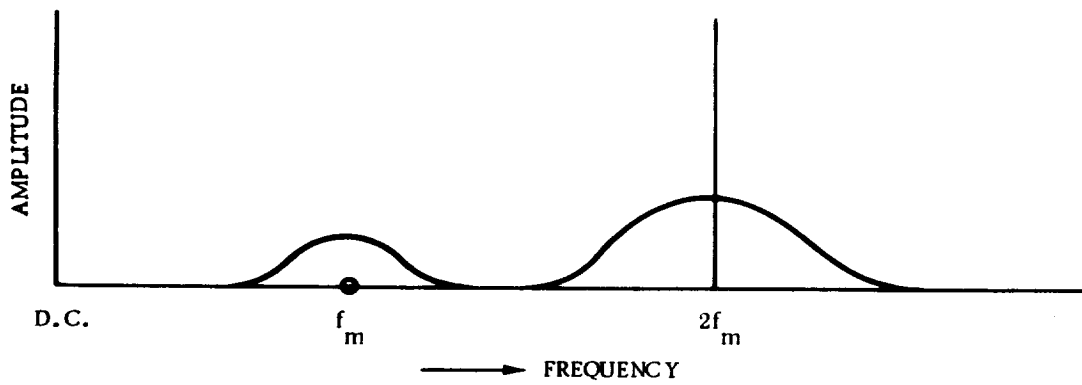


Figure 9. Altimeter Signal After Squaring

transmitter modulation signal (located at  $2f_m$ ) in order to make the altitude measurement in accordance with the theory described earlier. The process of reconstructing the "carrier" spike also affords the opportunity for additional narrow-banding which is advantageous from a signal-to-noise ratio viewpoint.

#### 1.3.4 Signal-to-Noise Ratio Characteristics

It can be shown starting with the well-known radar range equation, that the signal-to-noise ratio of a radar operating against a beam-filling target, such as the earth, can be expressed as:

$$\frac{S}{N} = \frac{P_t G_o \omega \lambda^2 \sigma_o LE}{16\pi^2 \cos^2 \psi r^2 NF KTB} \quad (18)$$

where

$S/N$  = signal-to-noise ratio in the bandwidth  $B$

$P_t$  = average transmitted power

$G_o$  = maximum antenna gain

$\omega$  = antenna pattern factor (accounting for the loss of power outside the main lobe 3-db limits), normally near 0.6

$\lambda$  = transmitted wavelength

$\sigma_o$  = Back-scattering across section per unit area of the scattering surface

$r$  = range to the scattering surface

$\psi$  = beam incidence angle

$NF$  = receiver noise figure

$K$  = Boltzmann's constant

$T$  = absolute temperature

$B$  = bandwidth (approximately equal to the Doppler spectrum width in the velocity function and less in the altimeter function)

**L = system RF losses**

**E = efficiency factor of modulation process.**

For an FM/CW system using the information in one of the sidebands the efficiency factor E is

$$E = J_n^2(M) \quad (19)$$

where n = sideband order.

This can be shown from the well-known identity

$$J_0^2(M) + J_1^2(M) + J_{-1}^2(M) + J_2^2(M) + J_{-2}^2(M) + \dots = 1. \quad (20)$$

The received modulation index M was previously shown to be

$$M = 2m \sin\left(2\pi f_m \frac{\tau}{2}\right). \quad (21)$$

From an examination of a table or curves of Bessel functions and of (21), it is seen that the efficiency factor E, and hence the resulting signal-to-noise ratio, will behave quite differently for different Bessel sidebands and is a function of the transmitted modulation index m, the modulation frequency  $f_m$  and the round trip delay time,  $\tau$ . Specifically, for sidebands other than the zero<sup>th</sup> order ( $J_0$ ), the signal will go to zero for a round trip delay time (and hence range) of zero. Also, due to the periodic nature of the sine function, the signal will again go to zero periodically at distances such that

$$2 f_m \frac{\tau}{2} = n \quad (22)$$

where n = 1, 2, 3, etc.; or when

$$r = n \frac{\lambda_m}{2} \quad (23)$$

where  $\lambda_m$  is the modulation wavelength.

As a result of the above, certain critical parameters, such as the sideband order, the transmitted modulation index m and the modulation frequency  $f_m$  must be carefully chosen, as a function of the system operational requirements. This is the subject of the next section.

### 1.3.5 Choice of Critical Parameters

Before a trade-off on the critical system parameters can be made, the system's operational requirements such as maximum speed, altitude, etc., must first be clearly established. Since the radar under discussion was primarily intended for space applications and for helicopters, VTOL aircraft and light aircraft, the maximum operating altitude was selected to be 30,000 feet and the maximum speed to be 350 knots, with radar operation required through hovering. In view of the nature of helicopter operation a very important requirement for the system was performance down to zero feet altitude and, in view of hovering and VTOL operations, the absence of any signal altitude holes.

#### 1.3.5.1 Bessel Sideband

One of the primary reasons for selection of an FM/CW Doppler system over a pure CW system is the much greater transmitter-receiver isolation and discrimination against echos from nearby objects which is afforded by the FM/CW system. This results because at and near zero relative delay between the local oscillator and received signal, in the case, for instance, of leakage signals, the received modulation index  $M$ , and hence the amplitude of all of the sidebands except the zero<sup>th</sup> order, go to zero. This was first shown by Glegg, (ref) and is demonstrated in Figure 10, which is a sketch of several Bessel functions of small argument. Since it is not true for  $J_0$ , this sideband is immediately ruled out for use in the system.

Ref: K. C. Glegg, "A low noise CW-Doppler technique" Proc. Nat'l Conf. on Aeronautical electronics, Dayton, Ohio pp 133-144 1958

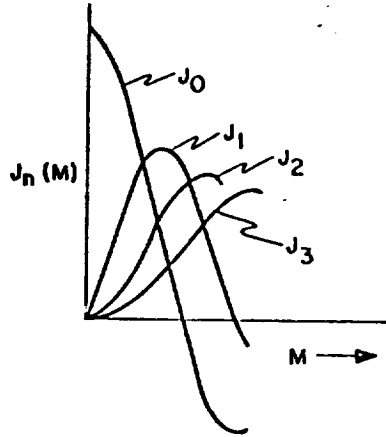


Figure 10. Bessel Functions for Small Arguments

Radar operation down to zero feet altitude virtually dictates the use of the first ( $J_1$ ) Bessel sideband for a narrow-beam system. This can be seen from an examination of the behavior of the various Bessel functions and the basic signal-to-noise ratio expression given by (18). In particular, the Taylor series expansion of the  $J_1(M)$  function is as follows:

$$J_1(M) = \frac{M}{2} \left[ 1 - \frac{M^2}{(2)^2(2)(1)} + \frac{M^4}{(2)^4(2)(3)(2)} - \frac{M^6}{(2)^6(2)(3)(4)(6)} + \dots \right] \quad (24)$$

From (21), we have

$$M = 2m \sin \left( 2\pi f_m \frac{T}{2} \right).$$

However, for small arguments,  $\sin x = x$ ; therefore, by combining (16), (21) and (23), we obtain

$$M = \frac{4\pi m}{\lambda m} r = Kr \quad (25)$$

where  $K$  is a constant for any particular system.

When  $M$  is small,  $J_1(M)$  is essentially equal to the first term of (24).

By combining (24) and (25) we get

$$J_1(M) = \frac{K}{2} r = K_1 r \quad (26)$$

or

$$J_1^2(M) = K_1^2 r^2 = K_2 r^2 \quad (27)$$

where  $K_1$  and  $K_2$  are constants.

Further, it will be noted from (18) that, for a particular radar, and a particular scattering coefficient  $\sigma_0$ , the signal-to-noise ratio can be expressed as

$$\frac{S}{N} = \frac{K_3 E}{r^2} \quad (28)$$

where  $K_3$  is a constant.

However, by virtue of (20),  $E$  was shown to be  $J_1^2(M)$ , which by virtue of (27) was also shown to be  $K_2 r^2$ . Hence, for small values of range  $r$ , the  $S/N$  is shown to be constant with range, or

$$\frac{S}{N} = K_3 K_2. \quad (29)$$

In other words, for the low-altitude region, the  $J_1$  Bessel function curve just compensates the inverse-square-law range versus signal curve of a beam-filling target type of FM/CW radar. This can also be seen graphically by examination of the  $J_1^2$  Bessel function curve for small arguments as shown in Figure 11, and that of the  $1/r^2$  curve shown in Figure 12. The product of the two curves (addition in the log domain) gives the resultant signal-to-noise ratio curve for a  $J_1$  FM/CW radar of this type, which is shown in Figure 13. The lower range region of the curve is seen to be flat as predicted by (29). Examination of the Taylor series or the shapes for the other Bessel sidebands, as shown in Figure 10, reveals that the  $J_1$  sidebands is the only one which has this desirable behavior in the low-altitude region.

For the signal versus range law within the system structure, i. e., from the antenna to the mixer crystal, the inverse square law no longer applies and only the  $J_1$  Bessel function law is applicable. This indicates that for near-zero relative delay between the local oscillator signal and

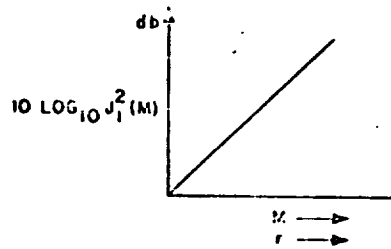


Figure 11.  $J_1^2(M)$  Function for Small Arguments

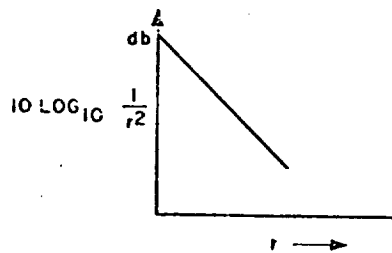


Figure 12.  $1/r^2$  Function for Small  $r$

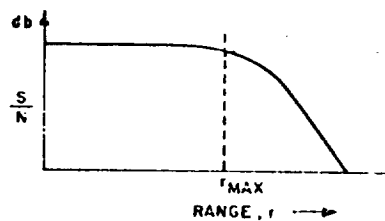


Figure 13. Signal-to-Noise Ratio vs Range for  $J_1$  FM/CW System

any leakage signal, the resulting output is near zero, providing good discrimination against such leakage signals. To the degree to which the leakage and local oscillator paths are not equal and due to reflections from



discontinuities such as antenna terminals, some amount of leakage signal will unavoidably get into the receiver. Also, if a klystron is used, some unavoidable AM may be present due to the shape of the klystron mode. These leakage and AM signals will be in the form of non-Doppler-shifted signals at  $J_1$  and  $J_{-1}$  frequencies. In order to eliminate these, some type of notch filter at these frequencies must be employed; this was done in the system under discussion, as will be shown in a later section. However, if a varactor multiplier power source is used, the incidental AM problems as well as any noise leakage problems should be greatly reduced or completely eliminated. **Theoretical analysis and experimental data have** shown that under certain conditions of microwave structure configuration a  $J_1$  sideband system can result in a larger residual leakage signal into the receiver than is desirable from a practical system viewpoint. Under these circumstances, it can be shown that use of the  $J_2$  or even the  $J_3$  sideband may represent a better compromise between residual leakage level and low altitude performance. It is clear from the previous development that there is no fundamental difference in the system approach, regardless of which particular sideband is used. The FM/CW radar technique affords the designer a very desirable flexibility in this respect.

The PTDLR system has been designed to permit rapid evaluation of performance obtained in three different sideband modes ( $J_1$ ,  $J_2$ , or  $J_3$ ), switch selected by front panel controls.

#### 1.3.5.2 Modulation Frequency

The choice of modulation frequency is dictated by a trade-off which is based on the maximum altitude of operation, the maximum speed of operation and the required accuracy of the altimeter function. Specifically,

the modulation frequency must be sufficiently low so that the maximum range  $r_{\max}$  is well below the range at which the SNR goes to zero, as indicated by Figure 13. It can be shown from (21), (22) and (23) that  $f_m$  must be in the region

$$\frac{c}{4r_{\max}} < f_m < \frac{c}{2r_{\max}}, \quad (30)$$

and preferably closer to

$$\frac{c}{4r_{\max}} = \frac{c}{4h_{\max} \sec \psi}.$$

Also, it can be shown that the altimeter function requires that for unambiguous altitude measurement at the maximum altitude of interest, the maximum modulation frequency is determined by

$$|f_m|_{\max} < \frac{c}{n2r_{\max}}.$$

This is seen from the fact that for unambiguous altitude measurement the maximum phase angle of the doubled modulation frequency ( $2f_m$ ) must be less than 360 deg or  $2\pi$ . From the previous development and (7) and (16), this implies that

$$2\pi > \frac{n \cdot 2 \cdot 2\pi f_m}{2} = \frac{n \cdot 2 \cdot 2\pi f_m \cdot 2r_{\max}}{2c}$$

or

$$2\pi > \frac{n4\pi f_m r_{\max}}{c} \quad (31)$$

or

$$|f_m|_{\max} < \frac{c}{n2r_{\max}} \quad (32)$$

For  $n = 1$ , (32) becomes

$$|f_m|_{\max} < \frac{c}{2r_{\max}} = \frac{c}{2h_{\max} \sec \psi}. \quad (33)$$

It is seen that (33) is quite compatible with the earlier criterion of (30). In fact, in the case of certain phase measurement techniques, it is necessary or desirable to keep the maximum phase angle below  $\pi$ , rather than  $2\pi$ . In this case (33) becomes

$$|f_m|_{\max} = \frac{c}{4r_{\max}} = \frac{c}{4h_{\max} \sec \psi} \quad (34)$$

which is exactly compatible with (30).

Unless special techniques are used, the maximum speed also places a restriction on the modulation frequency, as can be seen by reference to Figures 4 and 5. In order to avoid spectral overlap of adjacent sidebands, the minimum modulation frequency is given by

$$|f_m|_{\min} = 2 |f_d|_{\max} \quad (35)$$

where  $f_d$  is the maximum Doppler shift in a beam; this is found from (9) as

$$|f_d|_{\max} = \frac{2V_{\max}}{\lambda} \cos \phi \quad (36)$$

Hence (35) becomes

$$|f_m|_{\min} = \frac{4V_{\max}}{\lambda} \cos \phi \quad (37)$$

There is one other factor which determines the desired modulation frequency; namely, absolute altitude accuracy. This can be seen by noting from (7) that, for a  $J_1$  system, the maximum phase-angle range (after doubling) of the phase measuring device is given by

$$\Phi_{\max} = 2\pi f_m \tau_{\max} \quad (38)$$

Assuming criterion (34) to hold, and substituting (34) and (16) into (38) considering  $r = r_{\max}$  and  $\tau = \tau_{\max}$ , we have the condition for

$$\Phi_{\max} = \pi \text{ maximum accuracy.} \quad (39)$$

### 1.3.5.3 Transmitter Modulation Index

The choice of transmitter modulation index  $m$  primarily affects the resulting signal-to-noise ratio at various altitudes. If the largest possible signal-to-noise ratio is desired at the maximum design range  $r_{\max}$  then the required modulation index  $m$  is given by (21) and the maximum value for the particular order of Bessel function of argument  $M$ . If (34) and (16) are substituted into (21), (21) can be rewritten as

$$M_o = 2m \sin \left( \frac{\pi}{M} \frac{r}{r_{\max}} \right) \text{ for } m \geq 2 \quad (40)$$

$$M_p = 2m \sin \left( \frac{\pi}{M} \frac{r}{r_{\max}} \right) \text{ for } m = 1$$

Then, from (17) and (18), it is seen that the signal-to-noise ratio is a function of  $J_n(M)$ . Thus, if the highest signal-to-noise ratio is desired at the maximum design range  $r_{\max}$ , (40) becomes

$$M_o = 2m \text{ for } J_2 \quad (41)$$

$$M_o = \sqrt{3}m \text{ for } J_3 \quad (42)$$

$$M_p = 2m \text{ for } J_1 \quad (43)$$

The optimum modulation index can be determined from a table of Bessel functions and it is seen that for  $J_1(M_p)$ :  $M_p = 1.84$ ; for  $J_2(M_o)$ :  $M_o = 5.14$ ; and for  $J_3(M_o)$ :  $M_o = 6.38$ . The transmitted modulation index,  $m$ , therefore should be 0.92, 2.568, and 3.69 respectively. These are the values selected for the system under discussion. In addition, a switch has been incorporated to increase the modulation index by a factor of two to provide improved S/N ratios at low altitudes. The improvement is 6, 12, and 18 DB for  $J_1$ ,  $J_2$  and  $J_3$  respectively.

#### 1.3.5.4 Frequency of Transmission

The two authorized frequencies for Doppler radar are 8.8 GHz and 13.350 GHz (actually a band of 13.25 to 13.4 GHz), the latter generally being preferred for recent military applications. The higher frequency has the advantage of permitting the generation of narrower beamwidths for the same antenna aperture, with a resulting improvement in over-water accuracy and only negligible change in weather performance. Also, microwave components are smaller at the higher frequency. Use of 13.350 GHz for the system under discussion has a pronounced advantage for the absolute altitude function, as contrasted to the frequencies used for conventional altimeters; namely, 1.6 GHz and 4.3 GHz. Based on available data, the 13.350 GHz frequency should provide greatly improved performance over ice and snow since the ice and snow penetration problems, which have been reported for the lower frequencies, should be largely eliminated at 13.350 GHz. Also, the narrow beams of the system should avoid the false target acquisition problems which have been troublesome in connection with the use of conventional wide-beam FM/CW altimeters for such applications as aircraft carrier landing operations.

#### 1.3.5.5 Type of Transmitter Source

One obvious choice of transmitter source for this system is a low-power klystron. However, a better choice appears to be a varactor multiplier microwave source. Such sources have recently become available and, as a result of the increase in efficiencies achieved with varactor diodes in frequency multiplication, power outputs of 1 - 2 watts at 13.350 GHz are now achievable. The unique advantages of these sources include their all-solid-state design, which results in the realization of a truly all-solid state radar, having unprecedented reliability, their excellent frequency stability (1 part in  $10^6$  is achievable), their low noise power spectral density and their low primary power supply voltage requirement. In contrast to lower-power klystrons, which usually require 300 to 1000 V, the varactor multiplier sources generally operate from 28 Vdc. In view of the high signal efficiency of the radar technique under discussion, the use of a varactor source furnishing 100 mw becomes feasible.

#### 1.3.5.6 Type of Antenna Stabilization

It is well known that in Doppler radars, aircraft pitch and roll can be dealt with either by physical antenna stabilization or by so-called data stabilization; i. e., correction of the data by means of pitch and roll signals. If good system performance during operation over water is required, a physically stabilized antenna is preferred. This is so because of the large change in scattering coefficient of water for changes in incident angle. This effect not only greatly reduces the signal available with fixed antenna systems under pitch and roll conditions over smooth water, but it also reduces their accuracy performance in view of the different over-water calibration shifts experienced by each antenna.

The altimeter function of the system also has increased accuracy when the antenna is physically stabilized, in contrast to when it is data-corrected. The scattering behavior over water is identical to that for the Doppler function mentioned. Also, a high altimeter accuracy requirement favors the stabilized antenna since unsymmetrical range-weighting of the antenna beams is avoided.

For space applications requiring terminal guidance equipment to effect soft landings, physical antenna stabilization is highly undesirable because of environmental considerations. The use of data stabilization then becomes mandatory. The PTDLR system therefore incorporates a fixed antenna configuration.





## 2.0 EQUIPMENT DESCRIPTION

### 2.1 Functional Description

The flight evaluation model of the Planetary Terminal Descent and Landing Radar, Autonetics Model R146A, is a combined velocity and range measurement radar. It uses a dual modulation technique, employing ICW for both velocity and range measurements at high altitudes, and Bessel sideband FM/CW modulation for velocity and range measurements at low altitudes. As a result of information gained on the three subsequent flight test programs, the system configuration has undergone a series of modifications. The reasons for the modifications and the chronological order of their occurrence is contained in Section 3.

The original system utilized a lightweight Luneberg lens, fed by multiple horn feeds near its surface, which generated 3 non-coplanar velocity beams at an incidence angle of 15 deg. A fourth range (or altimeter) beam was pointed directly downward. This antenna was replaced with dual constant K antennas later in the program.

When operating in the FM/CW mode, the system was initially designed to utilize the  $J_3$  Bessel sideband only but was subsequently modified to permit operation of the  $J_1$  and  $J_2$  Bessel sideband modes as well.

A description of the final Bimode system configuration is best given with reference to the simplified block diagram shown in Figure 14. The FM/CW mode will be discussed first.

The varactor multiplier power source is frequency modulated by means of the 378 KHz ( $J_1$ ), 189 KHz ( $J_2$ ), or 126 KHz ( $J_3$ ) modulation oscillator signals generated in the master frequency generator (MFG)

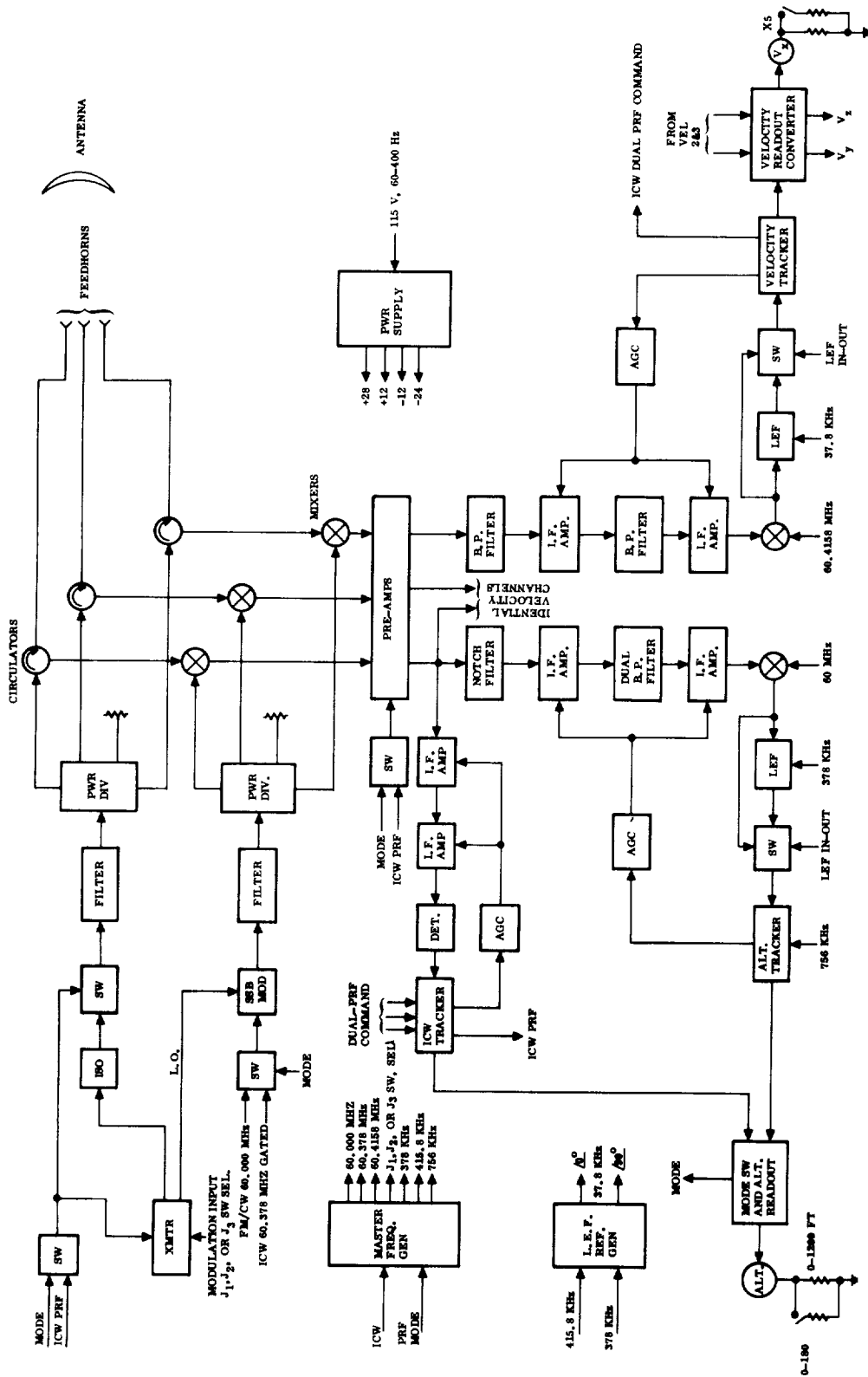


Figure 14. PTDLR Block Diagram

and switch selected from the control panel. The frequency modulated transmitter output is fed through an isolator, "pin" diode microwave switch (in the "on" position for this mode), a microwave filter and a four-way power divider. The signal then branches into three paths (originally four) containing individual circulators and arrives at the antenna feedhorns and is then radiated. The feedhorns share a common aperture and are positioned to provide the desired beam splay and clock angles. The signal is backscattered by the ground, received by the same antenna, and fed through the circulators to the balanced crystal mixers. The second output port on the transmitter contains a signal that is identical in all respects (including frequency modulation) to the main transmitter output but is at a lower power level. This signal is fed to a single-sideband modulator (SSB) which receives its other input from the 60 MHz or 60.378 MHz source contained in the MFG. This input frequency is 60 MHz in the FM/CW mode and 60.378 MHz in the ICW mode. The SSB output is an FM spectrum identical to the transmitted spectrum but centered 60 MHz above the transmitted frequency. This signal is fed through a waveguide filter (to remove the spurious sidebands), a four way power divider, and is then used as the local oscillator (L.O.) drive for the balanced signal mixers. The output of the signal mixers includes a signal located in the 60 MHz region and is amplified in the 60 MHz preamplifier. Since the transmitted signal (hence any leakage signal), and the L.O. signal are frequency modulated at a difference frequency of 60 MHz, a large 60 MHz spike will appear at the output of the preamplifier. Careful design of the preamplifier must be employed to insure that saturation does not occur. Subsequent amplification and processing of

the velocity information is identical and independent in each of the three velocity channels so that only one channel will be discussed. The preamplifier output contains the previously mentioned  $J_0$  spike and a number of sidebands occurring at multiples of the modulation frequency. The narrow band postamplifier chain is centered at 60.378 MHz and provides approximately 130 db gain for the desired sideband and filters out the unwanted sidebands and the  $J_0$  spikes. The postamplifier output signal (nominally  $60.378 \pm f_d$ ) is fed to mixer and is down converted to  $37.8 \text{ KHz} \pm f_d$ . The 60.4158 MHz mixer reference is produced by a crystal oscillator contained in the MFG. The received signal, now centered  $37.8 \text{ KHz} \pm f_d$  is fed to the velocity tracker either directly or through the Leakage Elimination Filter (LEF) as a function of a control panel selector switch. This filter rejects any non-Doppler-shifted leakage signal located exactly at the sideband frequency. This is accomplished by heterodyning down to dc in two channels, using two switching signals at the same frequency which are in quadrature with one another, by ac coupling; remodulating by quadrature signals and then recombining. This technique rejects the leakage signal by converting it to dc and maintains single-sideband operation after remodulation by means of the quadrature phase relationship in the two channels. It can be shown that, with certain designs, the notch filter bandwidth can be made as small as one pleases, in order to permit system operation during hovering. The output of this circuit is the original Doppler spectrum, minus any non-doppler shifted leakage, located at a convenient offset frequency (37.8 KHz) representing the positive or negative velocity components contained in the individual antenna beam.

The signal level at the input to the frequency tracker is sensed by the Automatic Gain Control (AGC) circuitry and is maintained at a relatively constant level by feedback adjustment of the postamplifier gain. It is the purpose of the velocity tracker to determine the single frequency which represents the center of area of this spectrum for each beam. In the system under discussion a so-called sine-cosine frequency tracker was used, a detailed discussion of which is given in a later section of this report. Functionally, it is a closed-loop discriminator which controls the frequency of a local oscillator which represents the beam Doppler shift,  $f_d$ . In order to obtain the three orthogonal vehicle velocity components,  $V_x$ ,  $V_y$  and  $V_z$  the three beam Doppler shifts are combined. This so-called Janus mixing makes the velocity accuracy highly insensitive to errors in pitch and roll stabilization. This operation is performed by the velocity readout converter. The three local oscillators mentioned above are running at an offset frequency in order to permit negative velocities and to maintain sense of direction. One method of performing the mixing operations is to convert the three frequencies into direct currents which are directly subtracted or added in operational amplifiers. The frequency-to-dc conversion is done in the velocity trackers and the mixing is done in velocity readout converter to produce the three dc analogs corresponding to  $V_x$ ,  $V_y$ , and  $V_z$ . These analogs are displayed to the observer on zero center microampere meters.

In order to obtain altitude information, the preamplifier output (common to velocity channel #3) is fed to a separate post amplifier chain having somewhat different bandpass characteristics than the velocity channel. It is necessary to retain both the upper and lower sideband to

the phase measurement necessary to derive altitude information. The postamplifier therefore, has a double bandpass characteristic with one passband centered at 60.378 MHz (60 MHz + 378 KHz) and the other centered at 59.622 MHz (60 MHz - 378 KHz). The double passband characteristic is generated by the dual bandpass crystal filter and the crystal notch filter which is centered at 60 MHz and removes the large  $J_0$  component. These filters remove all but the desired upper and lower sideband. The post amplifier output is fed to a mixer that has 60 MHz on the other input. The 60 MHz reference signal is produced by a crystal oscillator contained in the MFG. This mixing process results in a folded signal spectrum centered at 378 KHz and contains the original upper and lower sideband symmetrically spaced from 378 KHz by the doppler shift,  $f_d$ . The upper sideband appears at 378 KHz +  $f_d$ , and the lower sideband appears at 378 KHz -  $f_d$ . This signal is fed to an LEF and the bypass route such that the filter may be removed or inserted by a front panel control. (The same switch is used to remove the three velocity channel LEF's simultaneously.) The operation of the altitude channel LEF is identical to velocity channel LEF's except for operating frequency. The altitude channel LEF is designed to remove the non-doppler shifted leakage appearing at 378 KHz while the velocity channel LEF's are designed to remove non-doppler shifted leakage appearing at 37.8 KHz.

The signal is then fed to the altitude tracker where the signal phase information is extracted. An AGC loop monitors the signal at the tracker input and regulates the post amplifier gain to maintain the signal at a relatively constant level. A detailed description of the altitude tracker is given later in the report. The Altitude Tracker output is a

730 Hz pulse train with a pulsewidth corresponding precisely to the phase shift between the received signal and an internally generated reference signal (generated in the MFG). As explained in a previous section, the phase shift, hence, pulsewidth varies directly with altitude. This pulse train is fed to the mode switch and altitude readout board where it is converted into a dc analog of altitude. The dc voltage is exponentially shaped, buffered, and applied to the range meter for display purposes. Additionally, it is compared to a preset reference such that when the reference level is exceeded the PTDLR system will switch from FM/CW Bessel sideband operation into the ICW mode. This mode switching is set to occur at 1200 ft altitude.

After switchover occurs, the PTDLR system functions as a multiple beam, pulse doppler radar operating at a 50 percent duty cycle. The changes in operating configuration are limited to the transmitter, L.O. and altitude channel processing. The velocity channels are unaffected by the mode change. Referring again to the block diagram in Figure 14, the modulation input to the transmitter is grounded (performed within the MFG) thereby removing the frequency modulation from both the main transmitted signal and the L.O. signal. At the same time, switching is activated that gates the main transmitted output off and on at a 50 percent duty cycle rate. The switching rate may vary from approximately 8 KHz (at 30 K ft altitude) to 333 KHz (at 750 ft altitude). The correct rate is determined by the ICW tracker. The low power port from the transmitter is an ungated CW signal fed to the SSB as in the FM/CW mode but with the frequency modulation removed. The signal to the SSB is, however, changed from a 60 MHz CW signal to a gated, 50 percent

duty cycle signal centered at 60.378 MHz. The gating rate of the resultant L.O. signal applied to the signal mixers is identical to the transmitter output but phased so that the L.O. is gated off when the transmitter is gated on and vice-versa. This results in an output capability from the signal mixers only during the period when the transmitter is turned off and thus defines the "receive" period. Because the L.O. signal is removed from the transmit frequency by precisely 60.378 MHz, the signal output from the mixers will be centered at 60.378 MHz plus or minus the doppler shift associated with the individual antenna beams. These are exactly the same conditions provided for the velocity channels when operating in the FM/CW mode. The velocity channels are therefore completely compatible in both modes and require no mode switching circuitry.

The altitude channel processing is completely different in the ICW mode and is performed in a separate channel. It does, however, utilize the same preamplifier output that supplies Doppler Channel #3 velocity information and the altitude channel information when in the FM/CW mode. This preamplifier is fed to a broadband post amplifier chain that provides up to 130 db gain for the received signal. The post amplifier output is peak detected and buffered with a video amplifier and fed to the ICW range tracker. The function of the ICW range tracker is to determine if the received signal is accurately centered within the "receive" period established by the previously mentioned gating sequence of the transmitter and L.O. outputs. This condition will occur when the round trip radar time delay is equal to the transmitted pulse length. By means of "early" - "late" gate sampling techniques in the ICW tracker, a non-centered condition of the received return is detected and an error



is generated that changes the transmitter gating rate, hence, the transmitter pulse length since a 50 percent duty cycle is maintained, so that the pulse length is indeed equal to the round trip delay time. Since the round trip delay time of the radar signal is proportional to altitude (or slant range of the beam being used) and since the gating rate or pulse repetition frequency (PRF) is continuously servoed to maintain received signal centering, the closed loop PRF generated by the system in the ICW mode is an accurate measure of altitude. The ICW tracker also provides a pulse train output to the Mode Switch and Altitude Readout board where it is converted into a DC analog of altitude. The DC voltage is properly scale factored and displayed on the range meter as an indication of altitude. Additionally, this voltage is compared with a preset reference such that when it drops below the preset reference the PTDLR system will automatically switch back into the FM/CW Bessel sideband mode of operation. The mode switching is set to occur at 750 ft altitude.

The system is preset to switch from the FM/CW mode into the ICW mode at 1200 ft altitude and into the FM/CW mode from the ICW mode at 750 ft altitude so that a hysteresis band of 450 ft is provided. The overlap was incorporated to prevent continuous switching between modes with small changes in altitude or vehicle roll and pitch angles when operating the system in this altitude region. After switchover into the FM/CW mode, pitch or roll angles greater than 25 deg can be accommodated without causing re-switching to occur.

## 2.2 Physical Characteristics

The flight evaluation model of the Planetary Terminal Descent and Landing Radar, Autonetics Model R146A, consists of the following major components:

1. **Transmitter-Receiver Unit**
2. **Antenna Unit**
3. **Control, Processing, and Display Unit**

There have been two Antenna Units fabricated for use with the PTDLR system. The first unit consisted of an 18 in. Luneberg lens, four waveguide feedhorns, and a supporting structure. Total weight is approximately 20 lbs. The second antenna unit consists of two constant K antennas with three feedhorns on each antenna. This unit, with supporting structure weighs approximately 100 lbs.

The transmitter-receiver unit is also mounted on the antenna support structure and weighs approximately 35 lbs. A photograph of the integral system with the Luneberg lens attached is shown in Figure 15.

The control, processing, and display unit is shown in Figure 16. The chassis contains all of the required system power supplies, velocity and altitude trackers, display meters, and system control functions. The unit weighs 61 lbs and consumes approximately 230 watts of 60 - 400 Hz, 110 V power.

## 2.3 Performance Characteristics

Table 2 presents a summary of performance and salient features of the PTDLR flight evaluation equipment.

## 2.4 Description of Equipment Components

### 2.4.1 Master Frequency Generator

The master frequency reference generator is contained in two separate boxes -- one containing the high frequency sources, and one containing the low frequency sources



Figure 15. Transceiver

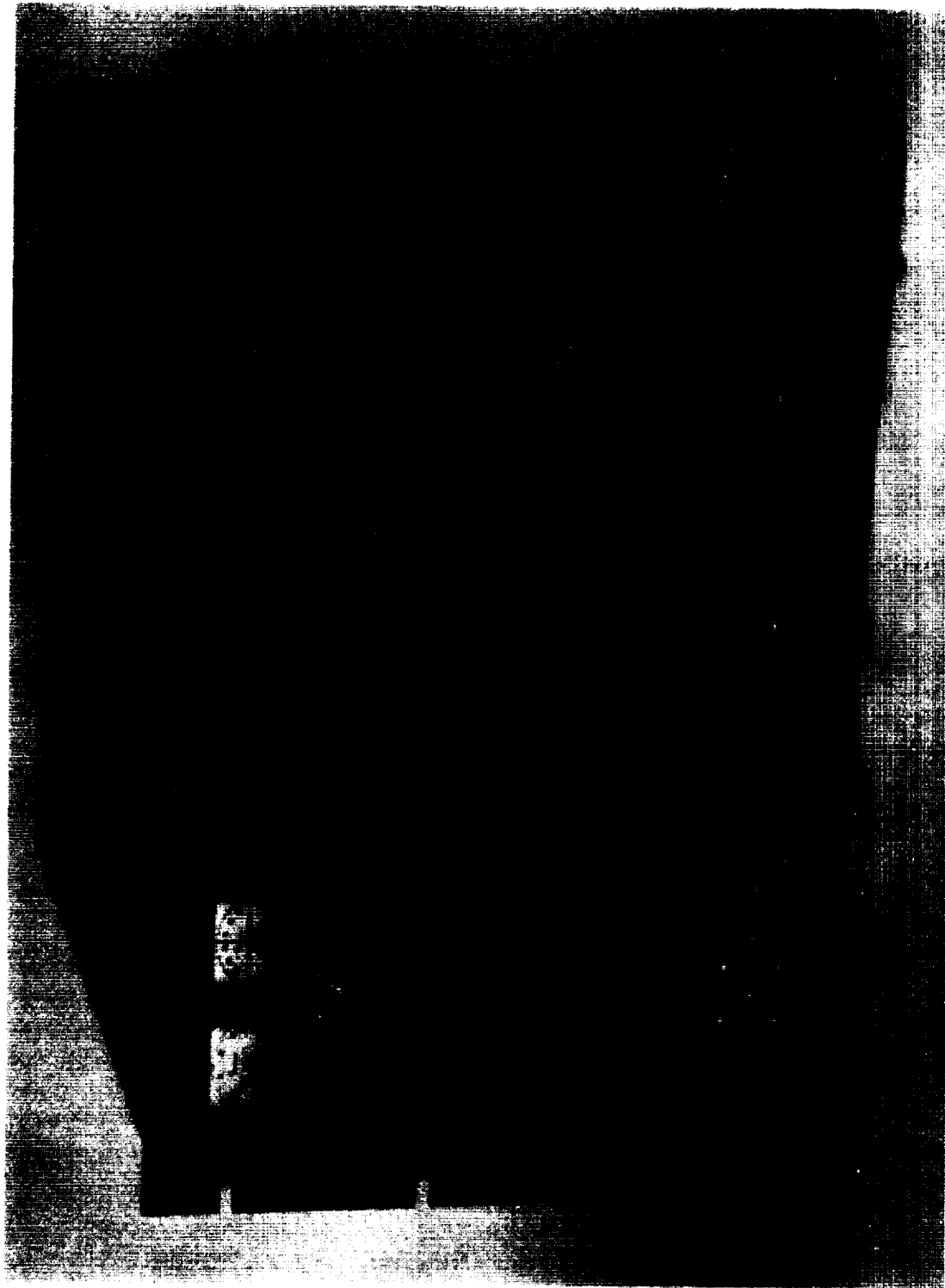


Figure 16. Processor

Table 2. Performance Characteristics

Operating Range (Altitude)	30,000 ft to 10 ft
Velocity Limits	±680 fps
Accuracy of Beam Velocity Components (D <sub>1</sub> , D <sub>2</sub> , D <sub>3</sub> )	5.5% V <sub>T</sub> or 3.5 fps
Range Accuracy	4.5% or 5 ft (3σ), whichever is larger
Smoothing Time	0.5 seconds
Precision Data Outputs (for airborne recording)	
D <sub>1</sub> , D <sub>2</sub> , D <sub>3</sub> (Doppler beam velocities)	square wave frequency analogs of velocity
Range - 30,000 ft to 750 ft	square wave representing radar PRF (range analog) - 8 KHz to 333 KHz
1200 ft to 10 ft	dc voltage proportional to range or pulsewidth prop to range
Modulation	
30,000 ft to 750 ft	ICW (50% duty cycle)
1200 ft to 10 ft	FM/CW (Bessel Sideband)
Modulation Frequency	
FM/CW	J <sub>3</sub> = 126 KHz, J <sub>2</sub> = 189 KHz, J <sub>1</sub> = 378 KHz
ICW	8 KHz to 333 KHz (variable with range)
FM/CW Bessel Sideband Order	J <sub>1</sub> , J <sub>2</sub> or J <sub>3</sub> selectable
Receiver Type	60 MHz IF
Frequency Tracker Type	Sine-Cosine
Meter Readouts	V <sub>x</sub> , V <sub>y</sub> , V <sub>z</sub> , range
Operating Frequency	13.35 GHz
Transmitter Power	500 mw (CW)

**Table 2. (Cont)**

<b>Transmitter Type</b>	<b>Solid-state Multiplier Chain</b>
<b>Antenna Type</b>	<b>Luneberg Lens (lightweight) and Dual Constant K lens</b>
<b>Number of Antenna Beams</b>	<b>Velocity - 3 Range - 1</b>
<b>Antenna Size</b>	<b>18-inch diameter</b>
<b>Antenna Gain</b>	<b>28 db (Luneberg) 31 db (constant K)</b>
<b>Antenna Polarization</b>	<b>Vertical</b>
<b>Antenna Beamwidth</b>	<b>4.1 deg</b>
<b>Beam Incidence Angle (Velocity Beams)</b>	<b>15 deg (Luneberg) 24° 10' (constant K)</b>

The high frequency generator (see Figure 17) contains two crystal oscillators and sufficient buffer amplifiers, mixers, switches, and driver amplifiers to supply the following signals:

1. Local oscillator offset frequency (60 MHz or 60.378 MHz)
2. Velocity channel if<sub>2</sub> offset frequency (60.4158 MHz)
3. Altitude channel if<sub>2</sub> offset frequency (60.000 MHz)
4. Partially formed zero doppler reference frequency (415.8 KHz)

The local oscillator (L.O.) offset frequency requirements are a function of the operating mode. In FM/CW, the offset frequency is 60.0 MHz and in the ICW mode the offset frequency is 60.378 MHz gated off and on with a fifty percent duty cycle operating at a pulse repetition frequency determined by the ICW range tracker output. This frequency is given by following equation:

$$f(\text{Hz}) = \frac{2.5 \times 10^8}{\text{Range (ft)}}$$



The 60.0 MHz L.O. signal is generated by a crystal oscillator operating in a modified Hartley circuit (see Figure 18). The oscillator output is amplified by a three stage buffer-driver. This output was initially used as the altitude channel reference directly as well as supplying other functions including the L.O. offset frequency. However, during tests, an oscillatory condition was observed and was eliminated by adding an additional two stage buffer amplifier, external to the high frequency master frequency generator box, in the line supplying the 60.0 MHz reference signal to the altitude channel IF phase detector.

The 60.0 MHz reference signal is also used to mix with 378 KHz to produce upper and lower sideband signals at 60.378 MHz and 59.622 MHz. (see Figure 19). These signals are further amplified and passed through a narrow band crystal filter (see Figure 20) that selects only the upper sideband (60.378 MHz). This signal is amplified in a gated driver and supplied to a broadband mixer (gate). The second mixer input signal is the square wave PRF train originating in the ICW tracking loop. The resultant mixer output is a gated burst at 60.375 MHz with a fifty percent duty cycle. This signal is supplied to a solid state switch that selects either the 60.378 MHz gated signal or the 60.0 MHz CW signal as a function of the operating mode. The switch output is fed to a broadband driver amplifier, and, as the L.O. offset frequency, is fed directly to the single sideband modulator in the microwave section.

A crystal oscillator operating at 60.4158 MHz is buffered, amplified, and fed to three individual driver amplifiers (see Figure 21). The outputs are used to supply the phase detector reference signal in a 2nd i.f. amplifier of each of the velocity channels.





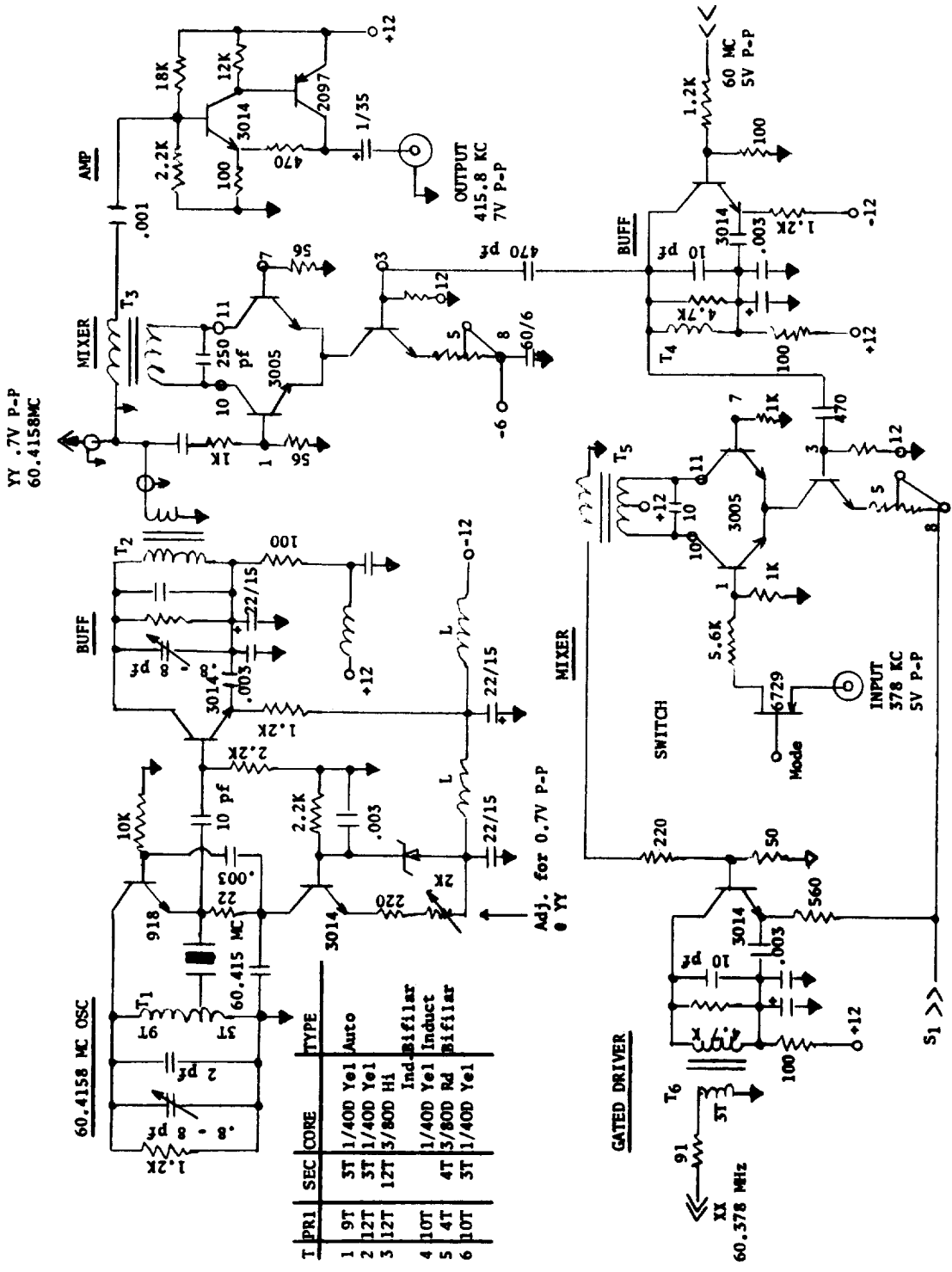


Figure 19. 60.378 MHz, 60.4158 MHz, and 415.8 KHz Reference Generators





The 60.4158 MHz is also mixed with the 60.0 MHz reference signal to produce a difference signal of 415.8 KHz. This signal is mixed with 378 KHz in the LEF reference generator board to produce a difference frequency of 37.8 KHz and represents the zero doppler velocity reference frequency.

The low frequency generator (see Figure 22) contains three crystal oscillators, shown in Figure 23, operating at 126 KHz, 189 KHz, and 378 KHz and are suitably buffered, amplified, gain-programmed and switch selected at the control panel to operate the FM/CW mode as a  $J_3$ ,  $J_2$ , or  $J_1$  Bessel sideband system. The selected output frequency is fed directly to the phase modulator within the transmitter at the correct amplitude to produce the desired modulation index. The modulation index can be changed by a factor of two by a front panel switch. This switch essentially changes the amplitude of the aforementioned oscillator outputs by a factor of two, which, in turn, changes the transmitter frequency deviation or modulation index by a factor of two. A schematic of the driver circuitry is shown in Figure 24.

The selected oscillator output is also used to generate a reference frequency of 378 KHz and a 756 KHz reference. This is done by feeding the selected oscillator (126 KHz, 189 KHz, or 378 KHz) to the harmonic generator shown in Figure 25 and extracting either the third, second or first harmonic in an amplifier tuned at 378 KHz, thus forming the 378 KHz reference. This signal is used to mix with 60.0 MHz to produce the 60.378 MHz ICW L.O. signal, mixed with 415.8 KHz signal (generated in the high frequency box) to produce the zero doppler velocity reference used directly as the altitude channel LEF reference, and is doubled in

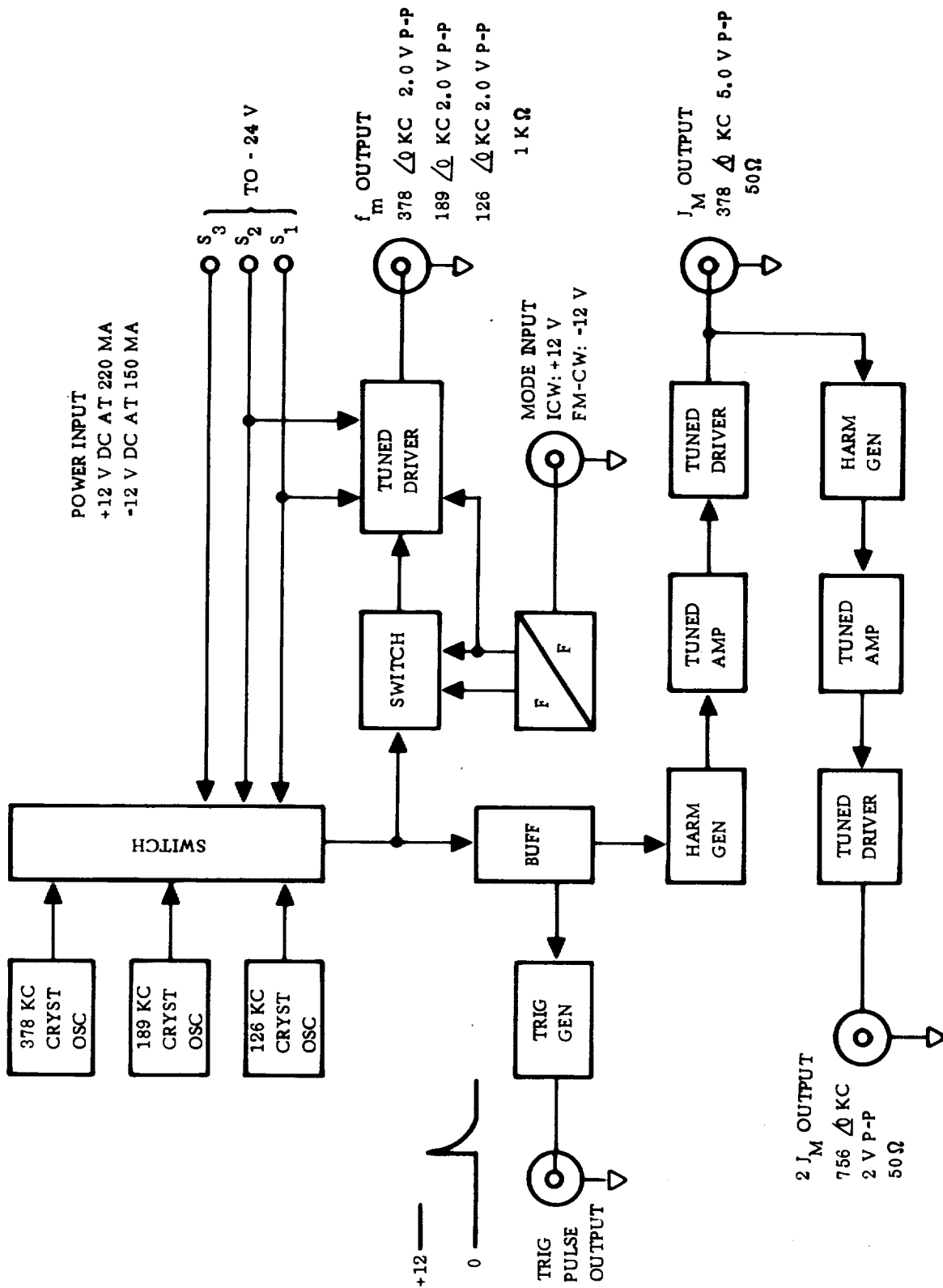
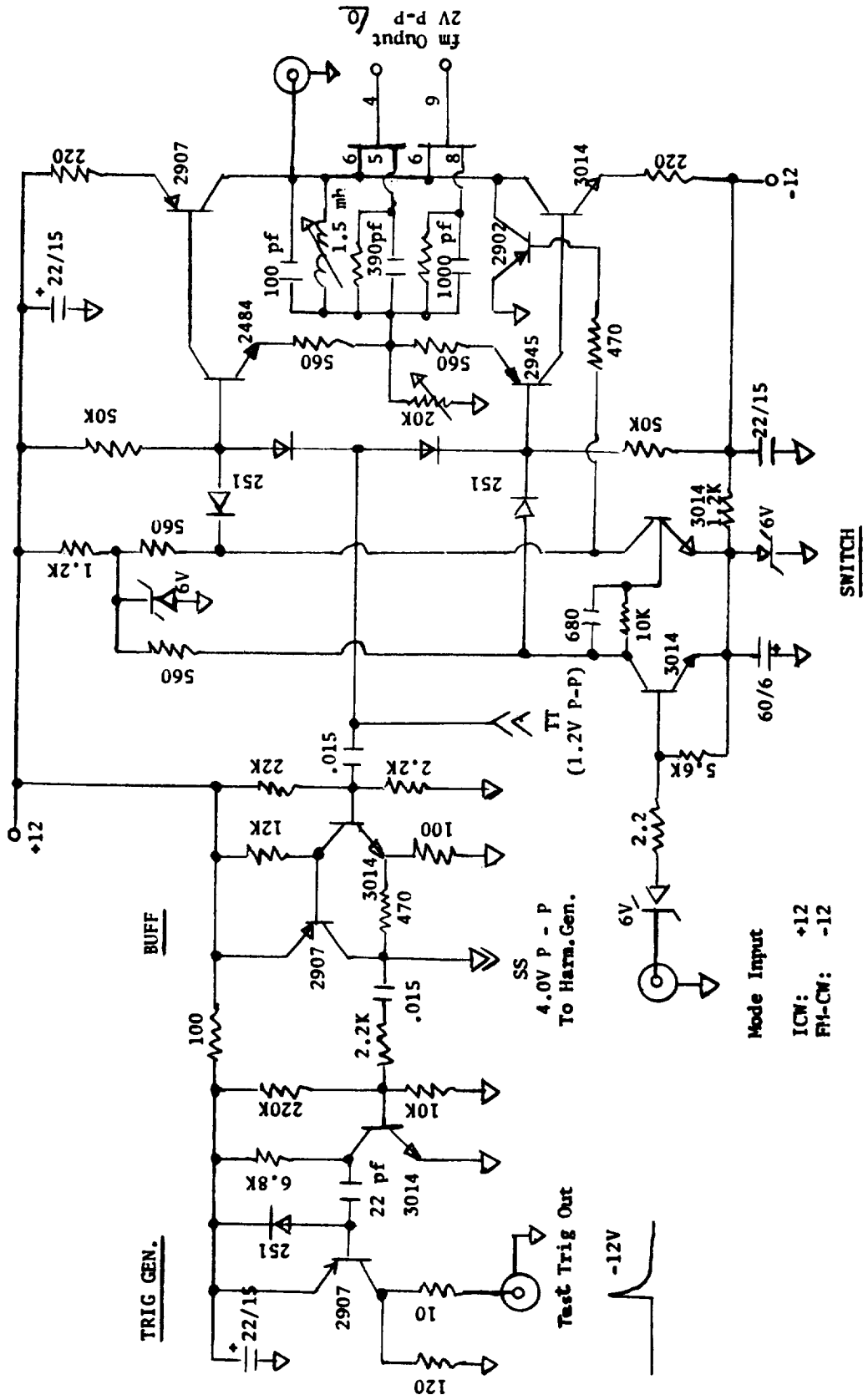


Figure 22. Low Frequency Generator



TUNED DRIVER



Mode Input  
 ICM: +12  
 FM-CW: -12

Figure 24. Modulation Frequency Driver





frequency by a X2 multiplier as shown in Figure 26 and used as the phase reference for range measurements in the FM/CW altitude channel.

#### 2.4.2 Mode Switching

The mode switching board performs the function of converting the FM/CW range variable pulse width signal and the ICW square wave variable frequency signal into D.C. signals whose amplitude is proportional to range. These D.C. signals are then compared to a preset D.C. level representing the desired mode switching points effecting a mode switchover when this level is exceeded. The D.C. analogs of range are also processed in a non-linear manner for meter display purposes.

In addition to the above primary functions, the board contains a linear amplifier used to supply the FM/CW range voltage at low impedance to an instrumentation recorder for evaluation purposes; an ICW mode indicator lamp driver with an interlock ICW tracking clamp; the summing amplifiers used to perform the transformation of the D.C. analogs of beam #1, beam #2, and beam #3 doppler frequencies into forward velocity ( $V_x$ ); sideways velocity ( $V_y$ ); and vertical velocity ( $V_z$ ).

Referring to the block diagram, figure 27, and circuit schematic, figure 28, the circuit description is as follows: Starting with the FM/CW input signal, it is applied to the driver amplifier that is essentially a two-stage saturation amplifier with a low impedance output (at least in the positive going direction) that is switching between gnd and the reference voltage ( $V_r = 6.0 \text{ V}$ ) supplied by the precision voltage regulation. The nature of the FM/CW input signal, hence the driver amplifier output signal, is a pulse train with a frequency of 730 Hz and a variable pulse width directly proportional to the slant range (loosely called altitude).



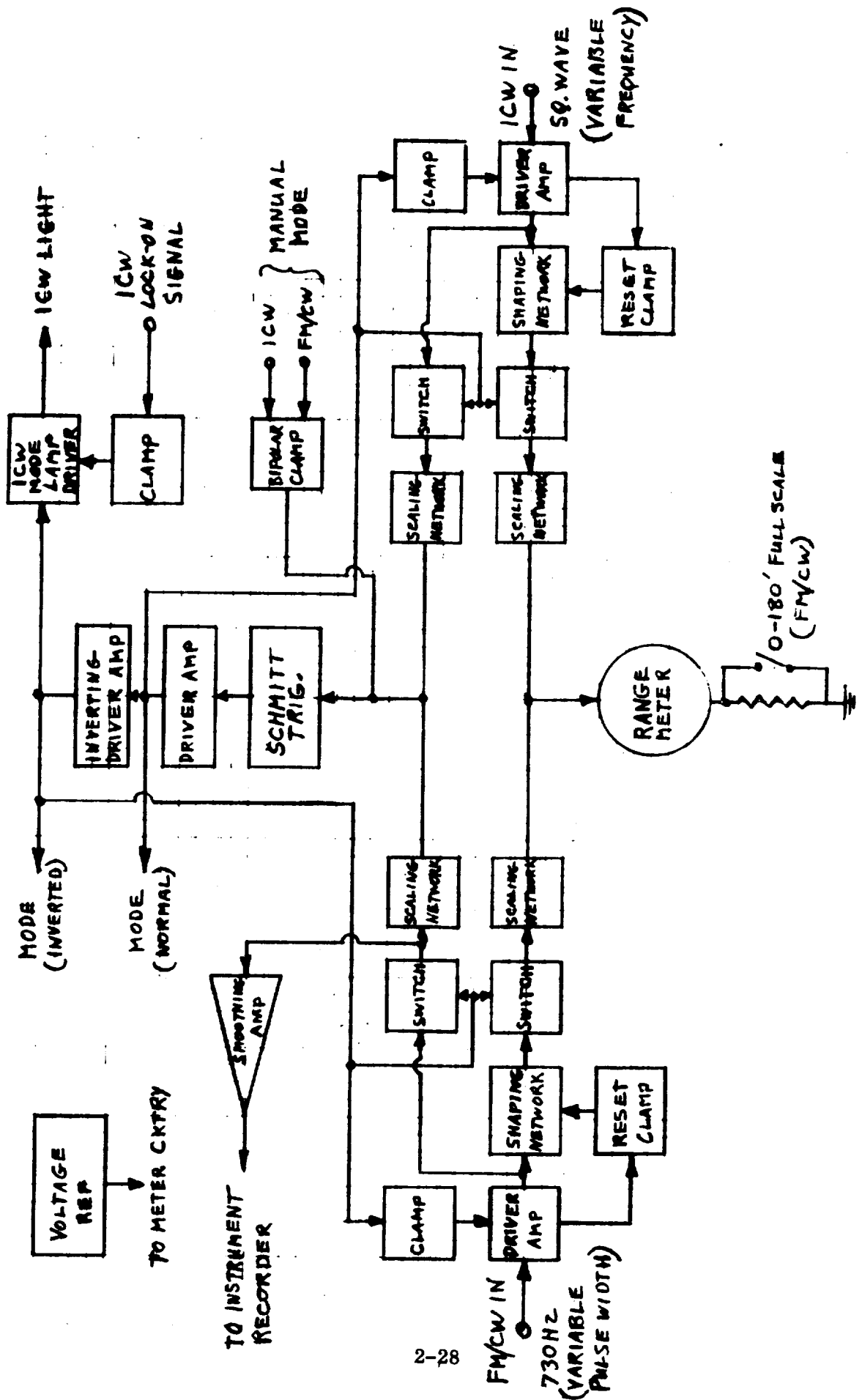


Figure 27. Mode Switching and Range Readout - Block Diagram



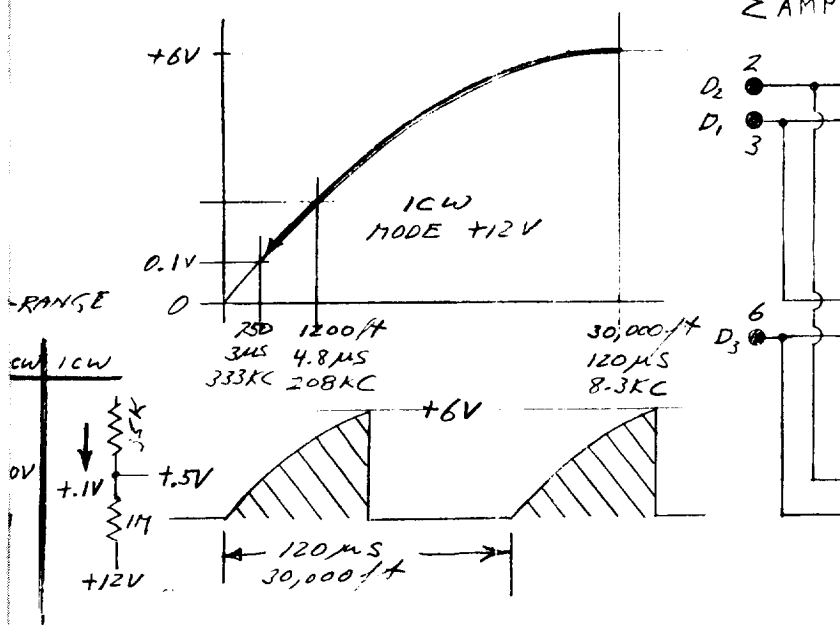
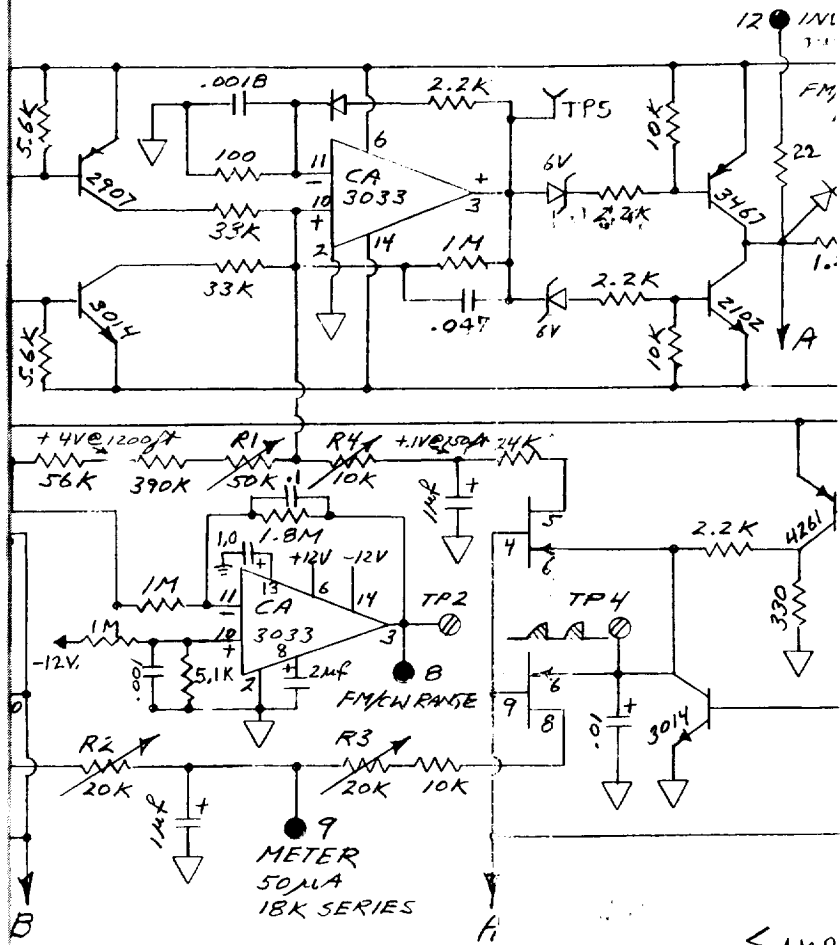
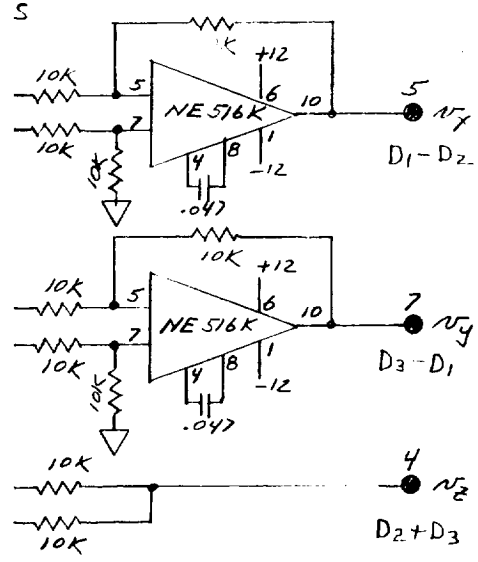
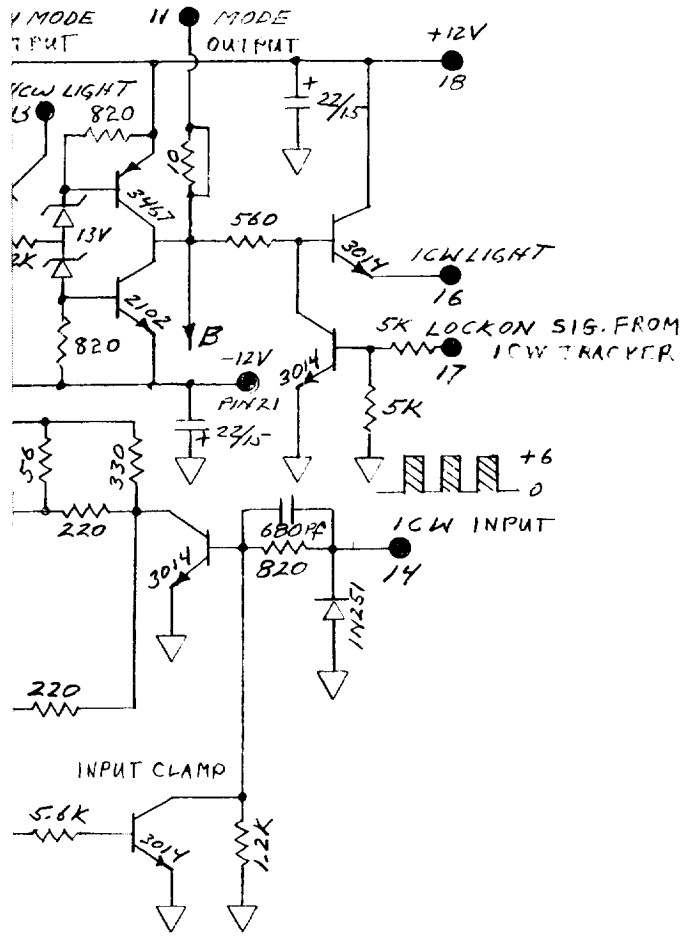


Figure 28. Mo  
2.



+12V PIN 18  
 -12V PIN 21  
 GND PIN 15

Mode Switching  
 -29/2-30

FOLDOUT FRAME 3

With a frequency of 730 Hz, the corresponding period of the pulse train is 1370 usec. The pulse width corresponds to the phase shift between the radar return signal and an internally generated reference signal. System parameters are such that the phase shift will increase from zero degree to 360 degrees linearly as the range (or altitude) is increased from zero ft. to approximately 1,302 ft. The pulse width of the FM/CW signal into mode board driver amplifiers, therefore, has a variation of:  $\frac{1370}{1302} = 1.052$   $\mu$ sec per ft. of altitude change. Since the waveshape out of the driver amplifier switches between precision voltages, direct averaging of the waveshape will produce a D.C. voltage directly proportional to altitude according to the relationship.

$$E_o(\text{D.C.}) = V_{\text{Ref}} \left( \frac{t}{\tau} \right) = V_{\text{Ref}} \left( \frac{r}{R_{\text{max}}} \right) = 5.53 \text{ MV/ft.}$$

In order to provide a more convenient scale factor and a lower source impedance to the instrumentation recorder, a feedback op-amp was added to increase the scale factor to -10 MV/ft. The required smoothing of the pulse train to obtain the D.C. component is obtained by adding a 0.1 ufd capacitor across the 1.8 meg. feedback resistor. This D.C. voltage could be used to drive the range meter, but, being linear with altitude, would require linear graduations on the meter face. This would be the most expedient utilization, but from an operational standpoint would be unsatisfactory. In a landing situation or low altitude maneuvering, the lower one becomes the more important it is to be able to determine altitude more precisely. This implies a scale expansion in the lower altitude region and a compression of the higher altitudes.



**This feature has been incorporated in the mode board by adding a shaping network to the pulse train that produces a logarithmic scale following the expression:**

$$e_o = 1 - e^{-\left(\frac{t}{RC}\right)}$$

**where t corresponds to the pulsewidth, hence, altitude and RC 47 ms is chosen to provide a scale expansion by approximately 10 times at the low altitudes. In addition, a scale expander switch is contained in the control panel to display 0-180 ft. full scale to provide even greater readout precision in the critical low altitude region.**

**Similar circuitry is provided for range processing the ICW input signal and non-linear shaping (RC = 22 usec) has been done to give a scale expansion of approximately 5 to 1 in the lower altitude region. The ICW input signal is a square wave with a frequency inversely proportional to range and, therefore, requires a different form of shaping network to provide the logarithmic scale. The D.C. analogs of the FM/CW and ICW input signals are switched, scale factored, and summed together. One branch drives the range readout meter and the other branch is applied to the Schmitt trigger circuit. The Schmitt trigger has a hysteresis window established by the feedback network between the op-amp output and the noninverting input. This window establishes the switching point overlap between the FM/CW mode and the ICW mode.**

**The present scaling and window values are set up to effect an automatic switchover from the ICW mode into the FM/CW mode at 750 ft altitude when descending and will switch from the FM/CW mode into the ICW mode at 1200 ft altitude when ascending. The system will operate**

satisfactorily in either mode in the region between 750 ft to 1200 ft altitude, but will be locked in one mode or the other until one of the above limits is exceeded. The bipolar clamp signal that is summed with the range voltages at the input of the Schmitt permits the system to be manually locked into either mode by a front panel control. This feature conveniently is used during laboratory and tracking bay checkout of the system.

The Schmitt trigger output is fed to two driver amplifiers in cascade, each supplying "mode" or "inverted mode" requirements to various parts of the system at +12 volt or -12 volt levels respectively.

#### 2.4.3 Transmitter

The transmitter used with this system was purchased from the Microelectronics Division of the Philco-Ford Corporation. Under the very capable direction of Messrs. Jack Joos and Joe DeBona of that division, the unit was delivered on schedule, within specifications, and, with the exception of three capacitor failures, has operated satisfactorily during the entire course of the program.

The unit is basically a crystal controlled oscillator-power amplifier-varacter multiplier source. Two modifications were incorporated by Philco to suit the bimode requirements consisting of adding a phase modulator between the crystal oscillator output and the power amplifier input and adding a second final varacter stage and RF switch. By varying the back bias voltage across a varicap tuned tank circuit, the phase modulator is able to change the relative phase of the signal driving the power amplifier with respect to the crystal frequency. The net phase change is proportional to the net voltage change across the varicap, which

is driven by the selected  $J_1$ ,  $J_2$ , or  $J_3$  modulation frequency (378 KHz, 189 KHz, or 126 KHz, respectively). The total phase change per unit time corresponds to the total frequency deviation. Because of the rather high multiplication factor of the transmitter (i.e.,  $\frac{f_{\text{transmitter}}}{f_{\text{crystal}}} = \frac{13.350 \text{ GHz}}{92.7 \text{ MHz}} = 144$ ) a very small phase change is required at the oscillator to produce a considerable frequency deviation at the transmitter output. For example, consider the  $J_2$  low modulation index case:

$$f_m = 189 \text{ KHz (modulation frequency)}$$

$$m = 2.568 \quad (\text{modulation index})$$

$$\Delta f = 384 \text{ KHz (frequency deviation)}$$

The transmitter frequency deviates from its center frequency ( $f_t$ ) by 384 KHz ( $\Delta f$ ) in one quarter cycle of the modulating frequency ( $f_m$ ). The next one quarter cycle of the frequency is returned to  $f_t$ , the next one quarter cycle the frequency deviates by  $\Delta f$  in the other direction, and so forth. One quarter of a cycle of the modulating frequency occurs in  $\frac{1}{4 (189 \text{ KHz})} = 1.323 \text{ usec}$  and since the frequency deviation during that time period was 384 KHz, using the relationship:

$$f \text{ (Hz)} = \frac{d\phi \text{ (degrees)}}{360 dt \text{ (sec)}}$$

$$\begin{aligned} d\phi &= \text{Total phase shift} = 360 f dt = 360 (384 \times 10^3) (1.327 \times 10^{-6}) \\ &= 183 \text{ degrees.} \end{aligned}$$

The phase deviation required at the phase modulator is reduced by the X144 multiplication factor of the transmitter chain. The total phase shift is, therefore, equal to approximately 1.27 degrees -- a very small amount!

The transmitter chain branches into two separate output stages preceding the last varactor multiplier. This was done in order to provide

a source of L.O. power and the gatable source of transmitter power required for ICW mode. Power splitting at the last possible point of the chain insures that both outputs have nearly identical FM noise components. This is a requirement for satisfactory FM/CW operation. Power division of a single high power output by using a coupler to supply L.O. power was not practical for two reasons. The first being the near impossibility of supplying the total power required from a single varacter stage with state-of-the-art components available at the time of this development. The second reason being the difficulty of obtaining the required "on-off" power ratio in the ICW mode using only microwave switches. This can be appreciated when it is realized that this "on-off" ratio must be approximately 145 db. Approximately 90 db of this requirement is realized by merely forward biasing the final high power stage during the desired "off" time. The additional 55 db attenuation is obtained by cascading two PIN diode microwave switches separated by an isolator. Suitable drivers are contained within the transmitter to simultaneously activate the varacter biasing and microwave switches with simple, low power, zero volt or +5 volt logic signals (high power output is on with "0" logic and turned off with "1" logic commands). Rise times of 10 NS and fall times of 4 NS are achieved. A delay time of approximately 80 NS occurs between the command signal and the RF output envelope. The high power output port (switched side) delivers 1.16 watts at 25°C and the L.O. port delivers approximately 0.49W. A block diagram of the purchased unit is shown in Figure 29. Specified parameters of the delivered unit appear in Table 3.

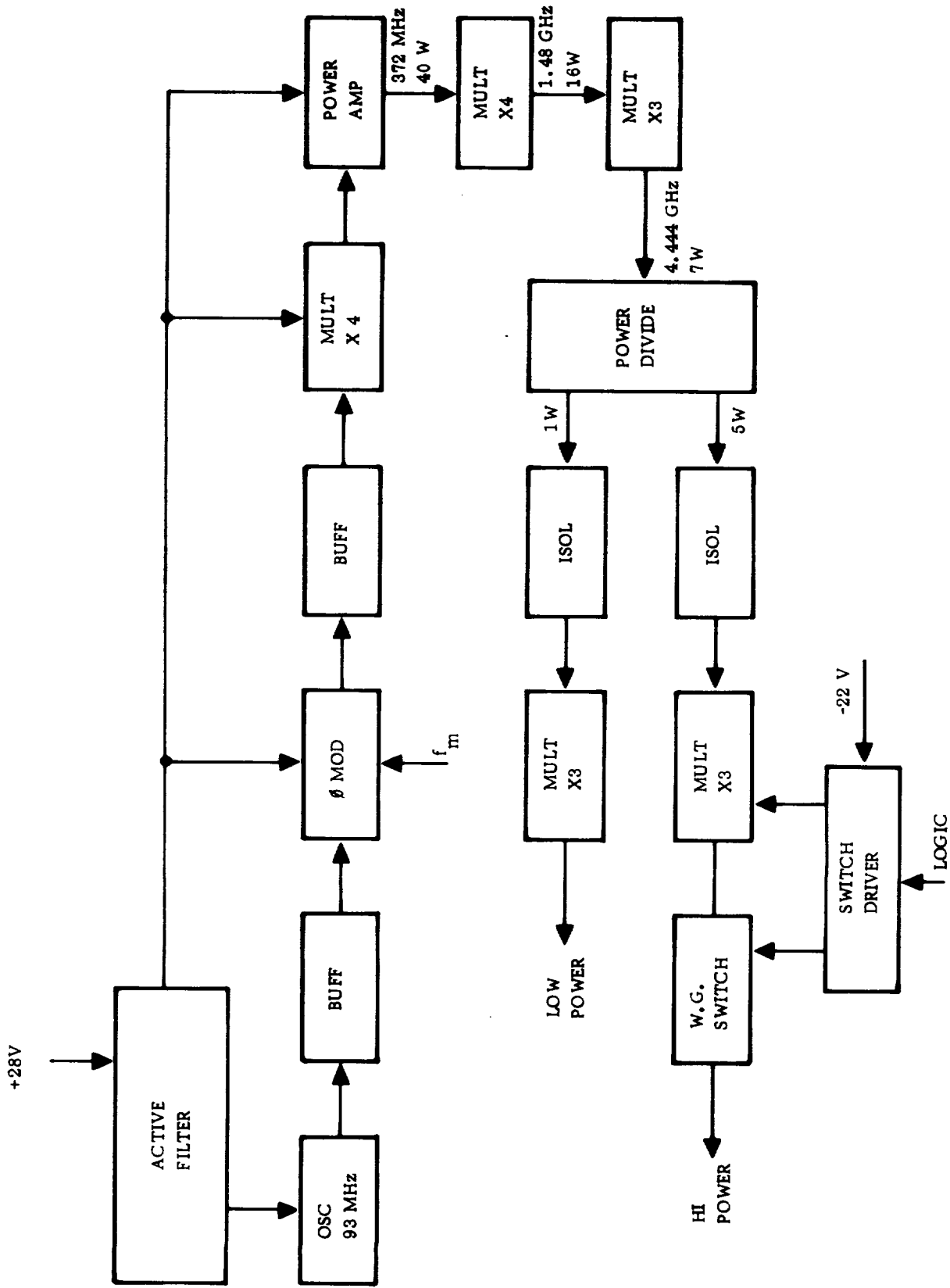


Figure 29. Ke Band Source

Table 3. K Band Power Source (Multiplier Amplifier Chain) T-3070

Electrical Specification

Output Frequency	13.350 GHz
Input Signal	
Frequency	92.708333 ± .001%
Power	10 milliwatts
Impedance	50 ohms
Output #1 Power	
Minimum	800 milliwatts
Typical	1 watt
Output #1 Switched Off	120 db Isolation
Output #2 Power	
Minimum	200 milliwatts
Output #1 and #2 Spurious outputs	40 db down
Output #1 logic signal	
On	0 to +1 volt
Off	+2 to +6 volts
Logic current required	10 MA
Switching time (Output #1)	
Rise time $T_R$	50 to 100 nanoseconds
Fall time $T_F$	50 to 100 nanoseconds
AM Noise	
$P_{AM}^*$	- 120 db/kc for 40 KHz bandwidth centered ±378 KHz from the carrier frequency.
FM Noise	
$f_{rms}$	20 cps/kc for a 40 KHz bandwidth centered ±378 KHz from the carrier frequency.
DC Power Required	
28 volts DC at I	3.5 Amperes

Mechanical Specifications

Weight 6#  
Output Connectors UG541A/U

\*Referred to maximum carrier power.

**Table 3. (Cont)**

**Environmental Specifications**

<b>Temperature</b>	<b>0 to 50°C operating -62 to +100°C storage</b>
<b>Shock</b>	<b>MIL-E-5400H</b>
<b>Vibration</b>	<b>5 g's or 0.02 inches pp (5 to 500 Hz) 50 g's (100 to 200 Hz at 20 Hz BW)</b>
<b>Humidity</b>	<b>MIL-E-5400H</b>
<b>Altitude</b>	<b>70,000 ft</b>

**2.4.4 Microwave Components**

The selection of "off the shelf" RF components is somewhat limited at 13.350 GHz and therefore tradeoffs regarding performance and cost between make or buy and between waveguide or stripline construction were also limited. The microwave unit finally selected was fabricated by Micro-Radionics, Incorporated. The unit consists of: two four-way power dividers to distribute the transmitter output and the L.O. power to each of four beams; four four-port circulators to direct the transmit power to the antenna and the received antenna power to the mixers; four balanced mixers to perform the signal down-conversion to IF frequency; a single sideband modulator to generate the L.O. offset frequency; a ten section narrow bandpass filter to suppress all but the desired L.O. offset frequency; and, several isolators and waveguide to OSM transitions. All of the components are of stripline construction and together form a fairly compact unit. An outline drawing of the RF hardware is shown in Figure 30. Also contained in the drawing are performance specifications relating to the various components.

Several problem areas associated with the RF section have been identified. The most significant occurring in the SSB filter. Proper cancellation of the Bessel sideband terms at the mixer output requires close matching of the electrical path lengths of the transmitter leg and the L.O. leg. During the hardware assembly phase of the program, the matching was done by measuring both the physical path lengths (transmitter-to-mixer and L.O.-to-mixer) and adding a small waveguide section in the transmitter leg to make the paths equal. During subsequent testing a considerable amount of Bessel sideband energy was noticed. Further investigation showed that the electrical length of the L.O. path was considerably greater than the measured physical length and the cause was traced to the SSB filter. It was not immediately apparent that the filter, physically consisting approximately of an eight inch piece of waveguide with ten 4-40 screws inserted in one wall, might electrically appear to be fifty feet long. Several calculations were performed to verify laboratory measurements made on a five section SSB filter.

The time delay through a waveguide filter is given by:

$$t_d = \frac{\ell}{V_g} \quad (1)$$

where

$\ell$  = length of filter (0.25 feet)

$V_g$  = group velocity in feet/second

The group velocity is obtained from the  $\omega$ - $\beta$  diagram for a filter by finding the slope at the frequency ( $\omega_o$ ) of interest.

$$V_g = \left. \frac{d\omega}{d\beta} \right|_{\omega = \omega_o}$$

where  $\beta$  is the phase shift per unit length of filter or filter section.



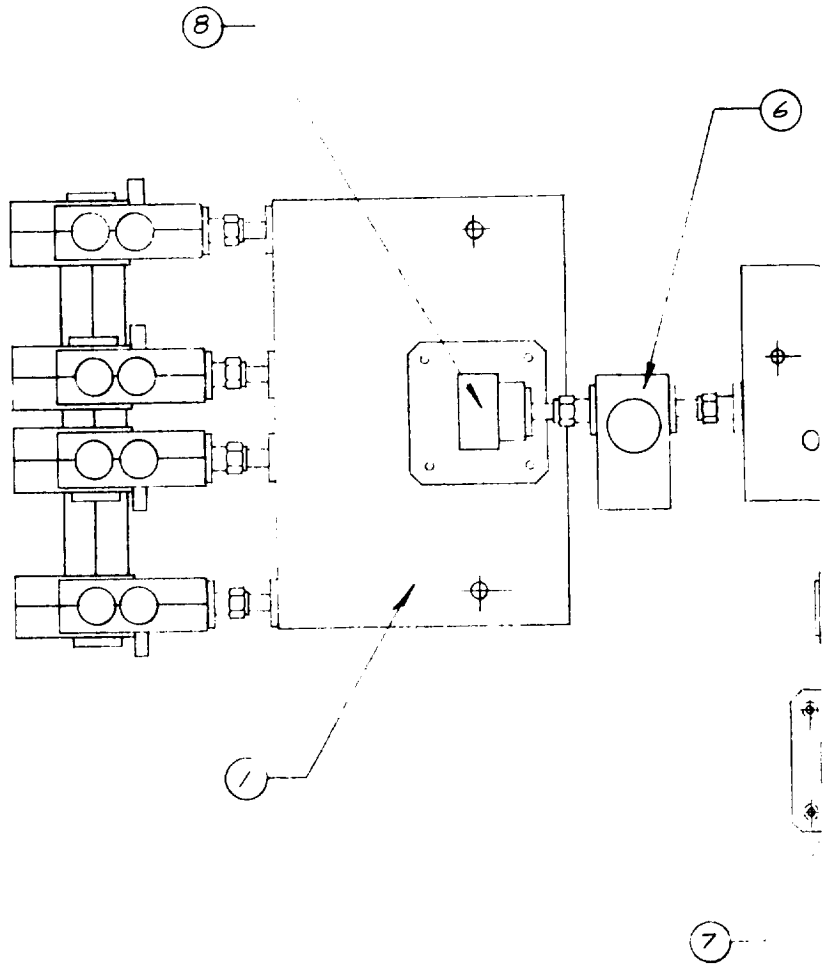


E

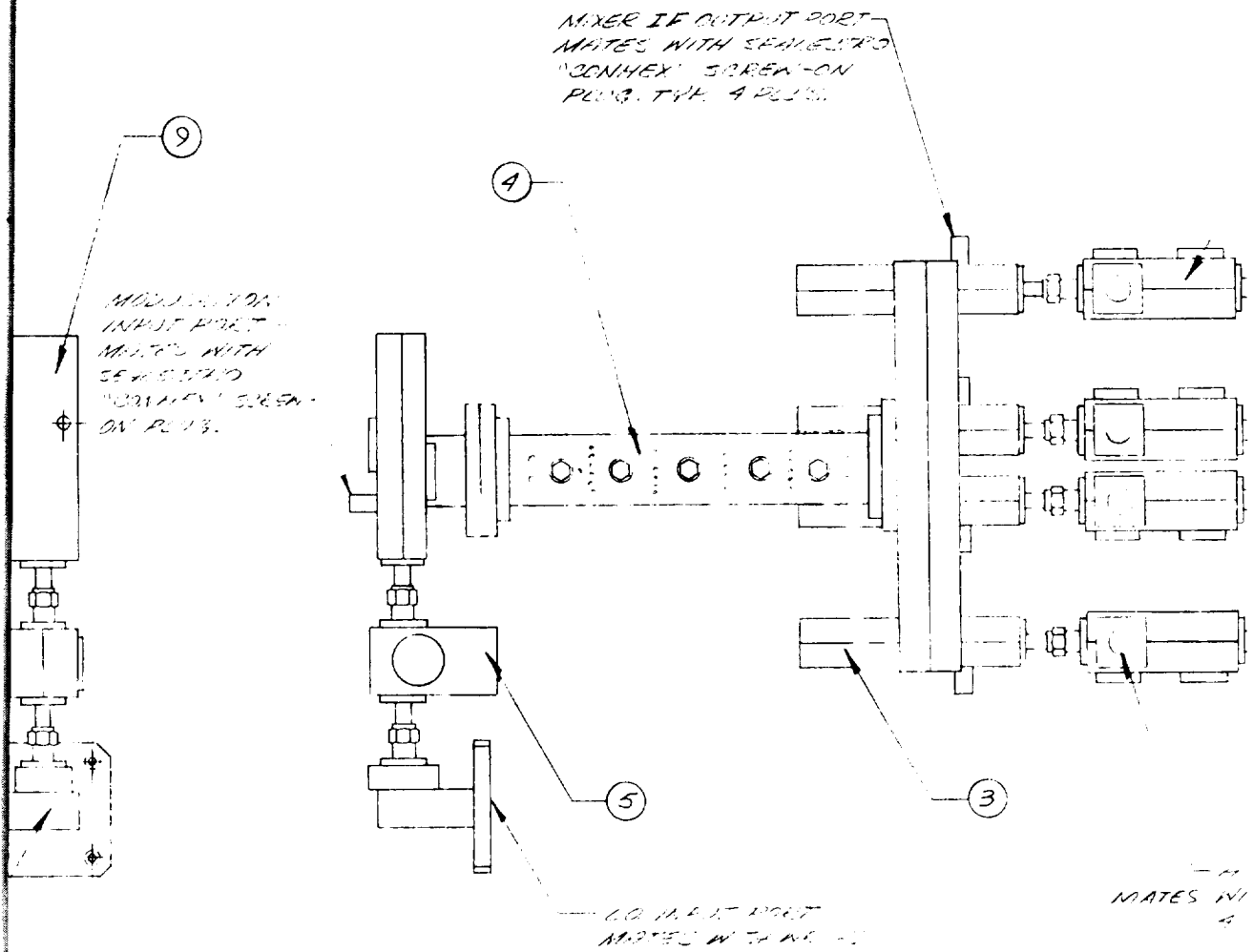
D

C

B

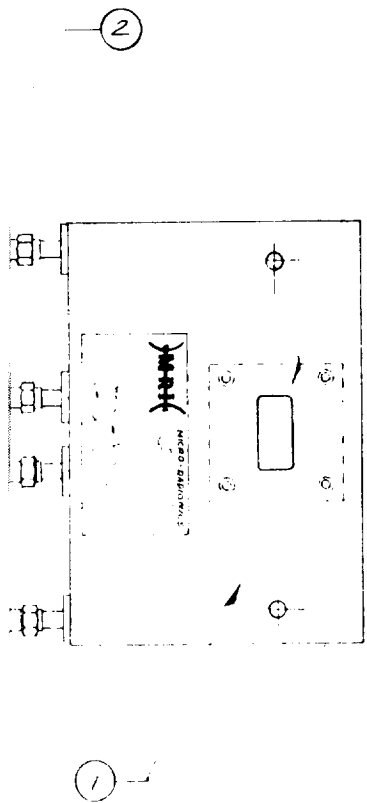


**EOLDOUT FRAME**



**BILL OF ASSEMBLYS**

ITEM	TITLE	PART NO.	QTY.
1	4-WAY PWR. DIV.	C995185005	2
2	4 PORT CIRC.	C995103007	4
3	MIXER	C995166011	4
4	FILTER	C995181005	1
5	ISOLATOR	C995100027	1
6	ISOLATOR	C995107028	1
7	TRANSITION	C995187002	1
8	TRANSITION	C995187003	1
9	MODULATOR	C995166011	1



- THE MOUNTED INPUT PORT MATCHES WITH THE BOARD.

### SPECIFICATIONS

<b>TRANSMITTER INPUT:</b>	
CENTER FREQ. FREQ. (F <sub>c</sub> )	13.35 GHz
BANDWIDTH	± 5 GHz
POWER LEVEL	+27 dBm MAX.
<b>INSERTION LOSS:</b>	
XMT. INPUT TO ANTENNA OUTPUT	1.0 dB MAX.
ISOLATION, MIXER TO XMT. PORT	30 dB MIN.
<b>L.O. INPUT:</b>	
CENTER FREQ. FREQ. (F <sub>c</sub> )	13.35 GHz
BANDWIDTH	± 5 GHz
POWER LEVEL	+23 dBm
MIXER L.O. POWER @ 13.31 GHz	+17 dBm MIN.
<b>REJECTED MODULATORS:</b>	
MOD. FREQ. RANGE	50 MHz
MOD. POWER LEVEL	+24 dBm MAX.
SPURIOUS SIGNAL REJECTION (MEASURED AT MIXER L.O. FREQ.)	20 dB
NOISE FLOOR (MEASURED AT ANTENNA PORT)	9 dB MAX (WITH 15 dB I.F. N.F.)
I.F. SOURCE IMPEDANCE	50 Ω NOM.

VIEW 1 FRONT  
 WITH 13.31 GHz L.O. INPUT  
 13.31 GHz

C995700 025 A

Figure 30. RF Hardware

For a single pole filter, there is a 90 deg phase shift from 3 db point to 3 db point. If the five section filter is stagger-tuned, then there is a 90 deg shift per filter section; each filter being about 5 MHz in width.

Hence

$$\frac{\Delta \omega}{\Delta \beta} = \frac{2 \pi (5 \text{ MHz})}{\pi/2 \text{ per } .05 \text{ feet}} = 0.05 (20 \times 10^6) \frac{\text{feet}}{\text{sec}}$$

$$V_g = \frac{\Delta \omega}{\Delta \beta} = 10^6 \frac{\text{feet}}{\text{sec}}$$

$$t_d = \frac{0.25}{10^6} = 250 \text{ nanoseconds}$$

For a synchronously tuned filter, there is a 90 deg shift per filter section; each filter being 24.5 MHz in width. Hence

$$\frac{\Delta \omega}{\Delta \beta} = \frac{2 \pi (24.5 \text{ MHz})}{\pi/2 \text{ per } .05 \text{ feet}} = .05 (98 \times 10^6) \frac{\text{feet}}{\text{sec}}$$

$$V_g = 4.9 \times 10^6 \frac{\text{feet}}{\text{sec}}$$

$$t_d = \frac{.25}{4.9 \times 10^6} = 51 \text{ nanoseconds}$$

Rise Time Method

For five single tuned sections, the noise bandwidth is

$$NB = 1.62(B) \text{ 3 db}$$

$$NB = 1.6 (10 \text{ MHz})$$

$$NB = 16.2 \text{ MHz}$$

The integration time is

$$\tau_I = \frac{1}{NB} = 62 \text{ nanoseconds}$$

The rise time is related in integration time by (Tiuri, Page 933)

$$\begin{aligned}t_r &= 2.2 RC \\ \tau_I &= 2 RC \\ t_r &= 1.1 \tau_I = 68 \text{ nanoseconds}\end{aligned}$$

The Radiation Lab Vol. I gives:

$$t_r = \frac{.7}{\Delta f} = \frac{.7}{10 \text{ MHz}} = 70 \text{ nanoseconds}$$

In any case, Millman and Taub relate time delay to rise time by equation 10-16:

$$N = 1.1 \left( \frac{t_d}{t_r} \right)^{1.5}$$

for  $N = 5$  sections

and  $t_r = 68$  nanoseconds

$$\frac{t_d}{t_r} = \left( \frac{5}{1.1} \right)^{.666} = (4.55)^{.666}$$

$$\frac{t_d}{68 \text{ nsec}} = 2.73$$

$t_d = 185 \text{ nanoseconds}$
---------------------------------

The diversity of the above answers is due to the large change of slope (or phase) in the 3 db passband of the filter  $\left( \frac{\Delta \omega}{\Delta \beta} \right)$ . Since these methods used the average slope over the passband, the answers are expected to be somewhat high. If the maximum slope is used, i. e., the signal is centered exactly in the passband, then:

$$t_d = \frac{Sl}{(\Delta \omega / \Delta \beta)_{\max}} = 37 \text{ nanoseconds}$$

Since some mistuning is quite likely (say 1 MHz), a good number to use is 50 nanoseconds.

NOTE: 2/1 passband skirts are not very realistic and probably 4/1 passband skirts shall be used for a 60 db filter. In this case, 40 MHz should have been used instead of 20 MHz. The time delay would be 18.5 nanoseconds.

The laboratory measurements indicated a time delay of 26.5 nanoseconds corresponding to approximately 26 ft. Since there are two of these filter sections in the L.O. path, a physically matched system could contain a 52 ft. electrical mismatch.

The final solution to this problem was obtained by installing an identical filter in the transmitter leg. This provided a good match and readily permitted adjustment by slightly returning any one of the filter sections.

An additional problem associated with the filter is the amplitude versus frequency response. Side bands appearing at  $J_1$ ,  $J_2$ , etc., can be produced either by frequency modulation or by amplitude modulation and it is extremely difficult by observing waveforms on a spectrum analyzer to determine whether a sideband is present because of FM, AM, or some of each. Because AM is difficult to isolate, it is necessary to design the basic system in a manner that will insure low AM characteristics. This is generally accomplished by maintaining broad bandwidth wherever possible. Hard limiting of signals to remove AM components is effective and is used in the transmitter. The SSB filter is the most likely component to introduce objectionable amplitude modulation with the changes in input frequency that occurs in the FM/CW mode. The situation is aided by the balanced mixer that provides approximately 20 db reduction in AM sensitivity of the mixer output with

respect to the L.O. input. During this program it has been found necessary, after bench alignment of the filter for proper bandwidth and minimum amplitude ripple, to slightly readjust the filter tuning while observing the leakage level of the desired sideband. A significant reduction in leakage levels has been obtained in this manner.

2.4.5 Antenna

2.4.5.1 Luneberg Lens

A number of different types of antennas were considered for use with the PTDLR System and a trade-off matrix indicated that a Luneberg lens had the significant advantage of being able to generate multiple, independently-positioned beams from a single lens.

In recent years, dielectric lenses have been employed in microwave systems in increasing numbers as a result of their inherent advantages over older, more conventional antenna devices. The Luneberg lens is an ideal radially-symmetric lens which can be made from plastics or metal-loaded plastic materials. Very efficient artificial dielectrics have recently been contrived and they make possible planar and spherical lenses having the required continuous gradation of refractive index. Typical characteristics are shown in Table 4.

Table 4. Luneberg Antenna Characteristics

Size	15 inch (diameter sphere)
Volume	1730 cubic inches
Weight (includes feeds and switches)	5.0 pounds
Aperture efficiency	> 60 percent
Beamwidth (3 db at 13.3 GHz)	4.1 $\widehat{\text{deg}}$ (one way)
Sidelobe level	< 20 db



During the last decade there have been many attempts to build lens antennas for use at radio-frequencies, and particularly at frequencies in the microwave portion of the spectrum. In 1944 the theory and functional design of a graded dielectric lens were set forth by Luneberg for a radially-symmetric device. The refraction index requirement makes the construction of such a lens for use at optical frequencies virtually impossible. Materials transparent to RF and meeting the needs are available, however, and several techniques have been used successfully in the building of practical lenses.

A dielectric Luneberg lens may take the form of either a cylindrical 2-D lens or a spherical 3-D device. The form it takes depends upon the nature of the focus desired and on the antenna feed configuration. In general, an object at some radius  $R'$  is exactly imaged on the surface of a lens of smaller radius  $R$  as shown in Figure 31. The limiting case where  $R'$  nears infinity is of particular interest. It is a special case of the general theory which predicts a principal focus  $F$  on the lens surface and its conjugate  $F'$  at a point external to the lens and diametrically opposite from  $F$ . When a focus exists an infinite distance from the imaging device, energy radiated from a source at  $F$  will be collimated and plane wave propagation will result. Reciprocally, electromagnetic energy in the form of a plane wave impinging upon the device will be concentrated at  $F$ ; for a cylindrical lens a line focus will result, while for a spherical lens, the focus will exist at a point. For the limiting case, Luneberg has shown that the refraction index,  $\eta$ , of the lens must vary as a function of the radial variable  $\rho$  according to an equation which reduces to

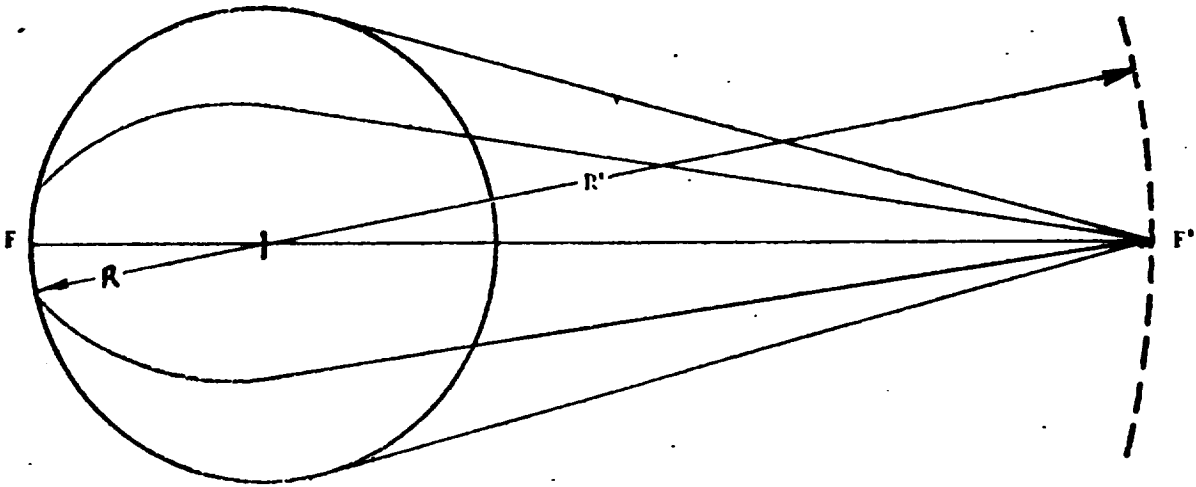


Figure 31. Luneberg Lens Geometry

$$\eta = \sqrt{2 - \left(\frac{\rho}{R}\right)^2}$$

A lightweight low-loss material for this purpose has been used since 1963. It is a precision artificial dielectric made of an array of needle-like metallic particles supported by a low density dielectric material. The particles are insulated aluminum slivers and are less than 1/10 wavelength long. The supporting matrix is a low-loss polystyrene foam similar to Armalite. Figure 32 shows the loss tangent variation over the refraction index range of interest for two low density polystyrene mediums using different size slivers. Table 5 has tabulated typical characteristics of the dielectric materials used for such lens antennas.

A Luneberg lens developed by Armstrong Cork, similar to the purchased lens, is shown in Figure 33 which is 10.5 inches in diameter. This unit, which was tested at 6 GHz, has an electrical diameter of seven wavelengths. The feeds are simple open-ended waveguides. The antenna has an efficiency of 66 percent. Shown in Figure 34 is a typical H plane pattern.

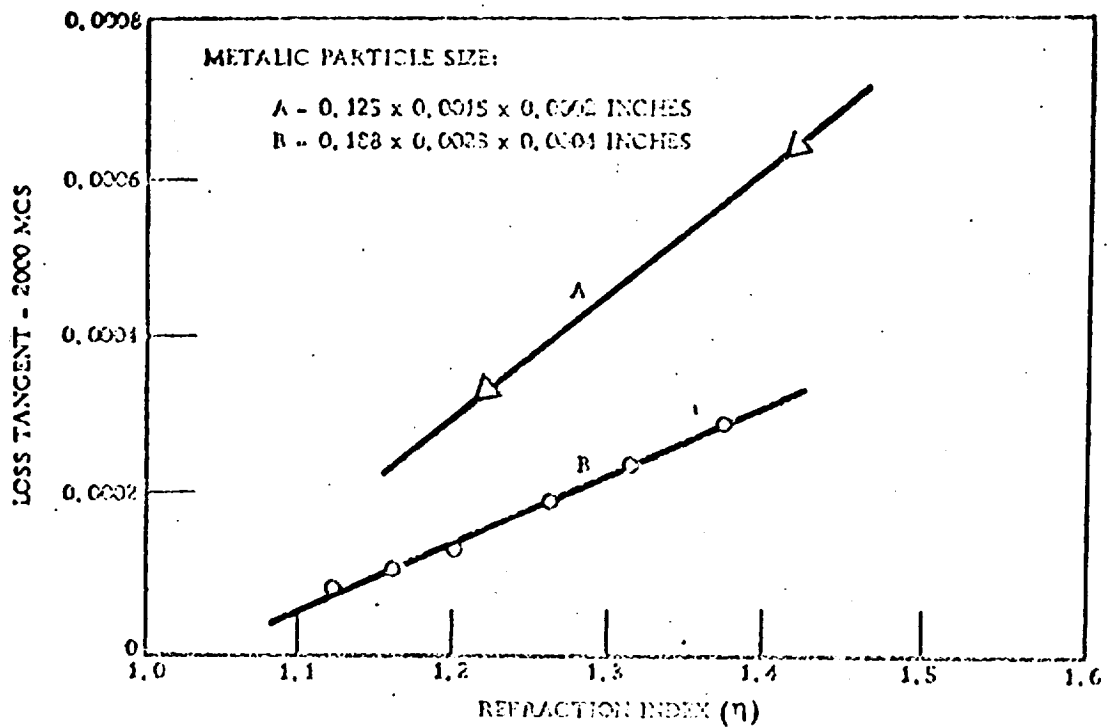


Figure 32. Graph of Loss Tangent as a Function of Refraction Index for Two Low Density Artificial Dielectrics

Table 5. Typical Properties of the Composite Luneberg Lens Medium Used by Armstrong Cork Co.

Density lbs/cu ft	2.5 - 3.5
Flexible Strength, lbs/sq inch	62.3
Modulus of Elasticity, lbs/sq inch	2160
Compressive Strength, lbs/sq inch	35
Tensile Strength, lbs/sq inch	47.8
Non-hygroscopic	
Dimensionally Stable	
Electrically Stable	
Withstands Hard Vacuum	

Table 5. (Continued)

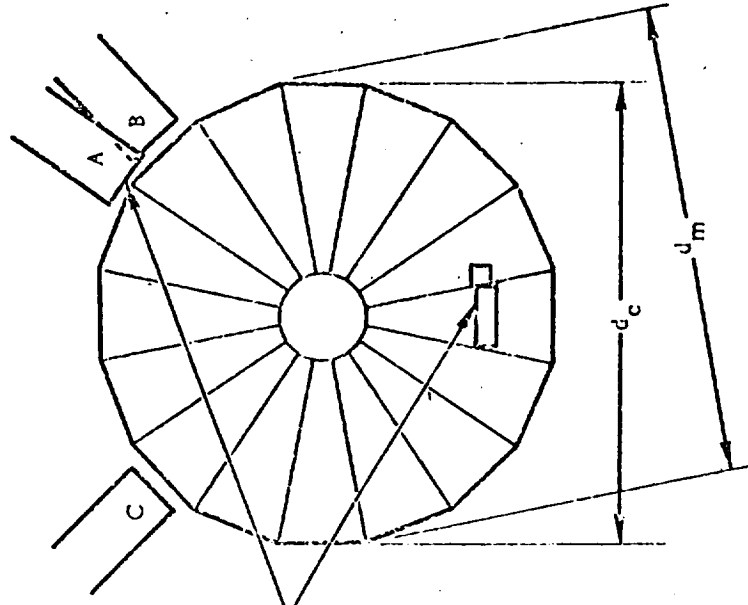
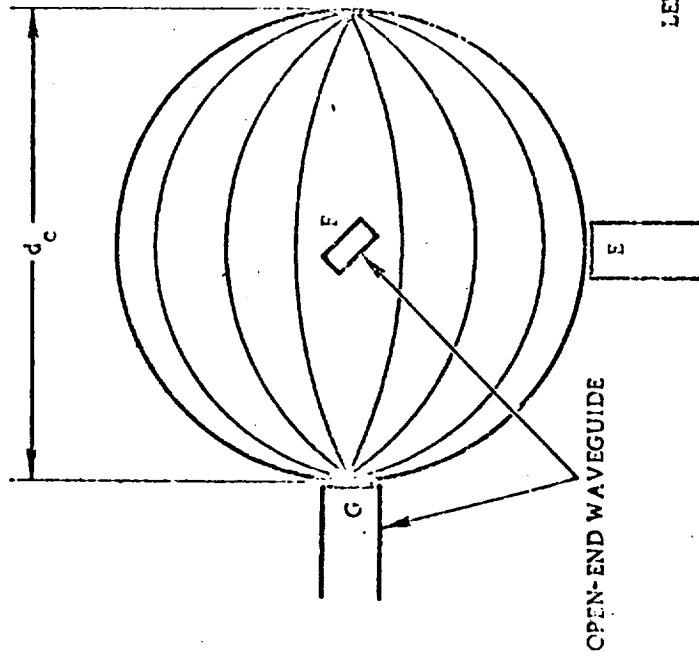
Electrical Stability of Lens Material				
Unit	Original Values		After 1 Year	
	Index	Lens	Index	Loss
1	1.368	0.00027	1.367	0.00025
2	1.361	0.00026	1.38	0.00026
3	1.368	0.00028	1.367	0.00026

Shown in Figure 35 is an H plane pattern using a 12-inch diameter Luneberg lens at 10 GHz with the waveguide feed 3/16 inch away from the lens surface. The primary manufacturers of Luneberg Lenses are Armstrong Cork Co. and Emerson Cummins, Inc.

The lens selected for use in the PTDLR program was purchased from Armstrong Cork Co., and subsequent antenna pattern tests using a variety of feedhorn designs indicated much poorer sidelobe structure than was expected based on the available literature and specifications. Unfortunately, the company discontinued the line shortly after purchase of the lens. Program funding and time schedule did not permit the purchase of a different unit for evaluation.

The antenna patterns taken on the completed assembly are shown as solid lines in Figure 40. Because of the rapid increase in the backscatter coefficient over specular terrain at beam angles approaching zero degrees (perpendicular to the surface), sidelobes in the zero degree region are of particular concern. As seen on the graph, the sidelobes were down at least 40 db (two-way) in the original patterns. The dotted patterns in Figure 40 show a significant deterioration of the beam patterns over a period of one year and four months. The two sets of

H-PLANE PATTERNS - 6.0 Gc  
 1-1/2 X 3/4 OPEN-END WAVEGUIDE PRIMARY ANTENNA  
 FEED RADIUS = 5.3 ± 1/16 INCHES



LENS DIMENSIONS:  
 $d_c = 10.3$  INCHES  
 $d_m = 10.6$  INCHES

FOCAL SPHERE (FEED LOCATION):  
 DIAMETER = 10.6 INCHES

Figure 33. Luneberg 10.5 in. Lens

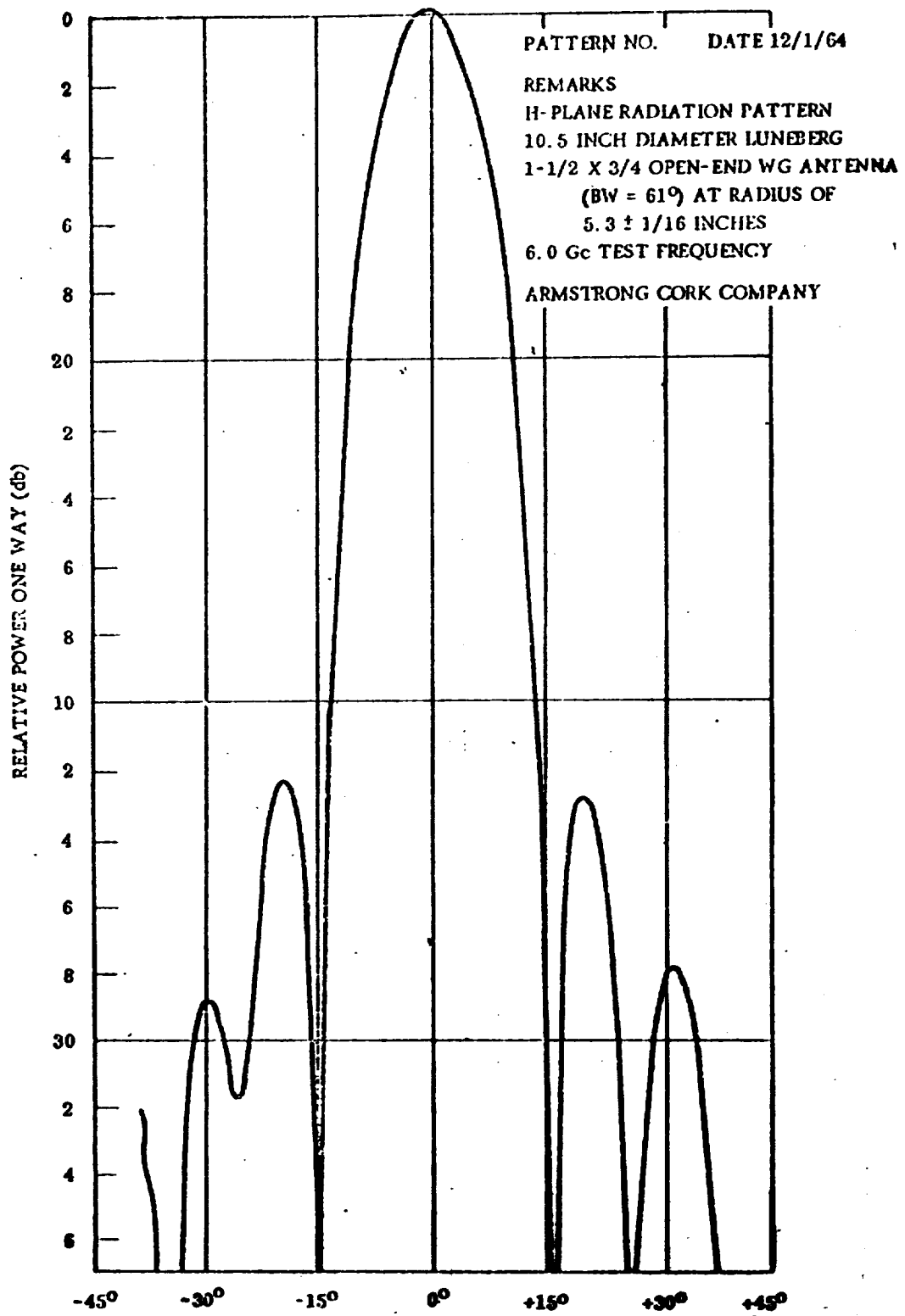


Figure 34. H-Plane Radiation Patterns for 10.5 in. Luneberg Lens

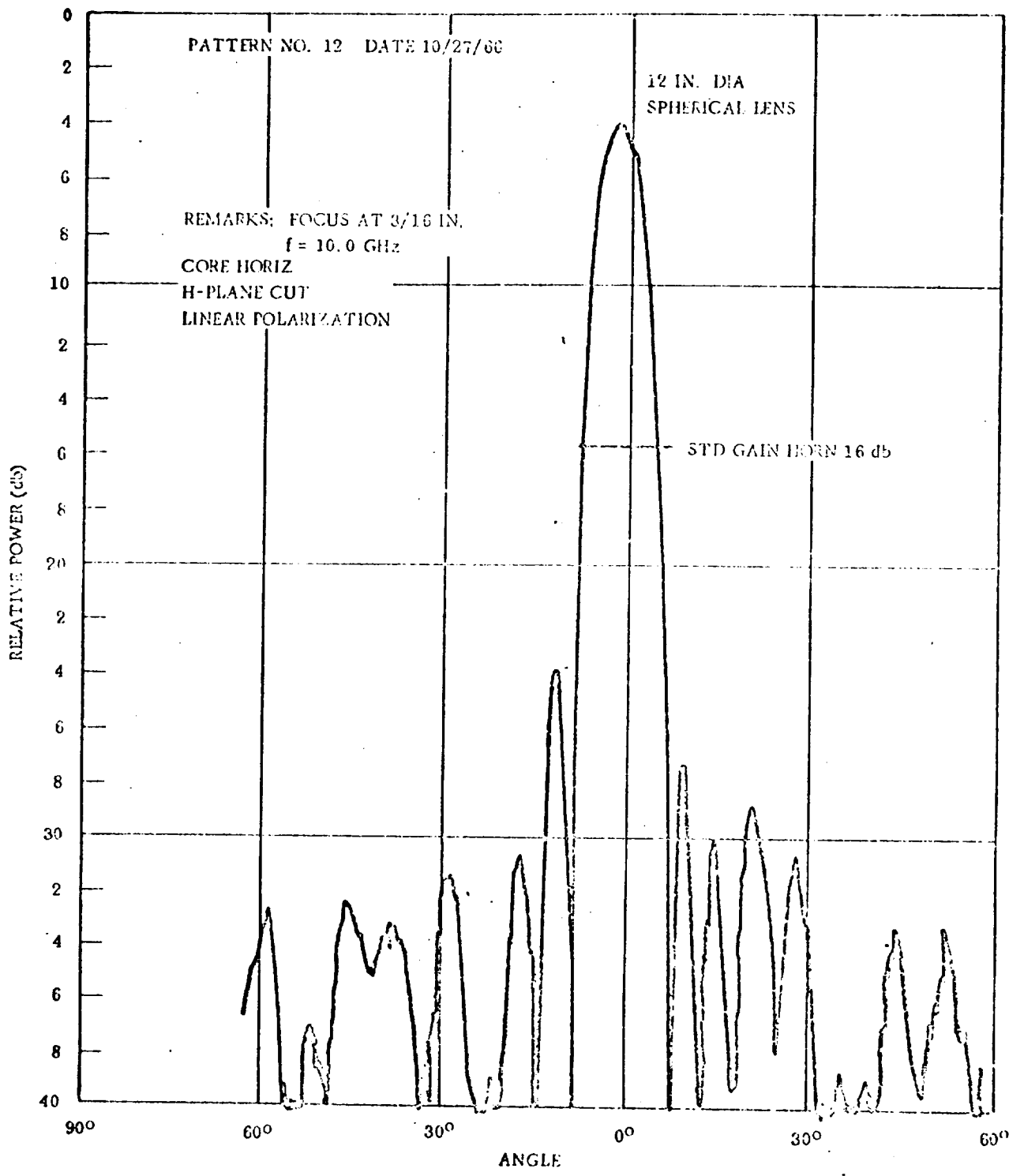


Figure 35. Luneberg Lens Beam Pattern

patterns were obtained from the same antenna assembly at the same antenna range facility and it has not yet been determined what caused the degraded patterns or when the change occurred. If, however, the dotted patterns existed (which is most probable) during the helicopter flight test program conducted September 1969, it would certainly explain the poor system performance obtained.

#### 2.4.5.2

##### Constant K Lens Antenna

The Luneberg Lens was replaced with a constant K multiple beam lens antenna in order to provide better sidelobe suppression. Two identical antennas were fabricated to enable evaluation of the PTDLR system with a single multiple beam antenna concept and a dual multiple beam antenna concept. The PTDLR system with a single multiple beam antenna concept utilizes a common multiple beam antenna for both transmit and receive while the dual multiple beam antenna concept utilizes a separate multiple beam antenna for transmit beams and receive beams. (See Figures 36(a) and 36(b)).

The multiple beam cap constant K lens antenna developed by Autonetics is a modified hemispherical constant K lens. (See Figure 37). A hemispherical constant K lens which can be designed for extreme wide angle scanning ( $>45^{\circ}$ ) has the disadvantage of large volume and weight. For limited scan requirements such as that of the PTDLR, much of the bulk of the lens dielectric can be removed without serious degradation with antenna radiation pattern. A theoretical design analysis and computer program was written to examine the properties of this cap scanning constant K lens.



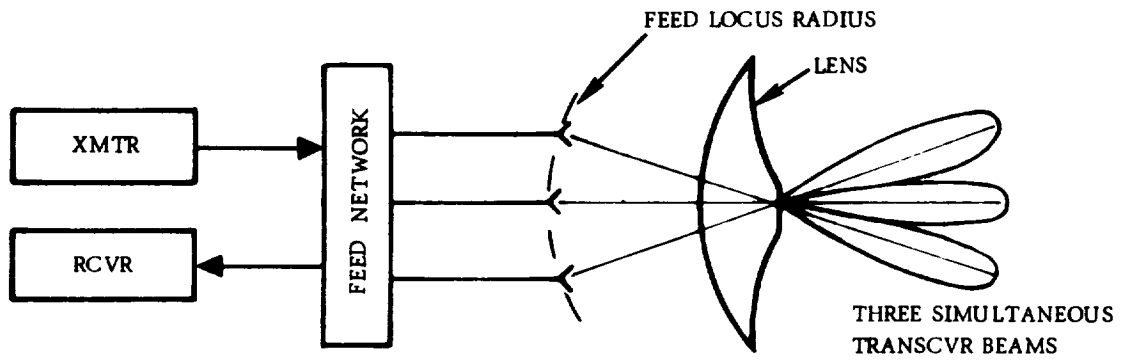


Figure 36(a). PTDLR Single Antenna Concept

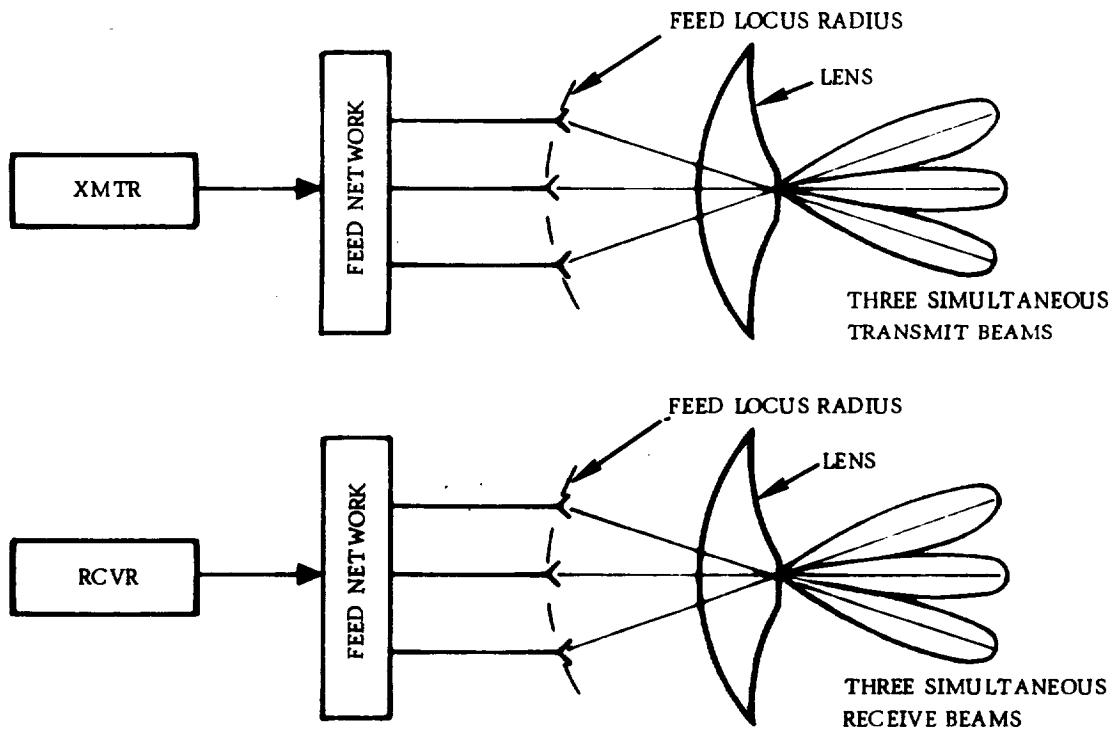


Figure 36(b). PTDLR Dual Antenna Concept

Let  $L_0$  be the reference path from a given horn to the lens aperture (See Figure 38).

$$L_0 = f + \eta \left( R - \sqrt{u^2 + v^2 + [w(u, v)]^2} \right) \quad \text{Eq. 2-1}$$

where:  $f$  = Focal length of lens

$R$  = Dielectric Lens Radius

$\eta$  = Lens Index of Refraction

The path length in any  $\theta$  direction from the given reference horn is:

$$L_1(\theta) = \ell_1 + \eta \sqrt{(A-u)^2 + (B-v)^2 + [f(A, B) - w(u, v)]^2} \quad \text{Eq. 2-2}$$

The normalized path length error is then:

$$SL = \frac{1}{R} (L_1(\theta) - L_0) \quad \text{Eq. 2-3}$$

The phase errors across a planar aperture (X-Y plane) can be examined by setting  $f(A, B) = 0$  and  $w(u, v) = 0$ . Equation 2-3 then can be reduced to:

$$\delta L = \frac{1}{R} \left[ \ell_1 + \eta \sqrt{(A-u)^2 + (B-v)^2} - f + \eta (R - \sqrt{u^2 + v^2}) \right] \quad \text{Eq. 2-4}$$

Equation 2-4 was evaluated on the computer using input parameters  $\eta, \psi, R$  and  $U$ . The thickness of the lens is zero when  $U = R$  and the thickness is equal to  $R$  when  $U = 0$ . Constraints on the analysis were dielectric constant less than 3.0, aperture size, and total lens depth. Equation 2-4 was then iterated for maximum  $U$  with allowable aperture phase error after correction.

The results of the analysis are shown in Figure 39. Using  $\epsilon = 4.0$ , lens radius of 19.0 inches focal length of 19.0 inches, and lens thickness of 3.0 inches, a Schmidt corrected aperture with maximum phase error of less than 0.1 wavelengths was achieved for all scan positions.

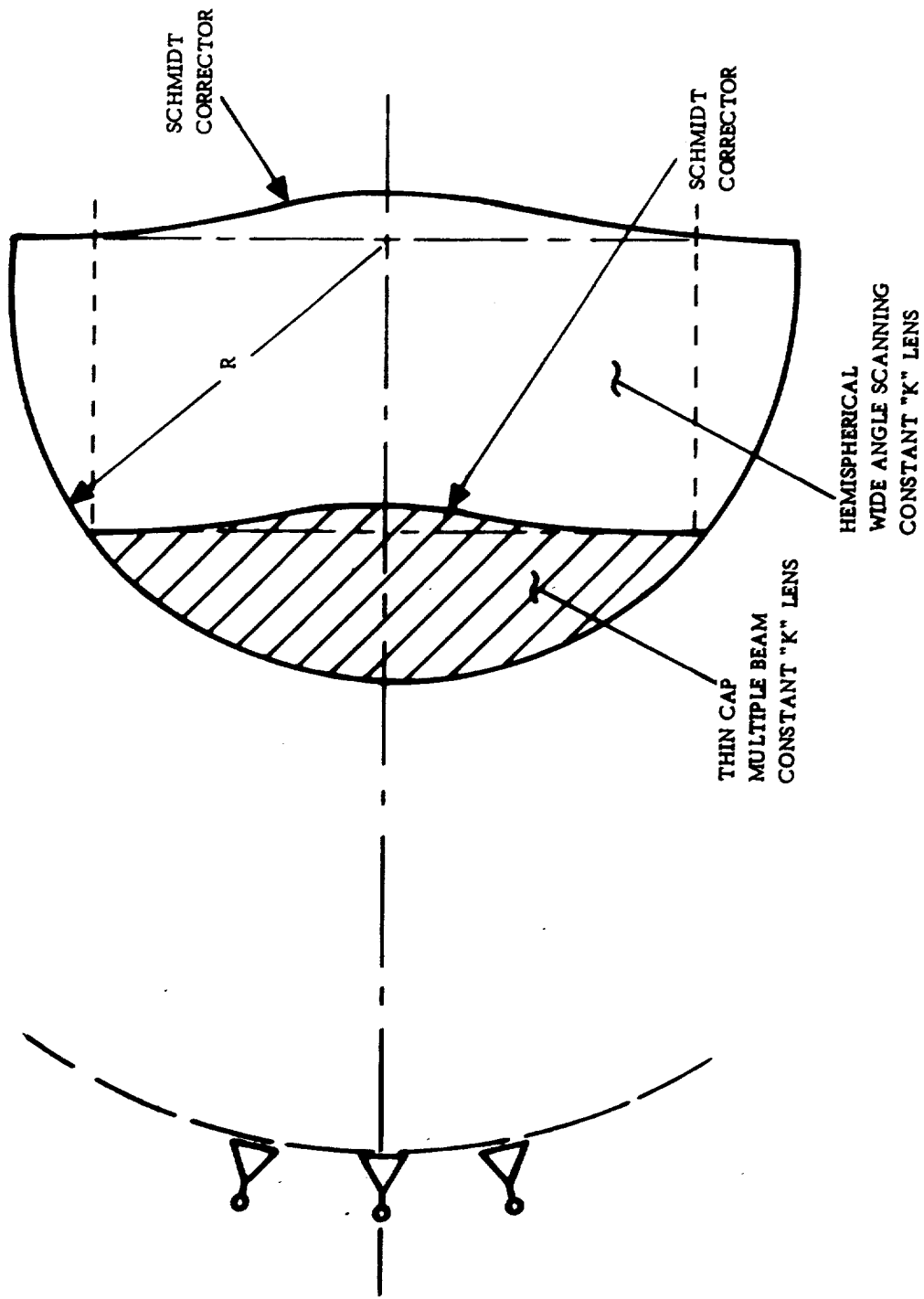


Figure 37. Physical Comparison of Geometrical Properties of Conventional Hemispherical Scanning Lenses with the Thin Cap Multiple Beam Constant "K" Lens

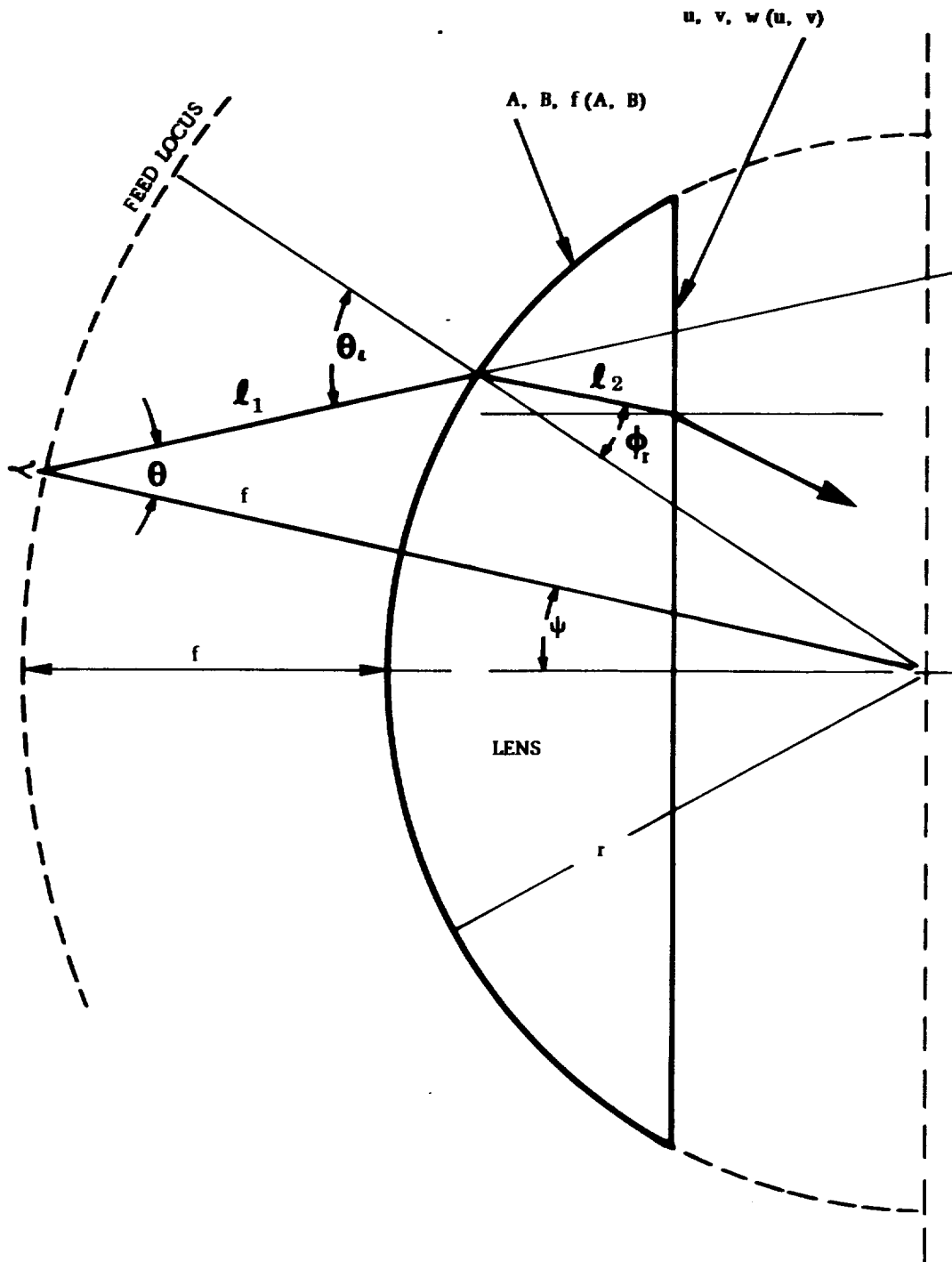


Figure 38. Constant "K" Cap Lens Geometry

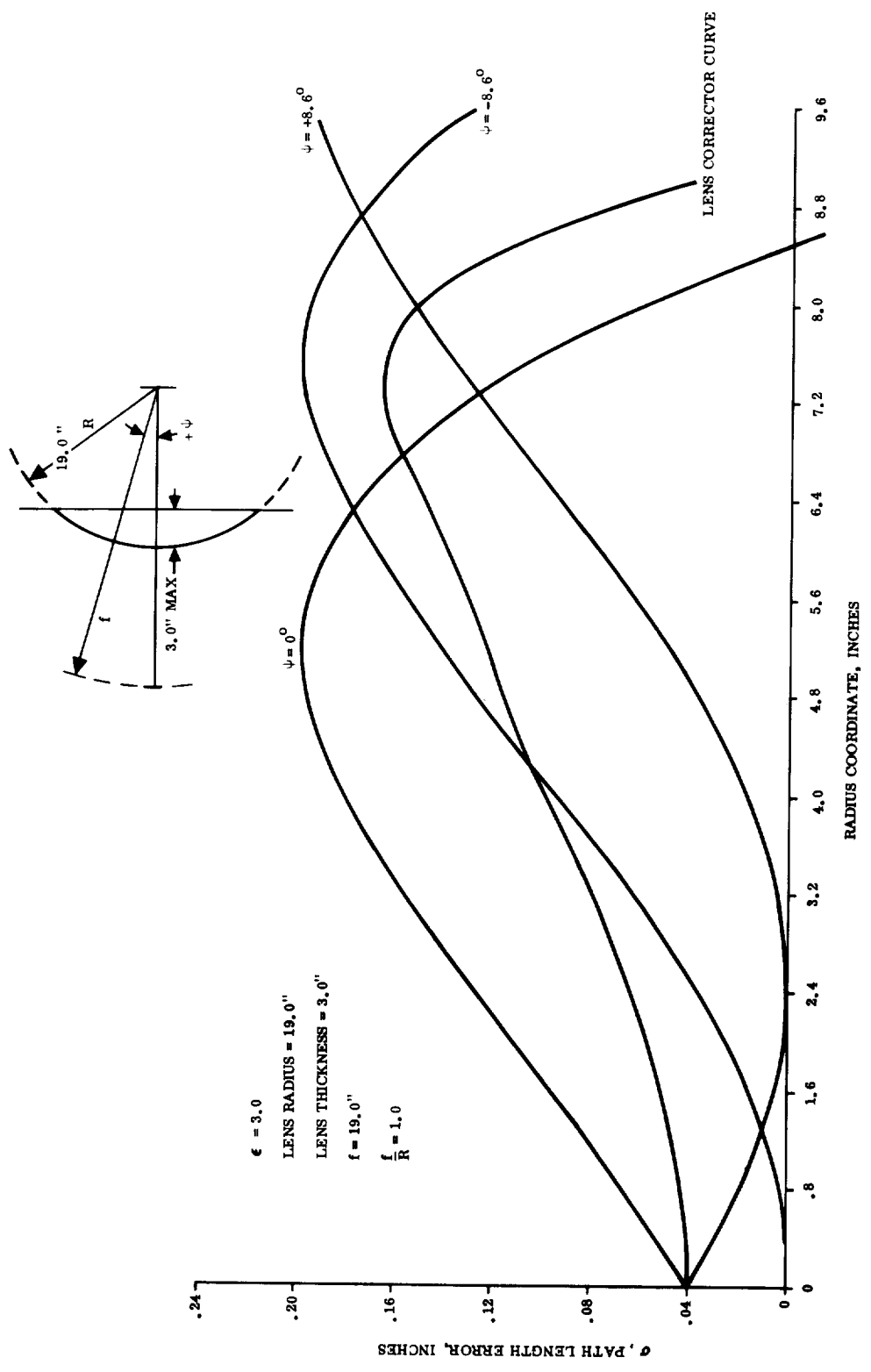


Figure 39. Aperture Phase Correction as a Function of Lens Radius

A total of 82 percent of the aperture could be utilized in the extreme scan position.

Beam patterns of the flight tested constant K antenna are shown in Figure 40. A significant sidelobe reduction over the Luneberg lens can be observed and approaches 70 db (two way) near the zero degree region. During the most recent flight test even over highly specular surfaces (ocean at Beaufort sea state 0-1) no noticeable sidelobe return was observed. The small spurious lobe appearing at approximately the image angle did produce beam-to-beam coupling. The spurious lobe appeared to be due to reflections from the lens mounting ring. Subsequent placement of absorbing material on this surface reduced the lobe to approximately -36 db. Further effort could probably eliminate it completely.

Table 6 shows the sidelobe improvement obtained by comparing the antenna patterns of the constant K with both sets from the Luneberg Lens.

Table 6. Sidelobe Improvement

<u>Degrees from Main Beam</u>	<u>Luneberg Lens</u>		<u>Constant K Lens</u>	<u>2 Way Improvement</u>	
	<u>Old Pattern</u>	<u>New Pattern</u>		<u>Old</u>	<u>New</u>
2	-3	-3	-2.5	-1	-1
4	-14	-8	-8.8	-10.4	-1.6
6	-18	-10.5	-20	+4	+19
8	-20	-12	-23	+6	+22
10	-21.5	-14	-25	+7	+22
12	-22	-16.5	-30	+16	+29
14	-23	-18	-31.5	+17	+27
16	-24	-19	-33.5	+19	+29

Table 6. (Continued)

<u>Degrees from Main Beam</u>	<u>Luneberg Lens</u>		<u>Constant K Lens</u>	<u>2 Way Improvement</u>	
	<u>Old Pattern</u>	<u>New Pattern</u>		<u>Old</u>	<u>New</u>
18	-25.5	-20.5	-35	+23	+29
20	-28	-22.5	-36	+16	+27

The last two columns tabulate the increased discrimination against sidelobe return expected by use of the constant K lens.

#### 2.4.6 Receiver Design Considerations

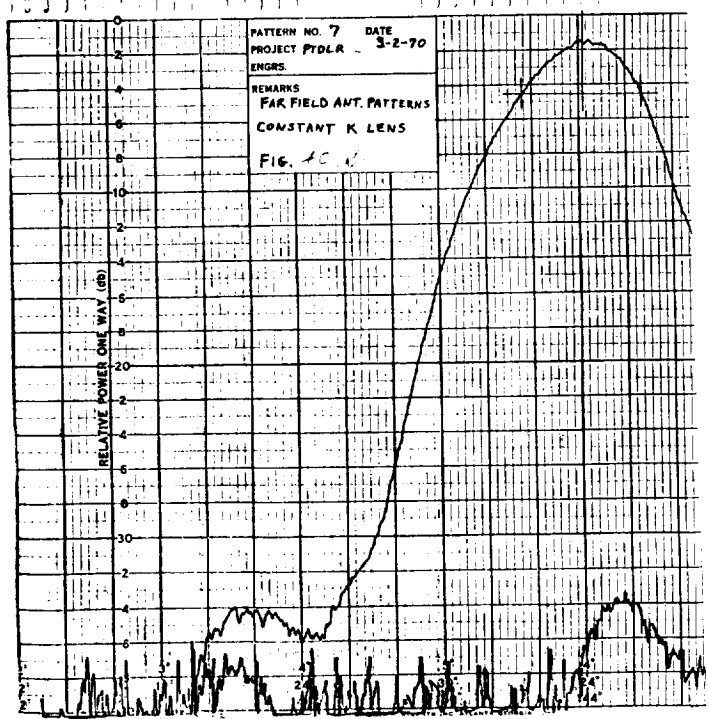
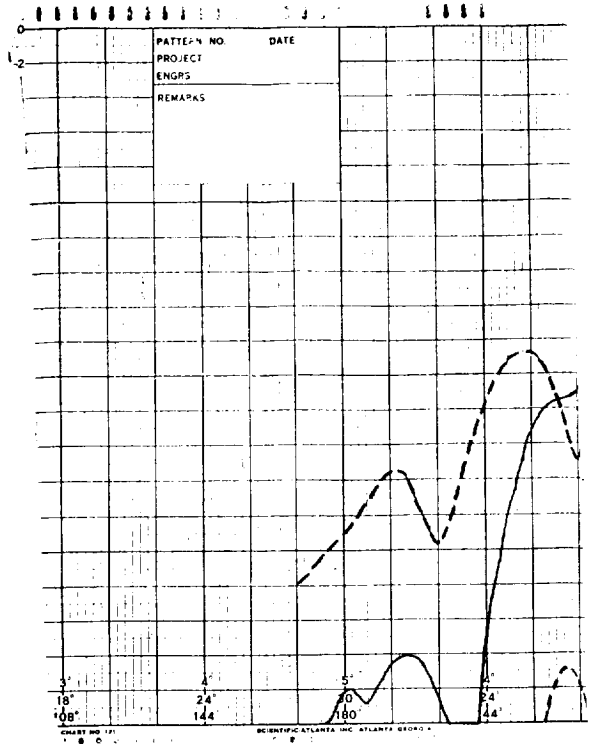
##### 2.4.6.1 FM/CW Bessel Sideband Mode

The frequency modulating signal applied to the transmitter and the L.O. generates a number of sidebands appearing at the mixer output simultaneously. These signals arrive at the mixer via two paths: a leakage path normally occurring as a result of an antenna mismatch or less than perfect port-to-port circulator isolation; and the desired path of receiving the reflected transmitter power from ground objects via the antenna. Of all the signals appearing at the mixer output, only one (two in the altitude channel) is used to measure doppler shift (or altitude) and the remaining signals are filtered out. Received signal as a function of Bessel sideband and range is shown in Figure 41.

Particular attention must be given to the distribution of gain in the receivers to insure that receiver saturation, with the attendant small signal suppression, does not occur. The general gain distribution requirements are determined from a knowledge of the sideband to be used, modulation index, leakage path magnitude, various sideband amplitude relationships, and rejection capabilities of typical crystal filters. An example of the required operating levels and gain distributions of the receiver chain is shown in Figures 42 and 43, and Tables 7,







FOLDOUT FRAME /

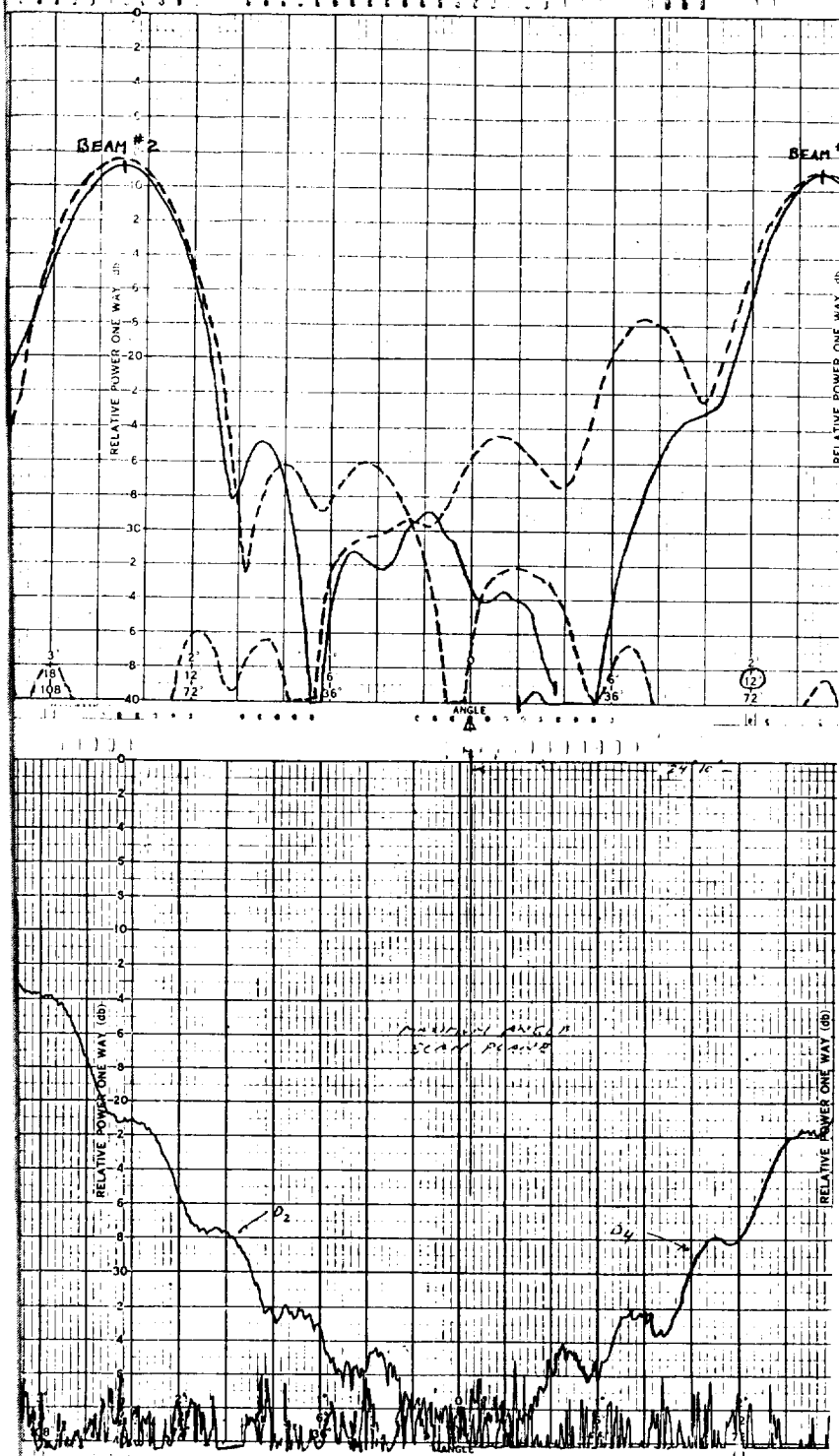
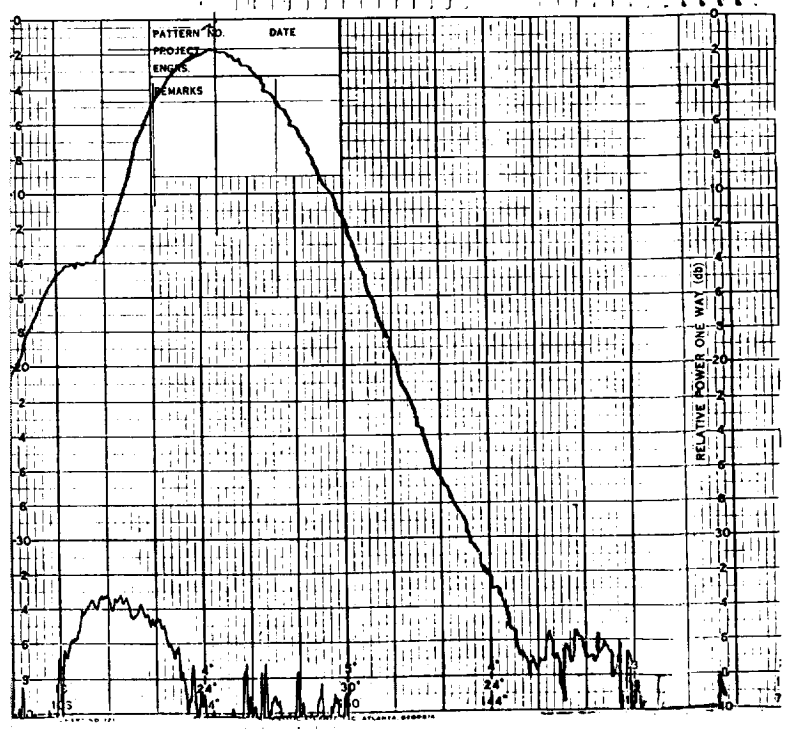
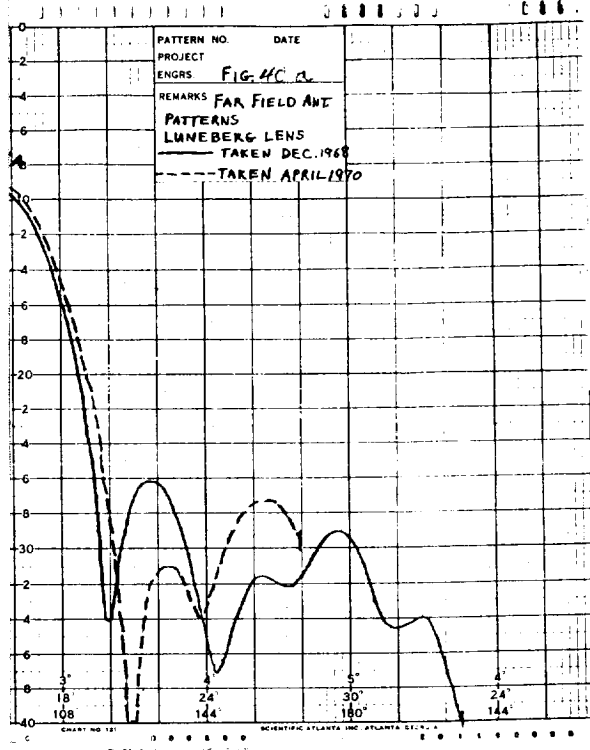


Figure 40. A



Antenna Beam Patterns

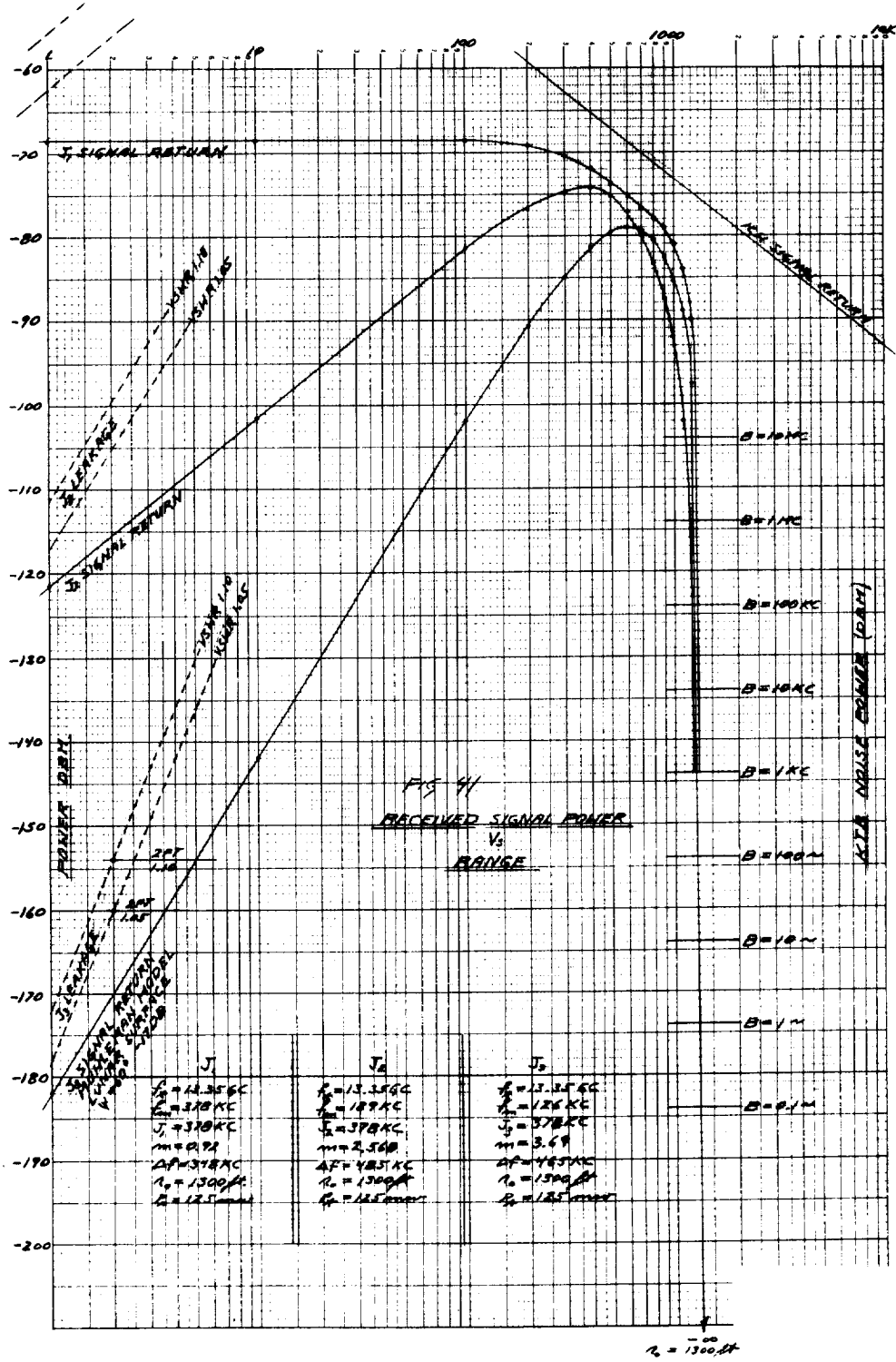


Figure 41. Received Power vs. Range

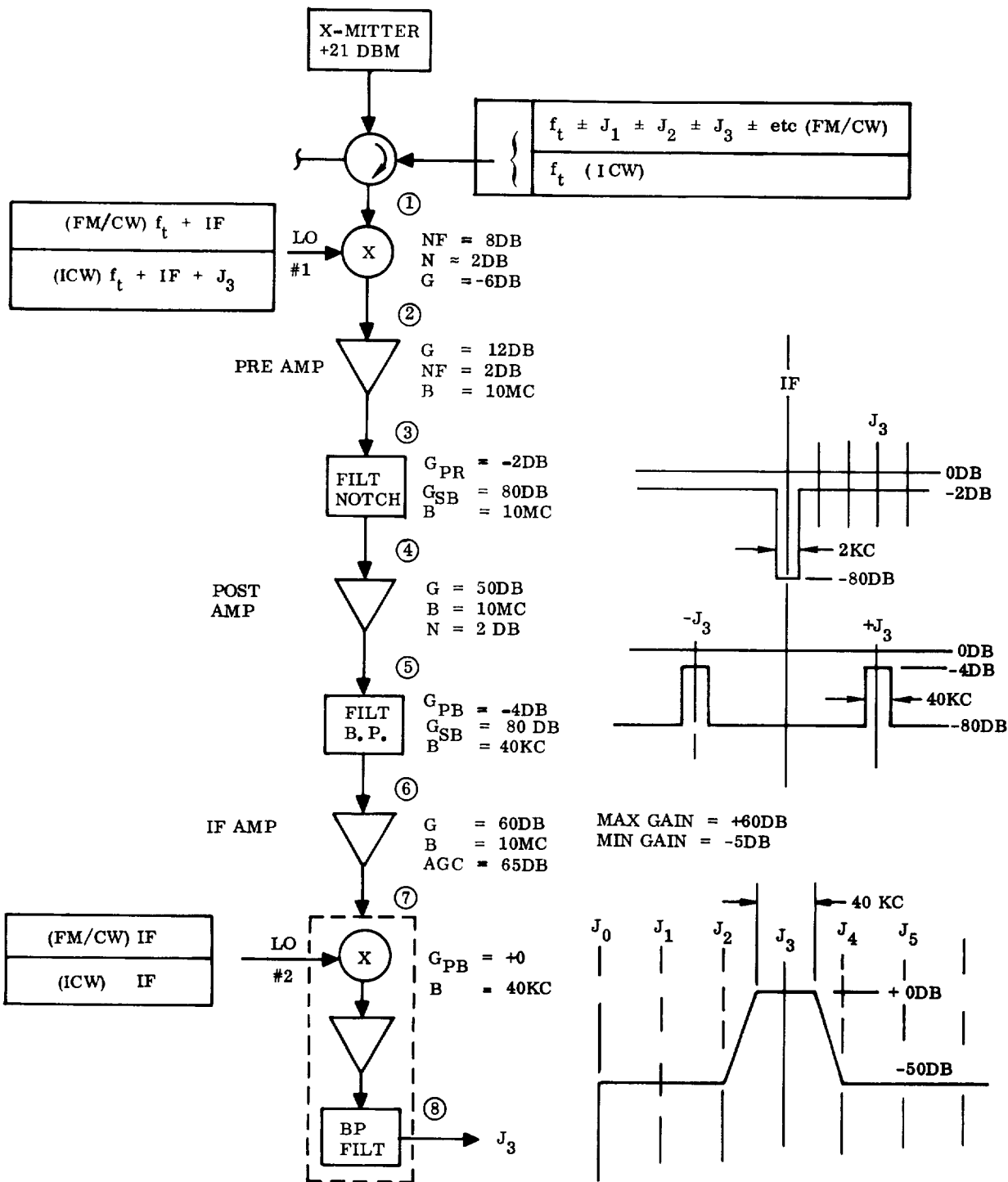


Figure 42. FM/CW Altitude Channel Gain Distribution

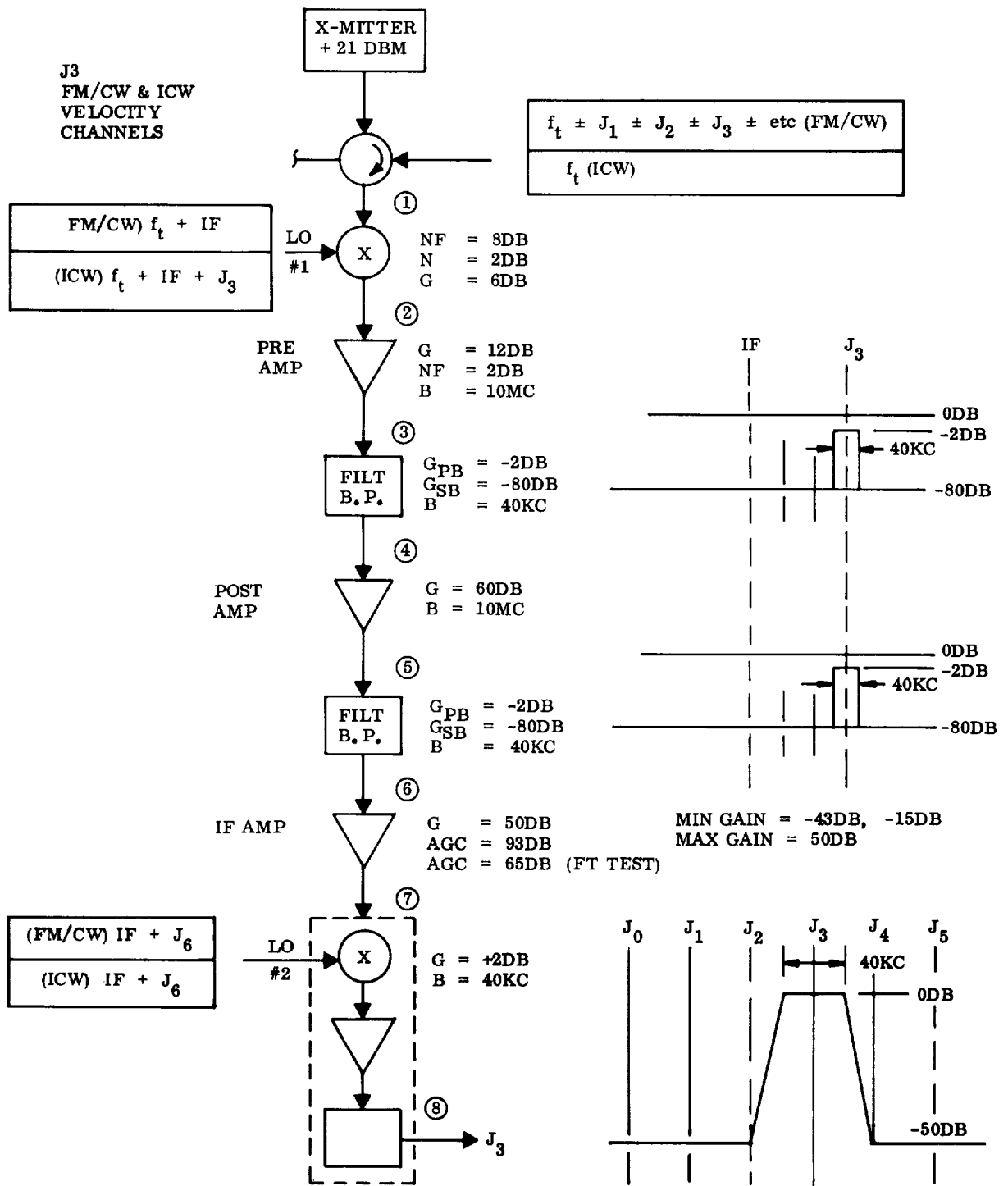


Figure 43. FM/CW Velocity Channel Gain Distribution

Table 7. FM/CW Altitude Channel Signal Levels

Sideband	Signal Points	1 DBM	2 DBM	3 DBM	4 DBM	5 DBM	6 DBM	7 DBM	8 DBM
J <sub>0</sub>	Leakage (30db Isol)	-9							
	1.1 VSWR (l = 2 ft)	-5	-11	+1	-79	-29	-129	-69	-119
J <sub>3</sub>	Min								
	Rough H <sub>2</sub> O @20 ft	-130	-136	-124	-126	-76	-80	-20	-20
	Max								
J <sub>1</sub>	Forrest @650 ft	-65	-71	-59	-61	-11	-15	-20	-20
	Leakage l = 2 ft	-150	-166	-154	-156	-106	-110	-115	-115
J <sub>1</sub>	Max 300 ft	-54	-61	-48	-50	-	-80	-20	-70
J <sub>2</sub>	Max 500 ft	-59	-65	-53	-55	-5	-85	-25	-75
J <sub>9</sub>	Max 1200 ft	-152	-159	-146	-148	-98	-178	-118	-168
Noise	KTB	-144/KC	-142/KC	-128/KC	-130/KC	-80/KC	-61/80KC	-1/80KC	+2/40KC -63/40KC
	Transmitter	-113/KC							

20 ft	S/N = 22db	S/L = +30	S/J <sub>1</sub> = +50db
650 ft	S/N = +43db	S/L = +95	S/J <sub>1</sub> = +115db

8, and 9 for the  $J_3$  case using known PTDLR parameters. No change was made in the receiver chain when evaluating system performance in the  $J_1$ ,  $J_2$ , or  $J_3$  Bessel sideband mode. This was accomplished by selecting the appropriate modulation crystal frequency such that the desired sideband ( $J_1$ ,  $J_2$ , or  $J_3$ ) at IF is maintained at 60.378 MHz and is thereby passed through the relatively narrow band (40 KHz) receiver chain;

#### 2.4.6.2 Pre-Amplifier

The pre-amplifier uses a low noise FET in a standard neutralized amplifier circuit. The unit is designed to provide a good match to the mixer output impedance and also provides a 50 ohm-output impedance to properly match the crystal filter input impedance. A nominal power gain of 15 db is produced over a bandwidth of approximately 15 MHz with a noise figure of 1.6 db.

Gating circuitry is provided in the source lead to gate the amplifier off during the ICW transmit period, turn it back on during the ICW receive interval, and maintains the amplifier in the "ON" position in the FM/CW mode of operation. The required waveform at the input to the gating amplifier is, therefore, a square wave switching between +12 volts and ground when in the ICW mode with the +12 volt portion of the square wave occurring during the receive interval. When operating in the FM/CW mode, a constant +12 volt DC level is applied to the gate input. A schematic of the pre-amplifier is shown in Figure 44.

#### 2.4.6.3 Crystal Filters

As discussed in Section 1.3, the crystal filtering is required to select the desired sideband from a number of sidebands appearing at



Table 8. FM/CW Velocity Channel Signal Levels ( $J_3$  Worst Case)

Sideband	Signal Points	1 DBM	2 DBM	3 DBM	4 DBM	5 DBM	6 DBM	7 DBM	8 DBM
$J_0$	Leakge (30db Isol)	-9							
	1.1 VSWR ( $l = 2$ ft)	-5	-11	+1	-79	-19	-99	-49	-97
$J_3$	Min (Still H <sub>2</sub> O @20ft)	-158	-164	-152	-154	-94	-96	-46	-44
	Max (Forrest @650ft)	-75	-71	-59	-61	-1	-3	-46	-44
	Leakage ( $l = 2$ ft)	-160	-166	-154	-156	-96	-98	-48	-46
$J_1$	Max (300 ft)	-54	-60	-48	-238	-68	-148	-98	-136
$J_2$	Max (500 ft)	-59	-65	-53	-133	-73	-153	-103	-151
$J_9$	Max (1200 ft)	-152	-159	-146	-226	-166	-246	-196	-244
Noise	KTB	-144/KC	-142/KC	-128/KC	-110/KC	-50/40KC	-52/KC	-2/40KC	0/40KC
	Transmitter	-113/KC							-93/40KC

20 ft	S/N = -44db	S/L = +2db
650 ft	S/N = +49db	S/L = +99db

Table 9. FM/CW Velocity Channel Signal Levels ( $J_3$  Nominal Case)

Sideband	Signal Points	1 DBM	2 DBM	3 DBM	4 DBM	5 DBM	6 DBM	7 DBM	8 DBM
$J_0$	Leakage (30 db Isol)	-9							
	1.1 VSWR $\ell = 2$ ft	-5	-11	+1	-79	-19	-99	-49	-99
	Min ( $\alpha = 30^\circ$ ) Rough $H_2O@20$ ft Max ( $\alpha = 90^\circ$ ) Forrest @650 ft	-130	-136	-124	-126	-66	-68	-18	-18
$J_3$	Leakage $\ell = 2$ ft	-65	-71	-59	-61	-1	-3	-18	-18
		-160	-166	-154	-156	-96	-98	-48	-48
$J_1$	Max (300 ft)	-54	-60	-48	-128	-68	-148	-98	-148
	Max (500 ft)	-59	-65	-53	-133	-73	-153	-103	-153
$J_9$	Max (1200 ft)	-152	-159	-146	-226	-166	-246	-196	-246
	KTB	-144/KC	-142/KC	-128/KC	-104/ 40KC	-44/40KC	-46/40KC	+4/40KC	+9/40KC -61/40KC
Noise	Transmitter	-113/KC							

20 ft    S/N = -22db    S/L = +30db  
650 ft    S/N = +43db    S/L = +95db

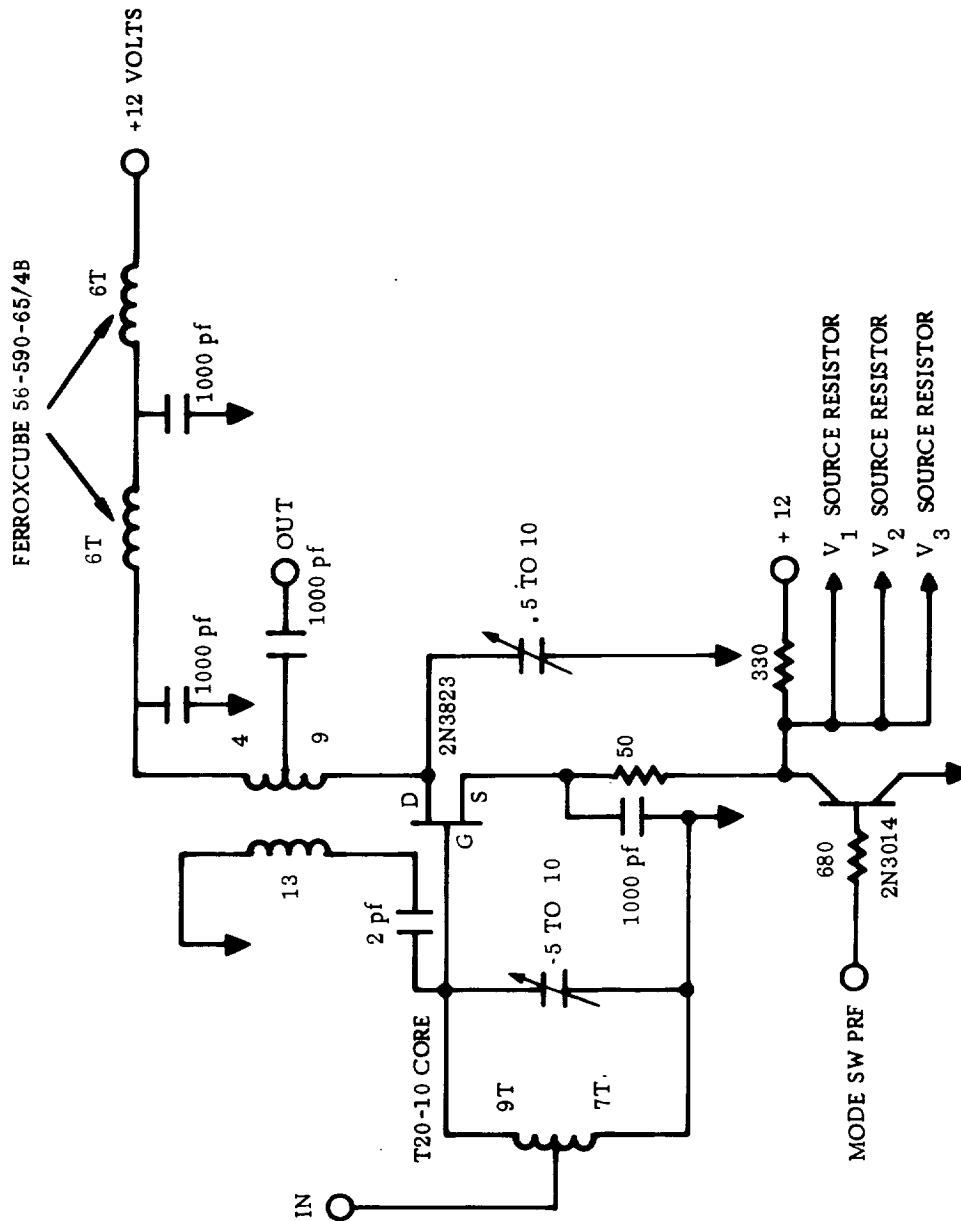


Figure 44. Preamplifier Schematic

the mixer output. The minimum bandwidth of the filters is set by the maximum doppler shifts that occur with a system design goal of 680 ft/sec maximum vehicle velocity. With a doppler sensitivity of approximately 27 Hz/ft/sec, the doppler shift will be  $\pm 18.36$  KHz. The resultant minimum bandwidth is therefore approximately 37 KHz. The specified -3 db bandwidth was increased to 45 KHz to insure relatively flat response over all expected values of doppler shift.

Specifications to the supplier, McCoy Electronics Co., Mt. Holly Springs, Pa., for the velocity channel crystal filter units were as follows:

#### PASS BAND FILTER 121B14

##### Electrical

##### I. Pass Band

- A. Center Frequency 60.378 MHz
- B. TOL  $\pm 0.001\%$  from  $0^{\circ}$  to  $50^{\circ}$ C
- C. 3 db B.W. 45 KHz (min)
- D. 60 db B.W. 120 KHz (max)
- E. Ripple  $\pm 0.5$  db
- F. Insertion loss 2 db max
- G. Impedance 50 ohms in and out

##### II. Stop Band

- A. Attenuation - 80 db min
- B. Spurious - 20 db min except on multiples of 126 KHz from center frequency and through B.W. of 40 KHz surrounding these multiples which must be -40 db (min). Attenuation must be -80 db (min) at 60.0000 MHz through  $\pm 20$  KHz.

## Mechanical

- A. Connector in and out OSM
- B. Case size 2-3/8 x 1 x 1-1/32

Two identical filters are used in each velocity channel. One is placed between the pre-amplifier and the first post-amplifier and the second filter is inserted between the first post-amplifier and the second post-amplifier. The velocity receiver channels, as implemented, are used without change for amplifying the signal returns in the FM/CW mode and in the ICW mode.

## NOTCH FILTER 121B16

### Electrical

#### I. Stop Band

- A. Center Frequency: 60.000 MHz
- B. TOL  $\pm 0.001\%$  from  $0^{\circ}$  to  $50^{\circ}\text{C}$
- C. 3 db bandwidth: 50 KHz  $\pm 25$  KHz max (inverted)
- D. 60 db bandwidth: 10 KHz  $\pm 5$  KHz min (inverted)
- E. Ripple  $\pm 0.5$  db
- F. Attenuation: 80 db min

#### II. Pass Band

- A. Insertion loss: 2 db max
- B. Within  $\pm 0.25$  db max gain variation in the 45 KHz bandwidth centered at 59.6220 MHz and 60.378 MHz.  
No spurious response in these critical regions.
- C. Spurious:  $\pm 20$  db max either side of critical regions.
- D. Ripple:  $\pm 0.25$  db

### III. Phase

- A. Phase track through critical region to within  $\pm 0.25^\circ$  centered at 59.6220 MHz and 60.378 MHz.

### IV. Mechanical

- A. Hermetic Seal
- B. Connectors: OSM
- C. Vibration: MIL 202
- D. Size: 1" x 1-1/32" x 2-3/8"

#### PASS BAND FILTER 121B10

### Electrical

#### I. Pass Band

- A. Center frequency 59.6220 MHz and 60.3780 MHz
- B. TOL  $\pm 0.001\%$  from  $0^\circ$  to  $50^\circ\text{C}$
- C. 3 db B.W. 45 KHz min
- D. 60 db B.W. 120 KHz max
- E. Ripple  $\pm 0.5$  db max
- F. Insertion loss 4 db max
- G. Impedance 50 ohms in and out

#### II. Stop Band

- A. Attenuation -80 db min
- B. Spurious -20 db min except on multiples of 126 KHz from center frequencies and through bandwidths of 40 KHz surrounding these multiples which must be -40 db min. Each filter section must have -80 db attenuation at 60.0000 MHz through  $\pm 20$  KHz. For a total attenuation of -160 db at 60 MHz.

### III. Phase

- A. Each pass band must phase track to  $\pm 2^\circ$  about the center frequencies.

#### Mechanical

- A. Connector in and out OSM
- B. Size 1-3/4 x 2-1/4 x 5/8
- C. Both filters to be in same housing

It can be seen that the filter requirements for the FM/CW altitude channel are considerably different from the velocity channel requirements. This is because both the upper and lower sideband (e.g.,  $\pm J_2$ ) must be passed by the altitude channel receiver.

In addition passing the two desired sidebands and rejecting all other signals, the filters must not modify the net differential phase shift between the two signals. This requires the specification for phase tracking of the notch filter and the dual filter over the design range of expected doppler shifts. A second dual filter could be used in the receiver chain to replace the notch filter, however, a notch filter is easier to fabricate and the phase tracking characteristics within the frequency bands of interest are inherently better, and a notch filter meets the filter requirements at the point it is placed in the receiver chain.

The crystal filters supplied by the vendor generally met the specifications with the exception of insertion loss. The insertion loss specifications were established by telephone conversations with the vendor prior to placement of the order. The receiver gain distribution was made using the specified insertion loss figures. The received

units measured 6 - 8 db greater insertion loss than expected and resulted in a somewhat poorer receiver noise figure. Increased pre-amplifier gain would improve the noise figure.

#### 2.4.6.4

#### Post Amplifiers

Five individual receiver chains have been used in the PTDLR system to satisfy the IF gain bandwidth requirements for three independent velocity (doppler) beam processing; FM/CW altitude channel processing; and ICW altitude channel processing. A reduction in the number of receivers could be made with some compromise in performance. Except for different band shaping requirements (performed by insertion of crystal filters at the appropriate points), all of the post amplifiers can be made identical. This is generally the case, except that the second post amplifiers in the velocity channels and FM/CW altitude channel also includes a phase detector and amplifier and the second post amplifier in the ICW channel additionally incorporates a video detector, amplifier, and low impedance line driver.

The IF amplifier sections are straight-forward designs utilizing a relatively low noise transistor input stage driving three substantially identical, cascaded integrated circuit amplifiers. Each stage provides a nominal gain of 16 db producing a total input-to-output gain of approximately 65 db. The -3 db bandwidth is 5 MHz centered at 60 MHz. AGC of greater than 50 db for each post amplifier (> 100 db per receiver chain) is produced by varying the effective bypassing of the auxiliary input of each of last three stages. The amount of bypassing is proportional to the impedance of the diode in series with the 0.001  $\mu$ fd bypass capacitor. The forward diode impedance is conveniently varied by simply changing the current through the diode by way of the AGC bus.



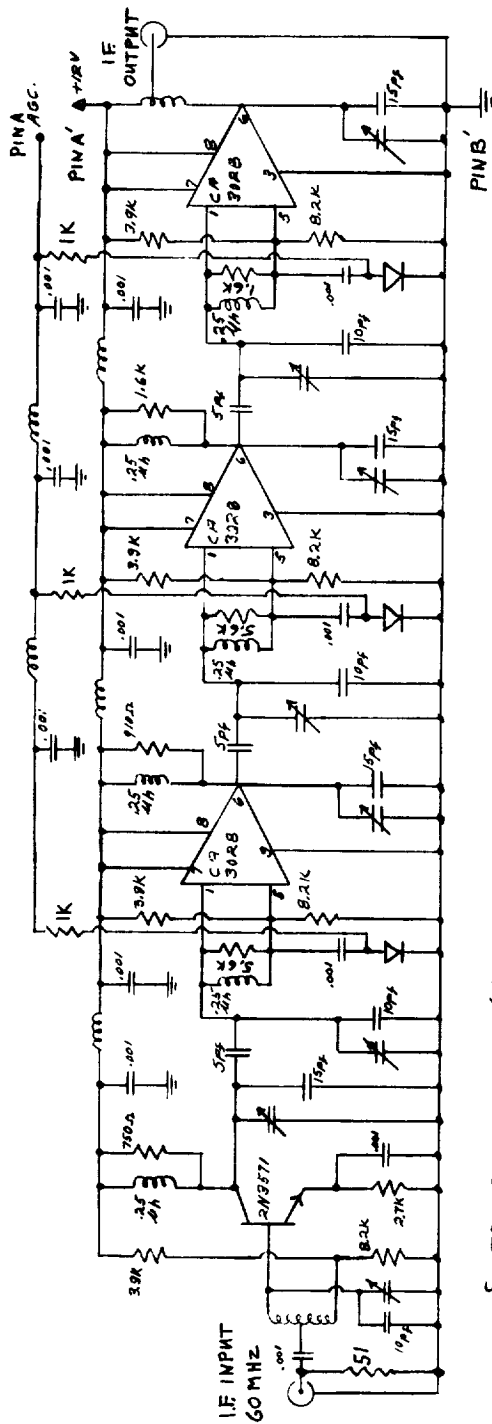
The phase detectors, video detectors, and video amplifiers are standard textbook varieties and need no discussion.

A schematic of the IF post amplifiers with or without phase detection, etc., is shown in Figure 45.

#### 2.4.6.5 Automatic Gain Control

A wide variation in the received signal power occurs during normal flight due to variations in the back-scatter coefficient with different types of terrain and variations in aircraft altitude and attitude. An automatic gain control (AGC) amplifier has been included in each of the five receiving channels to maintain the signal level at a relatively constant value at the post amplifier output. The basic AGC action is mechanized by envelope detecting the receiver output signal which is then compared with the desired preset level (d-c bias). If a difference in the two levels exists, an error signal is formed.

The error signal is amplified in a single stage high-gain amplifier-integrator followed by an emitter follower. This output signal is applied to the AGC bus of the IF post amplifiers and results in a change in overall receiver gain in the proper direction to null the error signal. A schematic of the AGC amplifiers is shown in Figure 46. It will be noted that the FM/CW altitude channel AGC amplifier and the ICW altitude channel AGC amplifier have an additional "mode" input. This signal turns off the unused altitude channel as a function of the operating mode.



SYSTEM CONTAINS FIVE (5) UNITS AS ABOVE; FOUR WITH OUTPUT STAGE MODIFIED TO INCLUDE PHASE DETECTOR SHOWN BELOW; ONE WITH AMPLITUDE DETECTOR

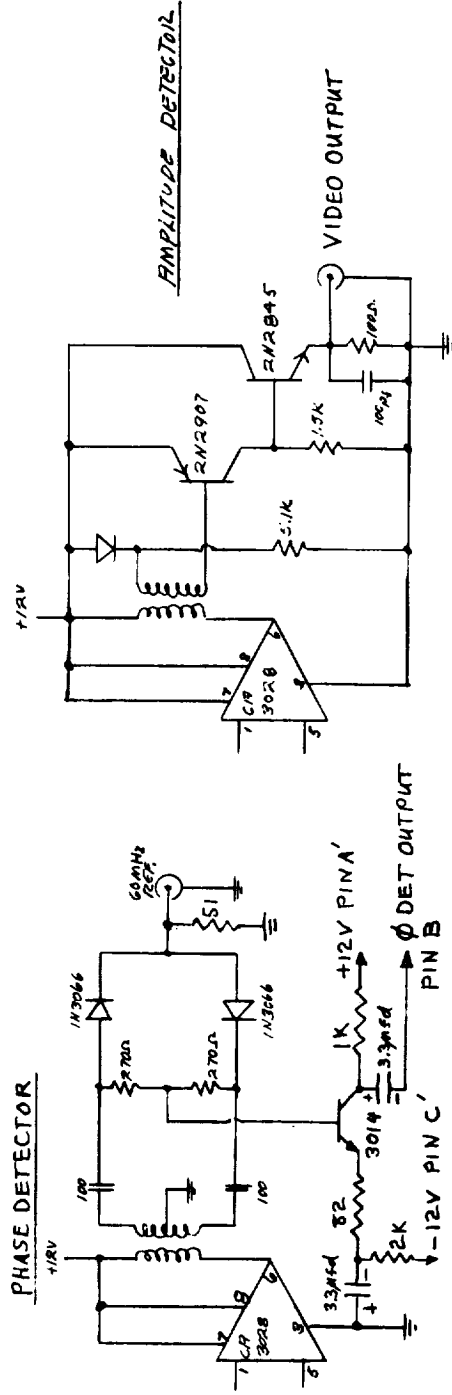


Figure 45. I. F. Amplifier



#### 2.4.7 Leakage Elimination Filter (LEF)

The leakage elimination filter removes phase coherent leakage from the doppler shifted signal with minimum additional alteration to the signal. It is essentially a notch filter within a bandpass filter, the notch existing for phase coherent stable leakage and zero doppler only.

Mechanization is as per Figure 47 for the velocity channel and Figure 48 for the altitude channel.

Circuitwise, the signal enters a pair of demodulators in quadrature which translates the leakage to zero frequency and the signal to its doppler components. The sum components of modulation are suppressed by low-pass filtering to prevent excessive third harmonic at the output. The low-pass time constant is set high enough to include the doppler extremes (up to 18 KHz) but exclude the harmonics. Notch width is determined by the high-pass filter which is set low to retain doppler close to zero. The cutoff frequency is 1 Hz. This is the filter that blocks the D-C generated by leakage and zero doppler. When the two doppler frequencies in quadrature are remodulated with quadrature references, they produce sum and difference sidebands that are in and out of phase respectively. A simple summing network allows the in-phase upper sidebands to reconstruct as the original doppler signal, and the out-of-phase lower sidebands to cancel. An adjustment is provided to effect the best cancellation.

Ideally, the notch provides infinite attenuation to phase coherent, stable leakage. This, however, is not achievable since the recombination mixers determine the degree of reference insertion and the mixers are less than perfectly balanced. This results in a leakage level somewhere between 35 and 45 db below the maximum signal output regardless of leakage input level.



ALL DIODES: CA3039 (6 PACK)  
 ALL XFMR'S: TRIAD SP-52

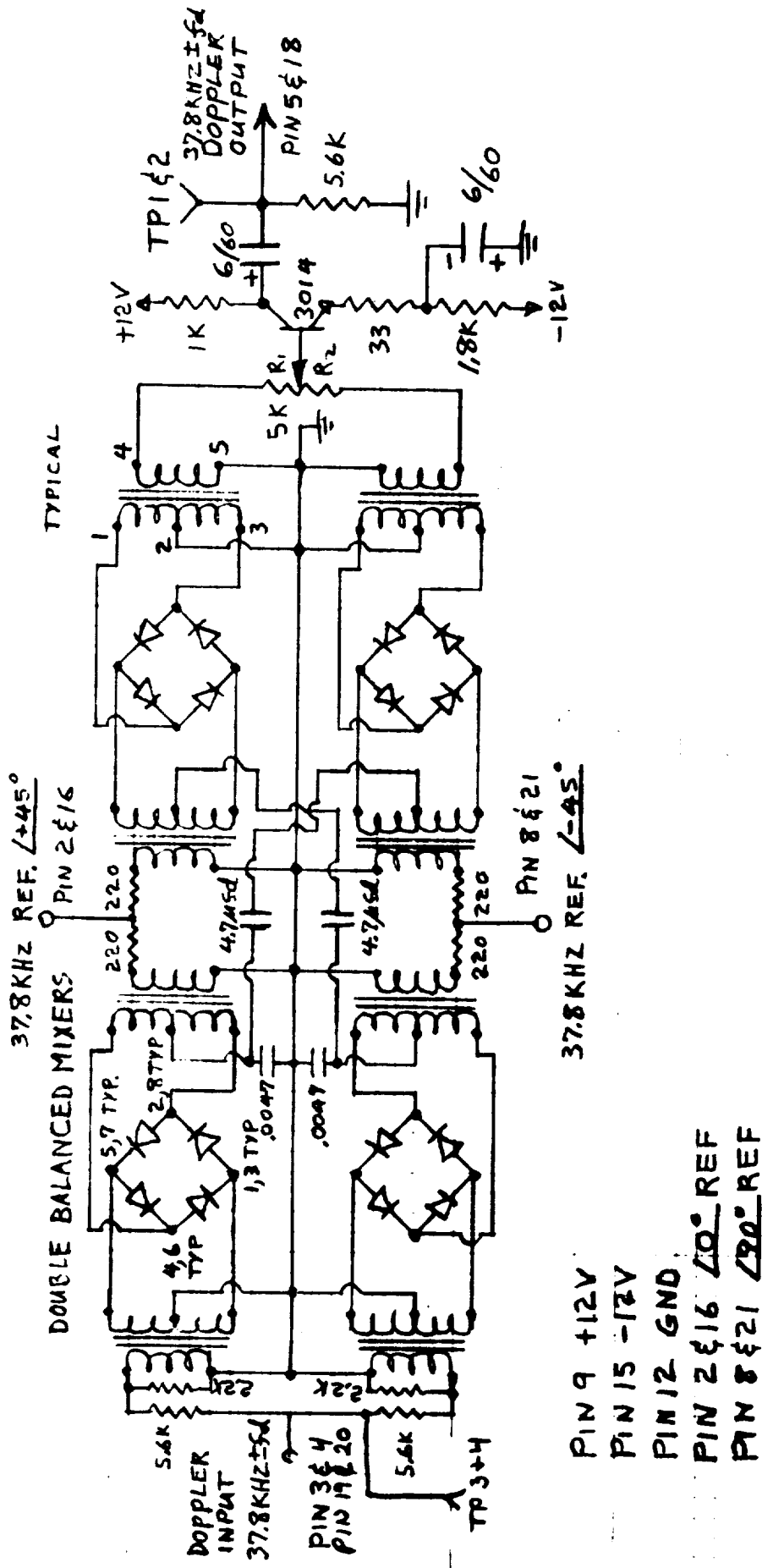


Figure 48. Leakage Elimination Filter (Velocity Channels)

Leakage that is to be eliminated by the LEF originates primarily from an RF delay mismatch between the transmitter-to-mixer leakage leg and the transmitter-to-mixer LO leg. It is controlled by matching the RF filter bandwidths lying in each leg which is in effect an adjustment to their respective group delays. The residual leakage for a particular Bessel sideband is then nulled to zero by a VSWR adjustment made to the transmit-receive leg. This is a nulling procedure and applicable to only one Bessel sideband at a time. At present, the system is nulled to  $J_3$  with  $J_2$  and  $J_1$  producing increasing amounts of leakage.

The LEF overall bandpass gain is unity, and its output impedance matches to the original source, allowing it to be switched into the video circuit with no further effect than to provide the leakage elimination required for  $J_1$  and  $J_2$ .

The quadrature references are generated from the  $J_3$  (378 KHz) phase coherent reference by RC  $45^\circ$  lead and lag networks. The 37.8 KHz velocity channel reference, Figure 49, is generated from  $J_3$  and 415 KHz. The difference sideband is filtered, buffered, and phase-shifted to provide the quadrature reference. This is then supplied to the three velocity filters from buffer-amplifiers to provide the proper gain and to minimize cross talk. The 378 KHz altitude channel quadrature reference, Figure 47 is obtained directly from  $J_3$  by RC phase shifters. It is supplied to the LEF from buffer-amplifiers to prevent contamination of the  $J_3$  reference.

#### 2.4.8 Velocity Tracker

Doppler navigation utilizes the doppler shift that occurs on the received signal if the range is changing during the observation time.





Unfortunately, the received signal contains fluctuations in both amplitude and frequency due to varying reflecting properties and finite angular coverage of the objects being observed. The velocity tracker is used to determine the average doppler shift of the received signal and to present a smoothed, constant amplitude doppler frequency to the computer for determining the desired velocity components.

Various types of velocity trackers have been developed over the years for use in doppler navigators. The type selected for use in the PTDLR system is the so-called "sin-cosine" tracker. This tracker has been used to provide the motion compensation function required for in-house Moving Target Indication (MTI) signal processing radar systems and a high confidence level has been formed.

A block diagram of the velocity tracker is shown in Figure 50 along with typical waveforms appearing at various points. The V.C.O. is a temperature compensated free running multivibrator with linear control voltage-to-frequency transfer characteristics over the design range of 39 KHz to 112.2 KHz. The device delivers two square wave outputs that are  $180^\circ$  out of phase with each other. Each output triggers a flip-flop that counts down the input rate by a factor of two. Two square wave signals are thus formed that are precisely 50 percent duty cycle and maintain a  $90^\circ$  phase relationship between them over a frequency range of 19.5 KHz to 56.1 KHz ( $37.8 \text{ KHz} \pm 18.3 \text{ KHz}$ ). The signals are similar to those shown in Figure 50, waveforms 2 and 3. They are applied to separate mixers that are simultaneously being driven by the doppler shifted received signal. The mixer outputs contain the sum and difference components of the two input frequencies and are low pass filtered to remove the sum frequency

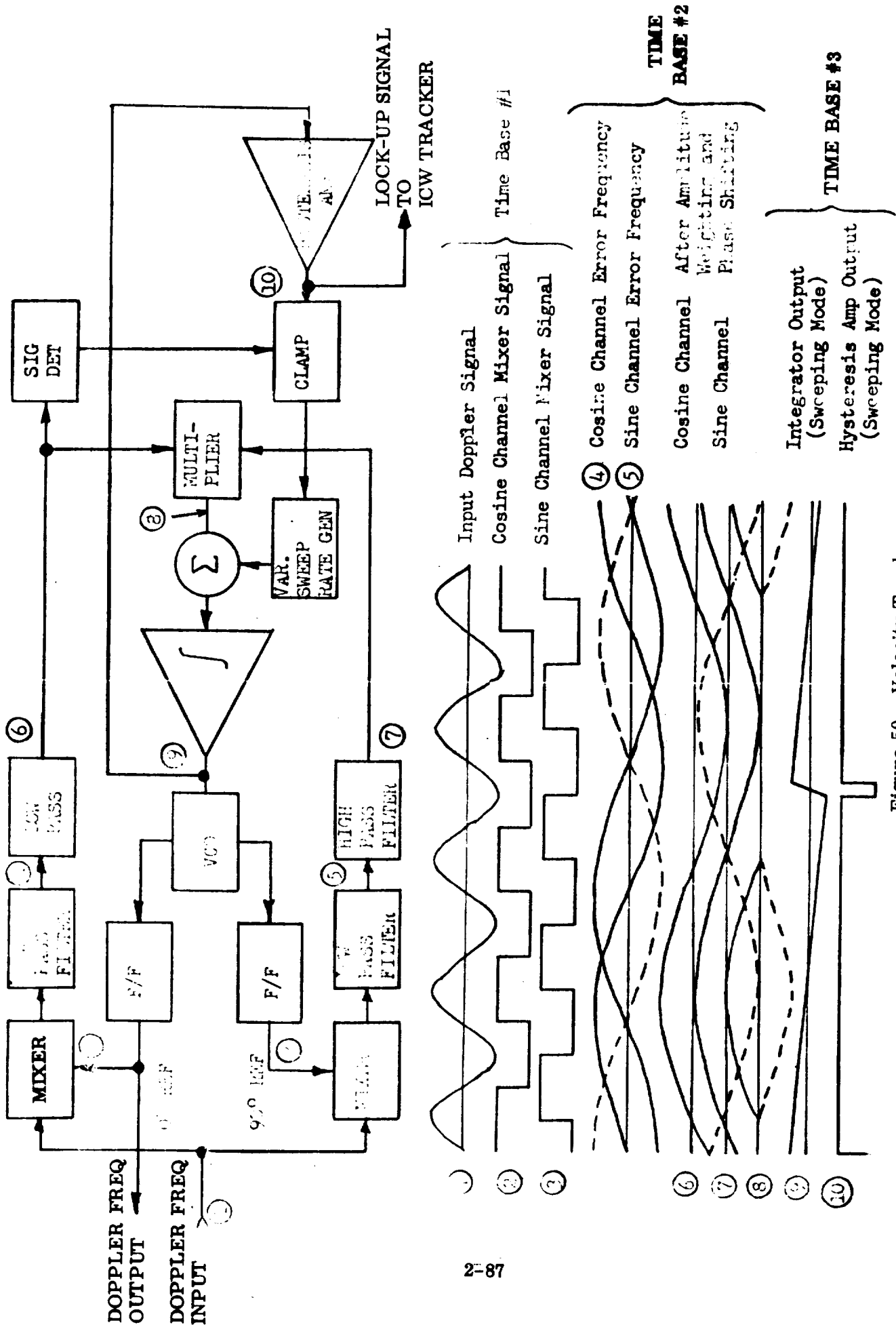
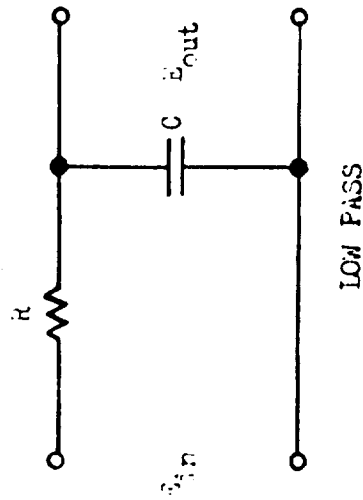
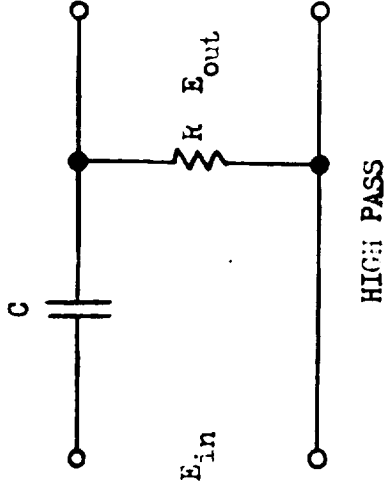


Figure 50. Velocity Tracker

components. At this point (see waveforms 4 and 5, Figure 50) the signals out of each filter are identical in frequency and structure but differ in their relative phase relationships. If the input frequency is higher than the reference frequency (V.C.O. + 2), the phase of the difference frequency in one channel will lead the signal in the other channel by precisely 90 degrees. If, however, the input frequency is lower than the reference frequency, the phase of the difference frequency of the same channel will lag the signal in the other channel by precisely 90 degrees. An abrupt 180 degree phase shift is experienced between the two outputs as the transition is made between a lower-than-reference frequency to a higher-than-reference frequency condition (or visa versa). If an additional 90 degree phase shift is inserted that is independent of sign or absolute value of the difference frequency, the two signals will then have an in-phase or out-of-phase relationship rather than a quadrature one (see waveforms 6 and 7, Figure 50). Multiplying the signals together produces a polarity sensitive error signal into the integrator whose output changes the V.C.O. frequency in the correct direction to null the error signal. This condition only occurs when the V.C.O. and the input are the same frequency - the desired result. The integrator time constant can be set to introduce the required amount of smoothing between the V.C.O output and the input doppler frequency that may contain a considerable amount of short term frequency variation with time or several closely spaced frequencies simultaneously or both, as is usually the case. In any case, the V.C.O. will represent the average frequency of the input doppler signal and that is the purpose of the velocity tracker. The phase shifting technique used to insert the required frequency independent 90 degrees

between the two difference frequency signals utilizes the phase-amplitude properties of a simple RC network as shown in Figure 51. When connected as a low pass filter the output will be approximately in phase with the input at very low frequencies and will approach a 90 degree lagging phase at very high frequencies, the -45 degree point occurring at  $\omega = \frac{1}{RC}$ . When connected as a high pass filter, the output phase will lead the input by approximately 90 degrees at very low frequencies and will approach a zero degree phase shift at very high frequencies, the +45 degree point occurring at  $\omega = \frac{1}{RC}$ . Thus, it can be seen that a differential phase shift of 90 degrees is maintained between the outputs of a high-pass, low-pass network driven from a common source, or, as in this application, if driven from separate sources of the same frequency.

In addition to providing the desired phase shift, the network also performs a useful amplitude weighting function. The low pass filter output (referred to as the cosine channel) remains essentially constant in amplitude out to the breakpoint,  $\omega = \frac{1}{RC}$ , and is then reduced at 6 db/octave. The high pass filter output (referred to as the sine channel) is increasing at the rate of 6 db/octave out to the same breakpoint frequency and then remains essentially constant in amplitude. It is apparent then that the product of these two signals will produce an output with the sign determined by the phase shift (zero degrees or 180 degrees) and an amplitude proportional to the value of the difference frequency at the input over frequency ranges from zero to approximately  $\frac{RC}{2}$ . The loop error signal thus has characteristics similar to an FM discriminator "S" curve. The loop restoring force decreases as the error is nulled and even with very high



RC NETWORK

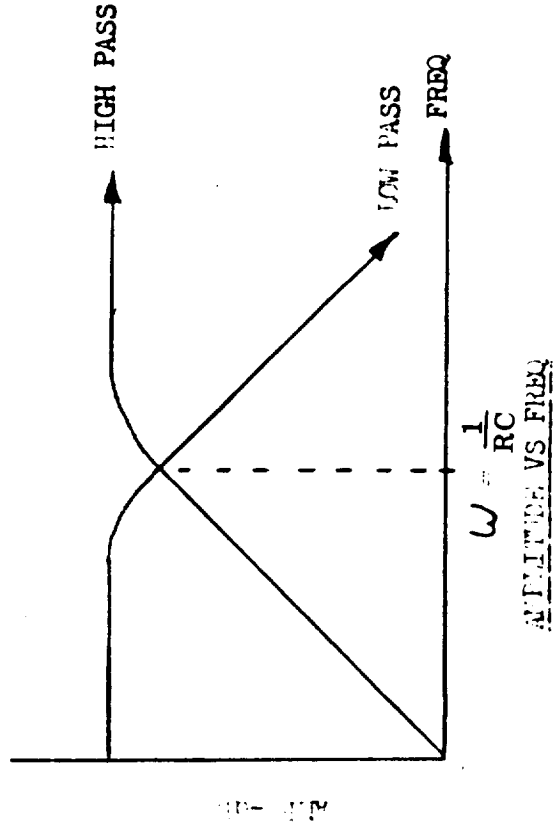
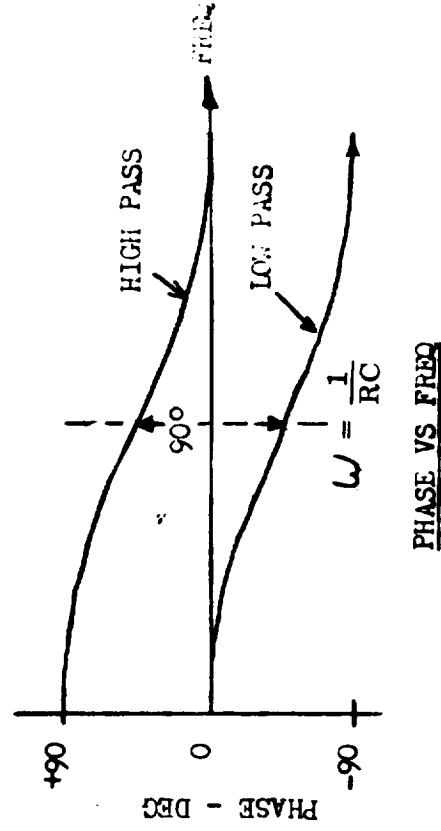


Figure 51. Amplitude and Phase Response

loop gain the mechanization is inherently stable. The filter corner frequency is selected to match the worst case short term frequency spread that occurs on the doppler input signal, thereby providing optimum signal-to-noise improvement. An effective bandwidth of approximately 400 Hz is used in the present filtering. The integrator time constant provides approximately 0.4 second smoothing between the input doppler frequency and the V.C.O. output.

The velocity tracker also contains an automatic searching mode to provide initial acquisition. The tracker has a capture range determined by the filter bandwidth (approximately 400 Hz) and will automatically lock up if the V.C.O. is operating within  $\pm 200$  Hz of the input doppler signal. This signal, however, can be any value between 37.8 KHz  $\pm 18$  KHz and it is therefore necessary to sweep the frequency of the V.C.O. so that during some portion of the sweep it is within 200 Hz of the input doppler signal. The sweep can be stopped at that point and the loop will automatically lock up. The sweep circuit is formed by feeding the integrator output into a hysteresis amplifier whose output is fed back to the integrator input. The hysteresis amplifier is merely a high gain operational amplifier with positive feedback around it. The feedback and input resistors are selected to produce a  $\pm 3$  volt hysteresis between the input and output. The output will remain in a negative state until the input exceeds +3 volts at which time the output will assume a positive state until the input exceeds -3 volts. This square wave output applied to the integrator input produces a triangular output that sweeps the V.C.O. over the 37.8 KHz  $\pm 18$  KHz frequency range. Actually, the integrator input is modified by the variable sweep rate generator shown on the block diagram (Figure 50) so that a

sawtooth waveform is generated rather than the described triangular wave. Typical waveforms are shown in 9 and 10 of Figure 50. The V.C.O. sweeps from 19.5 KHz to 56.1 KHz in approximately 1.2 sec and retraces 36 KHz in 10 milliseconds. The retrace time is so rapid that lockup can occur only on the upswing. This minimizes the possibility of acquiring on harmonics of the input doppler frequency, if they should be present. No difficulty has been experienced during simulation or flight testing.

A signal strength detector monitors the output of the cosine channel to stop the V.C.O. from searching when a signal is present. A signal will only appear in this channel when the V.C.O. and input doppler frequency are within approximately 200 Hz of each other. The search stop is performed by clamping the hysteresis amplifier output (Integrator input) to ground when sufficient signal is present in the detector. This stops the integrator output at the correct value to permit the tracker to automatically acquire and track the input doppler frequency. A schematic of the velocity tracker is shown in Figure 52.

#### 2.4.9 FM/CW Altitude Channel

This section will describe the mechanization used to extract altitude information from FM/CW systems. It is necessary to recall that the altitude information in an FM/CW system is contained in the phase shift of the received sideband with respect to the modulation frequency that initially produced the sideband. Since the phase shift of the received signal is directly proportional to altitude and since the mechanization is expected to measure this phase shift precisely, extreme care must be given in the design to insure that extraneous phase shifts are minimized.

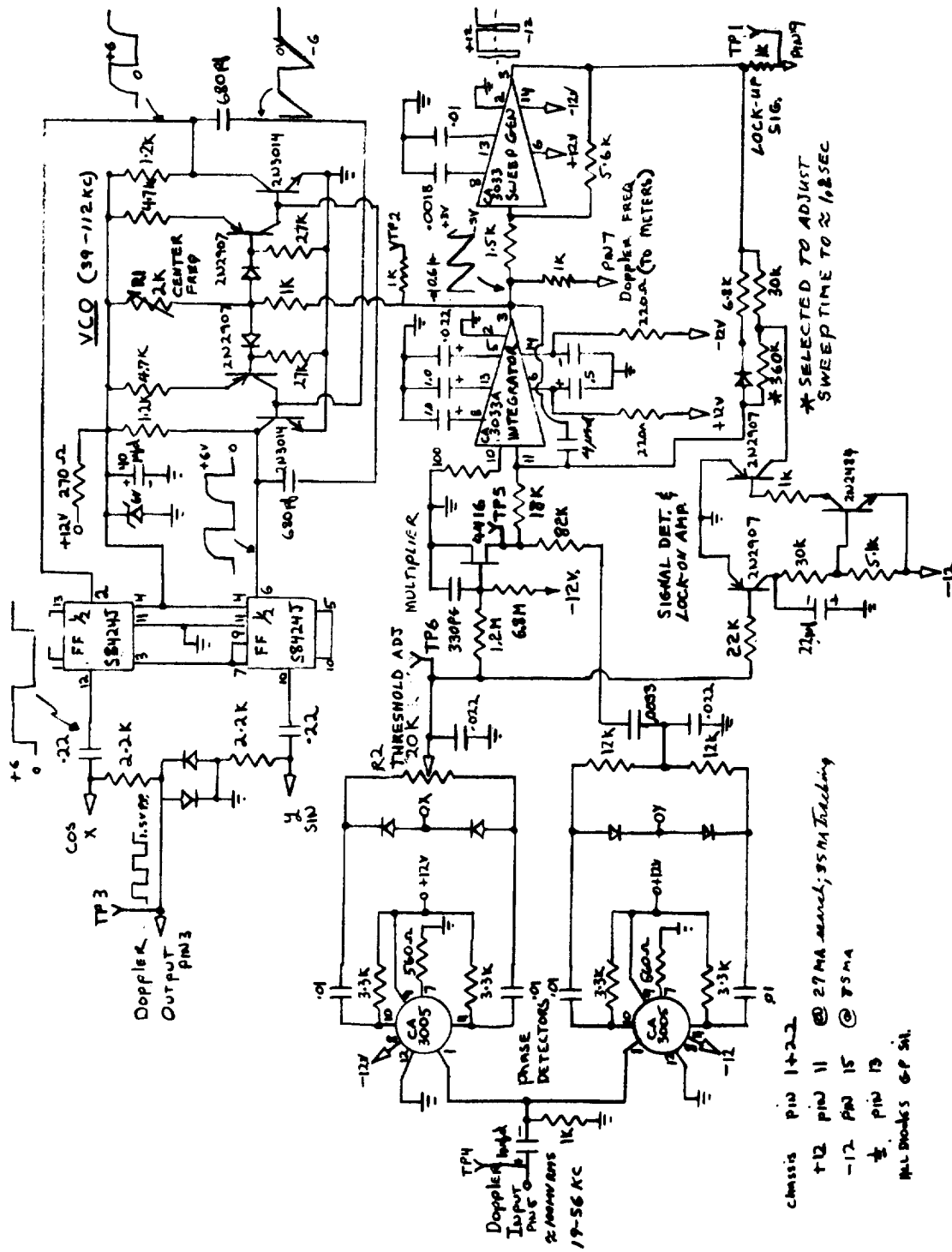


Figure 52. Velocity Tracker Schematic



In general, this requires broad bandwidths and phase tracking considerations (similarity of processing both signal and reference channels). Broad bandwidths have been maintained through the square law doubler and circuit similarity has been maintained through the mixers and band-pass amplifiers.

The following description refers to the block diagram shown in Figure 53 and the schematic shown in Figure 54. The waveforms appearing at various points are also shown and will be referred to in order to gain a better understanding of circuit operation.

Direct phase comparison of the received sideband signal would be difficult because of the doppler shift that may be present. Phase measurement of two signals that are slightly different in frequency would be meaningless since a  $360^\circ$  variation would occur at the difference frequency rate. However, by folding and utilizing both the positive and negative (e.g.  $J_1$ ) sidebands in a square law doubler, a single frequency carrier is generated independent of doppler shift on the received input. Waveform 1 in Figure 53 shows the received spectrum after folding. Except for the spectral width on the signals, the picture depicts the essential characteristics of a suppressed carrier modulator output being modulated by a signal equal to  $f_d$  where the sidebands produced are mirror images centered around the carrier. The received spectra are mirror images since they originated from the same sideband of the same signal at the same time. The desired cross products appearing at the output of the square law doubler are at twice the carrier frequency or in this case 756 KHz. A meaningful phase comparison can now be made. Care has

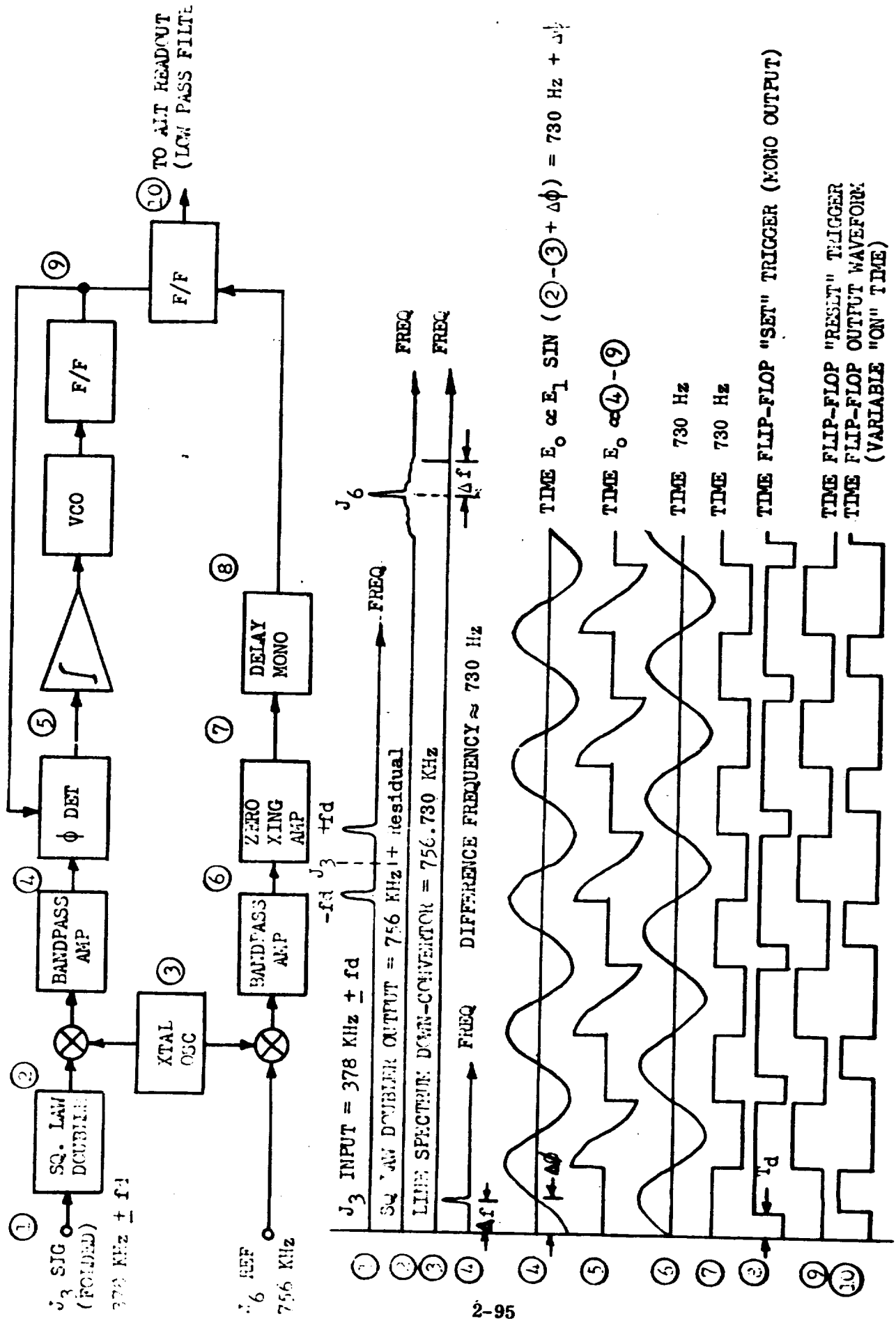


Figure 53. FM/CW Altitude Tracker



been taken in the design of the doubler to maintain broad bandwidths and symmetry with respect to the expected doppler spread and attention has been given to balancing and overall dynamic range to insure a distortion free output so that no phase errors are produced over the expected operating range of frequency and amplitude variations. The reference signal that will be used to make the phase comparison has been generated in the master frequency generator by multiplying the modulation frequency.

A direct phase comparison could be made between the doubler output and the reference signal but an accurate mechanization might be extremely difficult to implement. A  $360^\circ$  phase shift of the frequency doubled output corresponds to approximately 1300 feet altitude change and also corresponds to approximately  $1.32 \mu\text{sec}$  time delay ( $\frac{1}{756 \text{ KHz}}$ ). This is equivalent to approximately 1 nanosecond time delay per foot and presents a very sensitive situation from a measurement point of view. It has been found to be much more accurate to make these measurements at a lower frequency hence longer equivalent time delays for the same  $360^\circ$  phase shift. This is done by mixing both the doubled signal frequency and the reference frequency in separate mixers with a stable crystal oscillator of somewhat arbitrary frequency. The frequency of the oscillator was chosen to produce a difference frequency of approximately 1 KHz. The actual frequency chosen was supposed to produce a time delay of  $1 \mu\text{sec}/\text{ft}$  altitude so that in-flight scope measurements of time delay could be rapidly converted to altitude (i.e.  $300 \mu\text{sec} = 300' \text{ alt}$ ). However, the received crystal oscillated slightly higher in frequency and gives a scale factor of approximately  $1.05 \mu\text{sec}/\text{ft}$  altitude.

The signal frequency out of the mixer (lower sideband  $\approx 730$  Hz) can now be conveniently narrow banded to improve the signal-to-noise ratio (waveforms 4 and 5 in Figure 53). This is done in the bandpass amplifier which incorporates a twin-T feedback network to provide gain shaping. A bandwidth of approximately 60 Hz centered at 730 Hz and a gain of two are obtained in this circuit. Unfortunately, wide phase variations occur across the passband and since small center frequency variations will result from drifts in either the master modulation crystal oscillator or in the down converting crystal oscillator ( $\approx 756.730$  KHz), an identical band-pass amplifier is inserted in the reference channel. This signal will exhibit the same frequency variations and will experience the same phase shift in the band-pass amplifier. The differential phase shift between the signal and the reference will therefore be unaffected by frequency drifts and measurement errors will be prevented.

The reference signal at the output of the band-pass amplifier is a very low distortion, constant amplitude, 730 Hz sine wave. This signal is a-c coupled into a zero crossing detector that is essentially a high gain, wideband amplifier with a differential input. One input contains the signal and the other input is grounded. Exact zero crossing detection is assured by virtue of integrated circuit production techniques whereby parameter matching of similar devices formed on a common substrate is relatively easy. Because of the high gain and wide bandwidth, a very small part of the positive input half cycle is required to saturate the output of the amplifier. Similarly, only a very small portion of the negative half cycle is required to saturate the amplifier output in the opposite direction. A square wave is thus formed with the transition of states occurring at the

crossover points of the input sine wave with extremely small hysteresis (see waveforms 6 and 7 in Figure 53). The leading edge of the square wave is used to trigger a delay monostable. The output of this stage will change states synchronously with the input trigger but the duration of the "down" state is manually adjustable. Time delay at this point corresponds directly to altitude changes ( $\approx 1.05 \mu\text{sec/ft}$ ), therefore a time delay can be inserted that will permit an altitude calibration of the overall FM/CW system. In the event that errors are produced in the altitude channel by environmental changes, this is a convenient point to apply compensating signals. The leading edge of the delay monostable (see waveform 8, Figure 53) is used to trigger the output flip-flop. Once triggered (set), this device will remain in one state until retriggered from another source at a different input. If this trigger were generated by processing the received signal in a zero crossing detector as is the reference channel and if the leading edge output were used to retrigger the output flip-flop, then the time duration,  $t$ , of the output would be an accurate measure phase shift between the two signals with respect to a one cycle time interval,  $\tau$ , of the 730 Hz reference frequency ( $\theta_{\text{deg}} = \frac{360 t}{\tau}$ ). If the flip-flop output switches between two closely controlled reference voltages (zero volts and +6 volts in PTDLR), a d-c voltage can be produced that is directly proportional to altitude by simply time averaging the output in a low pass filter. This may then be used for altitude meter deflection and mode switching. This is the mechanization that was implemented at the beginning of the program and was used during the early phases of the flight test program. A considerable amount of short term phase variation was observed during flight and

although an adequate amount of smoothing could be done after the cycle-by-cycle phase measurement a more satisfactory solution would be to smooth out short term phase variations on the signal before the phase measurement was made.

#### 2.4.10 Phase Lock Loop

Two approaches were mechanized to perform the required altitude smoothing function. The first approach utilized conventional phase lock loop techniques and was used during most of the flight testing. A significant improvement was obtained, but results were still generally unsatisfactory at low altitudes. A phase lock loop is basically a two slope loop and is difficult to stabilize since the input signal amplitude is not constant. The second approach utilized novel techniques and, because it is a one slope loop, is inherently stable. Unfortunately, the mechanization was implemented late in the program and limited flight test data was accumulated with this loop installed. Operator evaluation and subsequent flight tape evaluation indicates that excellent altitude performance was obtained..

The following is a description of both mechanizations:

##### a. Phase Lock Loop #1

As pointed out in the FM/CW altitude section, the altitude information is contained in the phase of the down-converted received signal with respect to an internally generated reference of the same frequency. The received signal has rather wide short term phase variations and, therefore, dictates the need for a smoothing device prior to phase comparison.

This was implemented by inserting a phase locked loop in the signal channel past the bandpass amplifier but prior to the output flip-flop (see Figure 55). A phase lock loop is basically comprised of a phase detector, integrator, and a V.C.O. It is





used to force an oscillator to operate at the same frequency and to maintain phase relationship with the input signal. Frequency errors cannot exist or the loop is not locked and phase errors can be made arbitrarily small by providing high loop gain. The advantage of the loop is that it permits control of the rate at which the V.C.O. tracks changes of phase (or frequency) of the input signal by adjusting the time constant of the integrator. This then provides the desired smoothing of short term phase variations of the input signal because the phase of the V.C.O. is now compared with the reference channel. The loops are self capturing in that, within limits, they will automatically lock to the input signal if the frequency difference is not too great. The V.C.O. is a temperature compensated multivibrator with linear voltage-to-frequency transfer characteristics.

The total programable frequency range over which it may be driven by the integrator is approximately  $\pm 30$  Hz centered at 1460 Hz. The leading edge of the approximately square wave output is used to trigger a flip-flop. This unit counts down the frequency to 730 Hz  $\pm 15$  Hz and also provides a precise square wave suitable for triggering the output flip-flop (phase comparator) and is fed back to the input of the phase locked loop (see wave for 9, Figure 53).

The input phase detector is really a transistor clamp operated by this square wave signal. The input signal is applied directly to the integrator during the negative portion of the square wave and is inhibited (clamped to ground) during the positive half cycle. If the sampling period straddles the zero

crossing of the input signal, equal positive and negative areas will be applied to the integrator and no net change in output will result (see waveform 5, Figure 56). If the sampling does not exactly straddle the zero crossing, unequal areas will be applied to the integrator causing a net change in the integrator output. This produces an effective change in the V.C.O. frequency in the correct direction and long enough for the error to be nulled. The integrator utilizes an integrated circuit with a gain of 90 db to provide the high loop gain necessary to insure negligible phase error contributions by the loop. A schematic of the  $\phi$ -lock loop is shown in Figure 55.

b. Phase Lock Loop #2

The second approach to implementing the required phase smoothing uses a time modulator technique. The time modulator is used to provide the variable delay corresponding to the average phase shift of the input signal compared to the reference signal of the same frequency.

Referring to the block diagram and waveforms shown in Figure 56, the loop operation is as follows: The reference signal waveform 1 (730 Hz), previously shaped into a square wave by a high gain amplifier, is applied to the monostable multivibrator. The time delayed leading edge of the monostable output pulse train waveform 2, corresponds to the zero degree phase shift or zero altitude reference point. This reference point can be adjusted by varying the monostable pulsewidth and thus provides a convenient means of performing altitude

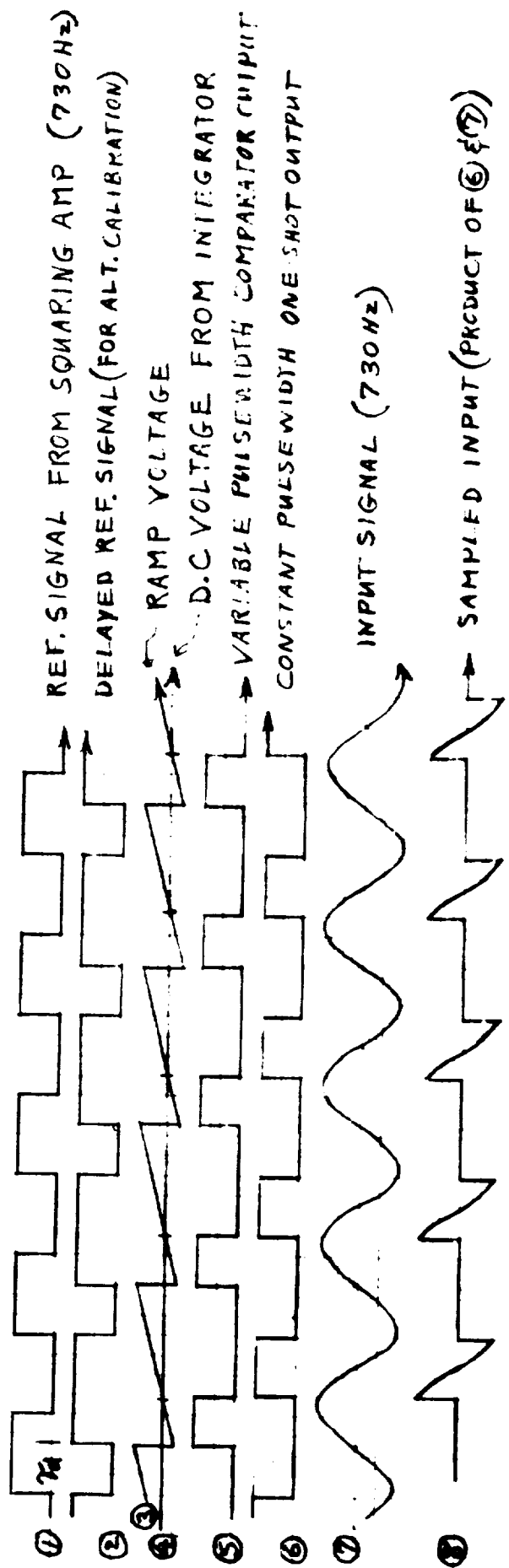
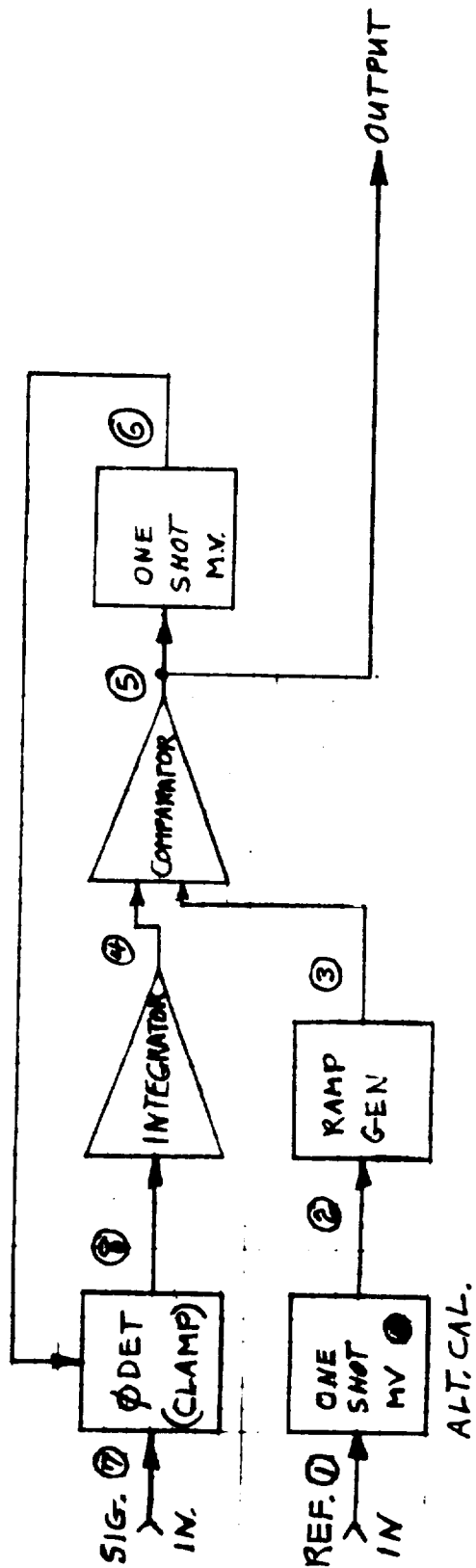


Figure 56. Phase Lock Loop #2

calibration. This leading edge is used to start a ramp voltage, waveform 3, at the output of the ramp generator. The voltage increases to approximately 4V during one reference cycle and is then reset to zero volts at the start of the next reference cycle. The process is repeated during each cycle. Since one reference cycle corresponds to  $360^\circ$  or the equivalent of 1302 ft. altitude, the scale factor at that point is equal to  $\frac{4 \text{ volts}}{1302 \text{ ft.}} = 3.07 \text{ MV/ft.}$  The ramp voltage is fed to the comparator where it is compared with the D.C. voltage output, waveform 4, from the integrator. The comparator is essentially a two state device whose output is, say, in the "one" state if one input is at a lower voltage than the other input and in the "zero" state if the input is at a higher voltage. The transition from one state to the other occurs when the two inputs are at nearly the same voltage. For any integrator output voltage of  $4 > V > 0$  this transition occurs twice: once during the reset time (zero alt. reference) and once during some portion of the ramp period (any equivalent altitude corresponding to the integrator D.C. voltage at a scaling of 3.07 MV/ft. of altitude). It can be seen that the resultant waveform 5, is a pulse train whose period is constant and equal to the reciprocal of the reference frequency ( 1370  $\mu$ seconds) and with a pulse width variable from 0  $\mu$ seconds to 1370  $\mu$ seconds as a function of the D.C. value of the integrator output. The leading edge of the pulse train always occurs at the reset time (zero altitude ref). The variable position trailing edge is used to trigger a monostable multivibrator. The monostable output,

waveform 6, is a constant width pulse train used to sample the input altitude signal. This is done in the phase detector and produces an output that is the product of the multivibrator waveform and the input signal sinewave. This results in waveform 8 Figure 56. It is apparent that the average value of this signal is zero only when the monostable pulse train sampling gate exactly straddles the input sinewave at zero crossing. This will occur at zero degrees and 180 degrees. This signal is fed to the integrator phased such that a non-straddling condition will produce a change in the D.C. level of the integrator output and a resultant change in the position of the trailing edge of the comparator output which shifts the monostable waveform in the correct direction to restore a straddling condition at the 180 degree point of the input altitude signal. At this point, the error voltage is reduced to nearly zero. High loop gain insures that the residual error is negligible. The integrator time constant determines the rate at which error is reduced to zero and, therefore, provides a convenient means of producing the required smoothing of short term phase variations on the input signal while providing accurate long term tracking of the average phase. Once calibrated, the waveform at the comparator output is a constant period pulse train set by the reference frequency (730 Hz) with a pulse width smoothly tracking the average phase of the input altitude signal. This waveform can provide an altitude readout by averaging the

waveform directly in a voltmeter. Further processing, however, is done (as discussed in the Mode Switching Section 2.4.2) in the present mechanization to generate a non-linear scaling such that readout errors are progressively reduced at lower altitudes. A schematic of  $\phi$ -lock loop #2 is shown in Figure 57.



### ICW Range Tracking Loop

The ICW tracker provides the ranging capability when in the ICW mode. The tracking loop is similar to the split gate range tracker used frequently in many radar systems. The mechanization to be described has, however, been designed specifically to meet PTDLR system requirements and therefore incorporates several features not normally found in this type of tracker.

The following PTDLR requirements and system considerations were used during the design phase.

- a. Desired range coverage: 30,000 ft. down to 750 ft.
- b. Automatic range capture
- c. Dual PRF capability (Velocity tracker requirement)
- d. Automatic dual PRF lockout
- e. Bimode compatibility
- f. Lock-up indication
- g. Interface requirements
- h. Calibratable

The design philosophy behind each of these considerations is now discussed.

The maximum range coverage of 30,000 ft. is somewhat arbitrary but is probably related to a particular mission profile requirement in the original voyager tradeoff studies. From a practical standpoint, however, the range could be extended to, say, 100,000 ft. if desired. The minimum range of 750 ft. is also somewhat arbitrary. It represents a compromise between the lowest altitude capability that could be easily mechanized (PRF approx. 333 Khz) without requiring particularly



fast rise times and high repetition rates and still provide adequate overlapping range coverage between the ICW mode and the FM/CW mode. The overlap of approximately 450 ft (up to 1200 ft. altitude in FM/CW and down to 750 ft. altitude in ICW) eliminates the possibility of continually switching between modes when operating near an altitude mode switching point. The lower altitude limit that could be obtained using the present transmitter and some circuit changes would appear to be approximately 100 feet.

Automatic range capture is highly desirable and is inherently provided by the mechanization.

The loop can, however, lock up and track at sub-multiples of the correct altitude. For example, assume an actual altitude of 10,000 ft. (25 Khz PRF). The loop could lock at the equivalent of 5000 ft (50 Khz), 2500 ft (100 Khz), or any integer divisor. The loop will close on the nearest integer that it was operating at under open loop conditions. In order to prevent a false acquisition, it is only necessary to insure that the open loop PRF is lower than the lowest expected closed loop PRF. Since the lowest tracking PRF corresponds to the 30,000 ft maximum design range (PRF  $\approx$  8333 hz), the V. C. O. has been designed to assume a PRF of approximately 7500 hz during equipment turn-on, mode switching, and during periods of signal loss. During the flight test program many equipment turn-ons and mode switchings were initiated at altitudes ranging from 750 ft. to 12000 ft. with the correct altitude being acquired in every case.

A dual PRF mode has been incorporated in the ICW tracking loop to prevent a false acquisition in the velocity trackers. Consider the

case of initial turn-on occurring at an altitude of, say, 30,000 ft. As stated above, under these conditions, the range tracking loop would normally be operating at an open loop PRF of 7500 Hz prior to acquisition and the velocity trackers would be sweeping over a doppler frequency range of approximately  $\pm 18$  KHz. Spectral lines will be produced because of the interrupted nature of transmission and, with a 50% duty cycle, the received signal will contain spectral lines symmetrically centered around the desired central line at all odd harmonics of the PRF. Figure 58 depicts a situation with a low and a high PRF.

It is seen from the diagram that several lines are contained within the velocity tracker search range in the low PRF case and erroneous results would occur if the tracker locked on any other than the central line.

It is therefore necessary to detect a searching condition in anyone of the three velocity trackers and insure the PRF at that time is high enough that no spectral line other than the central line will appear within the search range of the velocity tracker during the acquisition phase. Since the central line may be doppler shifted up to  $\pm 18$  KHz and the tracker searches  $\pm 18$  KHz, it is necessary to maintain the PRF at least as high as 36 KHz until all trackers have locked on.

At a given PRF, however, complete eclipsing of the signal can occur at particular altitudes. This condition will exist when the delayed return signal is received during the simultaneous radiation of the next (or multiple) transmission. The received signal is completely masked at that time and is therefore unusable. To prevent possible masking, the PRF is alternately shifted between two frequencies. The frequencies

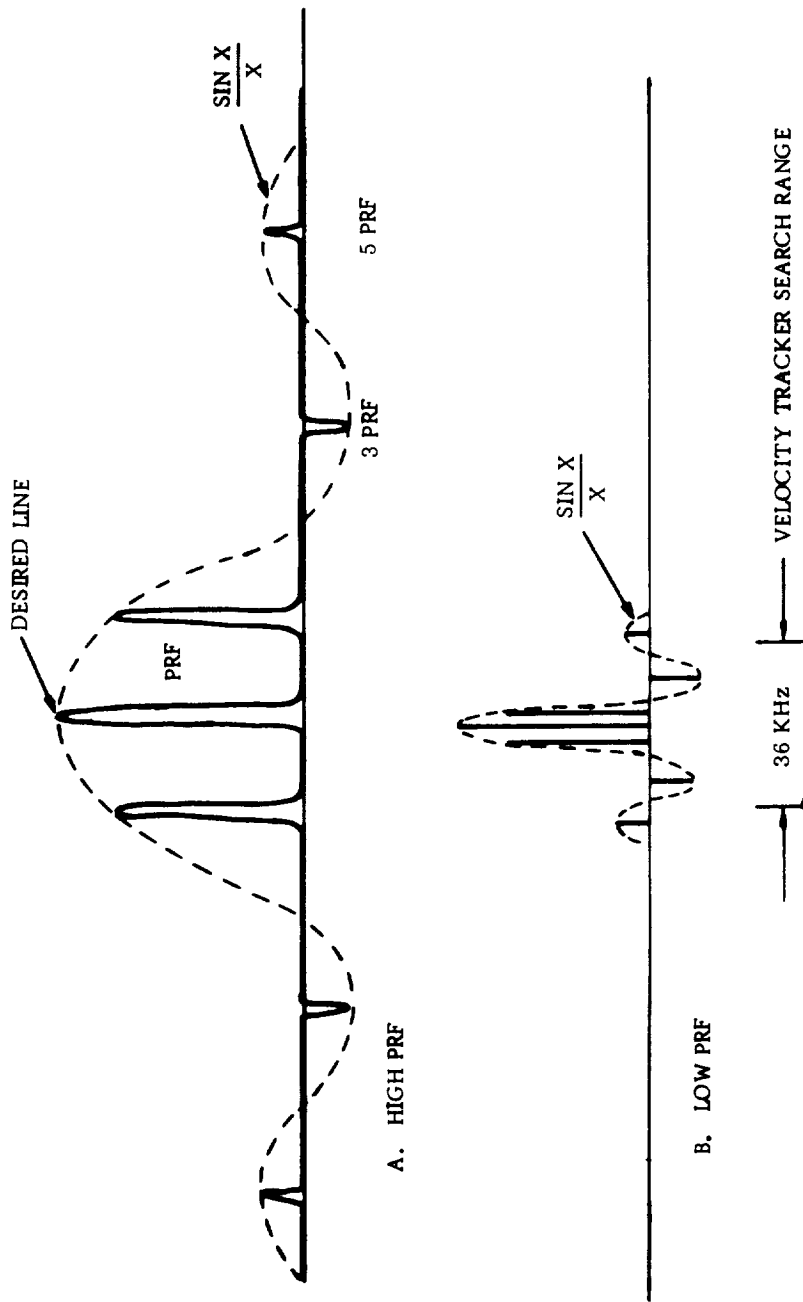


Figure 58. Received Spectra (ICW)

are chosen such that if complete masking should occur at one frequency, it cannot occur at the other frequency at that same altitude. This is true over the entire range of altitude coverage. The frequencies selected are approximately 45 Khz and 51 Khz.

The rate of alternation is a function of the sweeprate and capture range of the velocity trackers. The rate must be slow enough that the tracking filters will build up sufficient amplitude for detection but must be fast enough that an uneclipsed PRF return is available at the tracker before it sweeps beyond its capture range. The sweep rate of the velocity trackers is approximately 100 Khz/sec (38 Khz/0.4 sec) and the capture range approximately  $\pm 200$  hz. The minimum PRF switching rate is then approximately 250 hz. A frequency of 300 hz is used in the present mechanization.

An additional feature is provided in the mechanization that locks out the dual PRF mode if the operating PRF happens to be greater than 45 KC during a velocity tracker search phase. This situation could occur at altitudes below 5560 ft. with the range tracker locked up satisfactorily. If for some reason any or all of the velocity trackers lost signal momentarily and started searching, there would be no reason to break the range tracking loop to go into the dual PRF mode since there would be no unwanted spectral lines within the velocity tracker search range under this condition. Maintaining range track insures maximum available signal at the velocity tracker since no eclipsing will occur. This feature maximizes the probability of velocity tracker reacquisition and eliminates unnecessary range tracker reacquisitions.

The operation of the various blocks shown in Figure 59 will now be given. Waveforms appearing at various points are also shown. Starting with the V. C. O. we have a blocking oscillator that has a free running frequency of 30 khz unless increased by either of the two sources present at the preceding input summing point. Assume for the moment that they are zero. The blocking oscillator output pulse (approx. 50 nanosecond wide) is fed to two points. The upper branch consists of two flip flops and a driver stage. The first flip flop counts down the B. O. pulse train by two, thus producing a 15 khz square wave which in turn triggers the second flip flop. Its output is now 7.5 khz and has precisely a 50% duty cycle (square wave). This output is buffered by the driver stage and then used to turn the transmitter on for 50% of the period (L. O. off) and then turn on the L. O. for the remaining 50% period (transmitter off).

The lower branch being triggered by the B. O. is doing the same thing (i. e. , counting down the B. O. frequency and producing square waves at 15 khz and 7.5 khz). The insertion of the delay monostable permits a small time displacement between the upper branch and lower branch waveforms. This adjustment is used for range calibration by matching the received signal sampling gate positions to the desired received signal delay.

The appropriate waveforms from the first and second flip-flop are combined in NAND gates to form the early and late gate signals. These two signals uniquely divide the receive interval into two equal periods over all ranges of PRF. The amplitude detected received signal is applied to both gates. The early gate channels this signal into the upper

low pass filter for 50% of the receive interval then the late gate channels the received signal into the lower low pass filter for the remaining 50% of the receive period. The received signal has the same pulse length as the transmitted signal and is also equal to the receive interval because of the 50% duty cycle. The received signal delay, however, is proportional to altitude and may or may not be centered within the receive interval. If it is centered, equal amounts of the received signal will be sampled by the early and late gates and the averaged d. c. voltage at the output of each low pass filter will be equal. These outputs are differenced in the high gain amplifier and, being equal, will produce no change in the amplifier output voltage and, therefore, no change in the V. C. O. frequency. If, however, the received signal is not centered within the received interval, either the early or late gate sample (or both if there is considerable error) will not contain the received signal for the full sample interval. The average d. c. values appearing at the output of the low pass filters will be unequal and the difference value is the error signal used to adjust the PRF to the correct value. The phasing is such that if more signal appears at the early gate - low pass filter output the V. C. O. frequency is increased and visa versa. The V. C. O. will be driven in the correct direction until the error signal is nulled indicating a centered condition of the received signal within the received interval.

Obviously, some error must exist at the amplifier input to maintain its output, hence the V. C. O. frequency, at any value within the design range. This error can be made arbitrarily small by increasing the amplifier gain, however, and a gain of greater than 90 db is used

in the present mechanization to insure that the error is negligible. This basically describes the closed loop operation of the ICW range tracker.

The additional input to the V.C.O. summing point generates the dual PRF capability. The free running astable multivibrator forms two current level states alternating at a 300 Hz rate capable of making the V.C.O. run at 180 KHz (45 KHz PRF) and 204 KHz (51 KHz PRF) respectively. The lock-on signal (tracking mode) obtained from each of the velocity trackers is summed in the AND gate thereby inhibiting the dual PRF signal if all trackers are locked-on. Loss of lock of any tracker will pass the dual PRF current to the V.C.O. As stated earlier, interlocking has been provided to force the tracking loop signal (amplifier output) to zero at this time and to clamp the input received signal to ground simultaneously so that erroneous error signals are not formed in the low pass filters. Conversely, the interlocking provides maintenance of range tracking capability and inhibits dual prf operation during velocity tracking loss if the PRF is greater than 45 khz.

The bandwidth of the input video is from D.C. to approx 5 Mhz in order to maintain zero droop across the video return and to minimize waveform distortion (rise and fall times) prior to sampling. After sampling, the signal bandwidth is reduced considerably by the 0.5 sec time constant low pass filters with a resultant increase in signal to noise ratio. A schematic of the complete tracker is shown in Figure 60.

#### **2.4.12 Velocity Readout Circuitry**

The doppler frequency obtained from each of the three antenna beams and smoothed by individual doppler trackers (commonly called velocity trackers) must be combined in the correct manner to resolve the

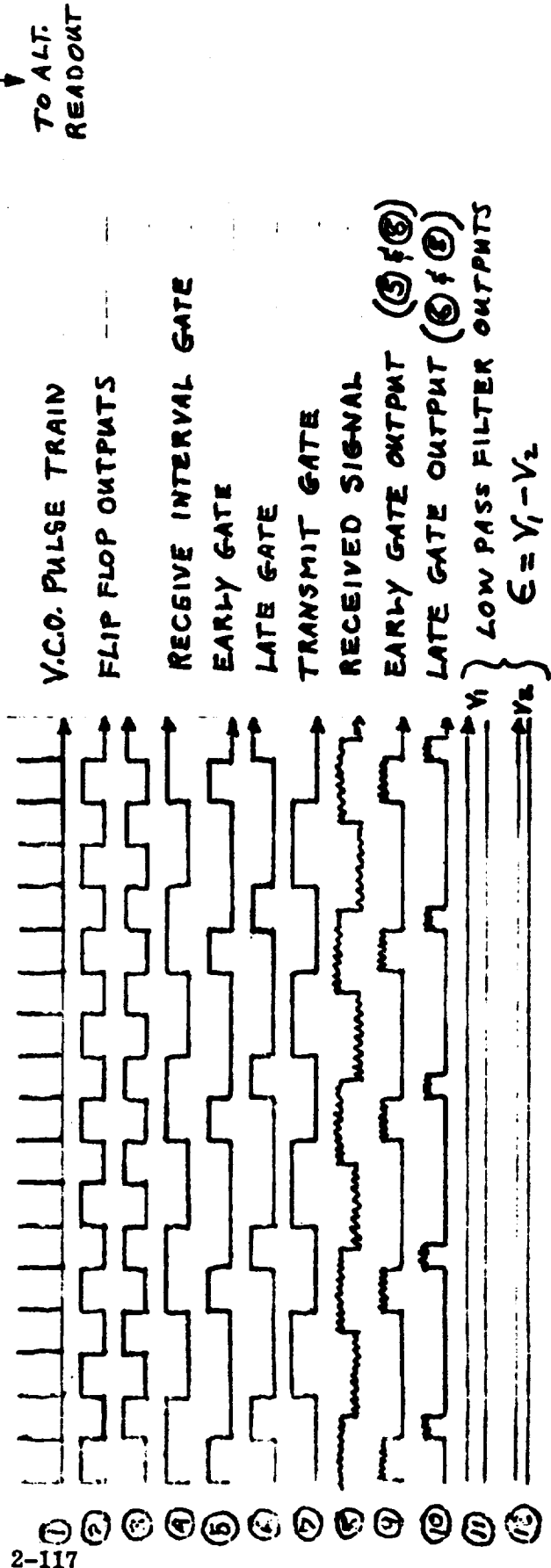
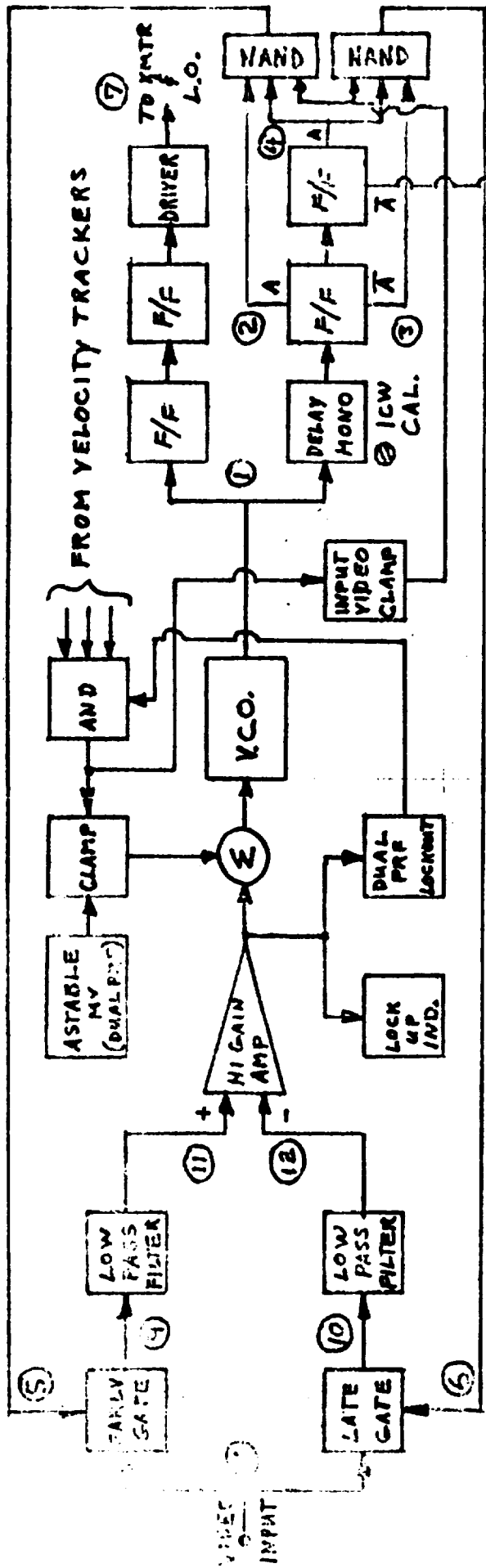


Figure 59. ICW Tracker





the various components of vehicle velocity. Defining a reference plane as being parallel to the skids of the helicopter, the resolved  $V_x$  velocity component is defined as a line passing fore and aft through the PTDLR antenna parallel to the reference plane. The resolved  $V_z$  velocity component is defined as the line passing vertically through the antenna and normal to the reference plane. The resolved  $V_y$  component is the velocity vector normal to both  $v_x$  and  $v_z$  and generally indicates sideways motion of the antenna (helicopter).

The doppler shift in each beam is first converted into a DC analog in the velocity trackers and are then weighted and combined in summing amplifiers located in the mode board (see Figure 28). The resultant, resolved, DC outputs are scaled in the meter board, Figure 61, and fed to three 50-0-50  $\mu$ amp meters. The meter scales have been calibrated to display 500-0-500 ft/sec ranges of velocity in the  $V_x$ ,  $V_y$ , and  $V_z$  components of velocity. Additionally, scale factor sensitivity can be increased by a factor of five by a push button located at each meter. During system evaluation it became apparent that the scale factor should be increased by a factor of, say, fifty (full scale display of  $\pm 10$  ft/sec) during a typical helicopter hover or landing maneuver.

The DC analog voltage proportional to doppler shift is actually the integrator output voltage that drives the VCO in the velocity tracker (see Section 2.4-8). The integrator output is an accurate analog if the voltage-to-frequency transfer function of the VCO is linear and contains no bias error if the VCO center frequency corresponds to the zero doppler reference frequency when the integrator output is zero volts. Linearity is obtained by using constant current sources to charge the timing

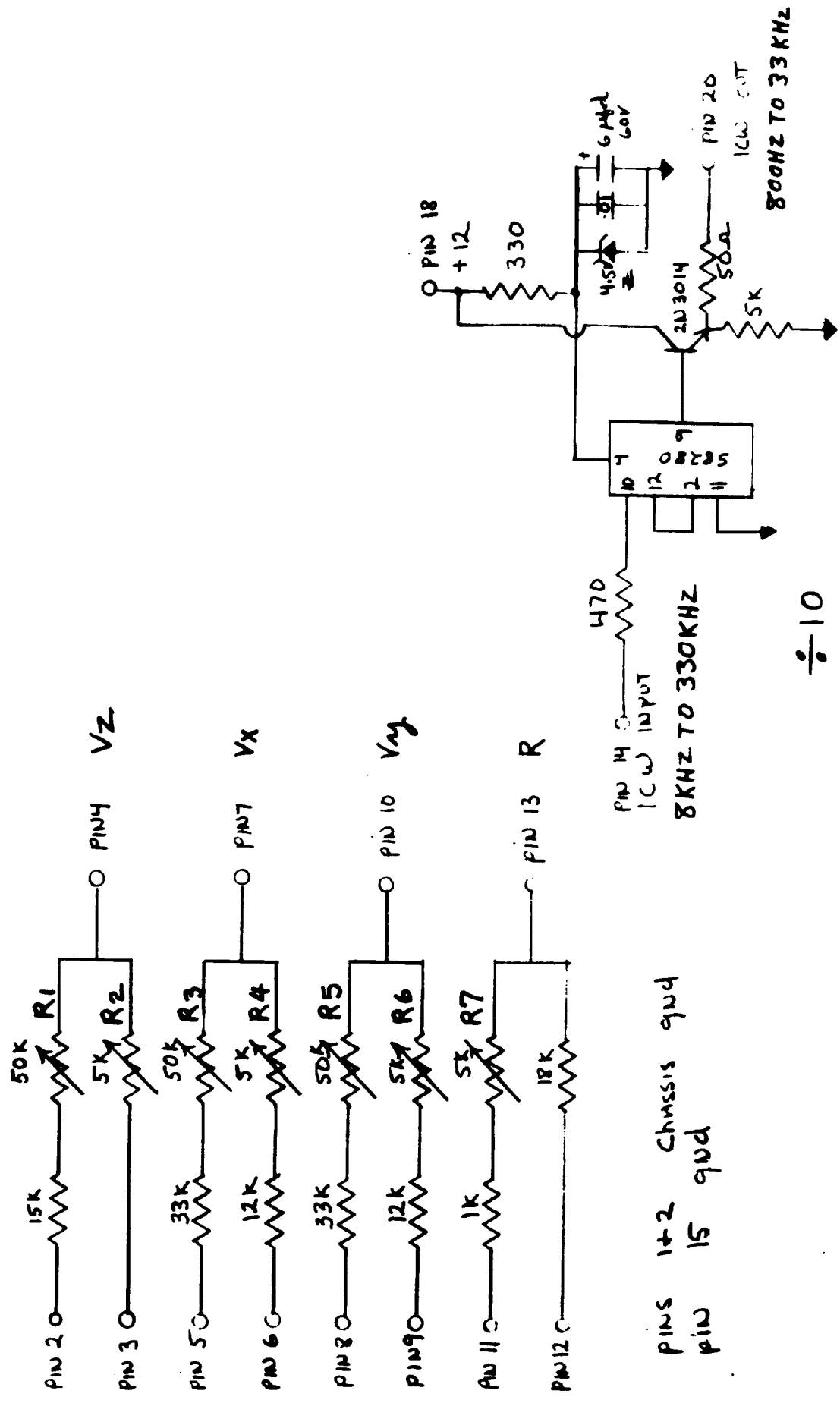


Figure 61. Meter Board

capacitors in the VCO. Linearity has been measured as better than 0.15 percent of value over the required operating range. The bias error is nulled by the center frequency potentiometer adjustment and is maintained by temperature compensating diodes.

The values of the summing amplifier weighting resistors and meter scaling resistors are calculated in the following manner:

Referring to the antenna beam geometry shown in Figure 62.

let:  $\rho_4 = 1$  (unit vector)

$$l_4 = \cos \alpha_4$$

$$m_4 = \cos \beta_4 \quad \text{(Direction Cosines)}$$

$$n_4 = \cos \gamma_4$$

from:

$$l_4^2 + m_4^2 + n_4^2 = 1$$

$$m_4^2 = l_4^2 \tan^2 \theta_4$$

$$l_4^2 (1 + \tan^2 \theta_4) = (1 - \cos^2 \gamma_4)$$

$$l_4^2 \sec^2 \theta_4 = \sin^2 \gamma_4$$

$$l_4 = \cos \theta_4 \sin \gamma_4 = \cos \alpha_4$$

$$m_4 = \sin \theta_4 \sin \gamma_4 = \cos \beta_4$$

$$n_4 = \cos \gamma_4$$

The individual doppler velocities can be resolved into their x, y and z components

from:

$$D_i = \frac{2}{\lambda_i} [V_x l_i + V_y m_i + V_z n_i]$$

$$D_1 = \frac{2}{\lambda_1} [V_x l_1 - V_y m_1 + V_z n_1] \quad (1)$$

$$D_2 = \frac{2}{\lambda_2} [-V_x l_2 - V_y m_2 + V_z n_2] \quad (2)$$

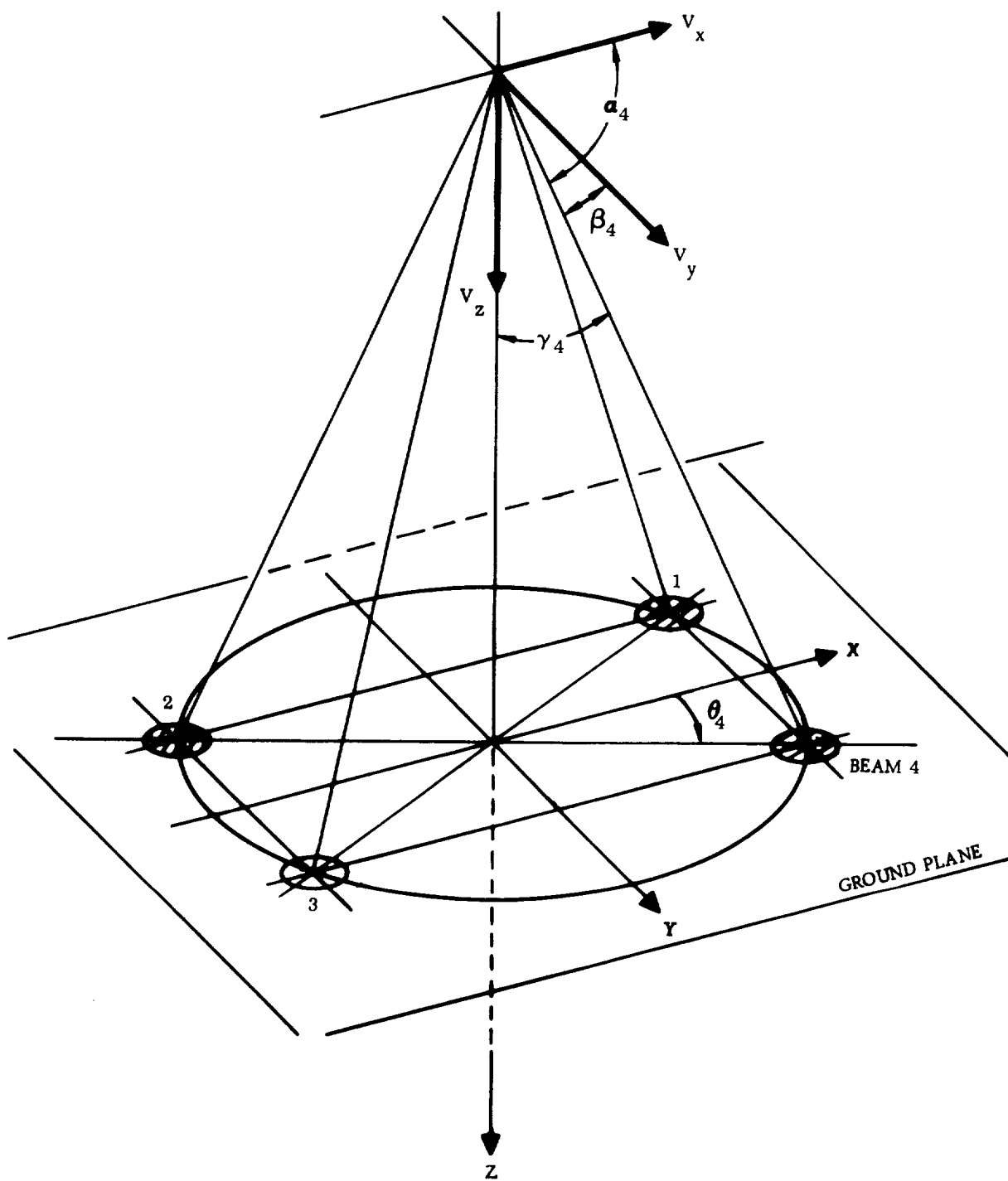


Figure 62. PTDLR Beam Geometry

$$D_4 = \frac{2}{\lambda_4} [V_x \ell_4 + V_y m_4 + V_z n_4] \quad (3)$$

solving (1), (2) and (3) for  $V_x$ ,  $V_y$ , and  $V_z$

$$V_x \ell_1 - V_y m_1 + V_z n_1 = \frac{\lambda_1 D_1}{2} \quad (1)$$

$$-V_x \ell_2 - V_y m_2 + V_z n_2 = \frac{\lambda_2 D_2}{2} \quad (2)$$

$$V_x \ell_4 + V_y m_4 + V_z n_4 = \frac{\lambda_4 D_4}{2} \quad (3)$$

$V_x$  Matrix:

$$V_x = \begin{vmatrix} \frac{\lambda_1 D_1}{2} - m_1 + n_1 \\ \frac{\lambda_2 D_2}{2} - m_2 + n_2 \\ \frac{\lambda_4 D_4}{2} + m_4 + n_4 \end{vmatrix} = \begin{vmatrix} -\frac{\lambda_1 D_1}{2} (m_2 n_4 + m_4 n_2) \\ +\frac{\lambda_2 D_2}{2} (m_1 n_4 + m_4 n_1) \\ +\frac{\lambda_4 D_4}{2} (m_2 n_1 - m_1 n_2) \end{vmatrix}$$

$$= \begin{vmatrix} \ell_1 - m_1 + n_1 \\ -\ell_2 - m_2 + n_2 \\ \ell_4 + m_4 + n_4 \end{vmatrix} = \begin{vmatrix} -\ell_1 (m_2 n_4 + m_4 n_2) \\ -\ell_2 (m_1 n_4 + m_4 n_1) \\ +\ell_4 (m_2 n_1 - m_1 n_2) \end{vmatrix}$$

let:  $V_x = K_1 D_1 - K_2 D_2 - K_3 D_4$

$$K_1 = \frac{\lambda_1}{2\ell_1} \left[ \frac{1}{1 + \frac{\ell_2}{\ell_1} \left( \frac{m_1 n_4 + m_4 n_1}{m_2 n_4 + m_4 n_2} \right) - \frac{\ell_4}{\ell_1} \left( \frac{m_2 n_1 - m_1 n_2}{m_2 n_4 + m_4 n_2} \right)} \right]$$

$$K_2 = \frac{-\lambda_2}{2\ell_2} \left[ \frac{1}{1 + \frac{\ell_1}{\ell_2} \left( \frac{m_2 n_4 + m_4 n_2}{m_1 n_4 + m_4 n_1} \right) - \frac{\ell_4}{\ell_2} \left( \frac{m_2 n_1 - m_1 n_2}{m_1 n_4 + m_4 n_2} \right)} \right]$$

$$K_3 = \frac{-\lambda_3}{2\ell_3} \left[ \frac{1}{1 + \frac{\ell_1}{\ell_4} \left( \frac{m_2 n_4 + m_4 n_2}{m_2 n_1 - m_1 n_2} \right) + \frac{\ell_2}{\ell_4} \left( \frac{m_1 n_4 + m_4 n_1}{m_2 n_1 - m_1 n_2} \right)} \right]$$

For PTDLR:

$$\ell = m = \frac{\sqrt{2}}{2} \text{ (45° clock angles)}$$

$$n_1 = n_2 = n_4 \text{ (equal splay angles)}$$

$$\lambda_1 = \lambda_2 = \lambda_4 \text{ (equal frequencies)}$$

$$K_1 = \frac{\lambda}{4\ell}$$

$$K_2 = \frac{\lambda}{4m} = \frac{\lambda}{4\ell}$$

$$V_x = \frac{\lambda}{4\ell} (D_1 - D_2)$$

$$K_3 = 0$$

Vy Matrix:

$$V_y = \begin{array}{c} \left| \begin{array}{l} \ell_1 + \frac{\lambda_1 D_1}{2} + n_1 \\ -\ell_2 + \frac{\lambda_2 D_2}{2} + n_2 \\ \ell_4 + \frac{\lambda_4 D_4}{2} + n_4 \end{array} \right| \begin{array}{l} \frac{+\lambda_1 D_1}{2} (\ell_2 n_4 + \ell_4 n_2) \\ \frac{+\lambda_2 D_2}{2} (\ell_1 n_4 - \ell_4 n_1) \\ \frac{-\lambda_4 D_4}{2} (\ell_1 n_2 + \ell_2 n_1) \end{array} \\ \hline \left| \begin{array}{l} +\ell_1 - m_1 + n_1 \\ -\ell_2 - m_2 + n_2 \\ +\ell_4 + m_4 + n_4 \end{array} \right| \begin{array}{l} -m_1 (\ell_2 n_4 + \ell_4 n_2) \\ -m_2 (\ell_1 n_4 - \ell_4 n_1) \\ -m_4 (\ell_1 n_2 + \ell_2 n_1) \end{array} \end{array}$$

$$\text{let: } V_y = K_4 D_4 - K_5 D_1 - K_6 D_2$$

$$K_4 = \frac{\lambda_4}{2m_4} \left[ \frac{1}{1 + \frac{m_1}{m_4} \left( \frac{\ell_2 n_4 + \ell_4 n_2}{\ell_1 n_2 + \ell_2 n_1} \right) + \frac{m_2}{m_4} \left( \frac{\ell_1 n_4 - \ell_4 n_1}{\ell_1 n_2 + \ell_2 n_1} \right)} \right]$$

$$K_5 = \frac{\lambda_1}{2m_1} \left[ \frac{1}{1 + \frac{m_4}{m_1} \left( \frac{\ell_1 n_2 + \ell_2 n_1}{\ell_2 n_4 + \ell_4 n_2} \right) + \frac{m_2}{m_1} \left( \frac{\ell_1 n_4 - \ell_4 n_1}{\ell_2 n_4 - \ell_4 n_2} \right)} \right]$$

$$K_6 = \frac{\lambda_2}{2m_2} \left[ \frac{1}{1 + \frac{m_1}{m_2} \left( \frac{\ell_2 n_4 + \ell_4 n_2}{\ell_1 n_4 - \ell_4 n_1} \right) + \frac{m_4}{m_2} \left( \frac{\ell_1 n_2 + \ell_2 n_1}{\ell_1 n_4 - \ell_4 n_1} \right)} \right]$$

For PTDLR:

$$\ell = m = \frac{\sqrt{2}}{2} \quad (45^\circ \text{ clock angles})$$

$$n_1 = n_2 = n_4 \quad (\text{equal splay angles})$$

$$\lambda_1 = \lambda_2 = \lambda_4 \quad (\text{equal frequencies})$$

$$K_4 = \frac{\lambda}{4\ell} = \frac{\lambda}{4m}$$

$$K_5 = \frac{\lambda}{4m}$$

$$K_6 = 0$$

$$V_y = \frac{\lambda}{4m} (D_4 - D_1)$$



$V_z$  Matrix:

$$V_z = \begin{vmatrix} \ell_1 - m_1 + \frac{\lambda_1 D_1}{2} \\ -\ell_2 - m_2 + \frac{\lambda_2 D_2}{2} \\ \ell_4 + m_4 + \frac{\lambda_4 D_4}{2} \end{vmatrix} = \begin{vmatrix} +\ell_1 - m_1 + n_1 \\ -\ell_2 - m_2 + n_2 \\ +\ell_4 + m_4 + n_4 \end{vmatrix}$$

$$\begin{matrix} +\frac{\lambda_1 D_1}{2} (\ell_4 m_2 - \ell_2 m_4) \\ -\frac{\lambda_2 D_2}{2} (\ell_1 m_4 + m_1 \ell_4) \\ -\frac{\lambda_4 D_4}{2} (\ell_1 m_2 + \ell_2 m_1) \end{matrix}$$

$$\begin{matrix} n_1 (\ell_4 m_2 - \ell_2 m_4) \\ -n_2 (\ell_1 m_4 + m_1 \ell_4) \\ -n_4 (\ell_1 m_2 + \ell_2 m_1) \end{matrix}$$

let:  $V_z = K_7 D_2 + K_8 D_4 + K_9 D_1$

$$K_7 = \frac{\lambda_2}{2n_2} \left[ \frac{1}{1 + \frac{n_4}{n_2} \left( \frac{\ell_1 m_2 + \ell_2 m_1}{\ell_1 m_4 + m_1 \ell_4} \right)} - \frac{n_1}{n_2} \left( \frac{\ell_4 m_2 - \ell_2 m_4}{\ell_1 m_4 + m_1 \ell_4} \right) \right]$$

$$K_8 = \frac{\lambda_4}{2n_4} \left[ \frac{1}{1 + \frac{n_2}{n_4} \left( \frac{\ell_1 m_4 + m_1 \ell_4}{\ell_1 m_2 + \ell_2 m_1} \right)} - \frac{n_1}{n_4} \left( \frac{\ell_4 m_2 - \ell_2 m_4}{\ell_1 m_2 + \ell_2 m_1} \right) \right]$$

$$K_9 = \frac{\lambda_1}{2n_1} \left[ \frac{1}{1 + \frac{n_2}{n_1} \left( \frac{\ell_1 m_4 + m_1 \ell_4}{\ell_4 m_2 - \ell_2 m_4} \right)} + \frac{n_4}{n_1} \left( \frac{\ell_1 m_2 + \ell_2 m_1}{\ell_4 m_2 - \ell_2 m_4} \right) \right]$$

For PTDLR:

$$\ell = m = \frac{\sqrt{2}}{2} \quad (45^\circ \text{ clock angles})$$

$$n_1 = n_2 = n_4 \quad (\text{equal splay angles})$$

$$\lambda_1 = \lambda_2 = \lambda_3 \quad (\text{equal frequencies})$$

$$K_7 = \frac{\lambda}{4n}$$

$$K_8 = \frac{\lambda}{4n}$$

$$V_z = \frac{\lambda}{4n} (D_2 + D_4)$$

$$K_9 = 0$$

#### Channel Mechanization

$$l = \cos \theta \sin \gamma$$

$$m = \sin \theta \sin \gamma$$

$$n = \cos \gamma$$

$$\phi = 45^\circ$$

$$\cos 45^\circ = \sin 45^\circ = 0.70711$$

$$\gamma = 24^\circ 10'$$

$$\cos 24^\circ 10' = 0.91236$$

$$\sin 24^\circ 10' = 0.40939$$

$$l = m = (0.70711)(0.40939) = 0.2894837629$$

$$n = 0.91236$$

Check:

$$l^2 + m^2 + n^2 = 1$$

$$2(0.28948)^2 + (0.91236)^2$$

$$0.16759734 + 0.83240077 = 0.99999811$$

Beams 1, 2, and 4

$$v_x = \frac{\lambda}{4l} (D_1 - D_2)$$

$$v_y = \frac{\lambda}{4m} (D_4 - D_1)$$

$$v_z = \frac{\lambda}{4n} (D_2 + D_4)$$

$$\lambda = \frac{c}{f} = \frac{9.8 \times 10^8 \text{ ft/sec}}{13.35 \times 10^9 \text{ Hz}} = 0.0738 \text{ ft/sec/Hz}$$

$$K_x = \frac{\lambda}{4l} = \frac{0.0738 \text{ ft/sec/cps}}{4 (0.28948)} = 0.063735 \text{ ft/sec/Hz}$$

$$K_y = \frac{\lambda}{4m} = \frac{\lambda}{4l} = 0.063735 \text{ ft/sec/Hz}$$

$$K_z = \frac{\lambda}{4n} = \frac{0.0738 \text{ ft/sec/Hz}}{4(0.91236)} = 0.020222 \text{ ft/sec/Hz}$$

$V_x$  Channel Mechanization

let:  $V_x = 500 \text{ ft/sec} = 340 \text{ mph}$  for full scale meter deflection of  $50 \mu\text{A}$   
 $K_v = 5 \text{ kc/volt}$  (velocity track output)

if:  $V_y = V_z = 0$        $D_1 = -D_2$

$$V_x = \frac{\lambda}{4l} (D_1 - D_2) = K_x (D_1 - D_2)$$

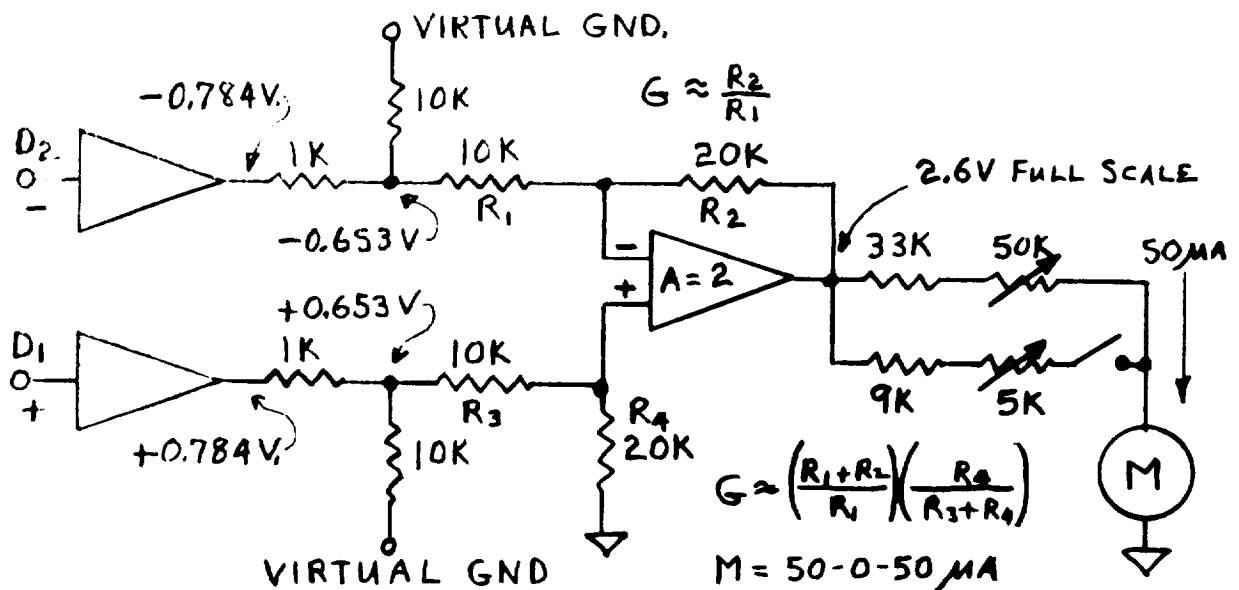
$$500 \text{ ft/sec} = 0.063735 \text{ ft/sec/Hz} \cdot 2D_1$$

$$-D_2 = D_1 \frac{500}{2(0.063735)} = 3.92249 \text{ KHz/500 ft/sec}$$

$$\frac{D_1}{K_v} = \frac{3.92 \text{ KHz}}{5 \text{ KHz/volt}} = 0.784 \text{ volts (full scale)}$$

$D_1 = +0.784 \text{ volts}$

$D_2 = -0.784 \text{ volts}$



$V_y$  Channel Mechanization

let:  $V_y = 500 \text{ ft/sec} = 340 \text{ mph}$  for full scale meter deflection of  $50 \mu\text{A}$ .

$K_v = 5\text{Hz/volt}$  (vel tracker output)

if:  $V_y = V_z = 0 \quad D_4 = -D_1$

$$v_y = \frac{\lambda}{4m} (D_4 - D_1) = K_y (D_4 - D_1)$$

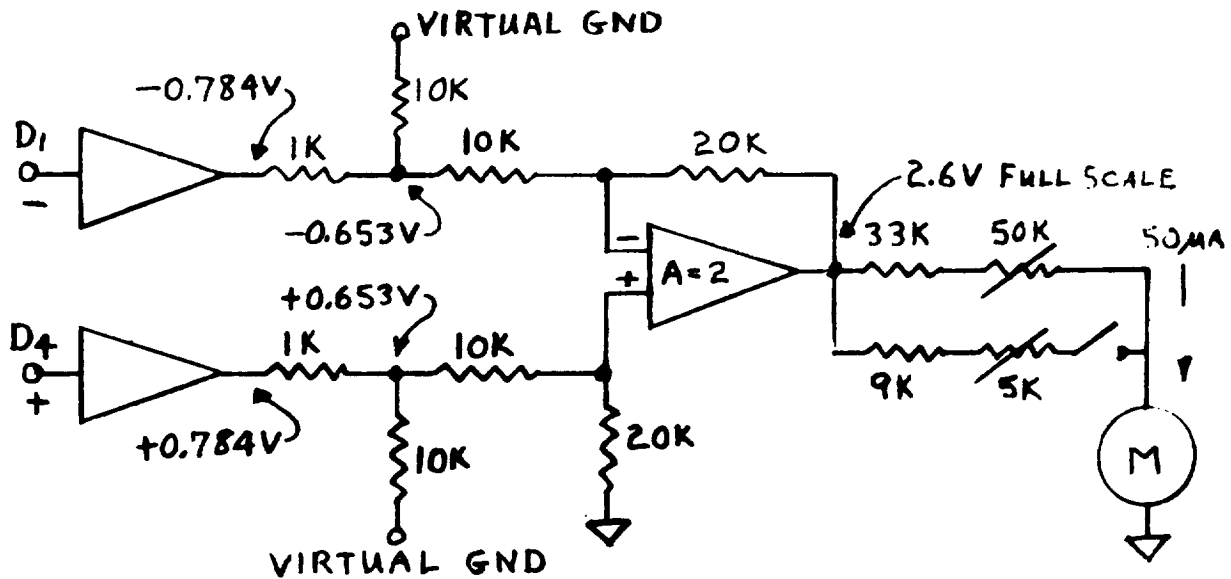
$$500 \text{ ft/sec} = 0.063735 \text{ ft/sec/Hz} (2D_4)$$

$$-D_1 = D_4 = \frac{500}{2(0.0637)} = 3.922 \text{ KHz}$$

$$\frac{D_4}{K_v} = \frac{3.92 \text{ KHz}}{5 \text{ KHz/volt}} = 0.784 \text{ volts (full scale)}$$

$D_4 = +0.784 \text{ volts}$

$D_1 = -0.784 \text{ volts}$



$V_z$  Channel Mechanization

let:  $V_z = 500 \text{ ft/sec} = 340 \text{ mph}$  for full scale meter deflection of  $50 \mu\text{A}$ .

$K_v = 5 \text{ Hz/volt}$  (vel tracker output)

if:  $V_x = V_y = 0 \quad D_2 = D_4$

$$V_z = \frac{\lambda}{4\eta} (D_2 + D_4) = K_z (D_2 + D_4)$$

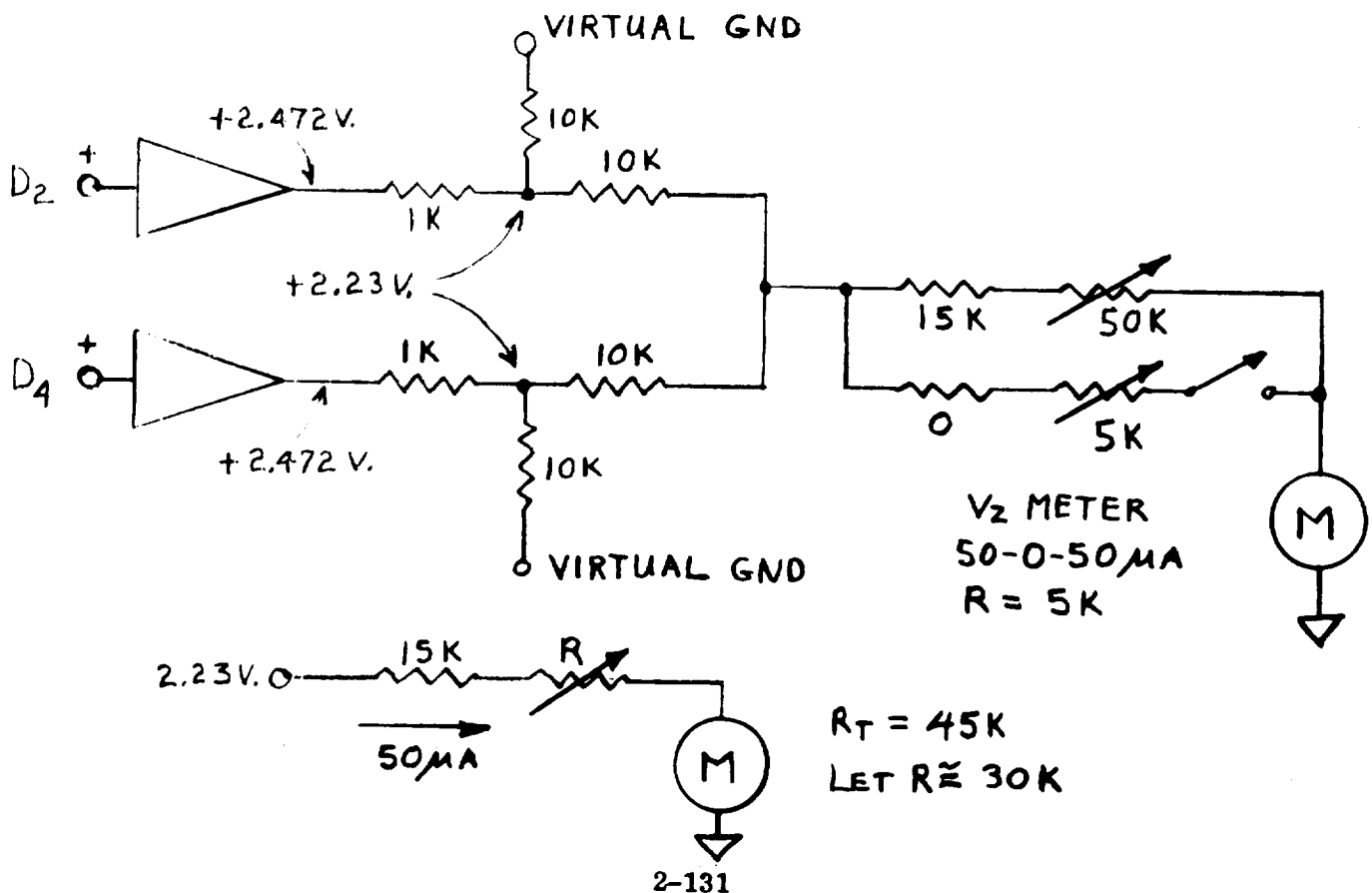
$$500 \text{ ft/sec} = .02022 \text{ ft/sec/Hz} (2D_2)$$

$$D_2 = D_4 = \frac{500}{2 \cdot 0.02022} = 12.36277 \text{ KHz/500 ft/sec}$$

$$\frac{D_4}{K_v} = \frac{12.363 \text{ KHz}}{5 \text{ KHz/volt}} = 2.472 \text{ volts/500 ft/sec (full scale)}$$

$D_2 = 2.472 \text{ volts}$

$D_4 = 2.472 \text{ volts}$



#### 2.4.13 Panel Controls and Electronic Chassis

The control panel and electronic chassis was designed to house the required system power supplies, electronic packages, and to provide sufficient switches, display meters, and critical test points to permit convenient system performance monitoring, mode configuration switching, and trouble shooting. The unit is mountable in a standard 19-inch instrument rack. Referring to Figure 63:

##### a. Meters

- (1)  $M_1$  is a 0-30 volt dc meter used to monitor the various power supply voltages. The power supply to be monitored is selected by the rotary switch,  $S_1$ .
- (2)  $M_2$  is a 100 - 0 - 100 (zero center) u-amp meter intended to be used to monitor agc levels, transmitter power, etc. Time did not permit development of the circuitry required to utilize this meter.
- (3)  $M_3$ ,  $M_4$ ,  $M_5$  are used to display  $V_x$ ,  $V_y$ , and  $V_z$  velocity components respectively. The meter faces are labeled to identify the direction of motion and the meter scales are calibrated to display individual velocity components in the range of 500 - 0 - 500 ft/sec. Directly above each meter is an illuminated push-button switch that may be used to increase the scale factor of the associated meter by a factor of five thus giving a full scale deflection sensitivity of 100 ft/sec. The push-button becomes illuminated when depressed into the X5 position.
- (4)  $M_6$  is the range (altitude) meter. The meter face was specifically designed for the PTDLR system and contains three separate scales. The lower scale is used in the ICW mode to indicate

altitude over the 0 - 30 K ft range. A green light adjacent to this scale is illuminated when in the ICW mode. The light is interlocked with the ICW range tracking loop such that it will extinguish if loss of range tracking occurs. Automatic mode switchover occurs when descending below 750 ft altitude and the 750 ft mark on this scale has been extended in length to visually identify where switchover should occur. After switchover occurs the green light is extinguished and the red indicator adjacent to the two upper scales becomes illuminated indicating operation in the FM/CW mode. The center scale indicates altitude over the range of 0 - 1200 ft and the upper scale indicates altitude over the range of 0 - 180 ft full scale. The upper scale is activated by depressing (momentarily)  $S_4$  which also becomes illuminated to identify that the upper scale is being used.

All altitude scales are highly non-linear to expand the low altitude end for more accurate readout.

b. Switches

- (1)  $S_1$  selects the power supply output voltage to be displayed on meter,  $M_1$ .
- (2)  $S_2$  has two functions. When switched into the  $J_1$  position, the PTDLR system operates in the  $J_1$  Bessel sideband mode. Likewise, when switched to the  $J_2$  or  $J_3$  position, the system operates in the  $J_2$  or  $J_3$  Bessel sideband mode respectively. When switched into any of the other positions, the system is locked into any one of the three Bessel modes of operation. The particular mode being pre-established by a wire change on the



**switch. The switch is then used to select from number of signals the signal that appears at the test connector adjacent to the switch. The signals available at the test connector as a function of switch position are:**

- a)  $V_1$  - the raw doppler received signal from beam No. 1 applied to velocity tracker No. 1.
  - b)  $V_2$  - the raw doppler received signal from beam No. 2 applied to velocity tracker No. 2.
  - c)  $V_3$  - the raw doppler received signal from beam No. 4 applied to velocity tracker No. 3.
  - d) REF - the zero doppler reference frequency, nominally 37.8 KHz.
  - e) ALT - the raw folded, altitude channel receive signal applied to altitude channel processor. Nominal frequency is 378 KHz.
  - f)  $\phi$  - the error signal within the altitude channel phase lock loop. Generally, appears as a sampled 730 Hz sine wave.
  - g) D.C. - A DC voltage proportional to altitude at a scaling of approximately 10 mv/ft.
  - h) ICW - the amplitude detected range channel video applied to the ICW range tracker.
- (3)  $S_3$  is used to control the primary line power and mode selection. In the standby position power is applied to all modules except the transmitter. The FM/CW position locks the system in the FM/CW mode. The auto position activates the automatic mode switching capabilities occurring as a function of altitude. The

ICW position locks the system in the ICW mode. The transmitter is on in each of these positions. The green light adjacent to this control is illuminated when the switch position is not in the "off" position and indicates a power "on" condition.

- (4)  $S_4$  is the FM/CW altitude scale expansion switch.
- (5)  $S_5$  changes the FM/CW modulation index by a factor of two.
- (6)  $S_6$  allows the insertion or removal of the leakage elimination filters in the signal path of each of the three velocity channels and in the FM/CW altitude channel.
- (7)  $S_7$ ,  $S_8$  and  $S_9$  provide a times five scale expansion of the adjacent meters.

c. Test Connectors

Eleven test connectors are provided on the lower left hand portion of the control panel. These connectors are wired directly to various signal points and were used as the data tape recorder interface point. The following is a list of the signals appearing at various connectors:

<u>Connector</u>	<u>Signal</u>	
$J_{16}$	Velocity tracker No. 1 output	} $\approx 1.5$ V p-p square wave at 37.8 KHz $\pm f_d$
$J_{17}$	Velocity tracker No. 2 output	
$J_{18}$	Velocity tracker No. 3 output	
$J_{19}$	$J_3/10$ reference (37.8 KHz)	
$J_{20}$	FM/CW range at $\approx -10$ mv/ft (DC)	
$J_{21}$	ICW range - frequency variable square wave	
$J_{22}$	FM/CW - 730 Hz variable pulsewidth	
$J_{23}$	Mode - +12V in FM/CW, -12V in ICW	

- J<sub>32</sub>**            Raw received doppler signal No. 1 (tracker input)
- J<sub>33</sub>**            Raw received doppler signal No. 2
- J<sub>34</sub>**            Raw received doppler signal No. 3

**d. Rear Chassis Connectors**

A number of connectors are contained on the rear of the chassis and the PTDLR RF head. The various signals and destinations are fully shown on the chassis wiring diagram, Figure 64.

**2.4.14 Power Supplies**

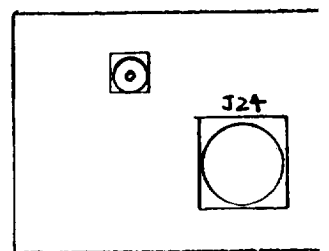
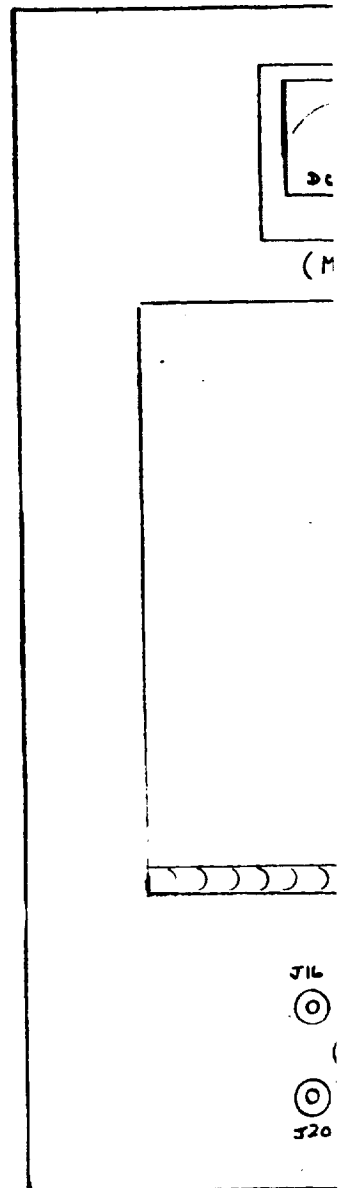
The power supplies are commercial AC to DC converters which operate from either 60 Hz to 400 Hz prime power. They are free convection cooled from a maximum ambient air temperature of 50 C.

The supply ratings are:

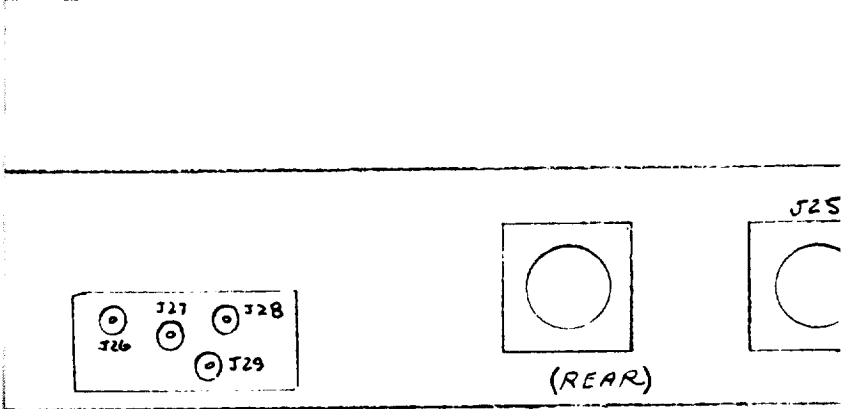
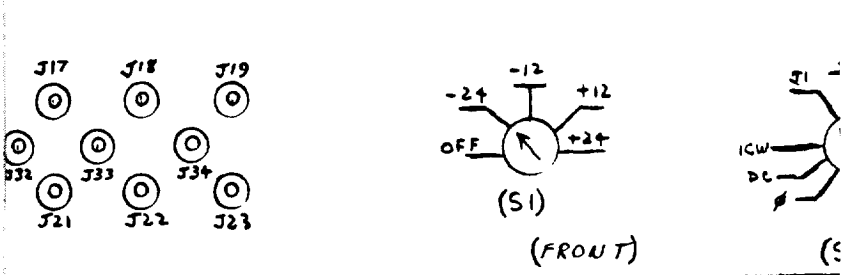
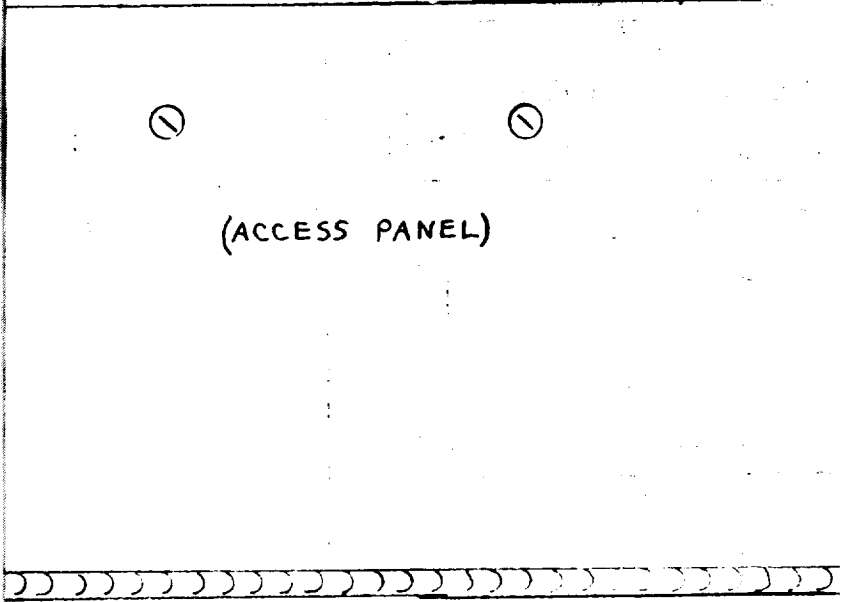
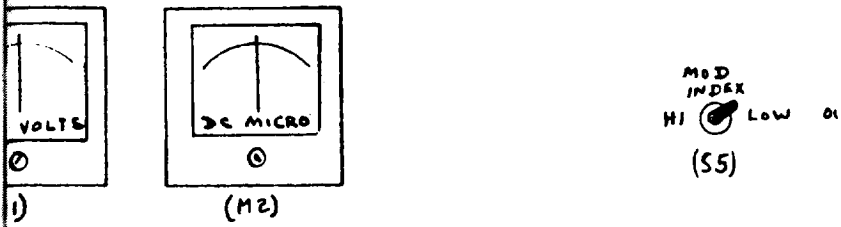
- +12V at 2.8A            Deltron A12-2.8
- 12V at 1.4A            Deltron A12-1.4
- +28V at 7.6A            Deltron A28-7.6
- 24V at 0.38A           Dresden Barns 25903

Regulation is 0.01 percent for all supplies.

The supplies have operated satisfactorily during the course of the program which included three flight test periods.



FOLDOUT FRAME



Fig

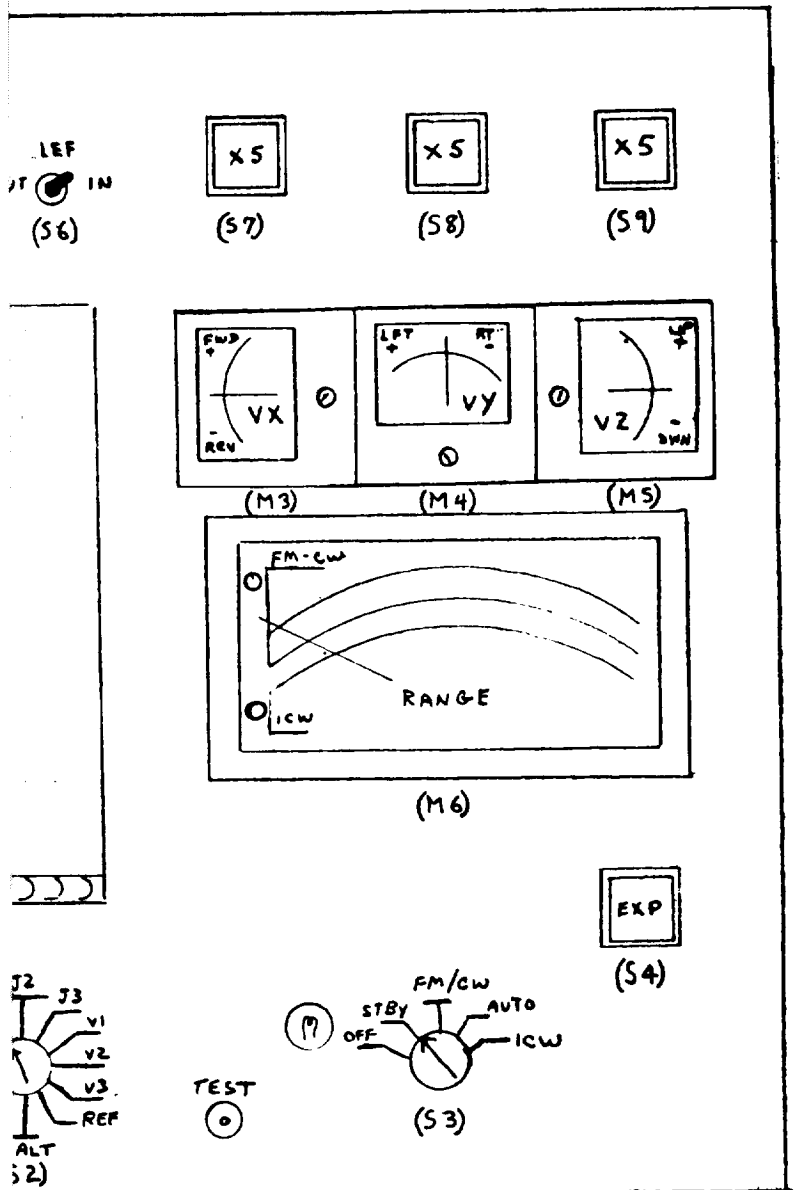
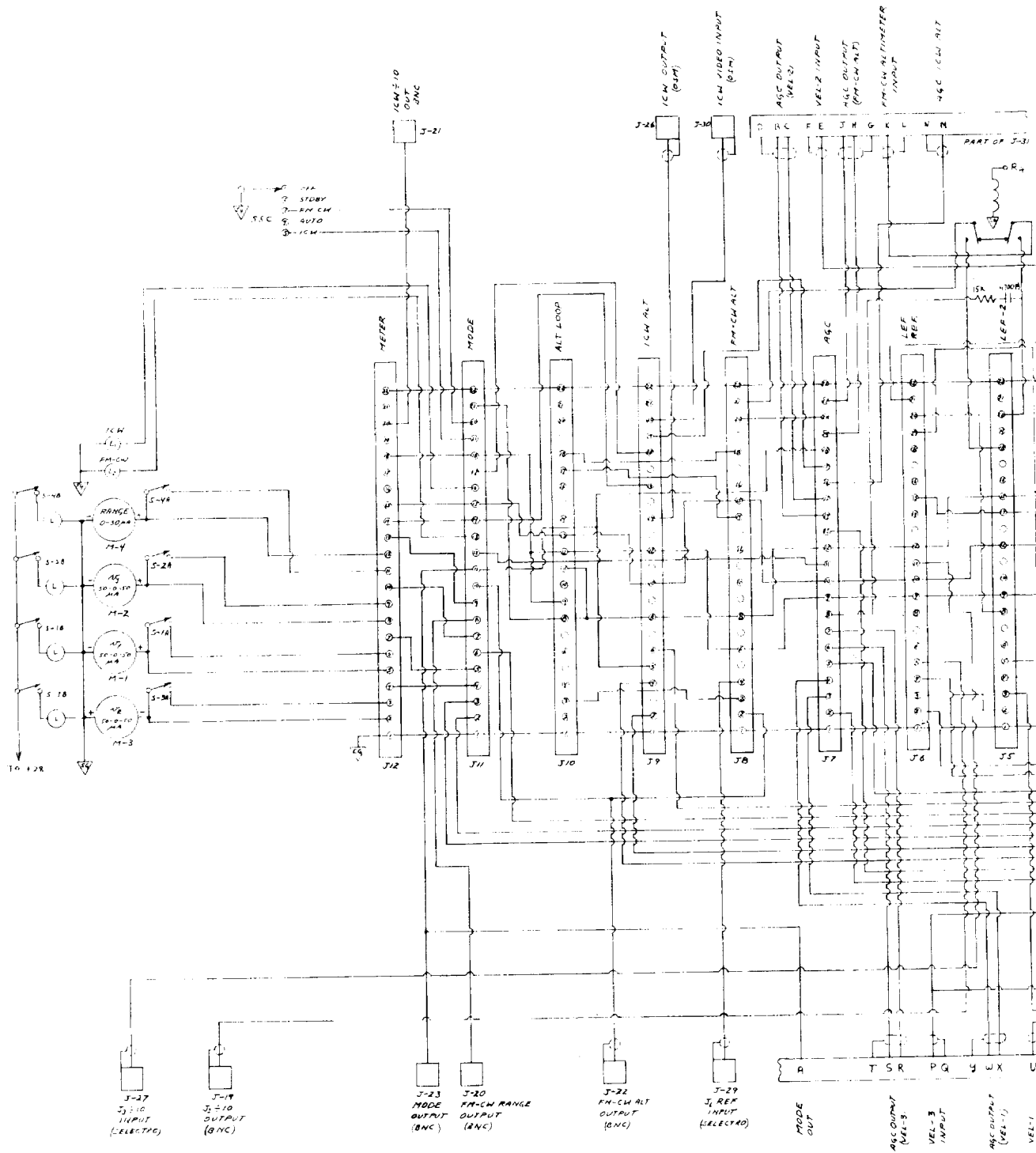


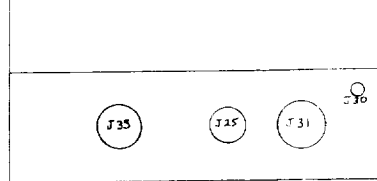
Figure 63. Control Chassis



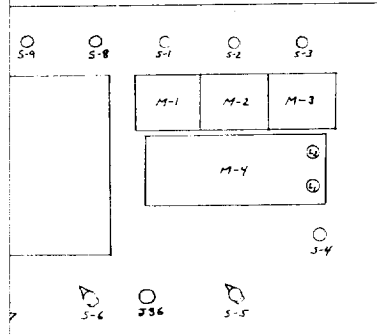
FOLDOUT FRAME







REAR VIEW



FRONT VIEW

POWER SUPPLIES

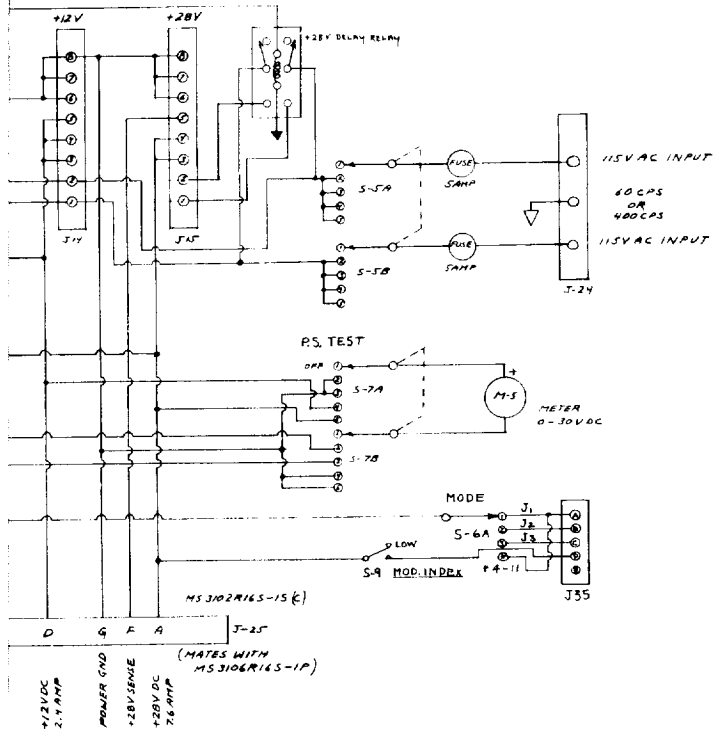


Figure 64. Wiring Diagram

2-139/2-140

FOLDOUT FRAME 3

**3.0**

**FLIGHT TEST**

**3.1**

**General Description**

The flight test program is intended to provide the means of determining the limitations and characteristics of the R146A radar under actual operating conditions. Ideally, the flight profiles would simulate the anticipated CBS, STOL and VTOL terminal descent and landing parameters (e.g., velocity and altitude ranges, attitude rates, decelerations, etc.).

The following altitude-velocity regions were considered representative:

<u>Altitude Range (Feet)</u>	<u>Velocity Range (Feet per Second)</u>
10 - 100	5 - 20
100 - 2000	20 - 350
2000 - 30000	100 - 1000

A flight test vehicle was not available that would permit evaluation of system performance over the entire altitude-velocity region.

The low altitude-velocity test region falls within a helicopter performance envelope and the high altitude-velocity test region would require the performance envelope of a jet-type aircraft. A considerable amount of on-board instrumentation is required to provide the qualitative and quantitative performance evaluation capability. After considering the required flight profiles and instrumentation, the company-owned B26B aircraft was selected as the most expedient vehicle in which to perform the initial flight test evaluation. This vehicle provided test capabilities in the nominal altitude-velocity region and was already fully instrumented.

Three separate flight test programs have been conducted under this contract. The first in the aforementioned B26B aircraft, and the latter two in a Bell-Jet Ranger helicopter. The helicopter provided the capability of fully evaluating the R146A performance in the low altitude-low velocity region. Altitudes down to zero feet and negative velocities in any direction were easily implemented.

The flight test program was divided into two phases. The first phase was used to establish, using on-board instrumentation, the velocity and altitude measuring characteristics and limitations of the landing radar system, and to determine the corrective action necessary if the performance did not meet design goals. The second phase was intended to establish quantitative system accuracy by comparing recorded ground truth data with recorded airborne radar data. Two Government-operated facilities were used to supply the ground truth data. During the second phase of the first flight test program, ground truth was supplied by Air Force Flight Test Center, Edwards Air Force Base, California. Ground truth for the second phase of the last helicopter flight test program was supplied by the Pacific Missile Range, Point Mugu, California.

### 3.2

#### B-26 Flight Test Program

This aircraft, originally a light attack bomber, was delivered to Autonetics Flight Test on June 9, 1966, and subsequently modified to perform service in flight testing avionics systems. A photograph of the aircraft is shown in Figure 65.

The original bomb bay section has been sealed and a floorboard installed with rails to accommodate instrumentation and equipment racks. The aircraft will carry a total of four personnel (one pilot, one qualified

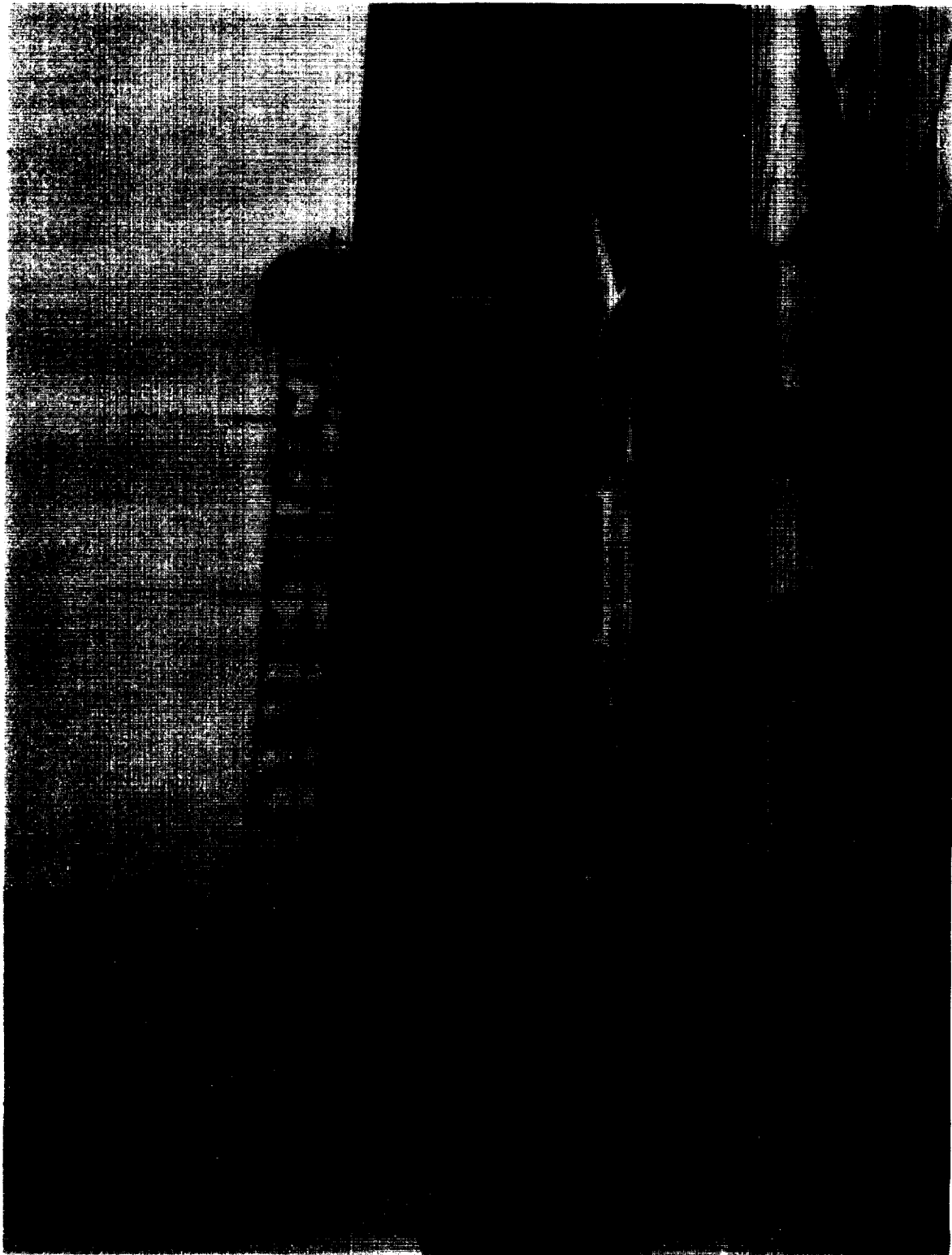


Figure 65. B-26 A/C

aircraft crew member, and two observer/operators) with ample additional space to accommodate the R146A radar equipment and the desired instrumentation.

The aircraft carries sufficient fuel for a three- to four-hour test flight. The maximum level flight speed is 300 knots (369 knots in a dive) with a minimum speed of 90 to 100 knots. The maximum service ceiling is 26,500 feet (with oxygen).

Basic electrical power is dc derived from two 300 amp, 28 volt, engine-driven generators. In addition, 115 v, 400 cycles is available from an inverter rated at 2500 va output. An auxiliary power unit (APU) is installed that will supply 20 K va output at 115 v, 400 cycles.

The R146A equipment was installed in the B26 during the week of February 6, 1969. The first flight occurred on February 10, and was generally conducted over desert terrain at altitudes varying from several hundred feet to 12,500 feet (mean sea level). Only two velocity channels were operating because the third velocity filter had not yet been shipped by McCoy Electronics Company.

The results of the first flight were quite encouraging, and the following observations were made:

- a. Velocity trackers locked-on satisfactorily and appeared to track changes in A/C velocity in both the ICW mode and the  $J_3$  Bessel sideband FM/CW mode.
- b. The ICW range tracking loop locked up satisfactorily and tracked altitude changes from 750 feet up to 10,000 feet (12,500' MSL).
- c. Automatic mode switchover operated satisfactorily (ICW to FM/CW).

The FM/CW altitude channel, however, did not operate correctly. Much greater amplitude modulation was noticed on the various signals that had been anticipated and required a change in the time constant of the AGC amplifiers in order to provide a more uniform signal level.

Thirteen flights were conducted between February 11, 1969 and March 21, 1969, during which time it was determined that the  $J_3$  Bessel sideband did not provide sufficient signal strength to permit satisfactory operation at altitudes below 125 feet in the FM/CW mode.

The R146A equipment was removed from the B26 A/C on March 28, 1969, and a modification program was initiated. The program consisted of adding a switch-selected capability of operating in either a  $J_1$ ,  $J_2$ , or  $J_3$  Bessel sideband FM/CW mode. Because of the higher transmitter leakage levels expected when operating in the  $J_1$  or  $J_2$  modes, it was necessary to incorporate Leakage Elimination Filters to remove the leakage frequency in the velocity channels and the FM/CW altitude channel. In addition to the above modifications, provision to increase the modulation index by a factor of two was added as a front panel switch.

The unfortunate loss of the B26 A/C necessitated the use of a different vehicle to resume flight testing of the modified R146A system.

### 3.3 Helicopter Flight Test Program

The modification program was intended to improve the low-altitude performance of the FM/CW mode and, therefore, a helicopter was selected as the most optimum flight test vehicle in which to investigate low-altitude performance of the R146A system.

A Bell Jet Ranger helicopter was modified by removing both rear doors and the rear seat. A special beam assembly was fabricated on

which were mounted the R146A radar system, operator's seat, and all of the necessary instrumentation. Photographs of the beam assembly and helicopter installation are shown in Figures 66 and 67.

During October 1, 1969 to October 9, 1969, six data flights were conducted. The primary purpose of these tests was to verify the predicted performance improvement that should have been obtained by changing from a  $J_3$  Bessel sideband system to a  $J_2$  Bessel sideband system.

Initial results indicated that the  $J_2$  sideband system operated down to approximately 20 to 25 feet with the low modulation index ( $m = 2.568$ ), and down to approximately 10 to 15 feet with the high modulation index ( $m = 5.136$ ).  $J_1$  sideband operation could not be evaluated because of extremely high leakage.

A detailed spectral analysis of the  $J_2$  mode doppler signals recorded on the flight tapes indicated the accuracy was being considerably impaired by the relatively high degree of sidelobe signal return. Antenna patterns were retaken on Luneberg Lens and a surprising deterioration of sidelobe patterns was noticed (Figure 40).

A new antenna design with low sidelobe levels was considered essential to obtain the desired accuracy and resulted in the development of the "Constant K" lens antenna. This antenna was designed to have low sidelobes and still provided the capability of three independent beams sharing common aperture. Rather high leakage levels were encountered when operating with a single antenna in the  $J_2$  sideband FM/CW mode and it appeared that a dual antenna system (separate transmit and receive antenna) should be evaluated. Two identical Constant K antennas were constructed and installed on the R146A system. A photograph of the dual antenna installation is shown in Figure 68.

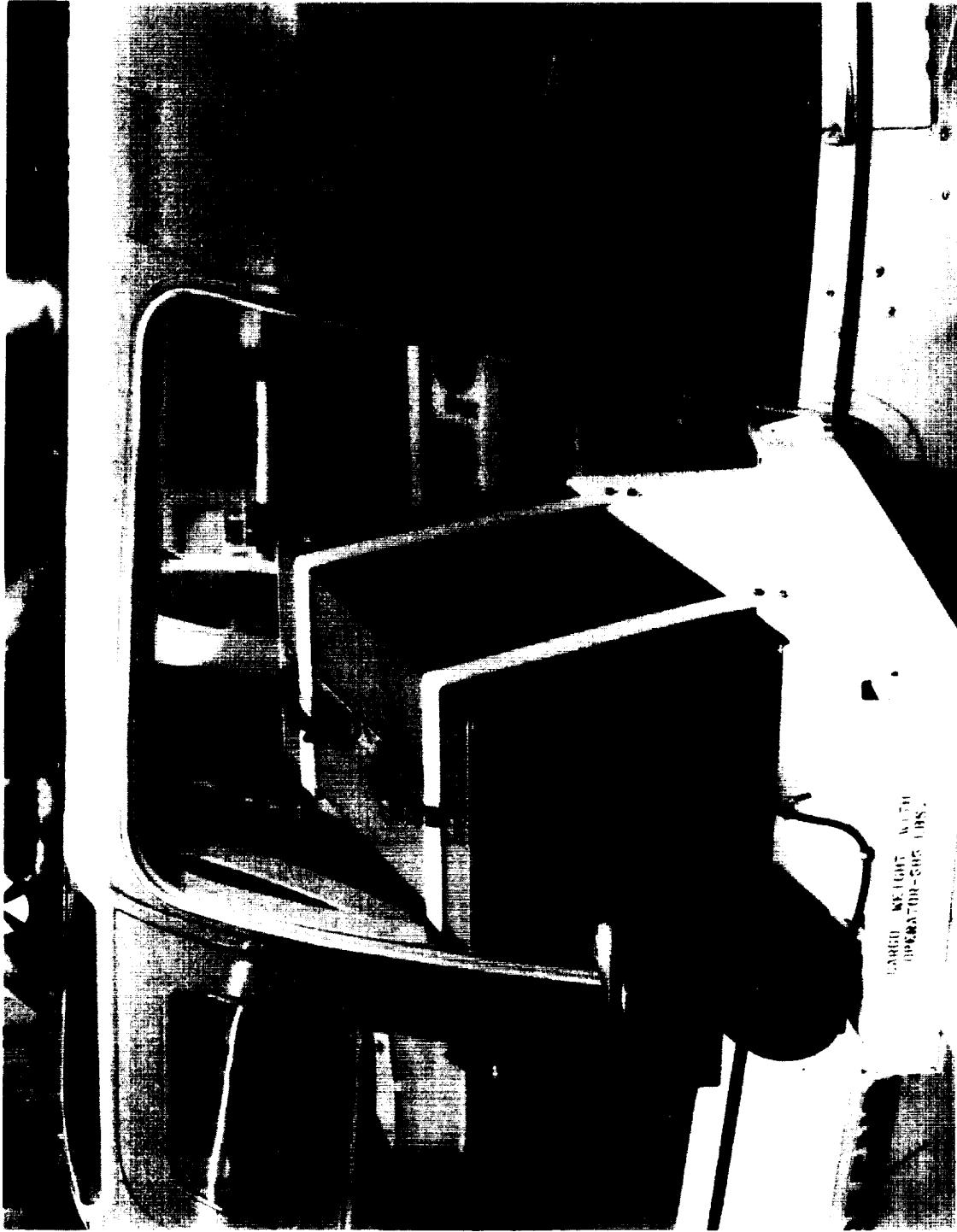


Figure 66. Helicopter Installation





Figure 67. Helicopter Installation

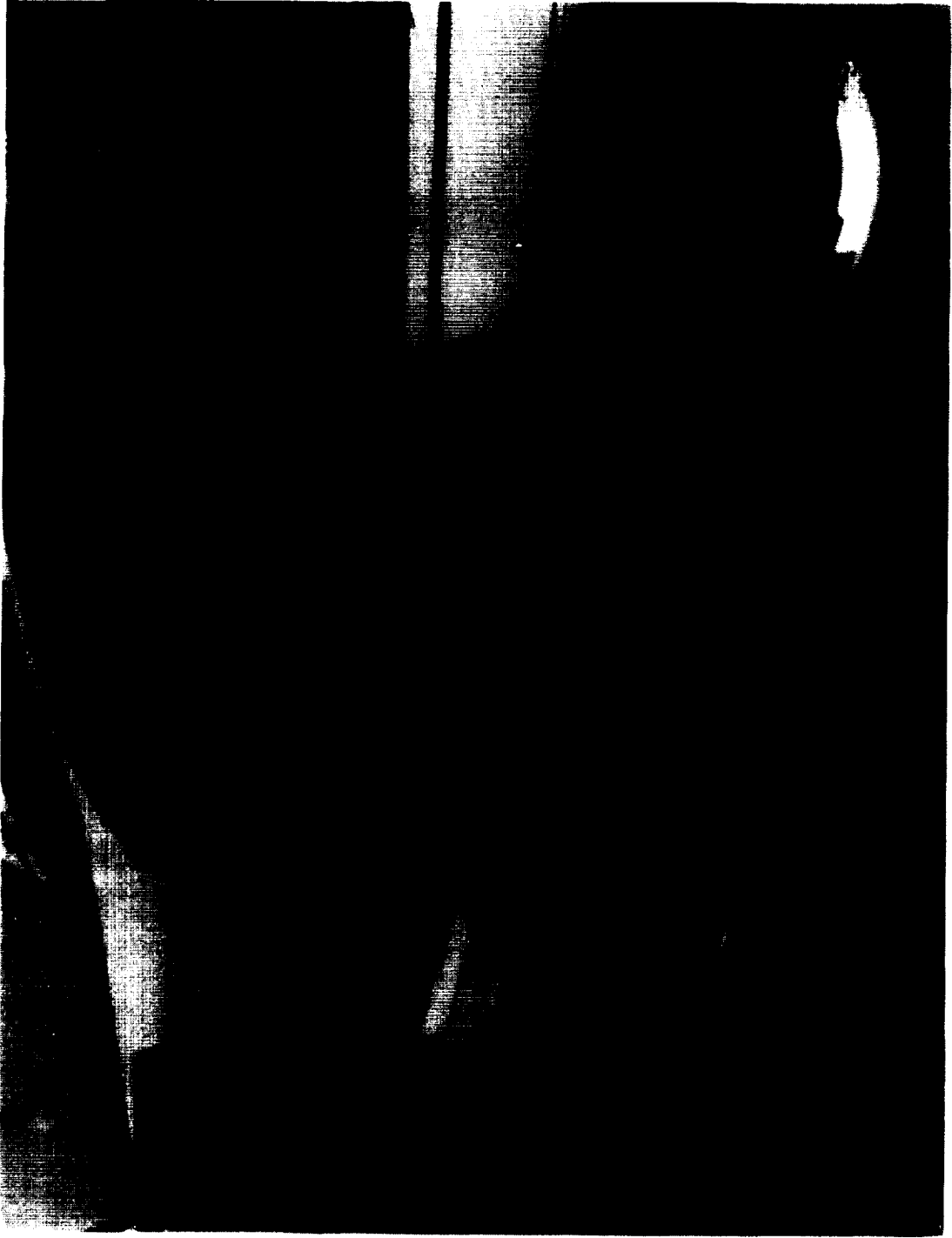


Figure 68. Dual Antenna Installation

A second helicopter flight test program was started on May 7, 1970, and consisted of 18 local data flights and 10 range data flights at the Pacific Missile Range, Point Mugu, California.

During the local flights, the most optimum system configuration from a performance point of view was selected. The best performance was obtained in the low modulation index,  $J_1$  Bessel sideband, dual antenna configuration. There was no requirement for Leakage Elimination Filters. The above configuration was the baseline system flown at PMR, but a considerable amount of data was generated on other system configurations. The last data flight was made on June 25, 1970.

#### 3.4 Instrumentation and Signals Recorded

The following equipment was installed to assist the operator during the local checkout phase and to provide flight geometry data as a permanent record during the controlled data flights:

- a. Vertical Reference Gyro - Kearfott Model 2105
- b. 14-Channel Tape Recorder - Leach Model MTR 3200
- c. Radar Altimeter - Minneapolis-Honeywell Model HG9050
- d. Oscilloscope - Tektronix Model 545 w/53/54C Dual Channel Plug-In
- e. Spectrum Analyzer Plug-In - Tektronix Model IL5
- f. Time Code Receiver - Supplied by PMR to enable accurate time correlation of flight tape data with ground data tapes.
- g. Beacon - Supplied by PMR to improve accuracy of tracking radars.
- h. Frequency Counter - Systron Donner Model 1505

A number of output signals from the R146A were recorded on tape to permit extensive post-flight analysis. Direct and FM recording techniques were used to record the following signals:

DIRECT RECORDING (15 IPS)	
Channel	Signal
1	Raw Doppler - Tracker Input No. 1
3	Raw Doppler - Tracker Input No. 2
5	Raw Doppler - Tracker Input No. 3
7	Velocity Tracker No. 1 Output
9	Zero Doppler Reference Frequency (37.8 KHz)
11	Velocity Tracker No. 2 Output
13	Velocity Tracker No. 3 Output

FM RECORDING	
Channel	Signal
2	A/C Roll
4	A/C Pitch
6	Altitude - R146A (FM/CW Mode)
8	Altitude, High Sensitivity - M-H Radar Altimeter
10	Altitude, Low Sensitivity - M-H Radar Altimeter
12	Voice
14	Time - IRIGB

Channel 5 was also used to record the ICW altitude signal when necessary.

### 3.5 Modes Tested

The R146A radar readily permits evaluation of system performance in a number of operating modes. During the flight test program the following modes have been evaluated in both a single antenna (common transmit-receive antenna) and a dual antenna (separate transmit and receive antennas configuration):

#### a. FM/CW Mode

(1)  $J_1$  Bessel Sideband ( $f_m = 378$  KHz), low modulation index

(a) Leakage elimination filters (LEF) in

(b) LEF out

2.  $J_2$  Bessel Sideband ( $f_m = 189$  KHz)

a. Low Modulation Index

(1) LEF in

(2) LEF out

b. High Modulation index

(1) LEF in

(2) LEF out

3.  $J_3$  Bessel Sideband ( $f_m = 126$  KHz)

a. Low Modulation index

(1) LEF in

(2) LEF out

b. High Modulation Index

(1) LEF in

(2) LEF out

B. ICW Mode

1. LEF in

2. LEF out

3. Automatic switchover, acquisition and tracking in an ascending condition

4. Automatic switchover, acquisition and tracking in a descending condition

3.6 Flight Profiles

A number of flight profiles were established to evaluate system performance as a function of altitude, velocity, and acceleration. The following list indicates the general profiles flown at a number of different velocities ranging from -10 feet per second (helicopter) to 330 feet per second (B26):

- A. Low level flights ranging from 5 foot to 10,000 foot altitude.
- B. Triangular ascents and descents ranging from 10 ft. altitude to 1000 ft. altitude.
- C. Vertical ascents and descents ranging from zero altitude to 80 ft. altitude and from 400 ft. altitude to 1500 ft. altitude. Hovering was also done over these same altitude ranges.
- D. Porpoising at several altitudes with slow, medium, and fast pitch rates.
- E. Figure "8" s at slow, medium and fast roll rates.

### 3.7 Terrain Types

A qualitative evaluation of system performance was made over the following terrain types:

- A. General terrain
  - 1. Hard packed, rolled dirt with sparse weeds.
  - 2. Plowed fields with furrows approximately eight inches apart and two inches high (planted and unplanted).
  - 3. Concrete runway aprons
  - 4. Blacktop runways
  - 5. Orange groves, etc.
  - 6. Sand
    - a. Flat (next to surf)
    - b. Rolling (dunes)
    - c. Wet
    - d. Dry
- B. Water (ocean)
  - 1. Beaufort scale: 0 - 1 (estimated)
  - 2. Beaufort scale: 2 - 3 (estimated)

### 3.8 Air Force Flight Test Center and Pacific Missile Range Tests

The first attempt to obtain ground truth altitude and velocity data was made at the Air Force Flight Test Center (AFFTC), Edwards Air Force Base, California. The Facility is located on the edge of a large, dry lake and excellent tracking radar coverage can be provided during low altitude runs over the lake bed. Unfortunately, system performance at that time was unacceptable when operating over highly specular terrain because of the high sidelobes of the Luneberg lens. The dry lake bed is an extremely flat, smooth surface and therefore highly specular. It was then decided to obtain high altitude performance data by selecting a course that did not require flight over the dry lake area. Low altitude flights were not possible over this course because intervening hills prevented adequate coverage of the tracking radar sites. Flight No. 311 was made in the B-26 aircraft on 21 March 1969 in the ICW mode at 1,000 ft and 3,000 ft altitudes and at velocities ranging from 130 knots to 240 knots. No further test flights were scheduled until it was established that the ground truth data tapes were being generated in a satisfactory manner. A review of the computer printouts from the ground truth tape data indicated that a problem did indeed exist at the facility. For this reason, and because of the unacceptable R146A performance over the dry lake area, further testing at AFFTC was discontinued.

After an extensive modification program to eliminate identified deficiencies, the R146A was installed in a jet ranger helicopter, locally tested, and was again ready for accuracy verification through the use of ground truth data. The use of the AFFTC facility was precluded because of the altitude ceiling of the helicopter in its test configuration.

Excellent facilities were available and accessible at the Pacific Missile Range (PMR), Point Mugu, California, and were therefore utilized. Ground truth data was generated by Askania Cameras and a space positioning computer at PMR. A typical flight card, shown in Figure 69, was prepared prior to each data flight to establish flight profiles. A copy was given to the test conductor before take-off and a second copy was retained in the helicopter during the data flight. Coordination was maintained by a VHF communication link. A summary of data flight activities is shown in Table 10. It is apparent from the table that a significant amount of data was obtained in a relatively short time period. This reflects the high degree of competence and cooperation exhibited by the following base personnel at PMR.

Bob Takarachek - Program Manager

Aldo Fatterelli - Range Data Engineer

Frank Nason - Test Conductor


Vic Bridges - Test Conductor



N6236N \_\_\_\_\_ MN \_\_\_\_\_ Date \_\_\_\_\_ Flt \_\_\_\_\_

Hover over west end runway 9 at 200 ft.

VHF frequency 123.3 MHz

Pass No.	Alt.	Vel (MPH)
1	1000	20
2	500	
3	300	
4	200	
5	150	
6	100	
7	75	
8	50	
9	30	
10	20	
11	15	
12	10	
13	5	
14	0 to 1	
15	100 to 0	20 to 0
16	100 to 0	20 to 0

**NOTE:** On pass No. 14 the altitude should be as low as the terrain will permit and velocity should be increased very slowly from 0 to approx. 5 MPH.

Figure 69. Flight Card

**Table 10. Pt. Mugu Flight Summary**

<b>Date</b>	<b>Flight Number</b>	<b>Configuration</b>	<b>Purpose</b>
12 June	017775	Dual Antenna	Variable Velocity and Altitude data
12 June	017773	Dual Antenna	Variable Velocity and Altitude data
15 June	018063	Dual Antenna	Hover data
16 June	018061	Dual Antenna	ICW Altitude and Velocity data
17 June	018064	Dual Antenna	Altitude data
19 June	018062	Dual Antenna	Mode comparison data
25 June	018324	Single Antenna	Altitude and Velocity data



## 4.0 DATA REDUCTION

### 4.1 General Discussion

Data reduction has been performed with two specific purposes in mind. Firstly, sufficient data reduction and spectral analysis were performed on each flight tape generated during the local flight test phase to establish problem areas and to optimize system parameters. Secondly, data reduction was performed to establish system accuracies using ground truth data supplied by the Askania facilities at PMR, Pt. Mugu.

The instrumentation and flight recorder on board this helicopter permitted the generation of a 14 channel flight tape as a permanent record. The recorded signals were used to provide system characteristics during both phases of the data reduction effort.

#### 4.1.1 Information Content on Signals

Optimization of the PTDLR system using flight tapes relied almost completely on the interpretation of the information contained on the various signals recorded.

The following is a discussion of the signals recorded and how they were used during system evaluation.

##### a. A/C pitch and roll signals

This signal was generated by a vertical reference gyro and, when properly aligned and erected in the helicopter, provided a continuous indication of helicopter flight attitude in space coordinates. By noting the pitch angle of the helicopter at any given time during level flight, one can determine the frequency difference that should exist between the forward pointing beams and the rearward pointing

beam since these beams are displaced from symmetry by the helicopter angle of attack. A pitch angle will result in the generation of an apparent vertical velocity ( $V_z$ ) component during level flight. Proper system operation can be estimated by comparing the measured  $V_z$  and forward velocity ( $V_x$ ) components with the measured pitch angle.

Roll angle information is useful in establishing velocity tracker lag and maximum tracking rates. Since a change in roll angle produces a companion change in each of the three doppler beams, a change in nominal doppler frequency of each beam will occur. Controlled roll rates produced by the pilot result in known doppler rates into the velocity trackers. A comparison of roll angle per unit time with the velocity tracker output frequency can establish the dynamic tracker characteristics. A further comparison of this data with laboratory test data will verify that the equipment is operating within design specifications.

b. Radar Altitude Signals

Radar altitude was provided from two sources and recorded on three tape channels. Two of the channels recorded helicopter altitude generated by the Minneapolis-Honeywell radar altimeter. Two scale factors were set representing a high sensitivity channel and a low sensitivity channel. The third channel recorded helicopter altitude as generated by the PTDLR system. The Honeywell altimeter was used to calibrate the PTDLR altimeter output and to determine the approximate accuracy. Unfortunately, the Honeywell altimeter was not useable below 50 ft or above

4000 ft and either a pilot estimate or a barometric altimeter reading was used to provide altitude information outside of this region.

c. Voice Channel

The voice was used to identify the various conditions that exist during the course of a test flight. The flight number, date, purpose of flight, system mode configuration, altitude, type of terrain being flown over, are examples of voice channel entries. An important function of the voice channel was to record observer comments regarding any unusual system performance or signal characteristics that might be noticed. Subsequent spectral analysis of taped signals could then concentrate on those areas identified by the voice channel as containing interesting or unusual phenomenon.

d. Zero Doppler Reference

This signal was derived from the MFG and was an accurate representation of the frequency that should appear at the output of each of the velocity trackers when the helicopter is in a precise zero velocity condition. As shown in the next section (4.1.2) the use of this signal during spectral analysis of the taped doppler signals virtually eliminates the effects of wow, flutter, and long-term tape speed variations on the quality of the data.

e. Velocity Tracker Output Frequency

The frequency output from each of the velocity trackers should approximate the average doppler frequency in each of the

three beams (subtracting the nominal 37.8 KHz reference frequency mentioned above). Spectral comparison of the frequency output vs the frequency input can establish the degree to which the tracker maintains accurate centering within the input spectrum. Input/output spectral widths can be compared to establish the smoothing provided by the time constant within the tracker. Lock-on and drop-out levels as well as tracking accuracy as a function of input signal-to-noise ratio can be determined.

f. Raw Doppler Velocity Signals

These were the most useful signals recorded during the development and testing phase. Careful evaluation of the characteristics permitted optimization of the AGC loop time constant and established the effects of antenna sidelobes as a function of terrain type, beam pointing angle, and helicopter attitude.

Signal-to-noise ratio as a function of altitude, terrain type, and operating mode (e.g.,  $J_1$ ,  $J_2$ , or  $J_3$  Bessel sideband operating in either high or low modulation index) could be readily plotted. Signal-to-leakage levels were conveniently evaluated during subsequent spectral analysis.

4.1.2 Data Reduction Techniques and Interpretation of Results

This section discusses the data reduction techniques used to generate a number of graphs from selected portions of flight tapes made during the PTDLR helicopter flight tests. The previous sections defined the signals recorded and the manner in which they were obtained. As stated before, the most interesting signal recorded is the raw doppler return from each of the three beams. Since this is the signal that

contains all of the information from which velocity information is derived, it is important to examine it carefully and understand each departure from predicted signal characteristics.

An attempt has been made to develop graphs and to interpret them such that meaningful conclusions can be made.

#### 4.1.2.1 Data Reduction Techniques

The raw doppler signal is directly recorded on magnetic tape and therefore this signal, consisting of a voltage that varies with time, is converted to a remnant magnetization that varies with distance along the tape. Any variation in tape speed (either short term or long term) during the recording process or subsequent playback introduces distortion in the form of frequency modulation (spectral broadening) of the original signal.

Wow and flutter figures specified by a tape recorder manufacturer, establish the degree of short and long term variation of tape speed that might be expected. Values of 0.25 percent are specified for the Leach recorder used in the helicopter and values of 0.2 percent are specified for the Honeywell machine used for playback. The overall spectral broadening that might be expected would be:

$$\Delta f = 37.8 \text{ KHz} \sqrt{.25^2 + .2^2} \approx 121 \text{ hz}$$

where 37.8 KHz is the nominal doppler frequency recorded and the quantity under the radical is the R.S.S. value of the two flutter figures.

The doppler spread expected on the input signal is approximately:

$$\Delta f = \frac{2v}{\lambda} \sin \theta d\theta$$



where

$v$  = vehicle velocity (fps)

$\lambda$  = radar wavelength (ft)

$\theta$  = antenna depression angle from the velocity vector

$d\theta$  = two-way antenna beamwidth

Letting

$v$  = 50 Kts  $\approx$  83 ft/sec

$\lambda$  = 0.074 ft

$\sin \theta$  = 80 deg

$d\theta$  = 2.65 deg

The doppler spread,  $\Delta f$ , is approximately equal to 102 hz. It is therefore apparent that the spectral spread introduced by wow and flutter of the tape machines during record and playback is even greater than doppler spread contained in the input signal. This condition must be eliminated in order to reproduce high quality data.

The technique used to minimize this problem during data reduction is quite similiar to the signal processing used in the FM/CW radar wherein the FM'd received signal is mixed with the FM'd L.O. signal to produce a constant difference frequency that is free of FM (matched time delay case). Recordings made during flight tests contain a 37.8 KHz reference, representing the zero doppler frequency, recorded on a separate channel simultaneously with the raw doppler signals. Since all signals are recorded in parallel, the percentage of FM'ing introduced by wow and flutter of the record and playback machines occurs equally on all channels.

The absolute value of spectral spreading is proportional to the individual signal frequencies recorded and since reference signal and raw doppler signals are very nearly the same frequency, close matching of the instantaneous deviations is obtained. Cancellation of the wow and flutter components is readily achieved by mixing the recorded reference signal with a stable oscillator of, say, 5 KHz and bandpass filtering the mixer output to extract the upper sideband only. This new reference frequency, nominally 42.8 KHz, contains the original reference FM'ing and is in turn mixed with the raw doppler signal of interest, bandpass filtered to extract the lower sideband, and is now centered nominally at 5 KHz and is free of wow and flutter distortion.

Figure 70 demonstrates the improvement obtained. The unprocessed reference curve shows a spectral width of approximately 140 Hz when analyzed directly off of the tape machine while the processed reference shows a spectral width comparable to the width of the filter within the spectrum analyzer.

A block diagram of the data reduction set-up is shown in Figure 71. The 10 Hz filter bandwidth within the spectrum analyzer requires relatively long sweep times to insure proper filter buildup during spectrum analysis (e.g., greater than 30 seconds is required to sweep 3 KHz). Because of the dynamic environment during helicopter flight test data gathering, a considerable change in conditions will occur in a 30-second period and would therefore destroy the usefulness of the reduced data. This problem is circumvented by transferring the selected portion of tape data to a Vibralyzer storage drum. This device has compatible bandwidths; up to 0.8 second of data can be stored on the drum surface;

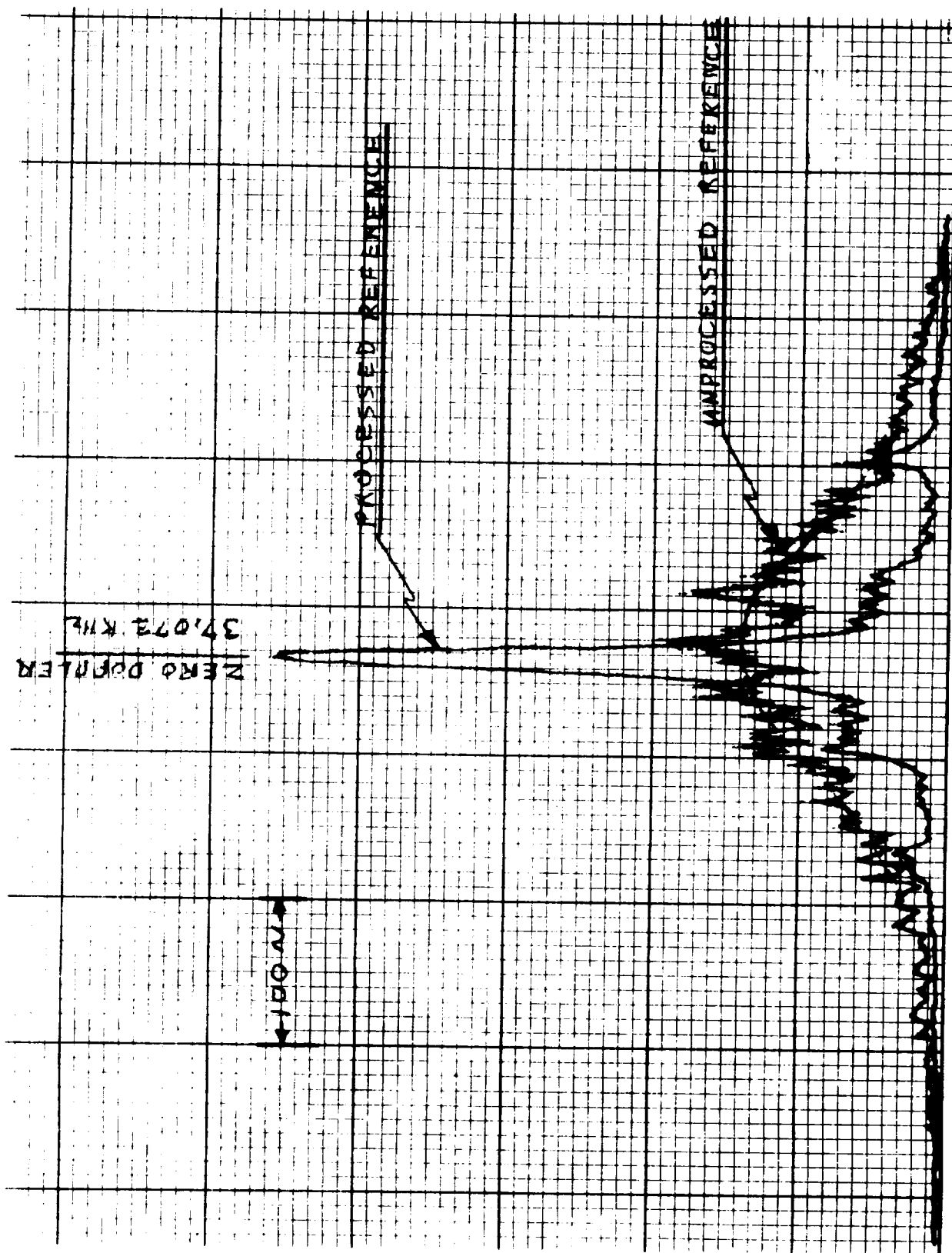


Figure 70. Processing Improvement

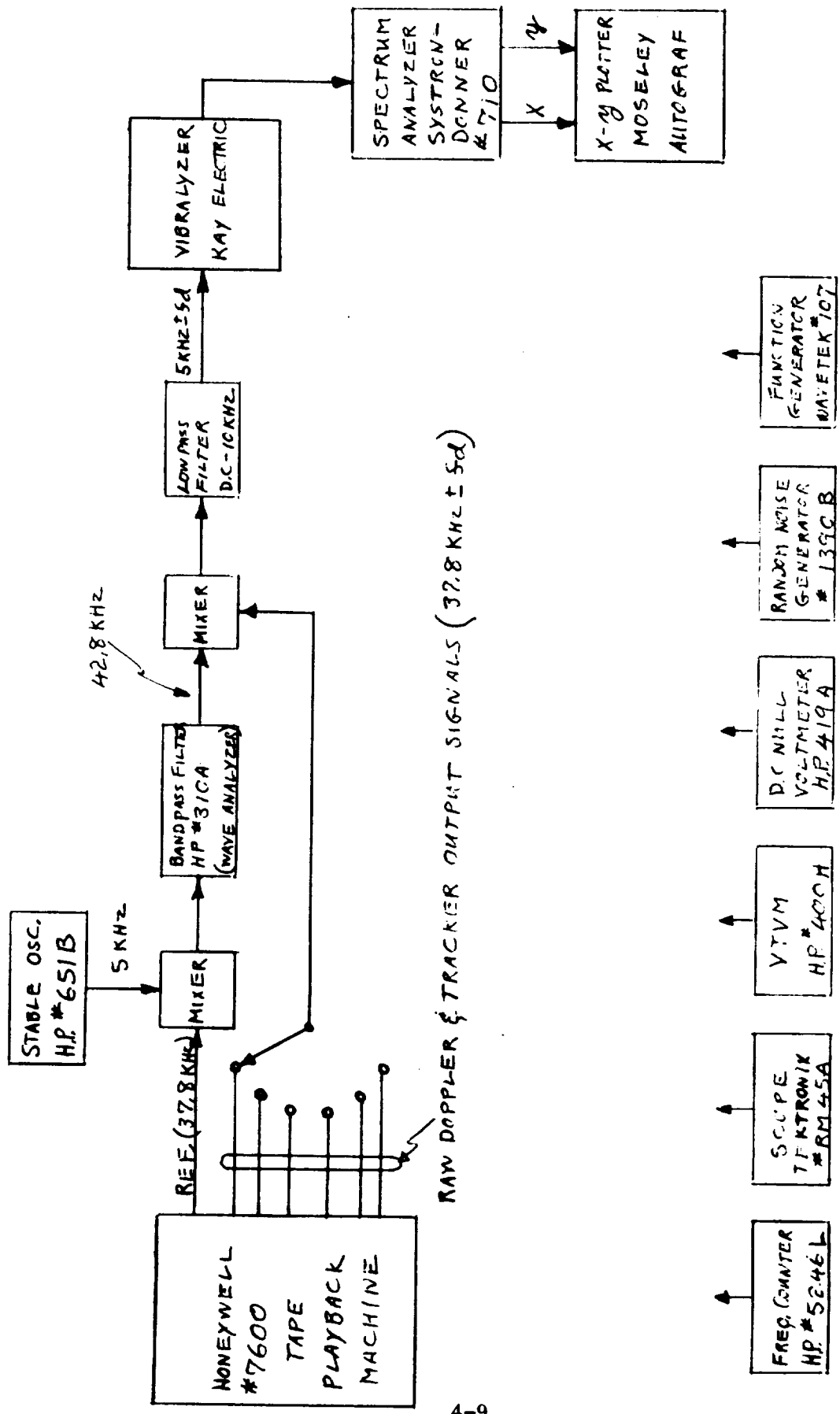


Figure 71. Data Reduction Set-Up

very low wow and flutter figures because of the extremely high drum inertia; and, data can be stored for as long as desired. The Vibralyzer output therefore supplies the selected portion of the raw doppler signal to the spectrum analyzer for as long as is necessary to sweep out the desired frequency coverage.

#### 4.1.2.2 Data Point Selection

Twenty-five reels of tape data were generated during the helicopter flight test program. Interesting data points were selected by monitoring the voice channel to identify such parameters as radar operating mode, altitude, terrain type, etc. At the same time, a footage counter on the playback tape machine was monitored and all pertinent information was logged together with any comments based on continuous spectral observations. Table 11 demonstrates typical data points identified.

After the data points have been identified, specific points can be selected for detailed analysis. This was the procedure used to generate the following graphs.

#### 4.1.2.3 Graph Interpretations

The graph shown in Figure 72 has been used to determine the approximate velocity and pitch angle of the helicopter at data point 5-1-1380 (Tape Number 5, Reel Number 1, footage counter reading 1380). From the graph, the following information can be obtained by measurements:

Channel No. 1

$f_d \approx 365 \text{ Hz}$  (Doppler Frequency)

$\Delta f \approx 150 \text{ Hz}$  (Spectrum Width)

Table 11. PTDLR Tape Data Points - Helicopter

J <sub>1</sub>	Mode		Mod		LEF		Alt	Terrain	Tape #	Reading	Data	1.5° Pitch Down
	J <sub>2</sub>	J <sub>3</sub>	LO	HI	In	Out						
	X		X		X		25	Blacktop		65 230	Zero Calib	
	X		X		X		50	Blacktop		256	Check Leakage Looks High	
	X		X		X		50	Blacktop		270	Notice LEF In and Out Check	
	X		X		X		140	Water		618	LEF In & Out Tracker	
	X		X		X		280	Water Smooth		696	Good Bias Example	
	X		X		X		290	Water Smooth		731	Good Bias Example	
	X		X		X		150	Water Smooth		791	Good Bias Example	
	X		X		X			Water		1108	LEF In and Out	
	X		X		X			Water		1200	Descent from 300 ft - 20 ft	
	X		X		X					1290	Ascent 20 - 380 ft	
	X		X		X					1300	Descent	
	X		X		X					1365	Ascent	
	X			X	X					1448	Descent	
	X			X	X					1500	Ascent	
	X			X	X					1600	Descent	
	X			X	X					1670	Ascent	
		X	X		X					1730	Descent	
		X	X		X					1763	Ascent	
X			X		X					1763	Descent	
X			X		X					1825	Ascent	
	X		X		X		20ft			1920	Good Signal @20 ft	
	X		X		X		200ft		to	2140	Porpoise	
	X		X		X		20ft			2199	Level Run Shows Bias	
	X		X		X		20ft			2228	Level Run	
	X			X	X		25ft			2242	Level Run	
	X			X	X		30ft			2267	Level Run	
		X		X	X		35ft			2293	May be good for S/N vs Mode	
		X		X	X		35ft			2293		
		X		X	X		35ft			2320		
		X		X	X		35ft			2327		
X			X		X		35ft			2348		

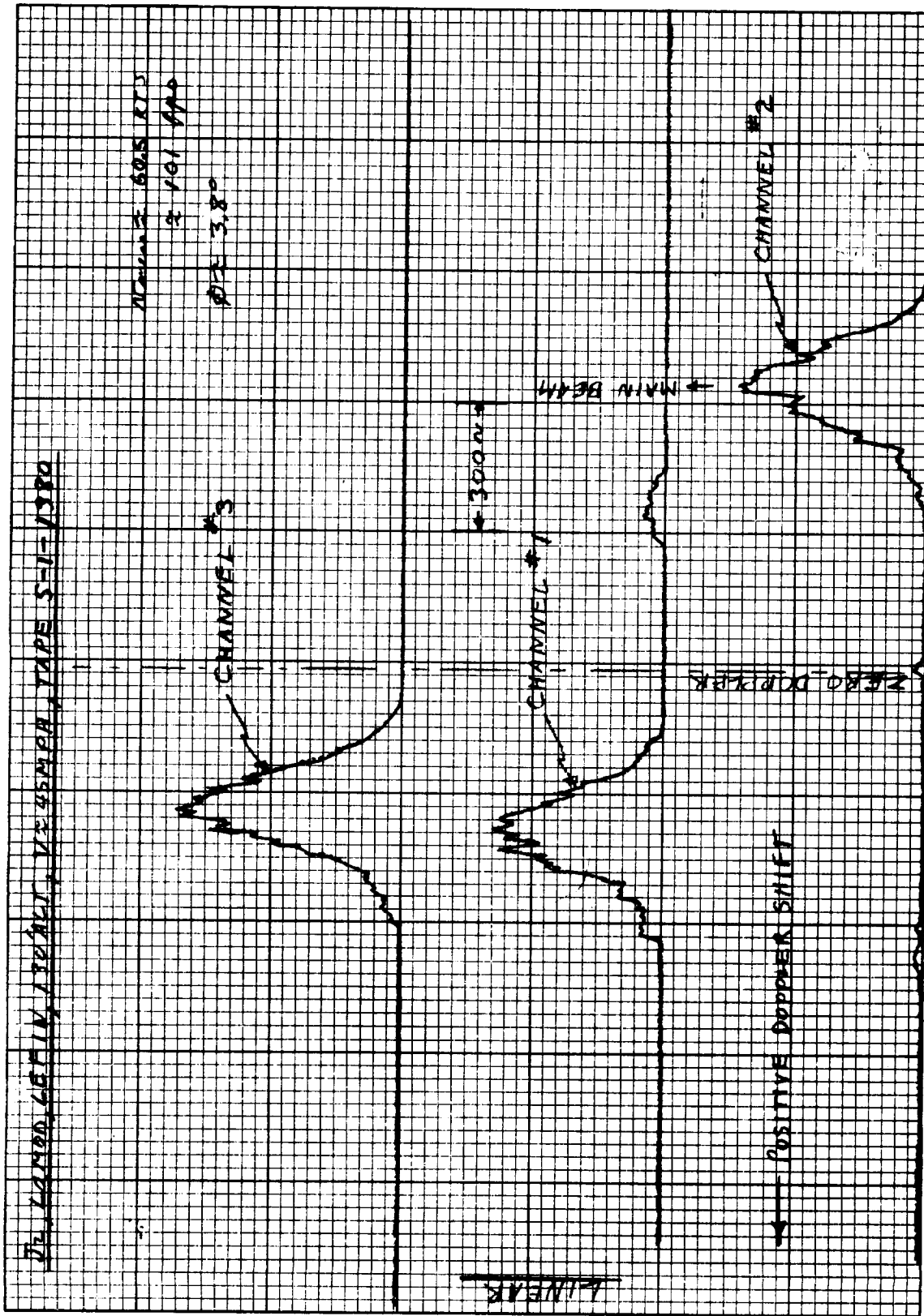


Figure 72. Doppler Spectra

Channel No. 2

$$fd \approx -665 \text{ Hz}$$

$$\Delta f \approx 120 \text{ Hz}$$

Channel No. 3

$$fd \approx 315 \text{ Hz}$$

$$\Delta f \approx 122 \text{ Hz}$$

The velocity components,  $V_x$ ,  $V_y$ ,  $V_z$  are computed from the following relationships:

$$V_x = \frac{\lambda}{4\ell} (fd_1 - fd_2)$$

$$V_y = \frac{\lambda}{4m} (fd_3 - fd_1)$$

$$V_z = \frac{\lambda}{4n} (fd_2 + fd_3)$$

where

$$\ell = 0.183$$

$$m = 0.128$$

$$n = 0.966$$

Substituting and solving:

$$V_x = 101 \text{ fps (forward)}$$

$$V_y = 5.05 \text{ fps (drift to the left)}$$

$$V_z = -6.7 \text{ fps (upward)}$$

Since the flight path was known to be approximately level, the presence of the upward  $V_z$  component implies a pitch down condition of the helicopter. The pitch angle can be determined from the relationship:

$$\alpha = \text{Tan}^{-1} \frac{V_z}{V_x} = -3.8^\circ \text{ (pitch down)}$$



The spectral width,  $\Delta f$ , of the doppler returns is:

$$\Delta f = \frac{2\mu}{\lambda} \sin \theta d\theta$$

where

$$V_x \approx 101 \text{ fps}$$

$$\lambda \approx 0.074 \text{ ft}$$

$$d\theta \approx 2.65^\circ \approx 0.046 \text{ rad}$$

$$\theta_1 \approx \theta_3 \approx 90 - 10.55 + 3.8 = 83.25 \text{ deg}$$

$$\theta_2 \approx 90 - 10.55 - 3.8 = 75.65 \text{ deg}$$

$$\sin \theta_1 \approx \sin \theta_3 = 0.993$$

$$\sin \theta_2 \approx 0.969$$

Therefore:

$$\Delta f_1 \approx \Delta f_2 = 125 \text{ Hz}$$

$$\Delta f_2 \approx 122 \text{ Hz}$$

These values compare favorably with the measured values from the graph. The graph shown in Figure 73 was taken from data point 4-2-1990. The operating mode was the  $J_2$  Bessel sideband, low-modulation index, 15 ft altitude over plowed dirt at a forward velocity of approximately 117 fps. During this data run the leakage elimination filters (LEF) were momentarily switched out. It appears that conditions are excellent for determining the effectiveness of the LEF at this data point for the following reasons:

- a. Forward velocity is great enough to give good frequency separation between the zero doppler line and the main beam doppler shift (approximately 580 Hz).
- b. The terrain roughness (plowed field) provides a high ratio of main lobe-to-side lobe signal.

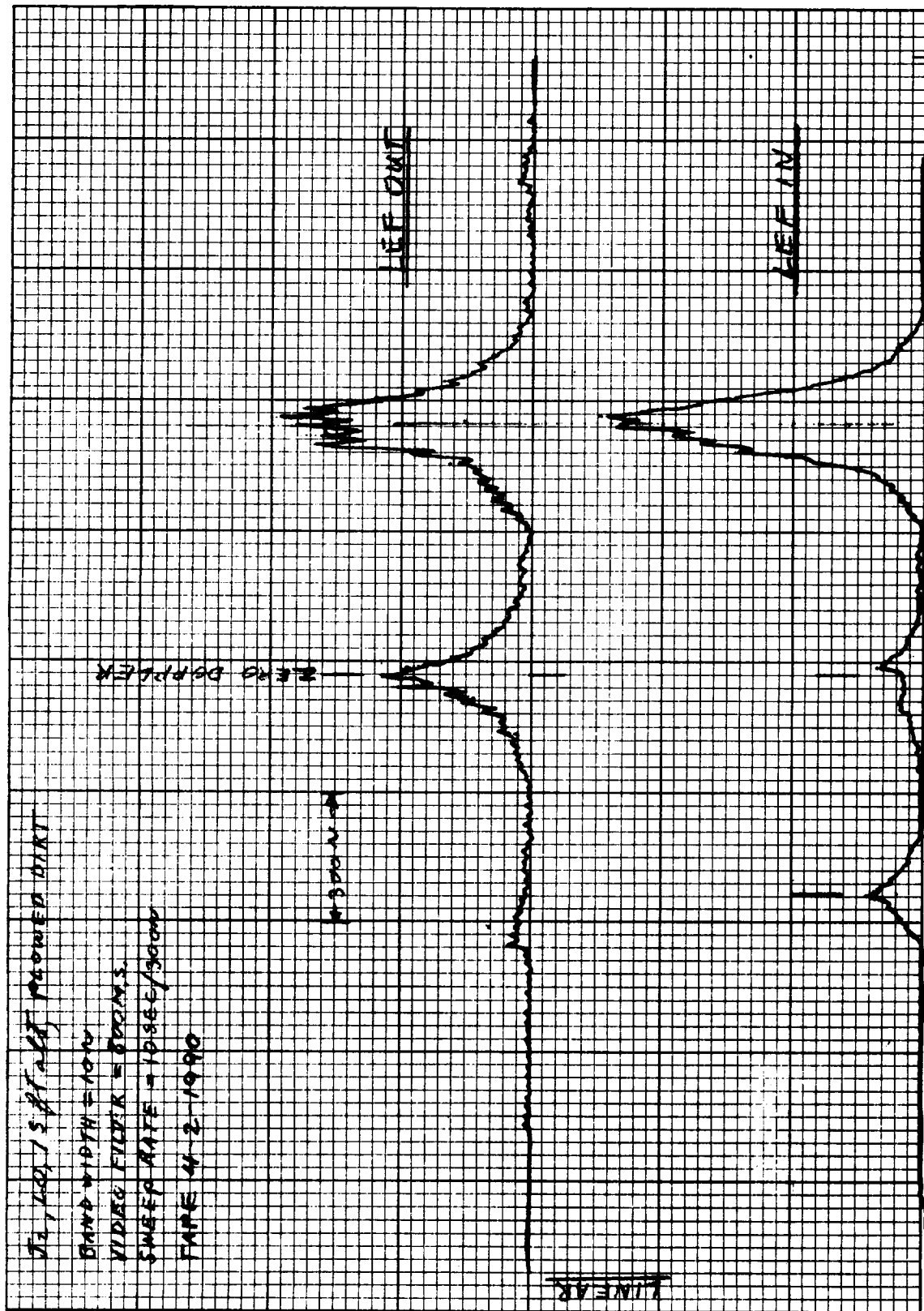


Figure 73. LEF Improvement

- c. Because of the low altitude and the resultant low signal return, the leakage level is more apparent.
- c. The two data points (LEF in - LEF out) are less than 1 second apart so that external parameters are nearly identical.

From the graph, the following measurements can be made:

$$\text{sig/leakage ratio - (LEF out)} \approx \frac{1.6}{1} \approx 4.1 \text{ db}$$

$$\text{sig/leakage ratio - (LEF in)} \approx \frac{2.3}{.2} \approx 21.2 \text{ db}$$

This indicates an improvement of approximately 17.1 db. Laboratory measurements indicate a 30 db rejection capability of the LEF. From the graph shown in Figure 70, it can be seen that pure leakage should exhibit a much narrower spectral width than is observed in Figure 73. It is probable then that the signal observed at and around the zero doppler line of Figure 73 is comprised of both leakage and sidelobe return and, since the notch width of the LEF is less than 5 Hz, the residue seen in the bottom trace is sidelobe energy.

The graph shown in Figure 74 represents the raw doppler output of Channel No. 2 over various types of terrain. While all of the data was not gathered on the same flight, the general operating conditions were equivalent except for terrain and helicopter velocity. The nominal altitude for each of the four data points plotted (identified on the right-hand side of each curve) was approximately 130 feet. The operating mode was:  $J_2$  Bessel sideband; low modulation index; LEF in. The four terrain types were:

- a. Plowed, unplanted field with furrows approximately 8 inches apart and 2 inches high.

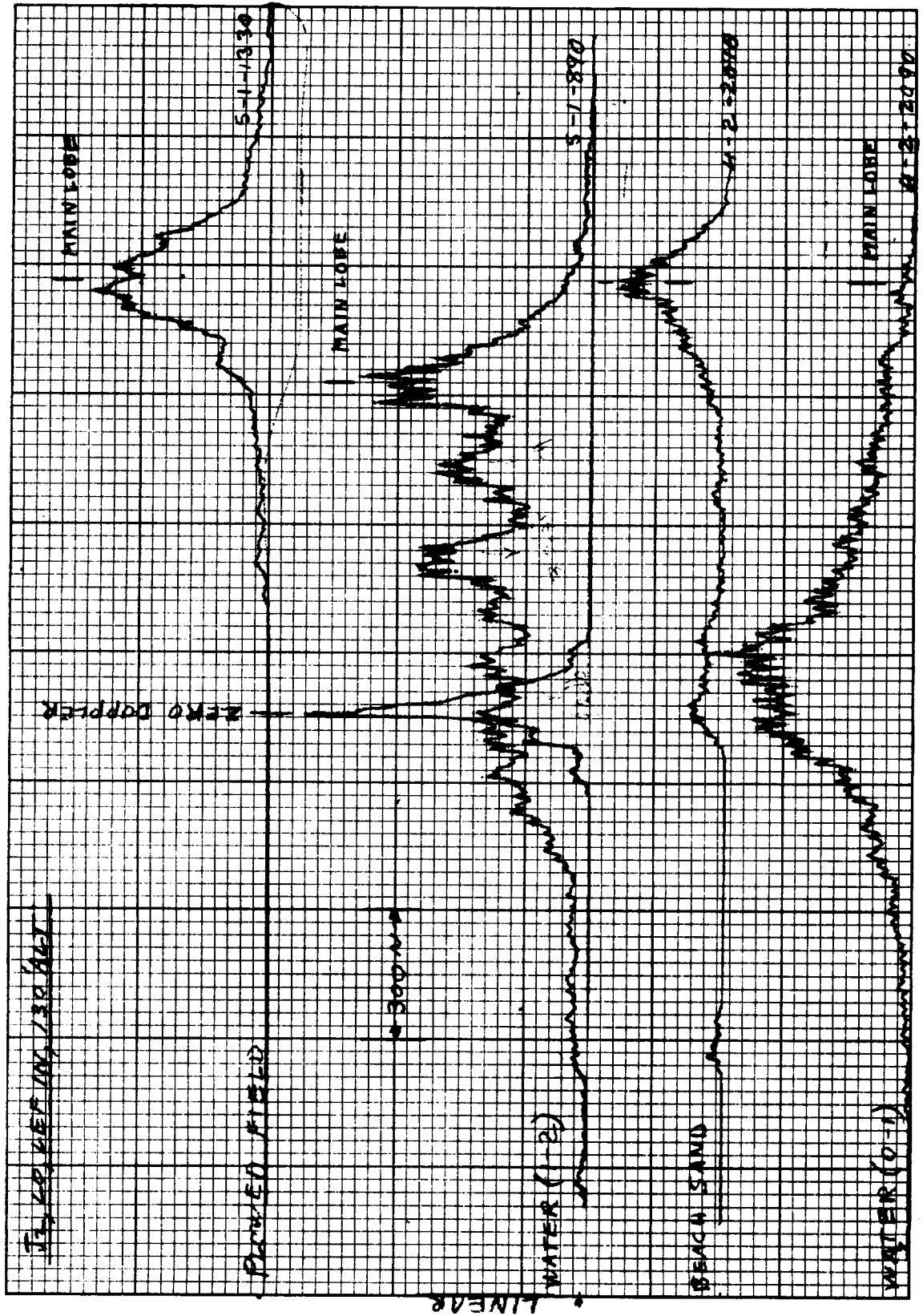


Figure 74. Doppler return vs Terrain Type

- b. Ocean surface at an estimated Beaufort number of 1-2.
- c. Beach sand with smooth surface and probable high moisture content.
- d. Ocean surface at an estimated Beaufort number of 0-1.

As stated earlier, the purpose of generating the graphs is to observe the raw doppler waveforms and compare them with theoretically predicted curves. Additionally, an attempt should be made to estimate the velocity measuring capabilities of the system from observing the various waveforms.

The first and third curves shown in Figure 74 (plowed field and beach sand) demonstrate a well-defined main lobe return. Well-controlled simulations of this type spectrum indicate that good velocity tracking will be achieved; hence, accurate velocity measurement will be obtained. Curve No. 2 demonstrates a deterioration in the definition of the main lobe because of the increased signal return from side lobe energy. The broadening of the spectral return produces a shift in the velocity tracker center frequency toward the zero doppler region as the tracker attempts to center over the average return power. Significant velocity errors occur with this type of spectral input. Curve No. 4 demonstrates an almost complete masking of the main lobe by side lobe returns. Under these conditions, the velocity tracker centers at near zero doppler frequencies and is only slightly effected by changes in vehicle velocity.

Some estimate can be made as to the improvement that would be obtained by reducing side lobe levels. An improvement of 10 db in the main lobe-to-side lobe ratio of a one-way antenna pattern would result

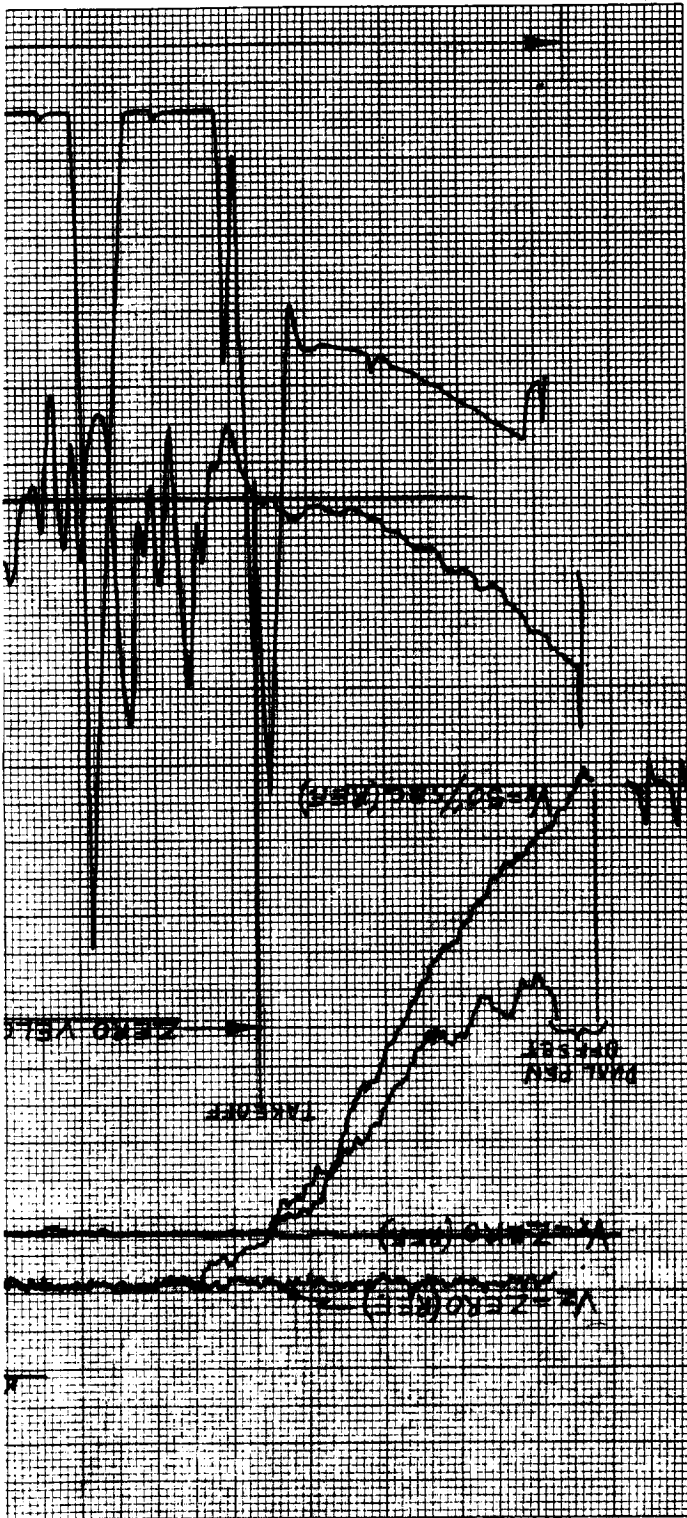
in approximately 20 db improvement in main lobe-to-side lobe energy of the raw doppler return. If the above improvements (10 db one-way) were applied to curve No. 4, Figure 74, a spectrum similar to curve No. 2, Figure 74, would result. By the same reasoning, Curves No. 2 and No. 3 would improve to the general shape of Curve No. 1, Figure 74, and it is reasonable to assume that a good velocity measuring capability will be obtained over all but the most specular types of terrain. All of the above data was obtained when the PTDLR system was using the Luneberg antenna. The decision to replace that antenna with the Constant K antenna was based primarily on the results of this data reduction effort. As shown in Table 6, Section 2.4.5 the Constant K design did in fact provide an improvement of approximately 29 db and subsequent spectral analysis of the doppler signals demonstrated well defined main lobe return (as in Curve 1, Figure 74) even when flying over quite specular terrain.

#### 4.1.3

##### Accuracy Determination

Accuracy testing was performed at PMR, Pt Mugu, California, and the mechanics of that flight test effort have been described in Section 3. This section discusses the subsequent data reduction activities performed on the resultant flight tapes and ground truth tapes. A preliminary reduction effort is shown in graphical form in Figure 75. This graph was generated from the original flight tape and represents flight 8064, run 15. This run was a typical helicopter landing profile from approximately 130 ft altitude to touchdown. A fairly large forward and vertical velocity component existed at the beginning of the run and decreased to zero at touchdown.

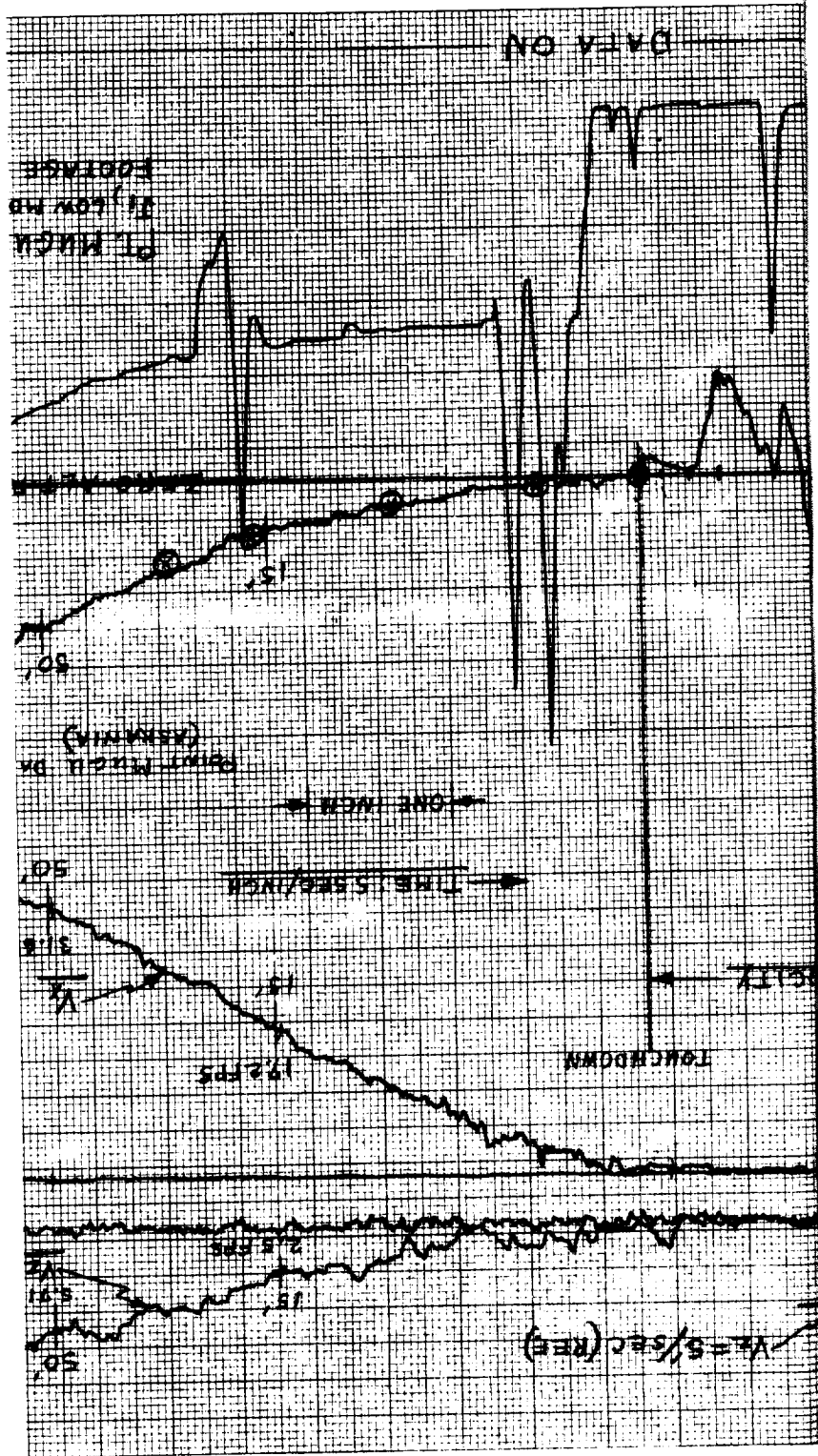
This run was selected for reduction because it demonstrated good PTDLR system operation down to zero feet, and positive, zero, and negative velocities. It also demonstrates the rather poor operation of the Minneapolis-Honeywell (M-H) altimeter that was used to provide reference altitude information. Both the M-H altitude trace (lower curve) and the PTDLR altitude trace (second curve from bottom) were generated directly from the appropriate flight tape channels by properly scaling the playback tape machine discriminators. The curves were recorded simultaneously on a dual pen chartrecorder. Because of mechanical constraints on the recorder, an offset lag of approximately 1 -1/2 seconds in time occurs between the PTDLR trace and the M-H trace. The traces were offset in altitude for graph clarity. Using the footage counter on the playback machine for time correlation, a second set of curves were plotted on the same graph to display the forward velocity and vertical velocity components during the let-down. The velocity components on the flight tape are recorded directly as the raw doppler frequency with the velocity trackers and as the processed frequency out of the velocity trackers. For graphical recording purposes, it is necessary to convert the doppler frequencies representing the various velocity components into a d. c. analog. This



FOLDOUT FRAME |

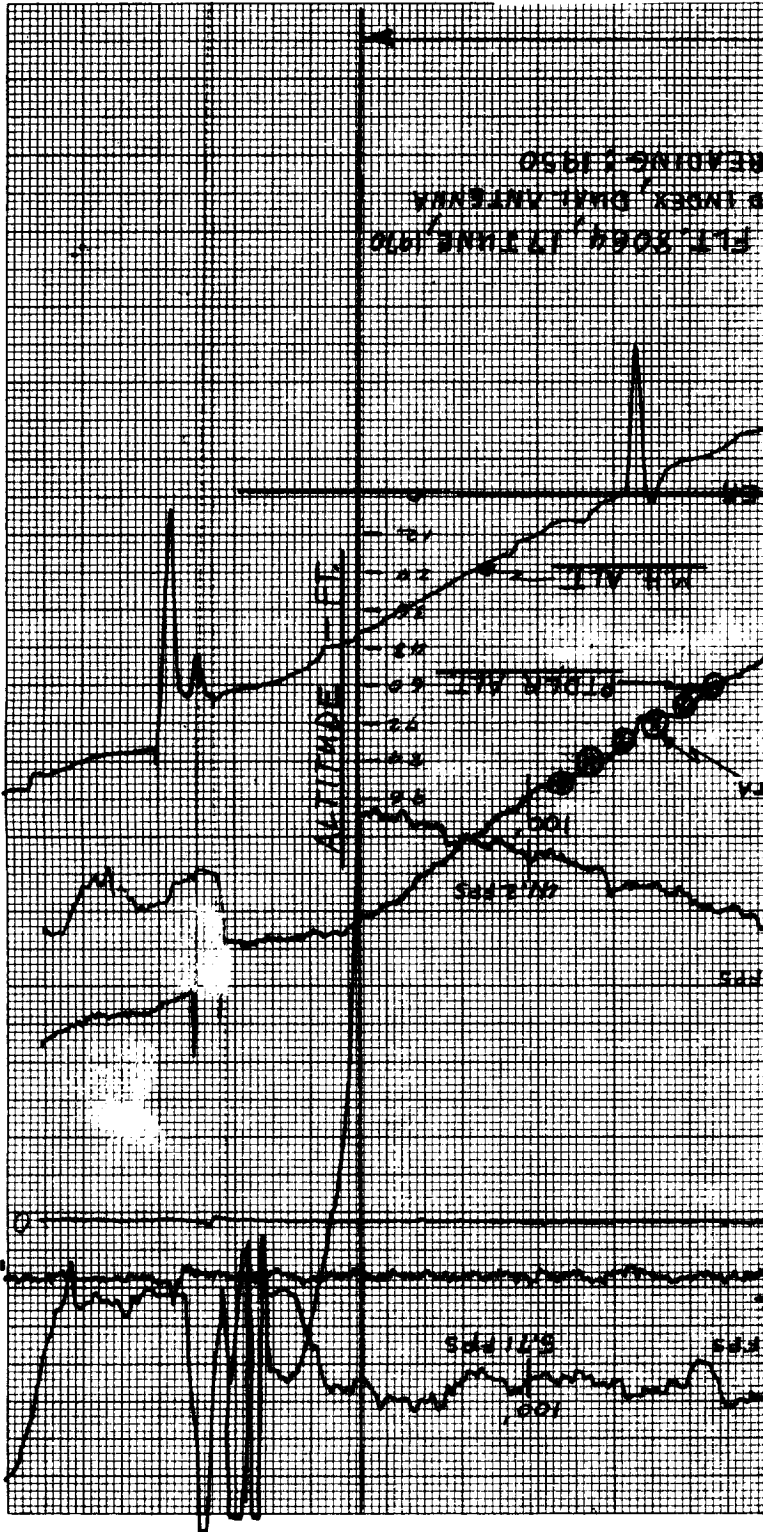


Figure 75. Pre



FOLDOUT FRAME 2

Primary Data Reduction



was most easily accomplished by playing the flight tape channels directly into the corresponding velocity trackers. The PTDLR system contains an analog computer that generates three d.c. voltages proportional to  $V_x$ ,  $V_y$ , and  $V_z$  based on the three beam velocities applied to the velocity track inputs. These signals are normally used in meter deflection for velocity display purposes. The PTDLR system had been removed from the helicopter, set up in the laboratory, and was available. The d.c. voltages out of the analog computer were used directly for pen deflection on the chart recorder. The zero velocity reference line for both the  $V_x$  velocity curve and the  $V_z$  velocity curve was generated by simultaneously playing the recorded zero doppler reference signal into all three of the velocity trackers and recording the resultant d.c. analog voltage. The velocity calibration references (i.e.,  $V_x = 50$  ft/sec and  $V_z = 5$  ft/sec) were generated by calculating the required doppler frequency in each beam, based on the PTDLR beam geometry and doppler sensitivity, that would be produced under theoretical conditions. These calculated frequencies were then set up on laboratory oscillators with the aid of a precision frequency counter and simultaneously played directly into the appropriate velocity trackers. The resultant d.c. signals were recorded on the same graph. For graph clarity the  $V_x$  zero reference and the  $V_z$  zero reference were displaced to minimize overtracing.

In addition to the above traces, the graph also contains a corresponding plot of the corrected ground truth data that was provided by PMR, Pt. Mugu. The data was in tabular form with one second printouts. Time correlation was obtained through the IRIG B timing signal that was recorded on both the flight tape and the ground truth tape and subsequently appeared on the printouts of both tapes.

From the graph the following observations can be made:

- a. The altimeter portion of the PTDLR does indeed operate down to touch down (at touchdown the antennas are a mere five inches off the ground).
- b. The PTDLR altitude profile is quite smooth compared to the M-H altitude profile which shows serious tracker dropouts particularly at lower altitudes.
- c. PTDLR altitude accuracy appears to be quite good based on the corresponding ground truth data generated by the tracking Askania cameras (Plotted as  $\otimes$ ).
- d. Velocity tracking is operative down to touchdown and has a negligible tracker offset at zero velocity.
- e. Negative velocities are demonstrated (Note  $V_z$  at takeoff).
- f. By integrating the  $V_z$  component over the time interval shown, an altitude profile is generated that is in close agreement with the actual flight profile.

Unfortunately ground truth was not available to define specific terrain features surrounding the exact flight paths. It is recalled, however, that there were gullies and somewhat elevated roadways in the vicinity of this flight that could account for the small perturbations in the PTDLR altitude profile.

Additional data reduction activities to establish PTDLR system accuracy have been conducted at the NASA Langley Research Center (LRC), Hampton, Virginia. The PMR, Pt Mugu ground truth tapes

were delivered to the LRC facility in a mutually agreeable digital format. The corresponding PTDLR flight tapes were also delivered to the LRC facility. The original goal was to digitize the PTDLR analog tapes and, using the appropriate conversion parameters, generate a compatibly formatted digital tape resembling the ground truth tape. Error plots could then be readily generated. For several reasons this program experienced difficulties and only minimal data will be available for inclusion in this report. While making an accurate measurement of the transfer function of the altitude readout circuitry after the flight test program, a nonlinear condition was observed. As described in Section 2.4.2 the altitude readout card contains a relatively simple circuit that converts a pulse width corresponding directly to altitude into a linear d.c. voltage used for recording altitude on an F.M. channel of the airborne tape recorder. The circuit is essentially a feedback operational amplifier with a d.c. gain of  $-1.8$  and a high frequency cutoff above 1 Hz and is intended to provide an averaging function on the input pulse train. The feedback resistor was originally selected to produce a scale factor of  $-10$  MV/ft altitude. Upon verifying this scale factor after the Pt Mugu flight test program, an increasing departure from the  $-10$  MV/ft scale factor with increasing pulse width was observed. The scale factor at 1000 ft altitude for example was approximately  $-6$  MV/ft. A nonlinear function is perfectly useable if it can be accurately defined. This nonlinearity, however, has a thermal time constant associated with it that is a function of the absolute operating level and ambient temperature at any given time of the flight and has thus far defied mathematical descriptions.

This problem has prevented LRC from generating an overall altitude accuracy plot in the FM/CW mode. The bulk of the altitude accuracy data reduction has been concentrated on flight 8064, runs 15 and 16 because the change in altitude is small, hence, the change in scale factor due to operating point and ambient temperature will contribute only small errors in the altitude data. Figure 76 through 81 show several plots of accuracy data produced at the LRC facility. Figure 76 is a plot of altitude vs time as determined by the PTDLR system and by PMR tracking camera during flight 8064, run 15. The PTDLR scale factor was established by assuming that the end points were correct. Figure 77 is a plot of run 16 that was similar flight geometry. Figure 78 and 79 are corresponding velocity vs time plots for run 15 and run 16 respectively.

Figure 80 is a velocity vs time plot at 1000 ft, 100 ft, and 10 ft altitude in the FM/CW mode ( $J_1$ ). The average velocity difference during the 1000 ft run is 1.1 ft/sec and corresponds to 2.75 percent of value (nominal velocity is 40 ft/sec) or 0.162 percent of the full scale value of 680 ft/second. The average velocity difference for the 100 ft altitude run is 1 ft/sec and corresponds to 2.6 percent of value (38 ft/sec) or 0.147 percent of full scale. The 10 ft altitude run shows a velocity difference of 2.3 ft/sec that corresponds to 7.4 percent of value (31 ft/sec) or .34 percent of full scale.

Figure 81 shows a plot of velocity vs time for three different runs at 2500 ft altitude with the PTDLR system operating in the ICW mode. The average velocity measured by the PTDLR system in the top graph was 44.45 ft/sec. The corresponding ground truth data indicated an

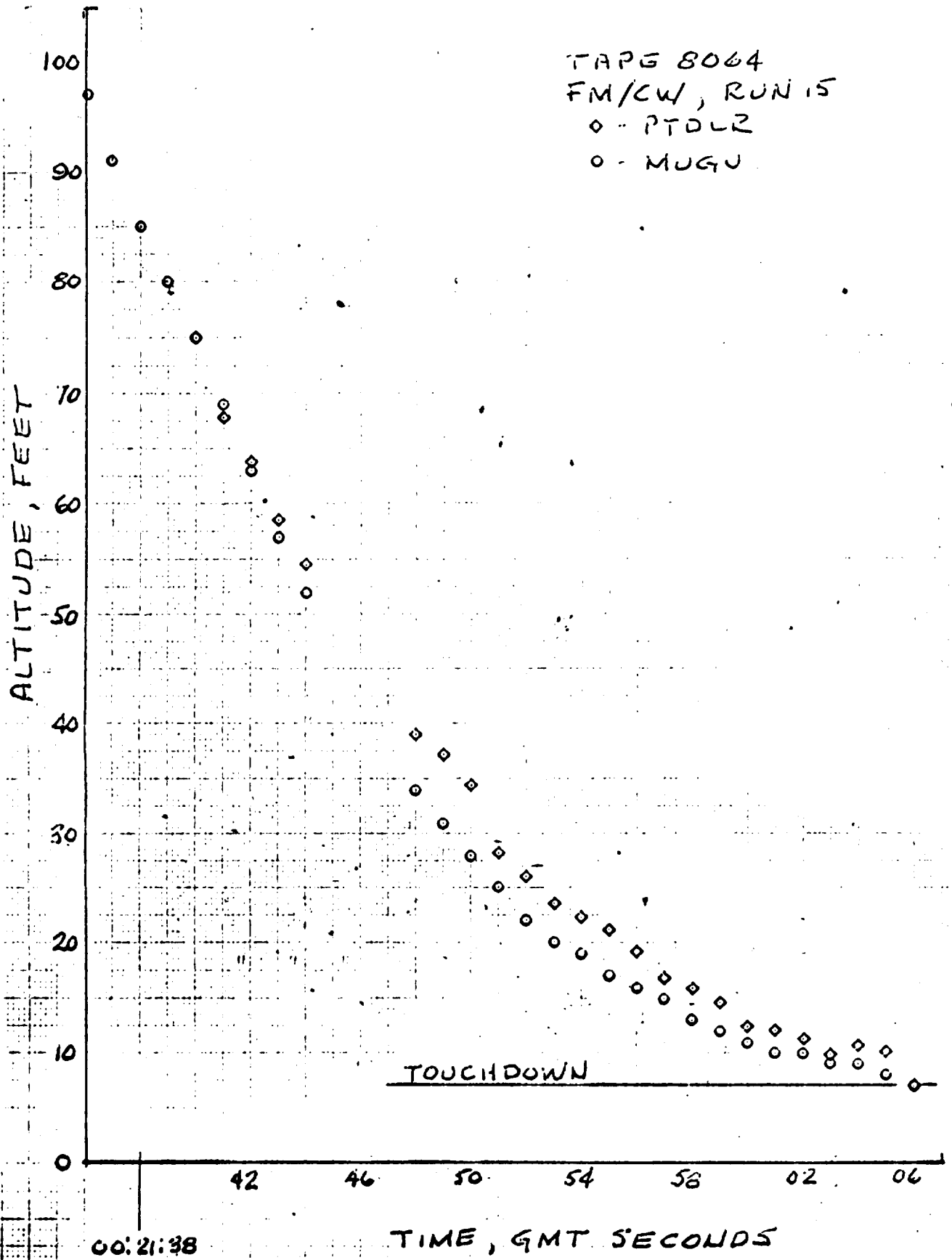


Figure 76. Altitude Comparison, Run 15

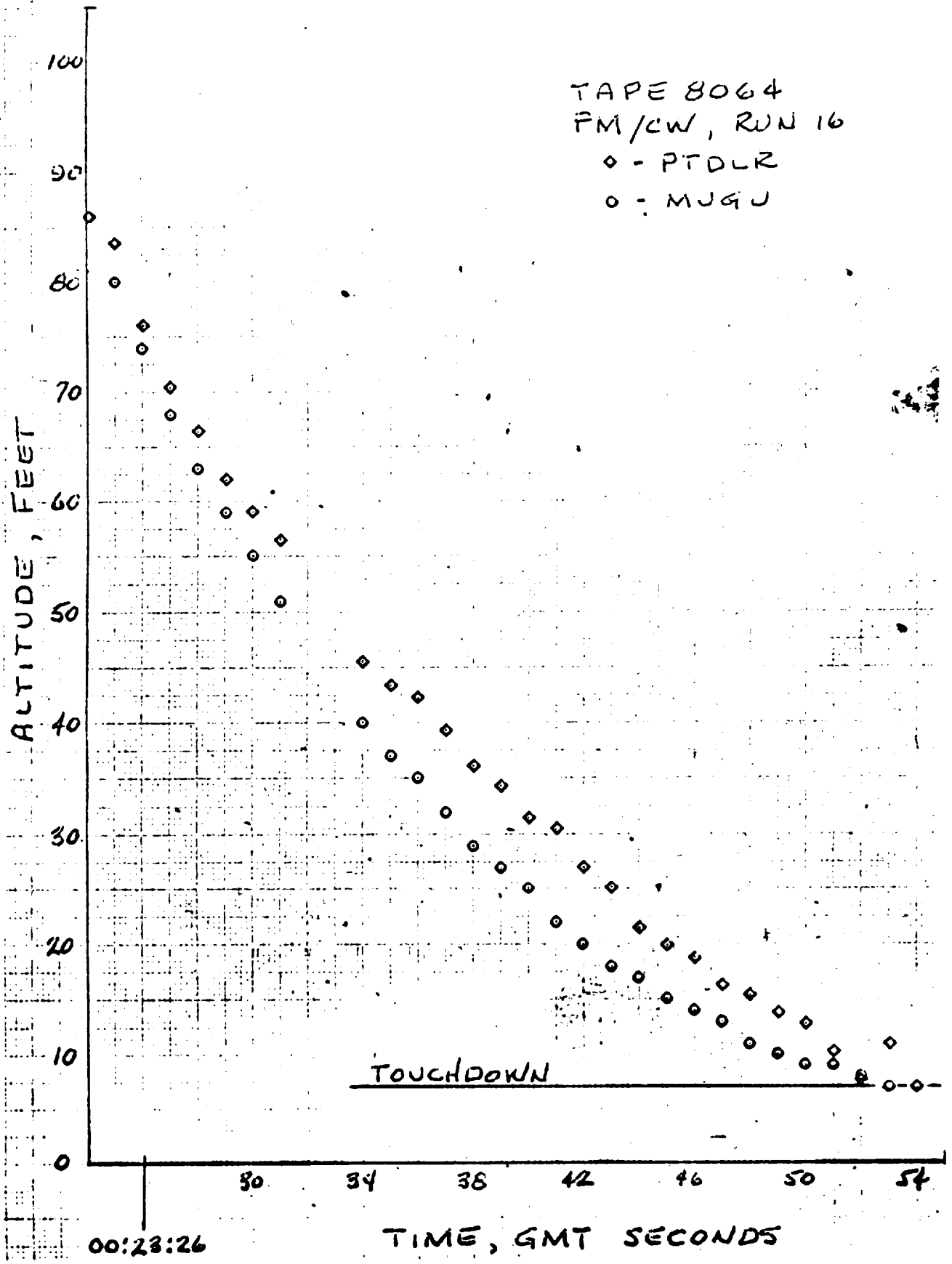


Figure 77. Altitude Comparison, Run 16



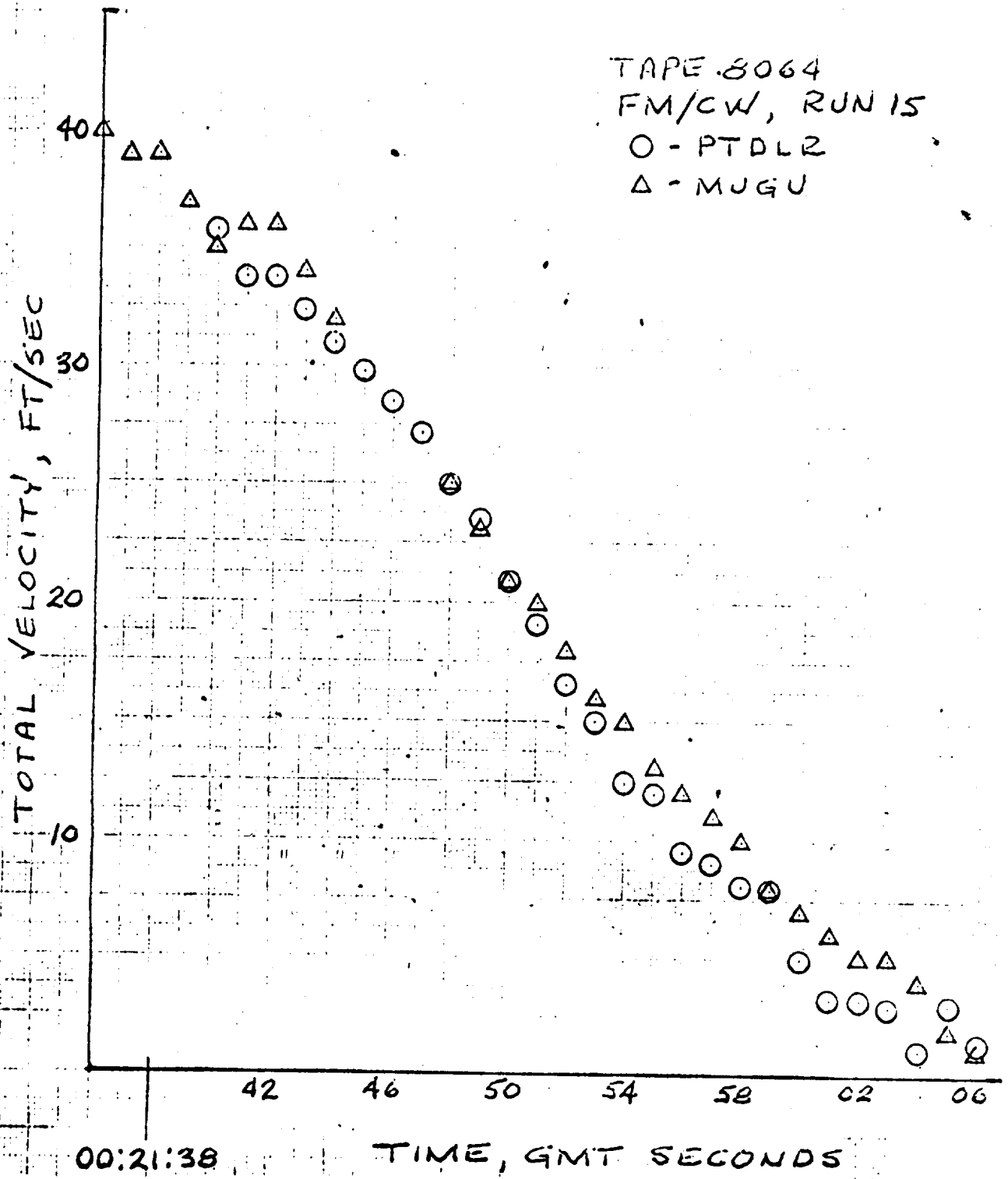


Figure 78. Velocity Comparison, Run 15

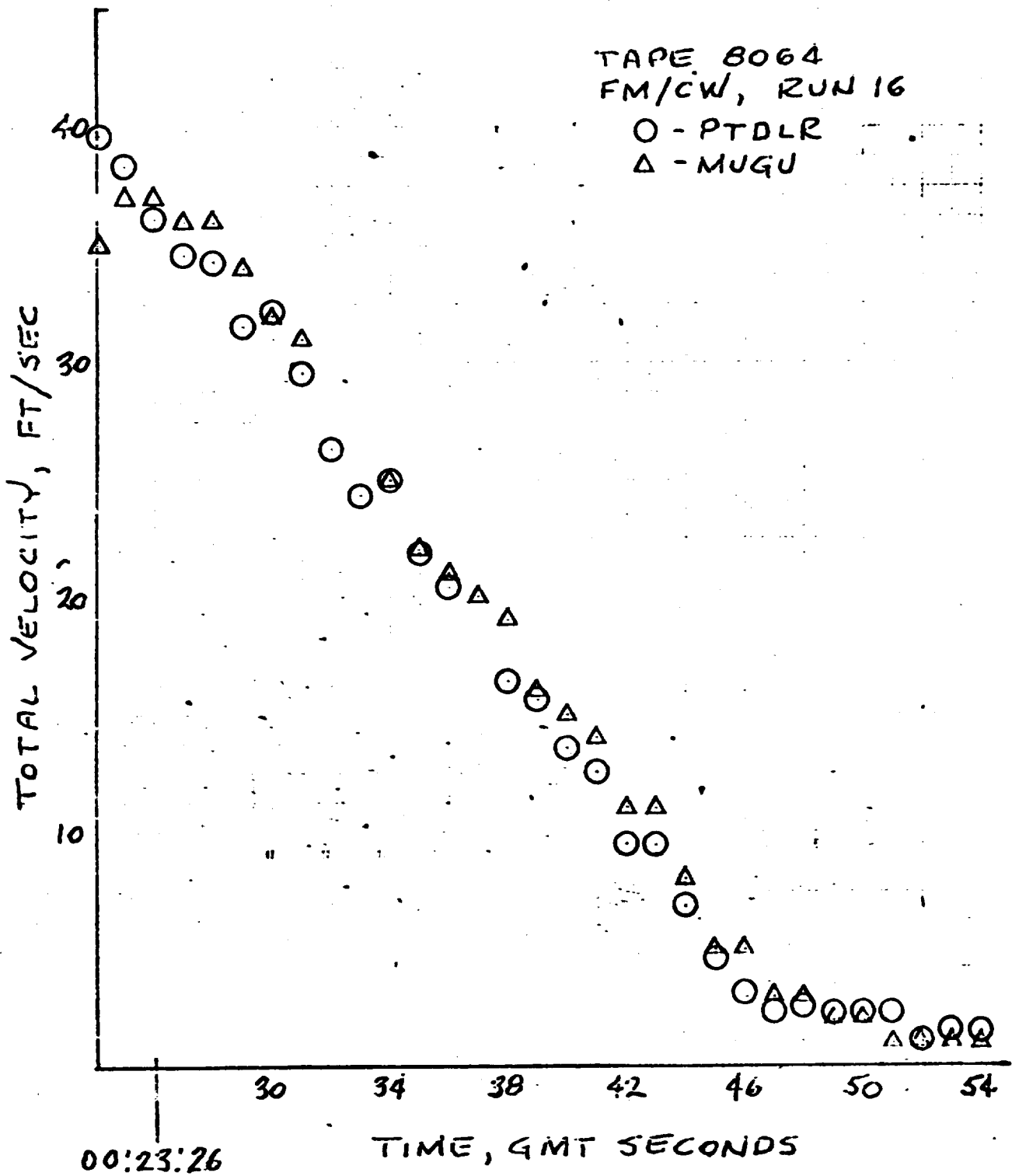


Figure 79. Velocity Comparison, Run 16

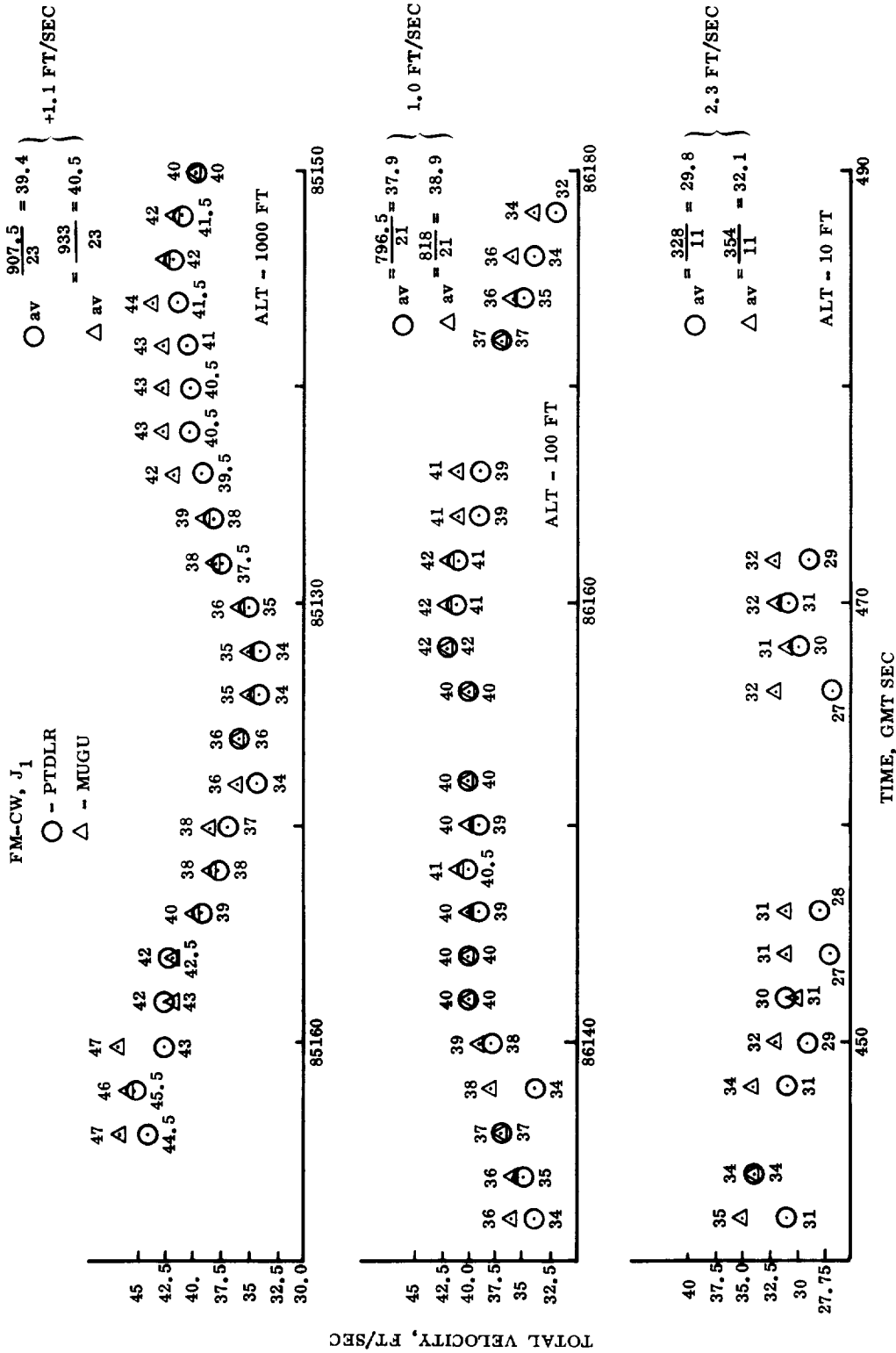


Figure 80. FM/CW Velocity Comparison

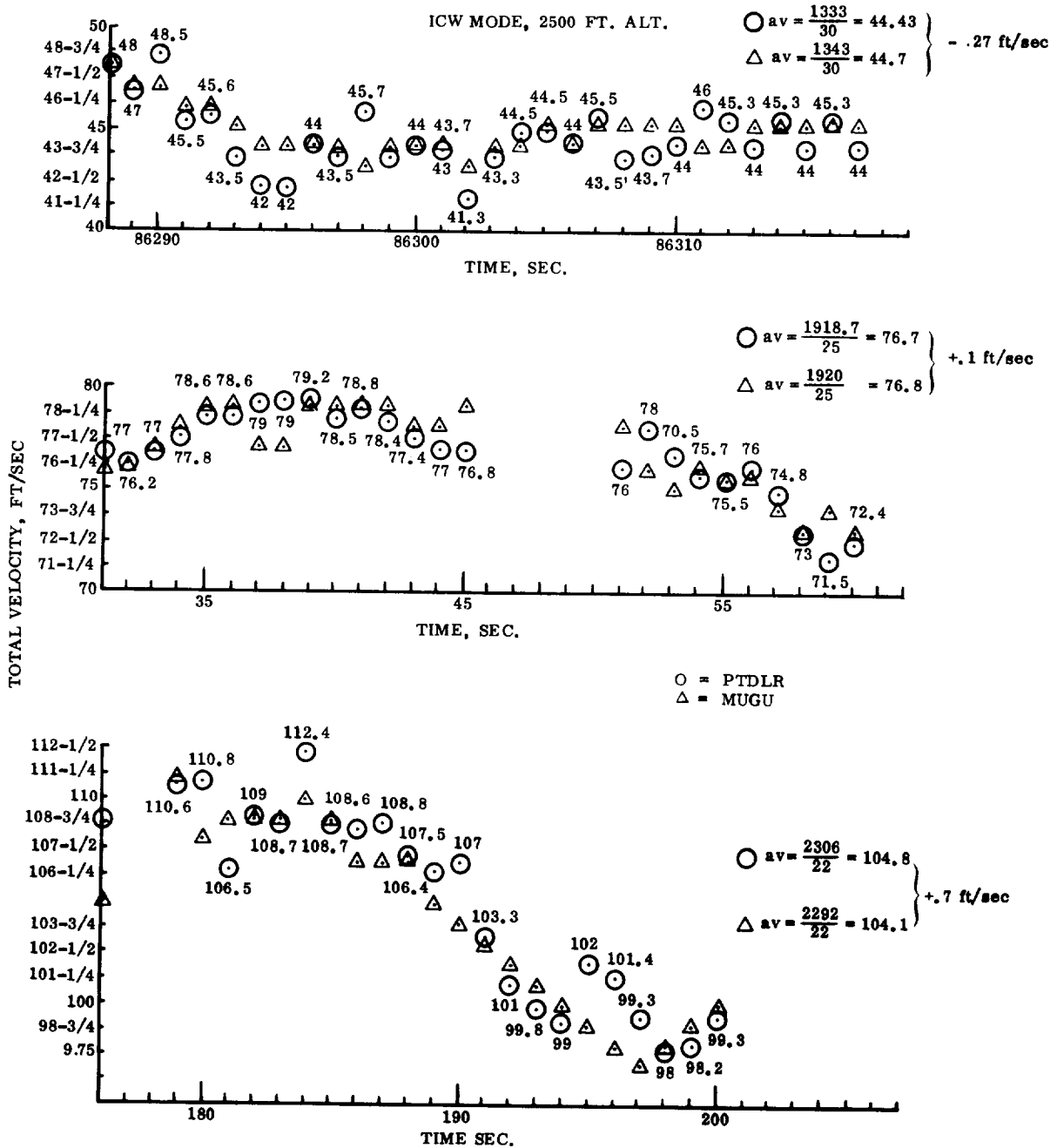


Figure 81. ICW Velocity Comparison

average velocity of 44.7 ft/sec. The difference velocity is, therefore, 0.27 ft/sec giving a 0.6 percent of value and a 0.025 percent of full scale accuracy figure. Similarly, the center graph with an average velocity of 76.8 ft/sec shows a 0.1 ft/sec velocity difference and a 0.13 percent of value or a 0.0147 percent of full scale accuracy figure. The bottom graph shows an average velocity of 104.5 ft/sec, a difference velocity of 0.7 ft/sec, and an accuracy of 0.67 percent of value or 0.103 percent of full scale.

The positional accuracy of the ground truth data supplied by PMR is stated to be  $\pm 2$  ft in altitude and the velocity accuracy is estimated to be  $\pm 1$  ft/second. Based on the LRC data it is apparent that the PTDLR velocity and altitude accuracy is considerably better than the original design goals stated in Table 2.



## 5.0 CONCLUSIONS AND RECOMMENDATIONS

### 5.1 Conclusions

A program of 30 months' duration that includes system and hardware design, fabrication, flight testing, and data reduction naturally leads to the formation of conclusive opinions. This section is intended to relate some of the events that occurred during the course of the program and the conclusions that were reached to the formulation of recommended activities that should be pursued.

The original system concept employing the bimode modulation technique has been shown to be sound. Theoretical calculations of system performance were based on hardware specifications assumed to be available as shelf items. Unfortunately, theory occasionally overlooks the influence of some subtle hardware characteristic that can be generally ignored but may have a significant effect on the performance obtained in a particular system configuration. One such item was the waveguide filter used in the output of the single sideband modulator. The filter output is used to supply the local oscillator power to the several receiver mixer channels. Local oscillator (L.O.) requirements for general radar applications are usually concerned with supplying the correct L.O. power to optimize the signal frequency conversion to the desired IF frequency. The L.O. is most often a single frequency whereby spectral purity is obtained by crystal or cavity stabilization and spurious frequency components are suppressed by simple filters.

FM/CW operation also requires high spectral purity and low spurious content in a signal that must be swept in frequency at relatively high rates. It is necessary that the instantaneous transmitter frequency and the

instantaneous L.O. frequency appearing simultaneously at the signal mixers maintain precisely the desired offset (IF) frequency. This requires that the electrical path length of the transmitter leakage-to-signal mixer (transmitter leakage occurring primarily from circulator isolation and poor antenna match in single antenna systems) and the L.O.-to-signal mixer path length be identical. While this is a well understood requirement for FM/CW systems, the original design calculations overlooked the large difference between the physical length of the L.O. filter section and its electrical length. As pointed out in Section 2.4.4, subsequent calculations and laboratory measurements indicated an electrical length of the filter of approximately 50 feet. This effect naturally produced a large path length mismatch and resulted in extremely high sidebands. The most expedient solution at the time was to install an identical filter in the transmitter leg. This matching approach significantly reduced the leakage sideband level. The amount of improvement was proportional to the degree to which two ten-section filters can be accurately matched initially and maintained in service. A reasonably good match could be obtained (with some difficulty) at a given transmitter frequency, modulation frequency, modulation index, and the antenna VSWR adjustment. Any variation of the above parameters produced unacceptable leakage levels, even when using leakage elimination filters, in the single antenna configuration (common transmit-receive antenna). Dual antenna operation (separate transmit and receive antennas), however, was excellent in any combination of operating modes (i.e.,  $J_1$ ,  $J_2$ , or  $J_3$ , high or low modulation index, etc.) without the need for any further adjustment of parameters after an initial alignment. Leakage elimination filters were not required since leakage was well below the receiver noise level even when operating in the  $J_1$  mode, high modulation index.



The basic system difference between a dual antenna and a single antenna configuration is the fact that the transmitted power is space coupled to the receiving antenna in the dual antenna case. In the single antenna case the transmitter is isolated from the receiver by the circulator. The isolation provided by a circulator is a strong function of the match into the antenna. The circulators used in the PTDLR system only provided an isolation of 17 db when operating into a good match (VSWR of 1.02). Much greater isolation (35-40 db) was obtained, however, when operating into a load with a VSWR of approximately 1.28. This is due to a bucking condition that is established wherein the normal circulator leakage is essentially cancelled by reflecting an equal amplitude signal with a 180-degree phase shift. Obviously this is a very delicate condition and only slight variations in any one of a number of operating parameters will upset the balance and will result in poor transmitter-to-receiver isolation.

It is estimated that the isolation obtained in the dual antenna configuration was approximately 55 db. This would imply that a circulator providing 55 db isolation should permit single antenna operation and give the same excellent performance as was obtained in the dual antenna flight tests. Circulators of this quality appear to be beyond present state-of-the-art capabilities. An in-house development, however, has produced switchable Ku-band circulators for use in Dicke type radiometers that provide 45 db isolation when operating into a matched load. The design uses a novel "magic T" approach and operates at  $19.3 \text{ GHz} \pm 20 \text{ MHz}$ . While the use of this type circulator in a single antenna configuration might increase the leakage level 10 db above that obtained in the dual antenna configuration, it is estimated that leakage would only approach the receiver noise level.

This should be acceptable but could be readily removed with the leakage elimination filters if necessary.

Since the initial design of the PTDLR equipment, a number of significant developments and improvements have been made in available components. In the transmitter area great strides have been made in the development of Gunn, Avalanche, and Impatt oscillators. Significant improvements have been made in power output capability, rf efficiency, and phase locking techniques.

A transmitter based on a phase locked Gunn oscillator approach would have several advantages over the varacter type presently used in the PTDLR system. A varacter multiplier power output of only 20 MW will supply the necessary L.O. and phase locking power. This is contrasted with the 1.4 watt varacter output requirement in the present transmitter. Since the Gunn oscillator is the equivalent of an rf power amplifier in this application, the generation of the required IF frequency offset between transmitter and the L.O. can be done at low power levels. This has several immediate advantages. The SSB modulator can now be placed in the transmitter leg rather than in the L.O. leg. This could not be done in the PTDLR mechanization because of the severe loss in available transmitter power due to the poor conversion efficiency of SSB modulators operating at high power levels and the additional power loss incurred in the subsequent filter. Operating the SSB at low power levels not only improves the conversion efficiency of the desired sideband, it also results in much greater suppression of the carrier and unwanted sideband frequencies. This materially reduces the subsequent filter requirement. The most significant advantage of this approach is that spurious frequencies appearing at the

transmitter output need only be suppressed, say, 40 db in order to have no significant effect on system accuracy. This is true since the received signal maintains the same spectral ratios as the transmitted signal (including spurs) and an undesired signal 40 db below the desired signal will not materially effect system accuracy. The most critical spurious frequency likely to be generated would be the image sideband produced by the SSB modulator since it is also displaced in frequency from the L.O. by the desired IF offset. However, the SSB modulator should provide 20-25 db suppression of this signal which reduces the subsequent filter requirement to a mere 20 db. This 20 db filter requirement occurs 120 MHz from the desired frequency (with a 60 MHz IF frequency) as opposed to a 90 db requirement only 60 MHz from the desired frequency in the present mechanization. Probably a single section rejection filter would suffice. A suggested transmitter approach is shown in Figure 82. The low power varacter multiplier output is power divided to supply the L.O. requirement to the three individual mixers directly. It is also supplied to the SSB modulator, offset by the IF frequency, filtered, and then used to phase lock a medium power Gunn oscillator. The Gunn oscillator output is power divided and is then used to phase lock three high power Gunn oscillators. Each supplying the transmitter power for an individual doppler beam. The configuration shown is a single antenna mechanization which would appear to be quite feasible since the path length matching problem previously discussed is all but eliminated with this transmitter mechanization. Obviously a dual antenna can be used by eliminating the circulator and adding the second antenna.

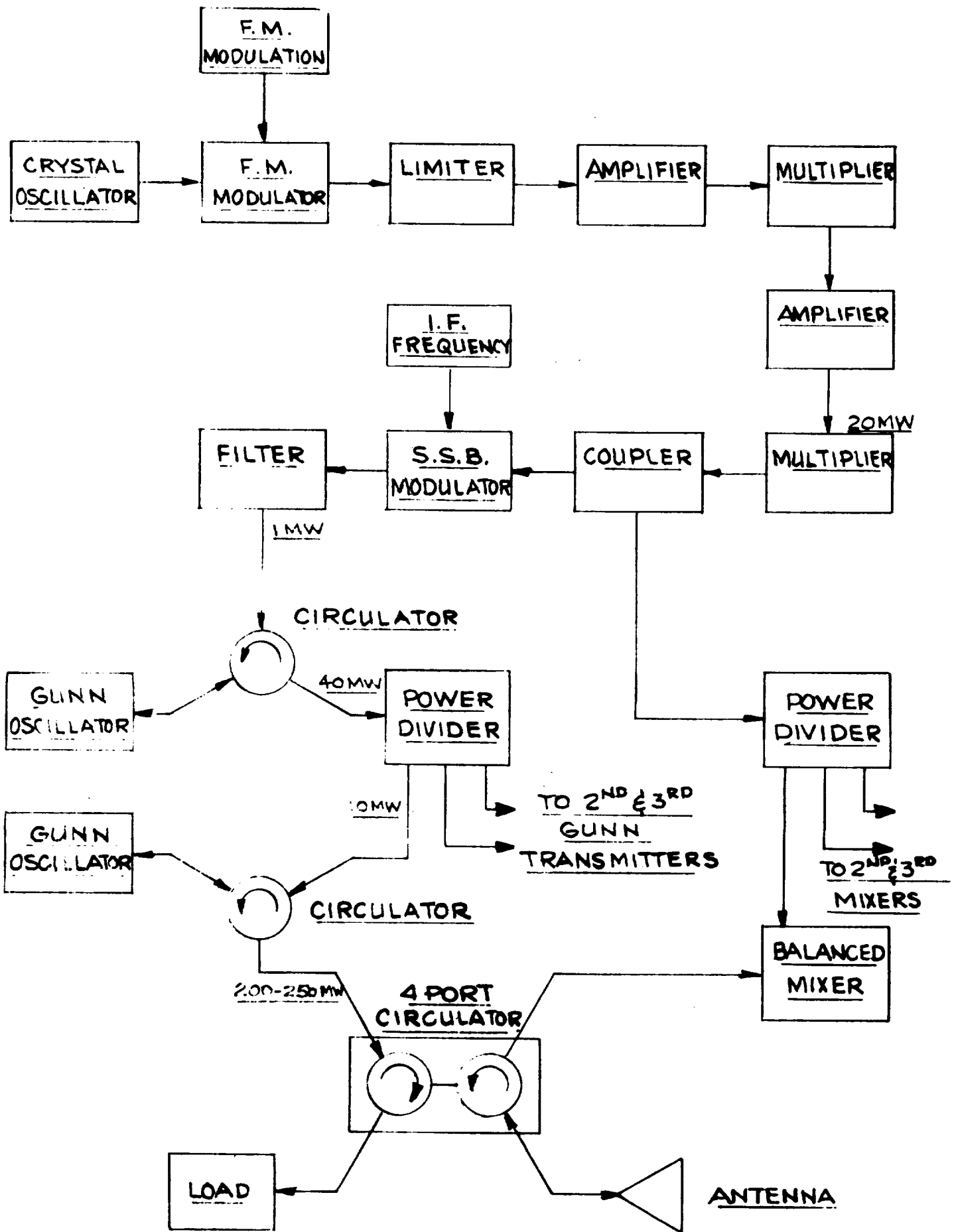


Figure 82. Proposed PTDLR Transmitter Mechanization

Significant in-house advances have recently been made in antenna fabrication techniques. Figure 83 shows a photograph of a low cost, light-weight flat plate antenna. This particular antenna was designed to operate at 35 GHz and has quite low sidelobes (30 db). The slot array is formed on two-sided copper clad material similar to a standard printed circuit board. The masking and etching process is, in fact, accomplished in the same manner. The array is fed by a simple pill-box feed structure on the back side of the plate.

This construction approach is very attractive from a cost, weight, and size point of view. Since the antenna array is easily reproducible by virtue of the simple etching process, one might consider a hexagonally shaped, relatively flat antenna composed of six identical, pie shaped elements. Opposite elements in the pie forming the transmit and receive antennas for each of the three beams. In order to provide the angular displacement required between each of the three beams, alternate sections are tilted about the apex through the desired angle, maintaining a planar relationship between opposite segments. The volume contained under each of the three alternate segments might conveniently be used to house the circuitry associated with that particular beam.

Needless to say, in the field of integrated circuits new developments are introduced almost daily and a number of components are now available that will considerably reduce the size and weight of the PTDLR electronics, particularly in the data processing circuitry. A digital velocity tracker has also been developed and tested that appears to provide a high degree of accuracy. It has the particular advantage of producing no offset bias error and can be completely fabricated using MOS technology.

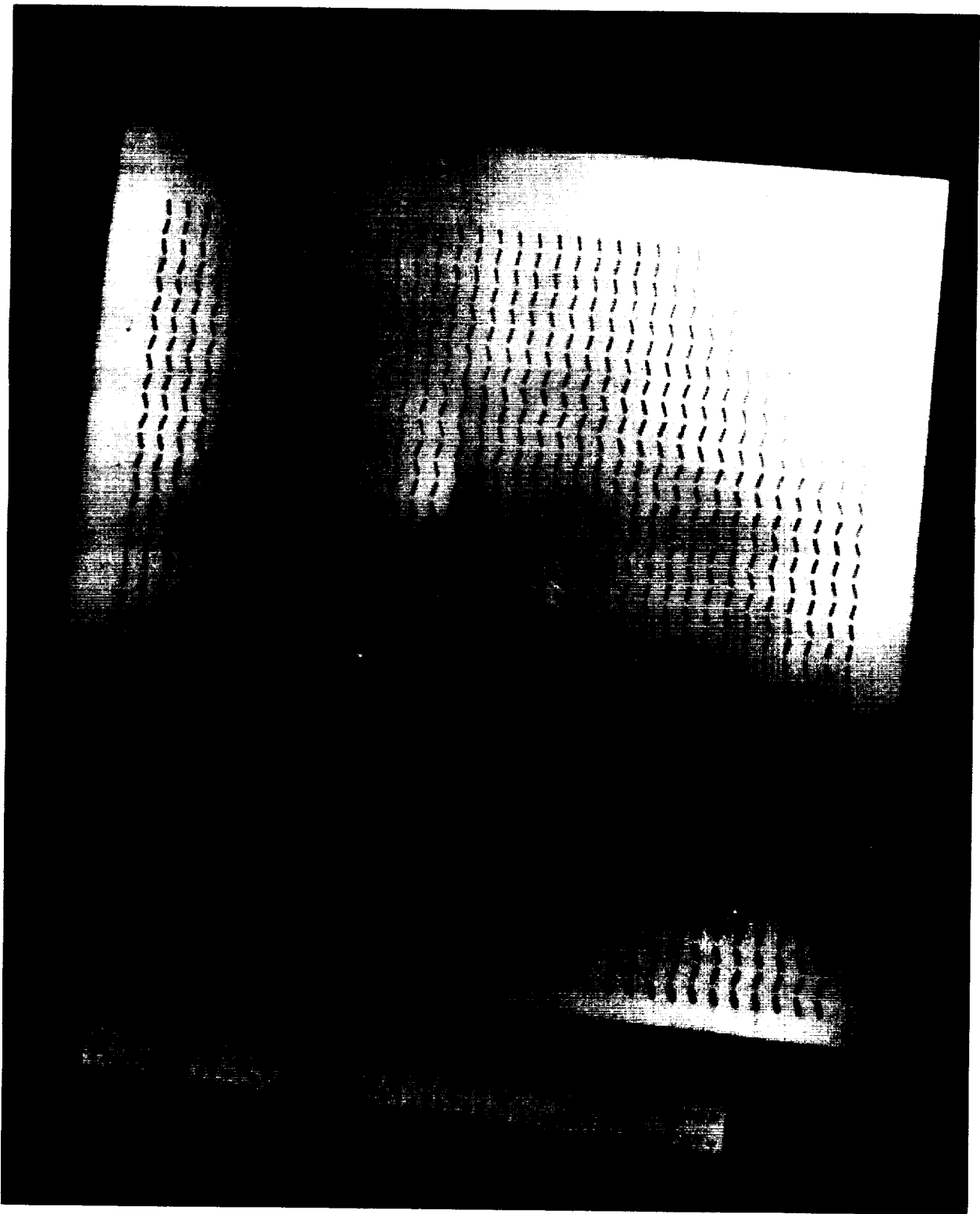


Figure 83.

## 5.2 Recommendations

The performance of the R146A has generally exceeded the original specifications for velocity and altitude with respect to both scale and accuracy. The system, however, is large in size and is quite heavy. As a development tool, it is very versatile and provides a good base from which new developments can be evaluated. As discussed in the previous section, several problem areas have been identified and promising solutions advanced.

It is recommended that a more thorough investigation of these suggestions be pursued. The Gunn transmitter would appear to simplify the mechanization considerably and minimize leakage and alignment problems. The flat plate antenna using printed circuit board fabrication techniques is a very promising approach to low cost, mass produced antennas. The lightweight construction technique is also attractive for application in space vehicles.

A successful development of both of these items coupled with a redesign of the electronics to incorporate the latest integrated circuitry would result in a highly compact, reliable, relatively low cost velocity and altitude sensor.